



Thèse

2018

Open Access

This version of the publication is provided by the author(s) and made available in accordance with the copyright holder(s).

Cellular delivery: thiol-mediated uptake of vesicles, diselenolane-mediated uptake and activation of cell-penetrating peptides

Chuard, Nicolas

How to cite

CHUARD, Nicolas. Cellular delivery: thiol-mediated uptake of vesicles, diselenolane-mediated uptake and activation of cell-penetrating peptides. Doctoral Thesis, 2018. doi: 10.13097/archive-ouverte/unige:106930

This publication URL: <https://archive-ouverte.unige.ch/unige:106930>

Publication DOI: [10.13097/archive-ouverte/unige:106930](https://doi.org/10.13097/archive-ouverte/unige:106930)

UNIVERSITÉ DE GENÈVE

FACULTÉ DES SCIENCES

Section de chimie et biochimie

Département de chimie organique

Professeur Stefan Matile

Cellular Delivery: Thiol-Mediated Uptake of Vesicles, Diselenolane- Mediated Uptake and Activation of Cell-Penetrating Peptides

THÈSE

présentée à la Faculté des sciences de l'Université de Genève
pour obtenir le grade de Docteur ès sciences, mention chimie

par

Nicolas Chuard

de

Lausanne (VD)

Thèse N° 5236

GENEVE

Atelier Repromail – Uni Mail

2018



**UNIVERSITÉ
DE GENÈVE**
FACULTÉ DES SCIENCES

DOCTORAT ÈS SCIENCES, MENTION CHIMIE

Thèse de Monsieur Nicolas CHUARD

intitulée :

**«Cellular Delivery: Thiol-Mediated Uptake of Vesicles,
Diselenolane-Mediated Uptake and Activation of
Cell-Penetrating Peptides»**

La Faculté des sciences, sur le préavis de Monsieur S. MATILE, professeur ordinaire et directeur de thèse (Département de chimie organique), Monsieur F. COUGNON, docteur (Département de chimie organique), Monsieur S. REGEN, professeur (Department of chemistry, Lehigh University, Bethlehem, Pennsylvania, U.S.A.), autorise l'impression de la présente thèse, sans exprimer d'opinion sur les propositions qui y sont énoncées.

Genève, le 2 juillet 2018

Thèse - 5236 -

Le Doyen

N.B. - La thèse doit porter la déclaration précédente et remplir les conditions énumérées dans les "Informations relatives aux thèses de doctorat à l'Université de Genève".

Acknowledgements

I would like first to thank Prof. Stefan Matile for allowing me to carry out my PhD in his group. All those years have enable me to grow scientifically as well as a person in general, and to find my way in life. All the work presented in this thesis would not have been possible without his guidance. I would like to thank equally Dr. Naomi Sakai for all her precious advices and abilities to provide answers to problems.

I am thankful to Prof. Steven L. Regen and Dr. Fabien B. L. Cougnon for accepting to read and judge this thesis. I am grateful to Dr. Giulio Gasparini, Dr. Saeideh Soleimanpour and Dr. Sebastian Benz for reading and correcting most of this thesis, and to Valentina Lorenzo for helping with the French translation.

I am grateful to all the collaborators that helped me on the different projects: Dr. Guillaume Molinard, Prof. Aurélien Roux, Dr. Samuel Lörcher, Dr. Viktoriia Postupalenko, Prof. Cornelia Palivan, Prof. Wolfgang Meier, Dr. Dimitri Moreau, Dr. Amalia Poblador-Bahamonde, Mrs. Jana Hildebrandt, Prof. Wolfgang Weigand, Mr. Jacques Saarbach, Prof. Nicolas Winssinger, Prof. Pierangelo Metrangolo and Prof. Giuseppe Resnati. Without all their help, it would have been impossible to do all the work presented in this thesis.

I would like to thank all the past and present member of the Matile group for providing an excellent working atmosphere. Especially Giulio who was first my mentor when I arrived in the lab, before to become a very good friend, and with his partner in life, Marta, hosting me about once a week during my whole PhD.

I am also grateful to all the members of the “monkey climbing team” allowing me to spread my remaining energy after long day work on the wall, and helping me to keep some mental sanity.

A special thanks to sweet Karolína for making me discover the joy of guitar duet and all our discussions after our repetitions. She gave me so much strength, helped me to become a better person and learn a lot on myself. I could not be more grateful to having meet her and getting to know her.

I would like to thank my friends from EPFL who were always present to remind me that there is a life out of the lab and all the memorable moments we spent together.

Finally I would like to thank my whole family, especially my parents Maria-Paz and Alain, and my brother Sylvain. I would not have been able to perform all those studies without their unconditional supports during all those years, trying to understand what I was doing in the lab and always being present when I needed them.

List of Publications

1. **Chuard, N.**; Poblador-Bahamonde, A. I.; Zong, L.; Bartolami, E.; Hildebrandt, J.; Weigand, W.; Sakai, N.; Matile, S. “Diselenolane-Mediated Cellular Uptake” *Chem. Sci.* **2018**, *9*, 1860–1866.
2. Macchione, M.; **Chuard, N.**; Sakai, N.; Matile, S. “Planarizable Push-Pull Probes: Overtwisted Flipper Mechanophores” *ChemPlusChem* **2017**, *82*, 1062–1066.
3. **Chuard, N.**; Gasparini, G.; Moreau, D.; Lörcher, S.; Palivan, C.; Meier, W.; Sakai, N.; Matile, S. “Strain-Promoted Thiol-Mediated Cellular Uptake of Giant Substrates: Liposomes and Polymersomes” *Angew. Chem., Int. Ed.* **2017**, *56*, 2947–2950.
4. **Chuard, N.**; Fujisawa, K.; Morelli, P.; Saabach, J.; Winssinger, N.; Metrangolo, P.; Resnati, G.; Sakai, N.; Matile, S. “Activation of Cell-Penetrating Peptides with Ionpair- π Interactions and Fluorophiles” *J. Am. Chem. Soc.* **2016**, *138*, 11264–11271.
5. Cotellet, Y.; **Chuard, N.**; Lascano, S.; Lebrun, V.; Wehlauch, R.; Bohni, N.; Lörcher, S.; Postupalenko, V.; Reddy, S. T.; Meier, W.; Palivan, C. G.; Gademann, K.; Ward, T.; Matile, S. “Interfacing Functional Systems” *Chimia* **2016**, *70*, 418–423.
6. **Chuard, N.**; Gasparini, G.; Roux, A.; Sakai, N.; Matile, S. “Cell-Penetrating Poly(disulfide)s: The Dependence of Activity, Depolymerization Kinetics and Intracellular Localization on Their Length” *Org. Biomol. Chem.* **2015**, *13*, 64–67.

Summary

Strained cyclic disulfides are new transporters that use thiol-mediated uptake to enter into cells. After demonstrating the ability of dithiolane to deliver fluorophores or small peptides into cells, we designed new transporters containing a thiol-sensitive head, a positive charge and an alkyl tail **S1** to deliver liposomes by thiol-mediated uptake (Figure S1).

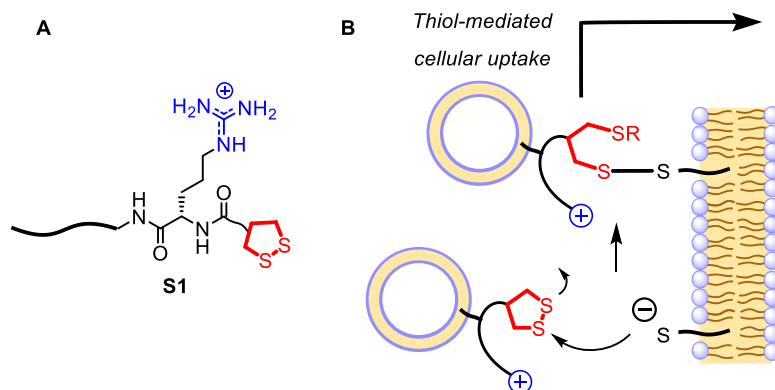


Figure S1. (A) Design of the amphiphiles for thiol-mediated uptake of vesicles. (B) Schematic representation of the entry of vesicles by thiol-mediated uptake.

Those probes can insert into the vesicle membrane after liposomes formation. The alkyl tail, the thiol-responsive head and the tuning of the liposome size were screened in order to obtain the best increase in cellular uptake. A maximum of 6-folds increase compared to the uptake of liposomes in absence of transporter, was obtained for the best activator. Treatment to block thiols on the cell surface and inactivity of transporter without the thiol-responsive head confirmed that the thiol-mediated uptake is the main entry mechanism. The fluorescence probe from the liposome core was localized in punctate location inside the cells that does not colocalize with endosomes,

lysosomes nor mitochondria. Therefore we postulated that they end up in the cytoplasm of the cells.

We were able to demonstrate that those transporters can also be used to deliver polymersomes into the cells despite the differences in the membrane composition and properties compared to liposomes.

Having reached the maximal ring tension with the epidithiodiketopiperazine scaffold, we decided to investigate compounds with diselenide instead of disulfide. Therefore we synthesized new probes containing a fluorophore and a diselenide bond. As in our initial study with disulfides, we investigated the diseleno asparagusic acid **S2**, the diseleno lipoic acid **S3** as diselenolane, and compared them to the linear diselenide of selenocystine **S4** (Figure S2).

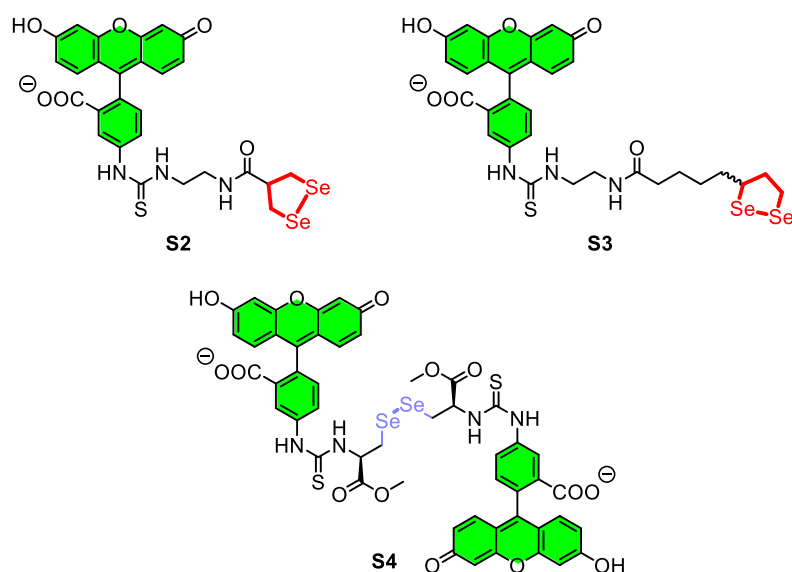


Figure S2. Fluorescent diselenide probes used in cellular uptake.

Unexpectedly from the results obtained with dithiolane, **S3** performed the best in cellular uptake. Its fluorescence was indeed higher than for **S2** for different incubation times and concentrations, and less cytotoxic for cells at

high concentration. The cellular distribution inside the cell was homogeneous with the exclusion of the nucleoli. On the other hand, incubation with **S4** showed lower and punctate uptake comparable to the original asparagusic acid.

The exact mechanism of entry into cells remains unclear for the diselenides compounds, since they are not inhibited by common endocytosis inhibitors. However some evidences of reaction with thiols point toward a possible thiol-mediated uptake.

Cell-penetrating peptides (CPPs) are powerful small polymers that can deliver substrates into cells. We have demonstrated in 2005 both in model membrane and in cells that pyrene butyric acid can be added to their membranes to increase the uptake of small polyarginine and to ensure their cytoplasmic delivery. The reason of this increase is an ion-pairing of the guanidinium cation with the carboxylate along with a good hydrophobicity and potential cation- π interactions of the peptide with the pyrene core.

In order to increase both the hydrophobicity and the ion-pairing interaction, we decided to develop new transporters based on naphthalene monoimide core **S5** (Figure S3A). On one side a carboxylate was introduced for ion-pairing with guanidinium groups from the polyarginine, while on the other side of the core, different alkyl chains were installed to increase the membrane insertion of the activator. Finally, a push-pull system was installed on the naphthalene core to polarize the π -surface for stabilization of both the positive and the negative charges at the same time.

We also investigated the ability of perfluorinated fatty acid **S6** to act as transporter (Figure S3B), and compared their activation of small polyarginine with fatty acids lacking the fluoride on carbons next to the carboxylic group.

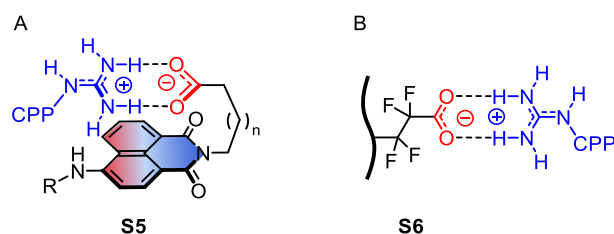


Figure S3. Activators of cell-penetrating peptides by ion-pairing on π -surface of naphthalene monoimide (A) or repulsion-driven ion-pairing with perfluorinated fatty acid (B).

Using model membrane, we screened the effect of the alkyl tail of **S5** on the transport of polyarginine to identify the best activator. The two best activators (a dodecyl and a perfluorinated alkyl tail) were tested for the uptake into cells, finding that the octaarginine could escape the endosomal capture and get released into the cytoplasm. With perfluorinated fatty acid, no activity in model membrane was observed. However when the cells were preincubated with **S6**, intracellular membrane was stained throughout the cell.

Résumé

Les disulfures cycliques sous tension sont des nouveaux transporteurs cellulaires utilisant l'administration thiol-dépendant pour entrer dans les cellules. Après avoir démontré la capacité des thiolanes à délivrer des fluorophores ou de petits peptides dans les cellules, nous avons synthétisé de nouvelles molécules constituées d'une tête réactive aux thiols, d'une charge positive ainsi que d'une chaîne alkyl pour envoyer des liposomes dans les cellules par administration thiol-dépendant (Figure S1).

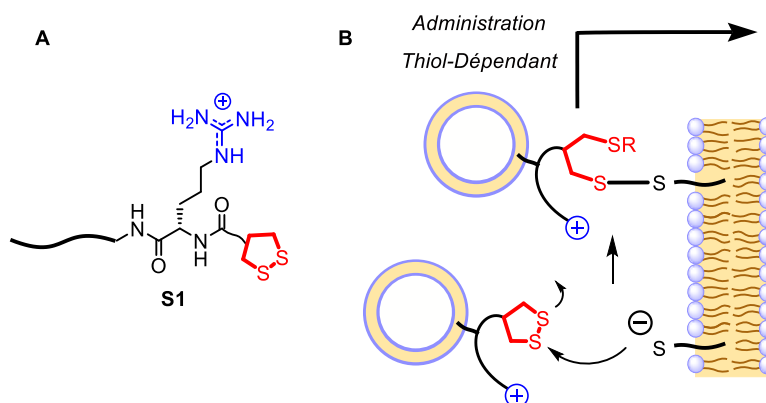


Figure S1. (A) Conception des molécules amphiphiles pour le transport de vésicules par absorption thiols-dépendant. (B) Représentation schématique de l'administration thiol-dépendant de liposomes.

Ces molécules peuvent s'insérer dans la membrane des vésicules après formation des liposomes. La chaîne alkyle, la tête réactive aux thiols et la taille des liposomes ont été testées pour obtenir la meilleure augmentation de pénétration cellulaire. Finalement, une augmentation maximale de 6 fois la pénétration des liposomes en l'absence de transporteur a été obtenue avec le meilleur amphiphile. Le traitement de la surface des cellules pour bloquer les thiols exofaciaux et l'inactivité d'un transporteur sans tête réactive aux thiols a

confirmé un mécanisme d'entrée thiol-dépendant. Le reporteur fluorescent à l'intérieur des liposomes est localisé en des points locaux à l'intérieur des cellules qui ne colocalisent pas avec les endosomes, lysosomes ou mitochondries. Par conséquent, nous avons postulé qu'ils se trouvent dans le cytoplasme des cellules.

Nous avons par ailleurs pu démontrer que ces molécules amphiphiles peuvent aussi transporter des polymersomes dans les cellules malgré les différences dans la composition et dans les propriétés de leurs membranes comparées à celles des liposomes.

Ayant atteint la tension de cycle maximale avec l'architecture de l'épidithiodiketopiperazine, nous avons décidé de passer des disulfures aux disélenures. Par conséquent, nous avons synthétisé de nouvelles sondes contenant un reporteur fluorescent et une liaison disélenure. Comme pour notre étude initiale avec les disulfures, nous avons testé l'acide aspartique disélenure **S2**, l'acide lipoïque disélenure **S3** en tant que disélenolane, et nous les avons comparés avec la disélenocystine comme disélenure linéaire **S4** (Figure S2).

Contrairement aux résultats obtenus avec les dithiolanes, la sonde **S3** a la meilleure pénétration cellulaire. Sa fluorescence est en effet plus forte que **S2** pour différents temps d'incubation et différentes concentrations, et sa toxicité est négligeable à haute concentration. Sa distribution cellulaire est homogène dans toute la cellule à l'exception des nucléoles. En revanche, l'incubation des cellules avec **S4** a montré une faible absorption ainsi qu'une localisation cellulaire comparable à l'acide aspartique.

Le mécanisme exact d'entrée dans la cellule n'est pas encore clair pour les composés disélenures. Ils ne sont en effet pas inhibés par des inhibiteurs communs d'endocytose. Par contre, des preuves de réactivité avec des thiols pointent vers un mécanisme d'administration thiol-dépendant.

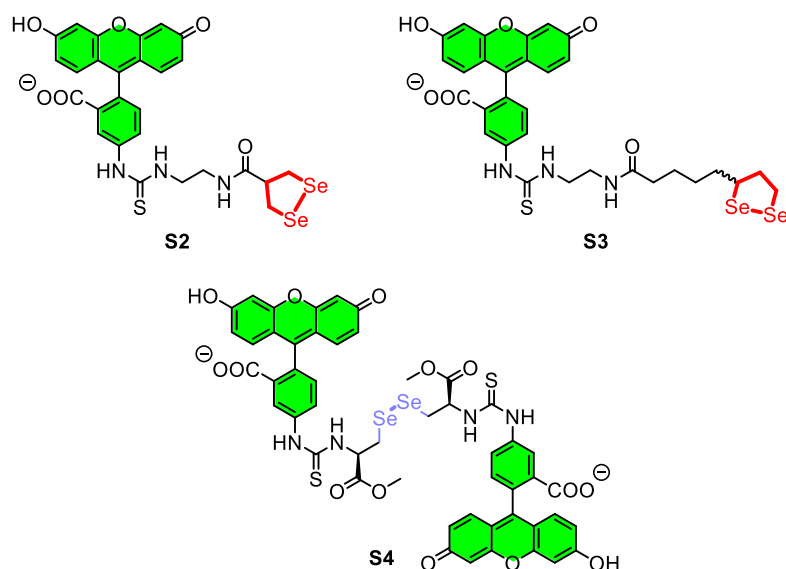


Figure S2. Sondes disélénures fluorescentes utilisées pour la pénétration cellulaire.

Les peptides à pénétration cellulaire (CPPs) sont de puissants petits polymères qui peuvent délivrer des substrats dans les cellules. En 2005, nous avons démontré dans des modèles membranaires et dans les cellules que l'acide pyrène butyrique peut être ajouté à leurs membranes pour augmenter la pénétration de petits polyarginines et s'assurer de leur relâchement dans le cytoplasme. La raison de cette augmentation est due à une interaction électrostatique entre le cation guanidinium et le carboxylate, ainsi qu'une bonne hydrophobicité et une potentielle interaction cation- π avec la surface pyrénique.

Pour augmenter l'hydrophobicité et stabiliser l'interaction électrostatique, nous avons décidé de développer un nouvel activateur basé sur un cœur naphthalène monoimide **S5** (Figure S3A). D'un côté de la surface, un carboxylate a été introduit pour l'interaction électrostatique avec les groupes guanidinium ; de l'autre, différentes chaînes alkyles ont été installées pour augmenter l'insertion du complexe dans la membrane. Finalement, un système

donneur-attracteur a été introduit sur le cœur naphthalène pour polariser la surface- π afin de stabiliser à la fois la charge positive et la charge négative.

Nous avons aussi évalué la capacité des acides gras perfluorés **S6** d’agir comme transporteurs (Figure S3B) et nous avons comparé leurs activations à des acides gras sans les fluorures sur les carbones adjacents à l’acide carboxylique.

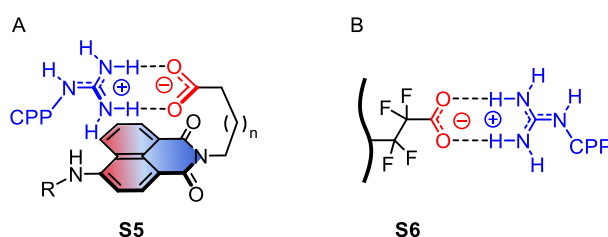


Figure S3. Activateurs de peptides à pénétration cellulaire par stabilisation de l’interaction électrostatique sur la surface- π du naphthalène monoimide (A) ou par interaction électrostatique poussée par répulsion avec les acides gras perfluoré (B).

En utilisant des modèles membranaires, nous avons étudié l’effet de la chaîne alkyle **S5** sur le transport de polyarginine pour identifier les meilleurs activateurs. Les deux meilleurs composés (une queue dodecyl et une chaîne alkyle perfluorée) ont été testés sur les cellules. Nous avons découvert que l’octaarginine peut échapper à la capture endosomale et être relâché dans le cytoplasme des cellules. Avec les acides gras perfluorés, aucune activité dans les modèles membranaires n’a été observée. Cependant, lorsque les cellules étaient préincubées avec **S6**, les membranes intracellulaires étaient marquées dans toute la cellule.

Table of Contents

CHAPTER 1	1
INTRODUCTION	1
1.1. Cellular Delivery Methods	1
1.2. Cell-Penetrating Peptides	4
1.2.1. Polyarginine	5
1.3. Poly(disulfide)s and Thiol-Mediated Cellular Uptake	10
1.3.1. Poly(disulfide)s	11
1.3.1.1. Cell-Penetrating Poly(disulfide)s	13
1.3.2. Thiol-Mediated Uptake and Strained Cyclic Disulfides	23
1.4. Selenium in Cellular Uptake	34
1.4.1. Diselenide in Cellular Uptake	34
1.4.2. Diselenolane	37
1.5. Vesicles in Cellular Uptake	42
1.5.1. Liposomes Delivery	42
1.5.2. Polymerized Vesicles and Polymersomes	47
CHAPTER 2	52
OBJECTIVES	52
CHAPTER 3	54
RESULTS AND DISCUSSION	54
3.1. Thiol-Mediated Uptake of Vesicles	54
3.1.1. Design	54
	IX

3.1.2.	Thiol-Responsive Head Screening	55
3.1.2.1.	Synthesis	55
3.1.2.2.	Flow Cytometry Assay	58
3.1.2.3.	Confocal Laser Scanning Microscopy	61
3.1.3.	Liposome Influence on Uptake	66
3.1.3.1.	Lipid Composition Screening	66
3.1.3.2.	Size Dependence	67
3.1.4.	Uptake Kinetics	70
3.1.5.	Colocalization Assay	74
3.1.6.	Tail Screening	79
3.1.6.1.	Synthesis	79
3.1.6.2.	Flow Cytometry Assay	82
3.1.6.3.	Confocal Laser Scanning Microscopy	83
3.1.7.	Polymersomes Uptake	86
3.1.7.1.	Confocal Laser Scanning Microscopy	87
3.1.7.2.	Flow Cytometry Assay	89
3.1.8.	Additional Transporters and Assays	90
3.1.8.1.	Epidithiodiketopiperazine Transporter	90
3.1.8.2.	Diseleno Lipoic Acid Transporter	92
3.1.8.3.	Addition of Positive Charges	94
3.2.	Delivery of Diselenides	95
3.2.1.	Synthesis	96
3.2.2.	Reactivity Toward Thiols	98

3.2.2.1.	Thiol-Exchange Affinity Column	99
3.2.2.2.	Oxidation of DTT	102
3.2.3.	Solutions Studies	106
3.2.3.1.	Reduction of the Diselenide Bond	106
3.2.3.2.	Fluorescence Quenching Effect	108
3.2.4.	Cellular Uptake Studies	110
3.2.4.1.	Flow Cytometry Assay	110
3.2.4.2.	Concentration and Time Dependences on Cellular Uptake	111
3.2.4.3.	Cytotoxicity Assay	119
3.2.4.4.	Uptake Inhibition Assay	121
3.3.	Activation of Polyarginine	124
3.3.1.	Design	125
3.3.2.	Solution Studies	130
3.3.2.1.	CF-Efflux Assay	130
3.3.2.2.	Absorbance of the ANI in presence of vesicles	135
3.3.3.	Cellular Uptake	137
CHAPTER 4		147
PERSPECTIVES and CONCLUSION		147
CHAPTER 5		151
EXPERIMENTAL SECTION		151
5.1.	General	151
5.1.1.	Reagents, Solvents, Medium and Equipment	151

5.1.2.	Chromatographic Equipment and Methods	152
5.1.3.	Equipment for Characterization	153
5.1.4.	Equipment used for Experiments	154
5.2.	Synthesis	155
5.2.1.	Thiol-Mediated Uptake of Vesicles	155
5.2.2.	Delivery of Diselenide Probes	171
5.2.3.	Activation of Polyarginine	174
5.3.	Methods	176
5.3.1.	Vesicles Preparation	176
5.3.1.1.	DSPC/DSPE-PEG ₂₀₀₀ LUVs	176
5.3.1.2.	DSPC LUVs	177
5.3.1.3.	EYPC LUVs (SRB)	177
5.3.1.4.	Brain PS/Rhod-PE LUVs	178
5.3.1.5.	Preparation of Vesicles for Thiol-Mediated Cellular Uptake	178
5.3.1.6.	EYPC LUVs (CF)	178
5.3.1.7.	Transport Activity in Fluorogenic LUVs	179
5.3.1.8.	EYPC LUVs (empty)	181
5.3.2.	Cellular Experiments	182
5.3.2.1.	Cell Culture	182
5.3.2.2.	Confocal Microscopy	182
5.3.2.3.	Colocalization Studies	183
5.3.2.4.	Flow Cytometry	185

5.3.2.5.	Endocytosis Inhibition	186
5.3.2.6.	Automated Microscopy	186
5.3.2.7.	MTT Assay	187
5.3.3.	Oxidation of DTT by Diselenolane	187
5.3.4.	Diselenolane Fluorescence Calibration	192
5.3.4.1.	Closed Cycle Correction Factor	192
5.3.4.2.	Open Cycle Correction Factor	192
5.3.5.	Absorbance and Fluorescence of CPP Activators	193
5.4.	Abbreviations	194
CHAPTER 6		198
REFERENCES		198

Chapter 1

INTRODUCTION

1.1. Cellular Delivery Methods

The development of an active principle of a drug against a specific disease can appear as finding a needle in a haystack. However once the design of the drug is efficient, another problem arises: how to deliver it efficiently to the targeted destination without altering its properties nor causing collateral damages to healthy systems in the process.

In order to solve this problem and unless the drug is so specific by itself or harmless to all systems except its target, there is also a need to develop a transporter called drug delivery system, to bring the drug to the specific site and release it in a time and space controlled manner without altering its function.

In the case of this thesis, the focus would be put on methods and transporters that can be used to deliver substrates into cells, thus crossing the cellular plasma membrane. There would be no discussion about administration methods, blood stability nor tissue targeting into living organisms.

Of course if the drug or the probe that need to cross the plasma membrane is small enough and with a good lipophilicity, it may enter by itself into the cell by passive diffusion through the membrane. However this is rarely the case. Therefore there has been a hard focus on the development of active and specific transporters. Some of the main characteristics needed are good membrane permeation, cell or organelle specificities and minimized cytotoxicity. Among the main transporters developed in recent years, we can find liposomes,^[1]

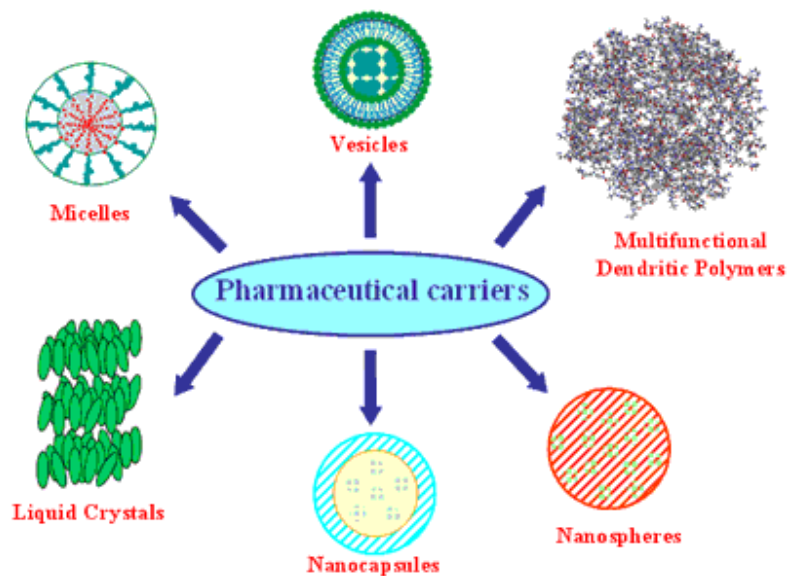


Figure 1. Common carriers used as drug delivery systems. Image from reference.^[2]

nanoparticles,^[3] micelles,^[4] or polymers^[5] (Figure 1). All those delivery systems mainly rely on the use of active transport (endocytosis) to deliver their cargoes into the cell at their specific location (Figure 2).

Under the term endocytosis different mechanisms are regrouped: the phagocytosis is an exceptional case for it is the uptake of solid particle or pathogens without the surrounding liquid environment by the cells to form phagolysosomes. In the human body macrophages are specialized cells that uses exclusively the phagocytic pathway to ingest pathogens or eliminate debris in the blood stream.^[6] All the other forms of endocytosis involve the uptake of the surrounding liquid along with the cargo and are regrouped under the pinocytosis pathway.

The pinocytosis pathway regroupes the macropinocytosis,^[7] the clathrin-mediated endocytosis,^[8] the caveolin-mediated endocytosis^[9] and the

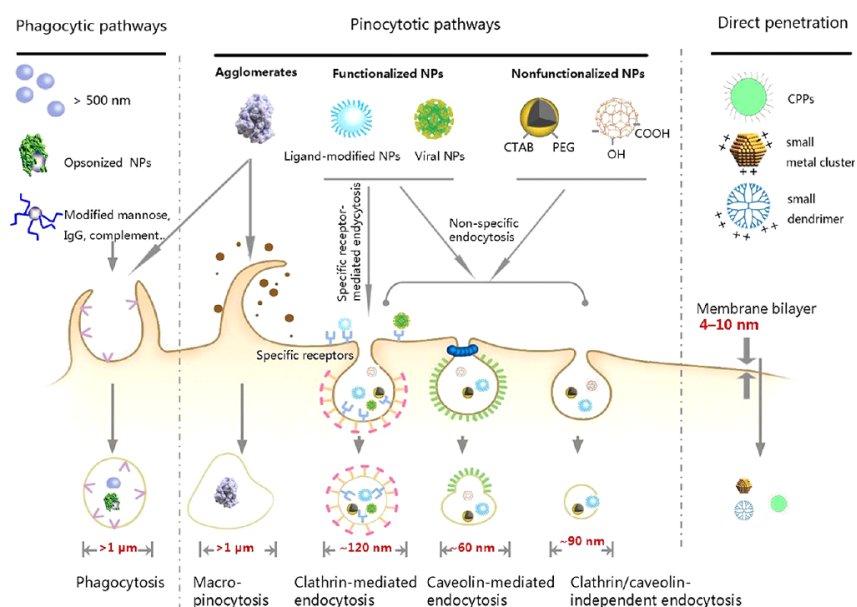


Figure 2. Schematic representation of the different cellular uptake mechanisms. Image from reference.^[10]

clathrin/caveolin-independent endocytosis.^[11] In all those different endocytosis pathways, the size, lipid composition and proteins involved to form vesicles called endosomes inside the cells, are different. Therefore there is the possibility to target specifically one type of endocytic pathway against another using chemical inhibitor or target all of them at once by depleting the cell from the energy needed for the mechanism by incubation at low temperature.^[12] The first endosomes formed in cells are the early endosomes which can mature into late endosomes and eventually into lysosomes. The whole maturation process is characterized by a decrease in the pH from the physiological 7.4 to about 5 in the lysosomes.^[13] This drop in the pH is commonly used by transporters to escape the endolysosomal pathway into the cytoplasm by introduction of a pH sensitive molecule.

1.2. Cell-Penetrating Peptides

Among all the drug delivery systems available and reported in the previous section, we decided in the Matile group, to focus first on polymers as transporters. The most common type of polymers used for cellular delivery are the cell-penetrating peptides (CPPs). CPPs were originally discovered in the transactivator of transcription (Tat) protein of the human immunodeficiency virus type 1 (HIV-1) simultaneously by the groups of Loewenstein^[14] and Pabo^[15] in 1988. They found that this protein can cross through the plasma membrane by itself. It is however only about ten years later that it was demonstrated that only a small and cation-rich sequence is efficiently responsible for the translocation (Tat₄₉₋₅₇: RKKRRQRRR).^[16] Surprisingly this specific sequence showed that its entry mechanism is not through endocytosis but by direct translocation through the membrane, thus confirming the result found for the antennapedia homeodomain transcription factor (later named penetratin) of *Drosophila* which displayed similar cell-penetration ability.^[17]

Encouraged by this very important discovery, many studies have focused on identifying different natural or synthetic peptide sequences that possess the cell-permeation ability. CPPs are short peptides (less than 40 amino acid residues) and can nowadays be classified in three main categories: amphipathic, cationic or hydrophobic. Some examples for each families are reported in Table 1.^[18]

The Tat sequence and the penetratin are part of the cationic type in which there is a large number of basic amino acids in the sequence, especially arginine and lysine residues. The hydrophobic type contains mainly hydrophobic amino acids which confer them the ability to pass easily through the plasma membrane by passive diffusion.^[19-20] Finally the amphipathic CPPs

Table 1. Type, name and amino acid sequences from some common CPPs. Table reproduced from reference.^[18]

Type	Name	Amino acid sequence
Amphipathic	Transportan	GWTLNSAGYLLGKINLKALAALAKKIL
	Pep-1	KETWWETWWTEWSQPKKKRKV
	MPG	GLAFLGFLGAAGSTMGAWSQPKKKRKV
	pVEC	LLIILRRRIRKQAHASK
	MAP	KLALKLALKALKAAALKLA
	CADY	GLWRALWRLRLSLWRLWRA
Cationic	Polyarginine	R8, R9, R10, R12
	Tat ₄₉₋₅₇	RKKRRQRRR
	Penetratin	RQIKIWFQNRRMKWKK
	P22N	NAKTRRHERRRKLAIER
	DPV3	RKKRRRESRKRRRES
	DPV6	GRPRESGKKRKRKRLKP
Hydrophobic	K-FGF	AAVLLPVLLAAP
	C105Y	CSIPPEVKFNKPFVYLI

are usually longer than the other types and contain a combination of hydrophobic and cationic residues conferring properties from both families.^[21-22]

1.2.1. Polyarginine

In the work presented in this thesis, we focused on one of the simplest CPP: polyarginine. It belongs to the cationic type and are constituted as its name imply, only of arginine residues. It was shown already in early 2000 that the guanidinium groups present on CPPs are responsible for the translocation

efficiency of the peptide.^[23] Working on optimizing the guanidinium-rich oligomer by introducing spacer, determining the stereochemistry and the number of arginine residue needed for good transport, various cargoes were delivered into the cells such as caspase,^[24] β -galactosidase^[25] or DNA^[26-27] by covalent or non-covalent conjugates.

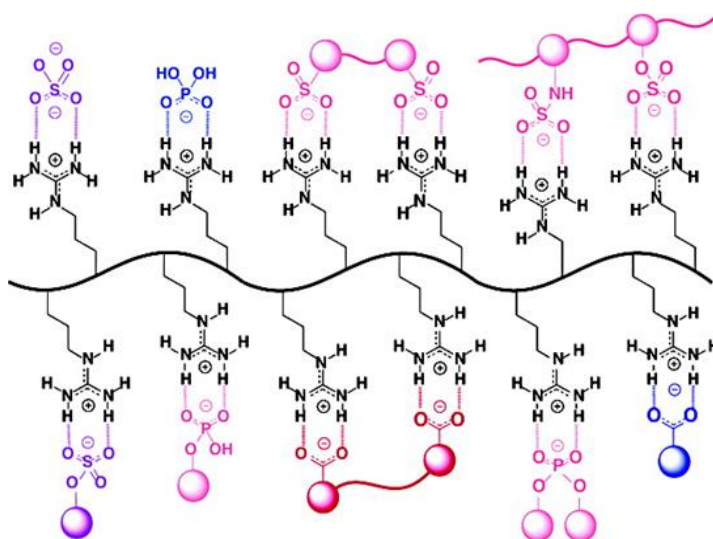


Figure 3. Example of bidentate ion-pairing of polyarginine with different anions. Image from reference.^[28]

Cationic arginines are preferred compared to lysine or histidine amino acids for two reasons. The first being that the guanidinium group can interact in a bidentate manner with anions such as phosphates, carboxylic acids and sulfates groups present on the cell surface (Figure 3), while the ammonium group in lysine can interact only by weaker electrostatic interaction.^[29] The reduction of cationic charges on the peptide by ion-pairing make them more lipophilic allowing them to pass through the plasma membrane.

The second reason is the difference in acidity between guanidinium and ammonium groups. Polylysine with a pK_a of their ammonium group around

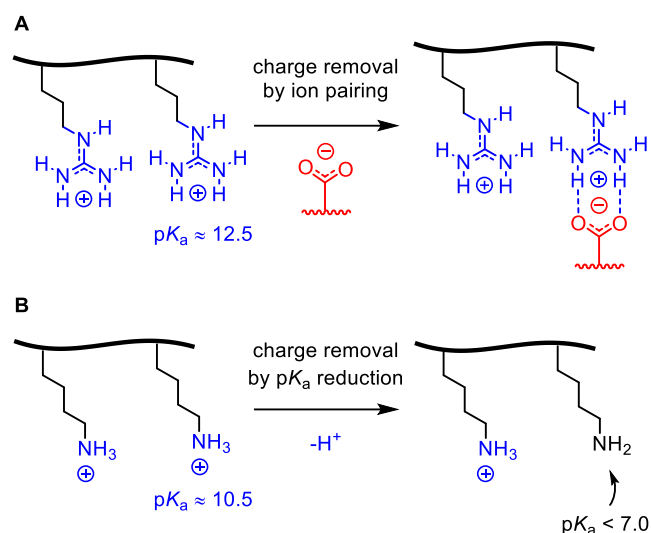


Figure 4. Charge repulsion by ion-pairing for polyarginine (A) or by protonation for polylysine (B). Image reproduced from reference.^[28]

10.5 demonstrated that upon charge proximity, a deprotonation of vicinal ammonium is possible by decreasing their pK_a to around 7 which, as a consequence, decrease the amount of positive charges available to interact with anion on the cell surface. In the case of arginine, the pK_a of the guanidinium is so high (around 12.5) that the pK_a of vicinal guanidiniums cannot decrease sufficiently to induce deprotonation. Therefore in order to reduce charge repulsion, polyarginine has to interact with anions to decrease the amount of positive charges present on the peptide (Figure 4).^[28]

Those two reasons explain the “arginine magic” that makes polyarginine such good transporters for cellular delivery compared to polylysine. However the exact transport mechanism of such carrier is still under debate, for there is a competition between direct translocation through the membrane, endosomal capture or even a combination of both depending on the size of the oligoarginine and the cargo to deliver.

For the direct translocation mechanism, different processes have been proposed such as the carpet model^[30] in which a transient inverted micellar pore is formed disrupting the membrane, the barrel stave pore formation^[31] where CPPs aggregate to form a pore, or the toroidal pores^[32] where the aggregation of the CPPs induce a membrane curvature until the thickness is so small that the polymer can pass by small pore formation.^[33]

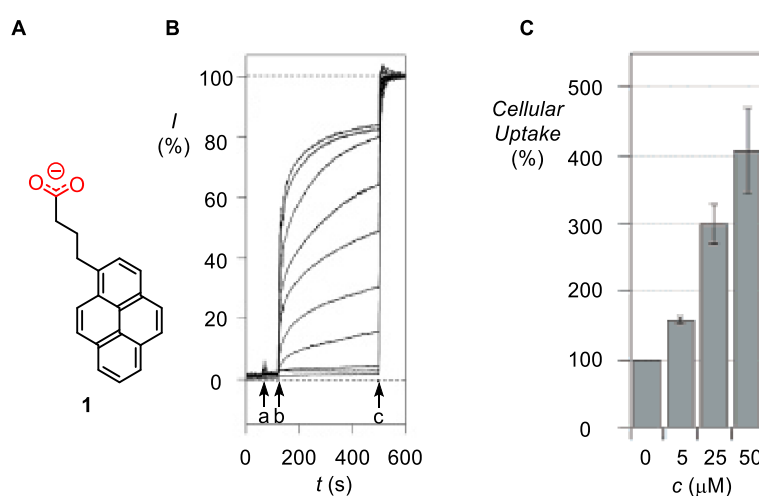


Figure 5. (A) Structure of pyrene butyrate **1** used as activator of polyarginine. (B) Activation of polyarginine in model membrane (large unilamellar vesicles, LUVs) by pyrenebutyrate: change in CF emission I as a function of time during the addition of **1** (a, 0 – 100 μM) and polyarginine (b, 250 nM), calibrated by final lysis with excess of Triton X-100 (c). (C) Quantification of uptake by flow cytometry of R₈ labelled with Alexa (5 μM) in HeLa Kyoto cells with increasing concentration of **1**. Images from reference.^[34]

However when the peptide cannot pass through the membrane by passive transport and get internalized into cells by endocytosis, escape into the cytoplasm become necessary. In order to overcome it, pH-responsive amino acid like histidine could be used in order to get release into the cytoplasm of the cell by “proton-sponge” effect (endosome osmotic swelling).^[35] Another strategy is to use small anionic molecules as activator that will interact electrostatically with polyarginine increasing its hydrophobicity and leading to

a passive uptake of the peptide. The only known activator used so far was the pyrenebutyrate **1** (Figure 5A), which demonstrated an increase of activity in model membrane (Figure 5B) and an increase of uptake in cells (Figure 5C). The increase of cellular uptake was accompanied by an escape of the endosomal pathway (Figure 6) for small polyarginine.^{[34],[36]} It was indeed demonstrated that labelled octaarginine (R_8) are mainly capture into endosomes (Figure 6B) when incubated alone, but preincubation of cells with **1** lead to the release of the peptide into the whole cell (Figure 6A).

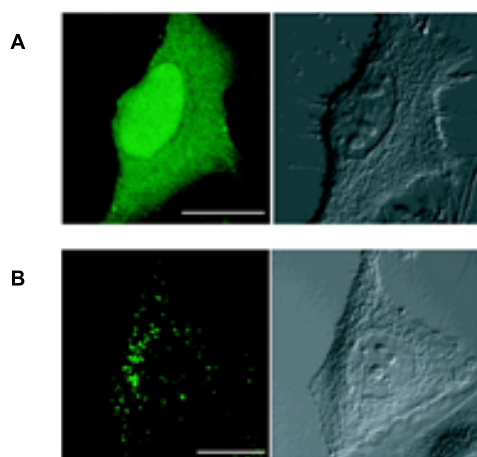


Figure 6. Confocal laser scanning microscope images from HeLa Kyoto cells incubated with R_8 -Alexa for 15 min with (A) or without (B) preincubation for 5 min with **1**. Left: Alexa fluorescence channel, right: DIC channel. Scale bar: 20 μ m. Images from reference.^[36]

Futaki and coworker further investigated the effect of addition of **1** on the membrane.^[37] In their report they showed that the addition of pyrenebutyrate to giant unilamellar vesicles (GUVs) have an effect on the membrane packing, disrupting the liquid-ordered phase and thus increasing the membrane fluidity (for more details on membrane phases, see section 1.5.1). Moreover it induced a negative membrane curvature which could help with the translocation of polyarginine.

In another report from Tomizawa and coworker, the pyrenebutyrate trick was applied for protein transduction in transdermal delivery.^[38] They managed to deliver hydroquinone fused to polyarginine in melanoma cells to inhibit melanin synthesis, before to successfully deliver the peptide in guinea pigs by topical therapy reducing irradiation-induced pigmentation.

One of the main drawback with such peptides is the cytotoxicity they display. Polyarginine starts showing cytotoxicity in HeLa Kyoto cells at a concentration as low as 10 μ M.^[39] In order to overcome this problem, one of the strategy is to modify the peptidic backbone to make it biodegradable by insertion of a pH-sensitive,^[40] hydrolysable^[41] or reducible bond.^[42] In our group we decided to investigate redox sensitive bond such as disulfide.

1.3. Poly(disulfide)s and Thiol-Mediated Cellular Uptake

The use of disulfide is advantageous because of the high control of the redox potential present in the cell naturally. While the extracellular medium is slightly oxidative, the cytoplasm is clearly a reducing environment with a high control of molecules such as glutathione (GSH), thioredoxin and free cysteine (Cys) kept at fix balance between their reduced and oxidized forms by highly regulated enzymes (Figure 7A).^[43] All those compounds contain a thiol to control the redox potential, which can be used in the thiol-disulfide exchange where the thiolate attack the disulfide bond releasing another thiolate (Figure 7B). For example the concentration of GSH outside the cell is in the micromolar range, while it is of 1 – 20 mM in the cytoplasm depending on the cell type and phase,^[44] 20 mM in the nucleus^[45] and about 5 mM in mitochondria.^[46] Due to this high control, the uptake of disulfide-containing transporters will be reduced once they reach the cytoplasm, releasing their cargoes and reducing their cytotoxicity depending on the localization of the redox sensitive bond on the polymer.

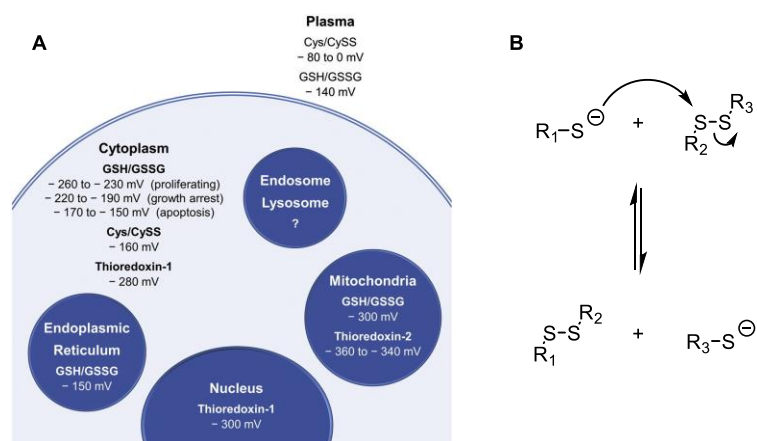


Figure 7. (A) Overview of the steady-state redox potential of the most abundant thiol redox couples in different cellular compartments. (B) Thiol-disulfide exchange reaction. Image from reference.^[43]

1.3.1. Poly(disulfide)s

Poly(disulfide)s are polymers that contain more than one disulfide bond in their chain. Most proteins for example are natural poly(disulfide)s when more than one pair of cysteines oxidize to form a correctly folded and mature protein.

In the last few years, the use of disulfide bonds in polymer to act as a carrier to transport substrates, have started to extend. Different strategies are used to incorporate them into the polymer (Figure 8). The disulfide can be already present in the monomeric unit to be polymerized (Figure 8A) by techniques such as reversible addition-fragmentation chain transfer (RAFT)^[47] or atom transfer radical polymerization (ATRP),^[48] or the disulfide bonds can be formed by oxidation of dithiols present on the monomer (Figure 8B).^[49] The disulfide can also be introduced on the side chain of the polymer mimicking natural peptides (Figure 8D). In particular, cysteine units are introduced in the polymer by solid phase peptide synthesis (SPPS), before to be functionalized with the substrate to be delivered.^[50]

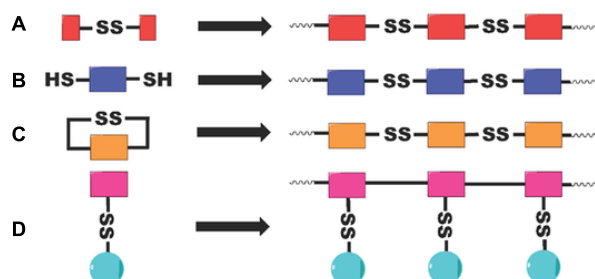


Figure 8. Strategies to introduce disulfide bonds in polymer. Image from reference.^[51]

Another interesting method for the introduction of disulfide in the polymer backbone, is through ring-opening polymerization of cyclic disulfide using thiol (Figure 8C).^[52] The first example of polymer for gene delivery made in this manner was given by Balakirev *et al.*^[53] in which they used the dilipoic acid **2** as monomer to form the poly(disulfide)s **3**. Surprisingly this polymerization method despite being prepared in mild conditions and the lack of side products, was not further studied with the exception of polymerized vesicles from the Regen group,^[54] and nearly forgotten.

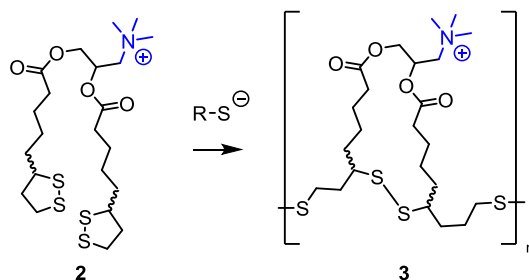


Figure 9. Monomer unit **2** used for ring opening disulfide-exchange polymerization by thiol and the corresponding poly(disulfide)s formed **3**. Structure reproduced from reference.^[53]

We decided in the Matile group to use this latest polymerization method to produce our own bioreducible polycations: the cell-penetrating poly(disulfide)s.

1.3.1.1. Cell-Penetrating Poly(disulfide)s

Cell-penetrating poly(disulfide)s (CPDs) are constructed by ring-opening thiol-disulfide exchange polymerization with asparagusic or lipoic acid derivatives. The driving force for the polymerization is the release of the ring tension contained in the dithiolane. This polymerization method was originally used in our group to build up functional photosystems on an electrode surface and was called the self-organizing surface-initiated polymerization (SOSIP).^[55-56] In this case, a thiol was bound to the surface of the electrode and performed a disulfide exchange with an asparagusic acid-containing monomer to grow a polymer perpendicular to the electrode. However in order to adapt this polymerization technique for cellular delivery, some optimization had to be performed in order to grow them in aqueous solution.

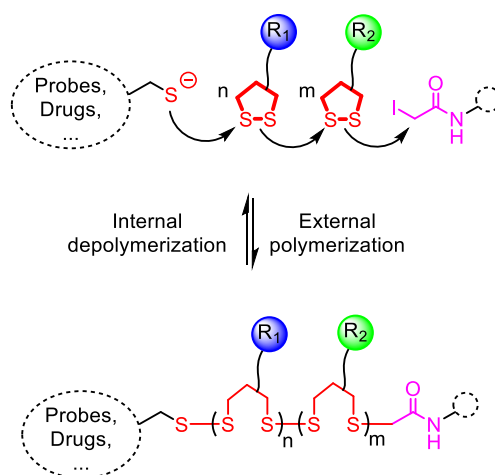


Figure 10. Schematic representation of ring-opening disulfide-exchange polymerization to grow CPDs. Image adapted from reference.^[39]

Those adjustments resulted in the substrate-initiated cell-penetrating poly(disulfide)s. Instead of installing a thiol on an electrode surface to initiate the polymerization, we introduced a thiol on the water soluble substrate to be delivered into the cell. This thiol will attack a monomer containing a dithiolane

ring on which a cation is linked to increase its water solubility and conferring, at the same time, similar propriety to CPPs. The attack release the ring tension contained in the cycle and a new thiolate to continue the polymerization. In order to quench the polymerization reaction, iodoacetamide or a derivative is added to the polymerization solution (Figure 10).

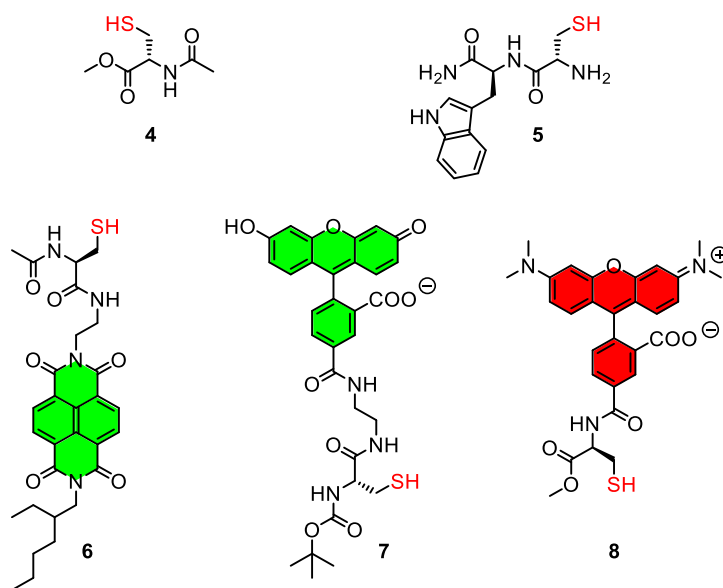


Figure 11. Initiator used to initiate the polymerization of CPDs.^{[39],[57-58]}

As a starting point, the proof of concept was established to demonstrate the possibility to grow polymer in mild conditions, i.e. in TEOA buffer at pH 7. The different initiators **4 – 8** (Figure 11), monomers **9 – 20** (Figure 12) and terminators **21** and **22** (Figure 13) were tested for the polymerization. The polymerization time, concentration of the different partners and the pH was tuned in order to obtain a polymer active in model membrane (CF-efflux assay). In this assay, carboxyfluorescein (CF) is entrapped in vesicles at a concentration high enough to ensure self-quenching. Upon the addition of a transporter, the recovery the fluorescence due to local dilution is measured in

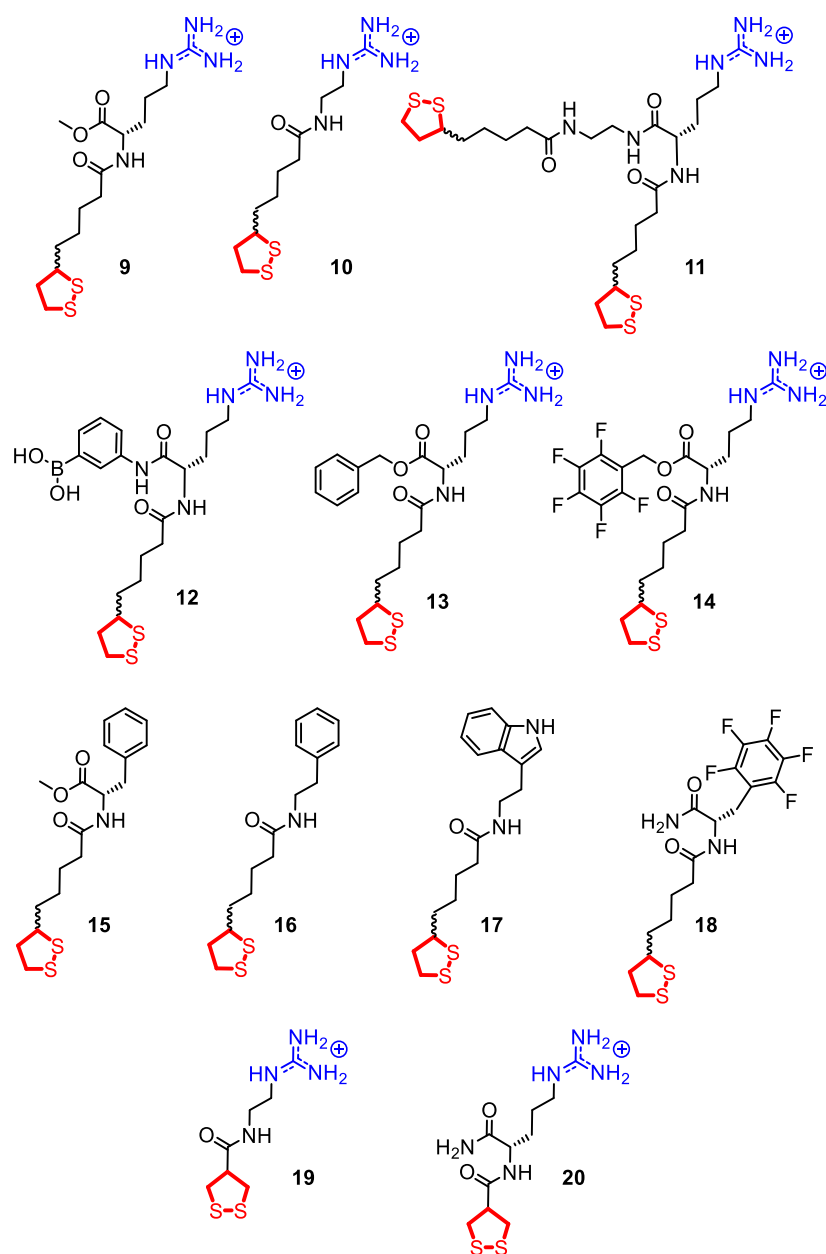


Figure 12. Monomer used in CPDs polymerization.^{[39],[57-58]}

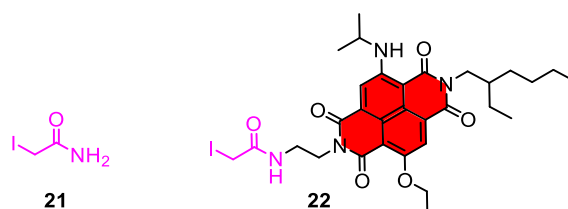


Figure 13. Terminator used to quench the polymerization of CPDs.^{[39],[57-58]}

time before full destruction of the vesicle. The activity correspond to the fluorescence before lysis upon normalization between the baseline and the destroyed vesicles fluorescence responses (Figure 5B).

The simple cysteine **4** was originally used to initiate the polymerization, but in order to facilitate purification by gel permeation chromatography (GPC), initiator **5** with a tryptophan, was introduced as molecule detectable by absorbance. The fluorescent initiator **6** and terminator **22** based on a naphthalendiimide core, were used to demonstrate the incorporation of both the initiator and terminator in the polymer by showing in a length dependent manner that Förster resonance energy transfer (FRET) was possible between those two moieties.^[57] In all other polymers grown in early studies, iodoacetamide **21** was used as terminator. Initiator **7** and **8** derived from CF and tetramethylrhodamine (TAMRA) respectively, were used as drug mimic for cellular uptake studies to track the final localization inside the cell by fluorescence.^[39]

The monomer used are derived from lipoic (**9 – 18**) or asparagusic (**19** and **20**) acids usually bearing a positive guanidinium cation. However the asparagusic acid-based compounds **19** and **20** showed random polymerization even in optimized buffer conditions without always incorporation of the initiator, and usually leading to small polymers with high polydispersity index (PDI). This is probably due to the high reactivity of the asparagusic acid with higher ring tension in the dithiolane cycle compared to lipoic acid. Therefore **19**

and **20** were quickly discarded as monomers to grow CPDs and the lipoic acid scaffold was preferred.

The first CPDs active in model membrane were grown using monomer **9** or **10** which are lipoic acid with a fused protected arginine or with a smaller linker terminated with a guanidinium cation, respectively.^[57] It was also demonstrated that it is possible to grow co-polymer using **9** with different monomers.^[58] This is interesting to incorporate new functions to the polymer: increasing its hydrophobicity using monomers **13** – **18** containing a π -basic or π -acidic ring to increase the cellular uptake by direct penetration as demonstrated with hydrophobic and amphiphilic CPPs; incorporating the boronic acid in **12** to target glycosaminoglycans on the cell surface; or cross-link different polymers using **11** containing two lipoic acids as the original CPDs developed by Balakirev.^[53] The different co-polymers were tested in the CF-efflux assay with usually good membrane activity, however when tested on cells, those CPDs tend to show lower activity and higher cytotoxicity than the original CPDs grow only with monomers **9** or **10**.^[39]

CPDs **23** and **24** grown from monomer **9** or **10** respectively and with initiator **7** or **8** were constructed, purified by GPC, lyophilized and desalted. The size was determined by GPC and the concentration by absorbance of the fluorescent initiator. In average polymers with the protected arginine **9** were longer with an average M_w around 10 kDa while the ones with **10** were smaller with an average M_w around 5 kDa. The PDI for both polymers was usually smaller than 1.2 which correspond to nearly monodisperse population. Their respective activity in the CF-efflux assay remained however similar with an effective concentration to reach 50% activity (EC_{50}) around 20 nM despite the difference in size. Interestingly, when the cellular uptake was tested, the fluorescent initiator were accumulating in different area: mainly in the nucleus, staining the nucleoli for CPDs **23** (Figure 14A and B), while mainly in the

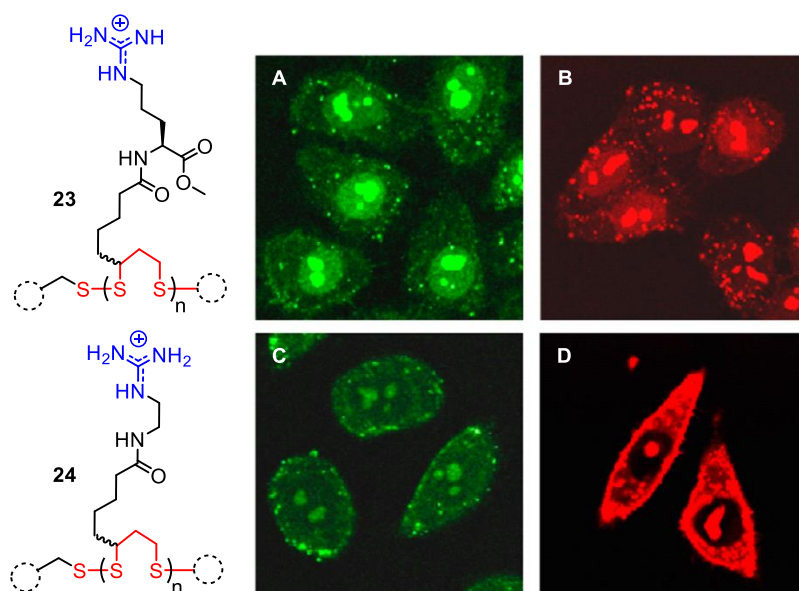


Figure 14. CLSM images of HeLa Kyoto cells incubated with polymer (500 nM) **23** (A and B) or **24** (C and D) with initiator **7** (A and C) or **8** (B and D). Images from reference.^[39]

cytoplasm with **24** (Figure 14C and D). The difference in uptake and localization was independent of the initiator/fluorophore as demonstrated by using **7** or **8** (Figure 14, A and C compared to B and D).^[39]

In order to understand better the difference in cellular localization, we studied in more details the factors determining the entry mechanism and the depolymerization kinetic inside the cytoplasm.^[59]

The CF-efflux assay was used in order to determine the transmembrane activity and the EC_{50} was determined for different sizes of **23** and **24**. We demonstrated that the activity is dependent on both the size and on the monomer used for polymerization. CPDs **24** were surprisingly more active at a low molecular weight compared to CPDs with **9** (Figure 15A). This result was indeed counter-intuitive from the cellular uptake experiments since **23** could

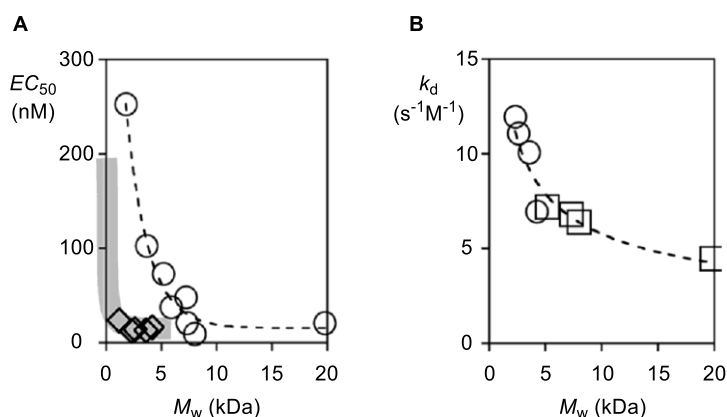


Figure 15. (A) Transmembrane activity of **23** (○) and **24** (◇) in function of the size. (B) Depolymerization kinetics of **23** (□) and **24** (○) in function of their size. Images from reference.^[59]

reach the nucleus whereas **24** remained mainly in the cytoplasm and thus we were expecting that **23** would have a higher transmembrane activity. However for typical size of polymers **23**, the transmembrane activity is the same as for **24**.

Since GSH is the main reducing agent in the cytoplasm, we decided to determine the depolymerization kinetics in solution for different polymer sizes with different concentrations of GSH. The transmembrane activity of the polymer was determined as a function of the incubation time with GSH to determine the t_{50} (incubation time needed to reach 50% of the activity). From the t_{50} at different concentration of GSH, the depolymerization rate constant k_d was determined for the CPD at a specific M_w . The curve of depolymerization kinetic in function of the size of the polymer (Figure 15B) proved that the depolymerization is only dependent on the size of CPDs and not on the monomer used to grow the polymer. This result was intuitive since it is the disulfide backbone that should be sensitive to GSH and the monomer itself should not have influence on it. Therefore only the number of disulfide bonds present on the polymer, i.e. the size, affect the depolymerization kinetic.

When polymer **23** at low molecular weight (5.7 kDa) was incubated in cell, a different cellular localization was observed compared to the original ones. The polymer was indeed mainly localized in the cytoplasm with non-negligible endosomal capture and weak nucleoli staining (Figure 16). The cellular localization of CPDs **24** did not change with smaller molecular weight. Unfortunately for unknown reasons, we were not able to produce larger polymer with monomer **10** to test for nucleus localization.

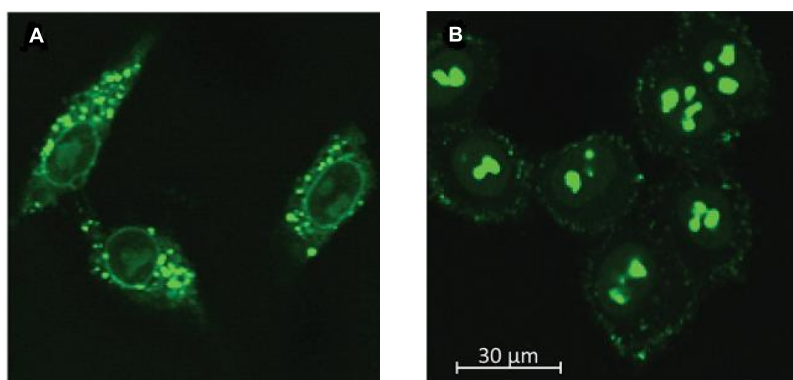


Figure 16. CLSM images of HeLa Kyoto cells incubated with **23** at low molecular weight (5.7 kDa, A) and high molecular weight (13.5 kDa, B). Images from reference.^[59]

Interestingly, increasing the concentration of CPD incubated in cell did not affect the cell viability (Figure 17A), countering one of the main disadvantage of usual CPPs such as polyarginine.^[39] The lack of cytotoxicity is probably due to rapid depolymerization of the CPD once it reaches the cytoplasm due to high concentration of GSH, as demonstrated before, releasing only non-toxic monomeric units and the substrate. When the cells were preincubated with the Ellman reagent (5,5-dithio-bis(2-nitrobenzoic acid), DTNB), a highly reactive disulfide that reacts with exofacial thiols, the uptake of CPDs was dramatically reduced (Figure 17B).

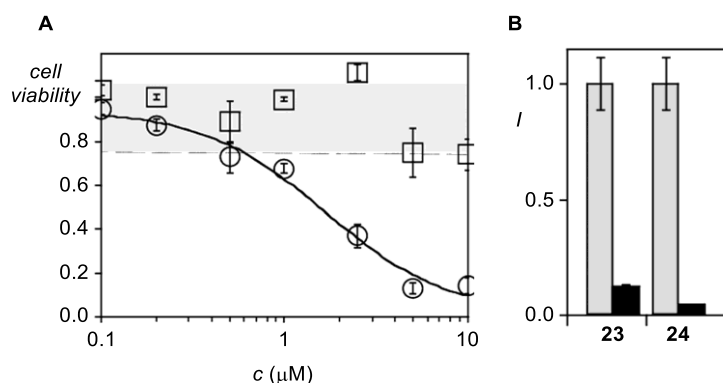


Figure 17. (A) MTT assay in HeLa Kyoto cells with CPD **24** (\square) and poly-*L*-arginine (\circ). (B) Cellular uptake quantified by flow cytometry of CPDs **23** and **24** without (grey) and with (black) preincubation with DTNB. Images from reference.^[39]

With all the results gathered at this point, we postulated that the mechanism of entry of CPDs into the cell occurs through a thiol-mediated and counterion-mediated uptake (Figure 18) where thiols exposed from proteins of the outer leaflet of the plasma membrane, could perform a disulfide exchange with the poly(disulfide)s backbone to anchor the polymer on the cell surface before to be endocytosed. Then, depending on the transmembrane activity, i.e. of the polymer composition and size, it can escape the endosomal pathway by transient inverted-micelle formation due to the presence of the positive charges and be released into the cytoplasm where it is depolymerized by the high concentration of GSH. If the polymer is long enough, it can reach the nucleus before full depolymerization. This mechanism would explain the difference observed between **23** and **24**, and the difference in cellular distribution observed for different size of **23**.

Further development of CPDs have been made on the initiator, monomer and terminator levels. In order to increase the scope of substrate to be delivered to the cells and since not all cargoes can be functionalized with a thiol to

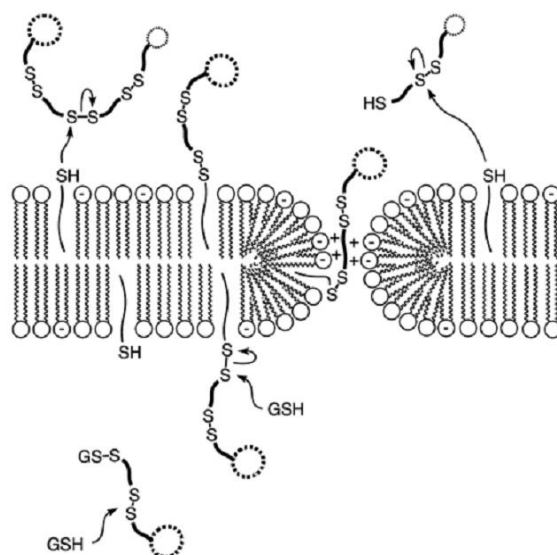


Figure 18. Proposed mechanism for the uptake of CPDs by thiol/counterion-mediated uptake. Image from reference.^[59]

initiate the polymerization, we successfully developed a thiol-containing biotin to interface CPDs with the streptavidin/biotin biotechnology and demonstrated the delivery of the whole complex into the cell.^[60] The Yao group also managed to develop several strategies on the initiator level^[61] to deliver various cargoes using CPDs in particular mesoporous silicate nanoparticles^[62–64] or native protein.^[65] Those interactions involve streptavidin/biotin biotechnology, electrostatic interactions with an anionic initiator, or inverted-electron-demand Diels-Alder cycloaddition.

On the terminator level, we used hypervalent iodine to quench the polymerization reaction. Those molecules have been shown to be more reactive than iodoacetamide toward thiols. By functionalizing such terminator with an azide, another substrate can be attached after polymerization by copper-catalyzed alkyne-azide cycloaddition (CuAAC). By using another fluorophore, we were able to demonstrate the incorporation of the terminator and the success

of the post-functional reaction, by FRET and colocalization of the initiator and terminator fluorescence inside cells.^[66]

Finally the monomer was functionalized with an azide on the C-terminus of the arginine in **9** to react after polymerization by CuAAC. The main advantage is that this small modification does not influence the polymerization and allow multiple post-modifications on the polymer after formation and purification. Using this method, additional cations or strained cyclic disulfides were grafted to increase the counter-ion mediated uptake or the thiol-mediated uptake pathways respectively, with a clear advantage for the addition of extra positive charges.^[67] More recently, sugars (glucose, galactose or trehalose) were grafted to the polymer with the double advantage to increase the possible uptake pathway through the respective sugar receptor on the cell surface, and to reduce aggregation observed when CPDs were incubated at high concentration in cells.^[68]

1.3.2. Thiol-Mediated Uptake and Strained Cyclic Disulfides

We have proposed that CPDs can enter into cells by a combination of ion-pairing between the cations on the polymer and anion on the cell surface, and by thiol-mediated uptake (Figure 18). This new uptake mechanism was first introduced in 2009 by the group of Sagan when they showed evidences of increased uptake of their CPPs when they contained a disulfide bond, and proposed that exofacial thiols play a role in the uptake (Figure 19).^[69] The group of Caruso also demonstrated the importance of exofacial thiols for the entry and release of a probe from their disulfides-containing capsules.^[70]

However, it was only in 2012 that Torres and Gait depicted how the thiol-mediated uptake might work^[71] in order to explain the difference in uptake they obtained with alkylated and non-alkylated cysteine present on their transporter.^[72] In their description, they proposed that thiol-disulfide exchange

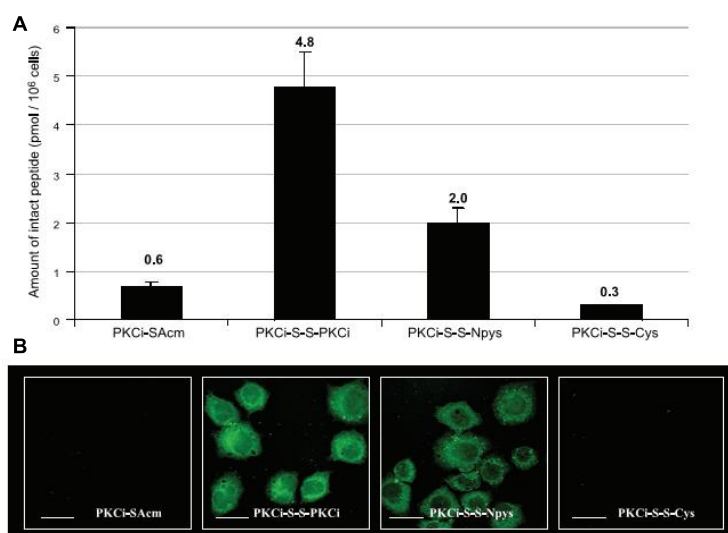


Figure 19. Quantification (A) and CLSM images (B) obtained with CPPs with a protected thiol (PKCi-SAcn), with a disulfide bond (PKCi-S-S-PKCi and PKCi-S-S-Npys) or with a disulfide and a thiol (PKCi-S-S-Cys). Images from reference.^[69]

or thiol-thiol oxidation could occur between the transporter and the cell surface protein in the extracellular environment, leading in a covalent anchoring of the transporter to the cell. The whole complex is then translocated into the cytoplasm where the cargo is released due to the reducing environment (Figure 20).

Despite the use of disulfide bonds in transporter long before those examples, the thiol-mediated uptake as part of the entry mechanism have been overlooked for many years. The disulfides were only used as redox sensitive bond to release the substrate once it reaches the cytoplasm, making it hard to attribute the real contribution of the thiol-mediated uptake mechanism in past studies. For example the comparison of transport between cysteine and cystine by Stanton and coworkers, showed differences in the transport mechanism.^[73] The mechanism for cysteine was quickly evaluated, but not for the cystine. The

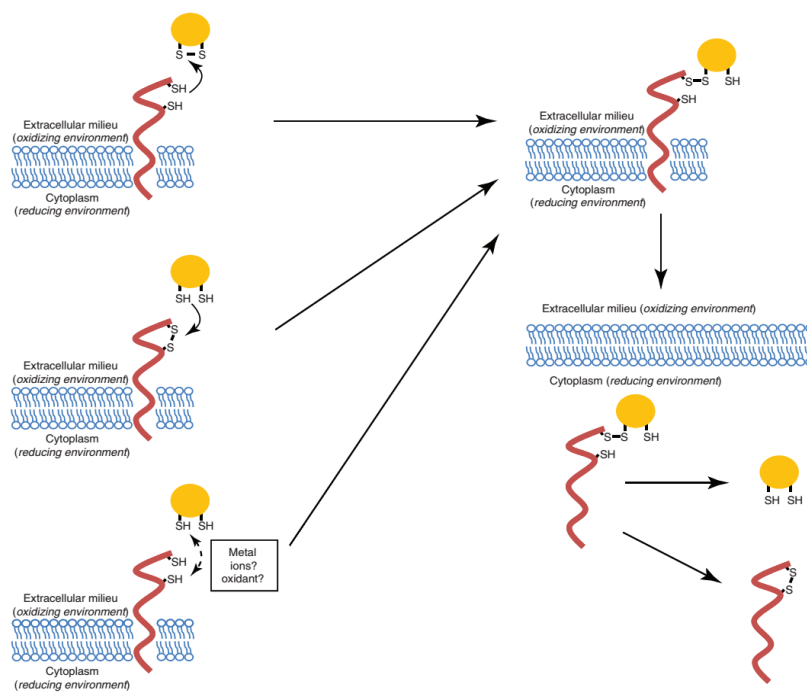


Figure 20. Possible mechanisms for thiol-mediated cellular uptake: disulfide-exchange or thiol-thiol oxidation to covalently link the transporter to proteins on the surface of the plasma membrane before internalization into the cell. Image from reference.^[71]

only observation they made about cystine entry was that it is reduced during the transport which is compatible with thiol-mediated uptake.

In our group, we wanted to demonstrate the existence and importance of the thiol-mediated uptake using the simplest molecules possible.^[74] Therefore we developed a library of fluorescent probes (Figure 21) containing either a disulfide bond (**25** – **29**) or a thiol (**30**). As a control, the fluorophore alone (**31**) was also added to the library. The uptake of **25** – **31** was tested on HeLa Kyoto cells. The only possibility for such molecules to enter into cells is by reaction of their disulfide or thiol with the cell.

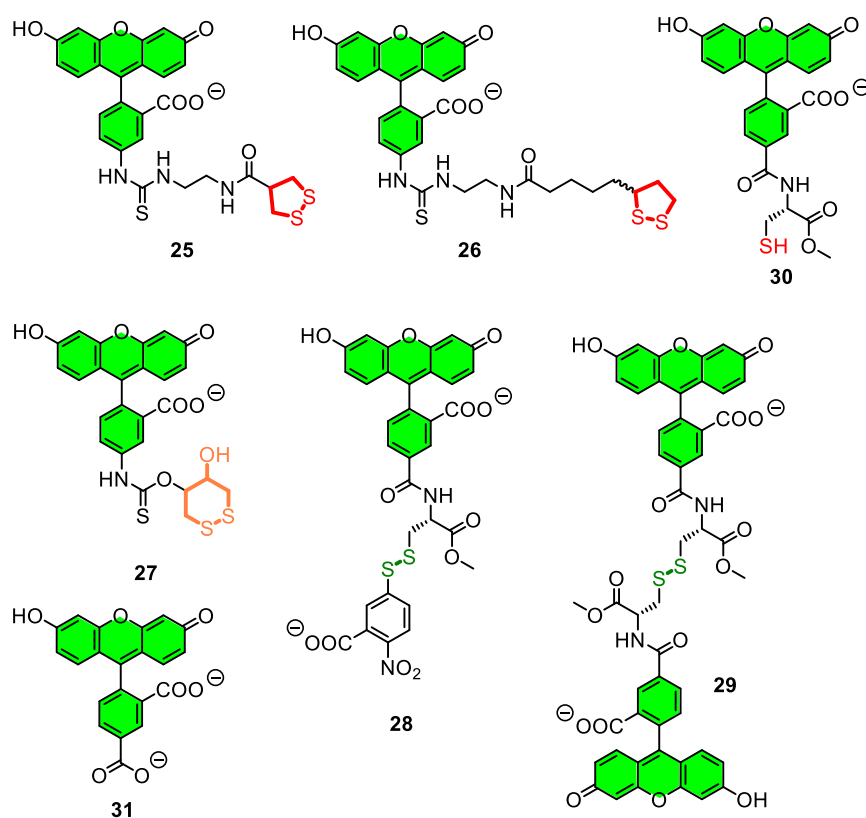


Figure 21. Library of probes containing different types of disulfide to test the thiol-mediated uptake. Image adapted from reference.^[74]

We decided to investigate not only linear but also cyclic disulfides. **25** and **26** are respectively an asparagusic or a lipoic acid attached to a fluorescein isothiocyanate (FITC) by an ethylenediamine linker. There is a small difference in the ring tension between those two compounds correlated to their respective CSSC dihedral angle of 27°^[75] and 35°^[76] making **25** more reactive than **26**. **27** contains a six-member ring disulfide based on oxidized DTT linked to FITC. The CSSC dihedral angle in this case is around 60°^[77] like in a normal chair configuration, making **27** less reactive than the dithiolane compounds. Finally

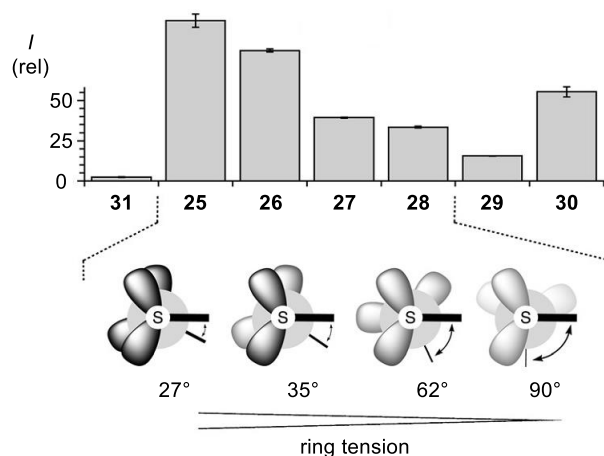


Figure 22. Flow cytometry data of HeLa Kyoto cells incubated with probes **25** – **31** (results are calibrated for the different emission intensities I of the different fluorophore) and the corresponding approximated CSSC dihedral angles for **25** – **28**. Image from reference.^[74]

linear disulfide **28** and **29** have a CSSC dihedral angle around 90° (76.4° for the Ellman reagent **32**,^[78] 79.2° for L-cystine)^[79] to minimize the repulsion of the lone pairs of electron on the sulfur atom.^[80] **28** is expected to be slightly more reactive due to the presence of a better leaving group than in **29**. Finally **30** was added to the library to study the effect of thiol on cellular uptake and their potential reaction with disulfides present on the cell surface.

The flow cytometry measurements (Figure 22) showed a good correlation between the CSSC dihedral angle, i.e. the ring tension, and the uptake. With higher ring tension, the uptake increased, with the best response obtained with asparagusic acid **25**. The cellular uptake then decreased with smaller dihedral angle in **26** and **27**. As mentioned before there is a small difference between the two linear disulfides, **28** being slightly better than **29** due to the presence of the better leaving group in **28**. The thiolated probe **30** showed a surprisingly good uptake demonstrating the presence of disulfide in the exofacial membrane

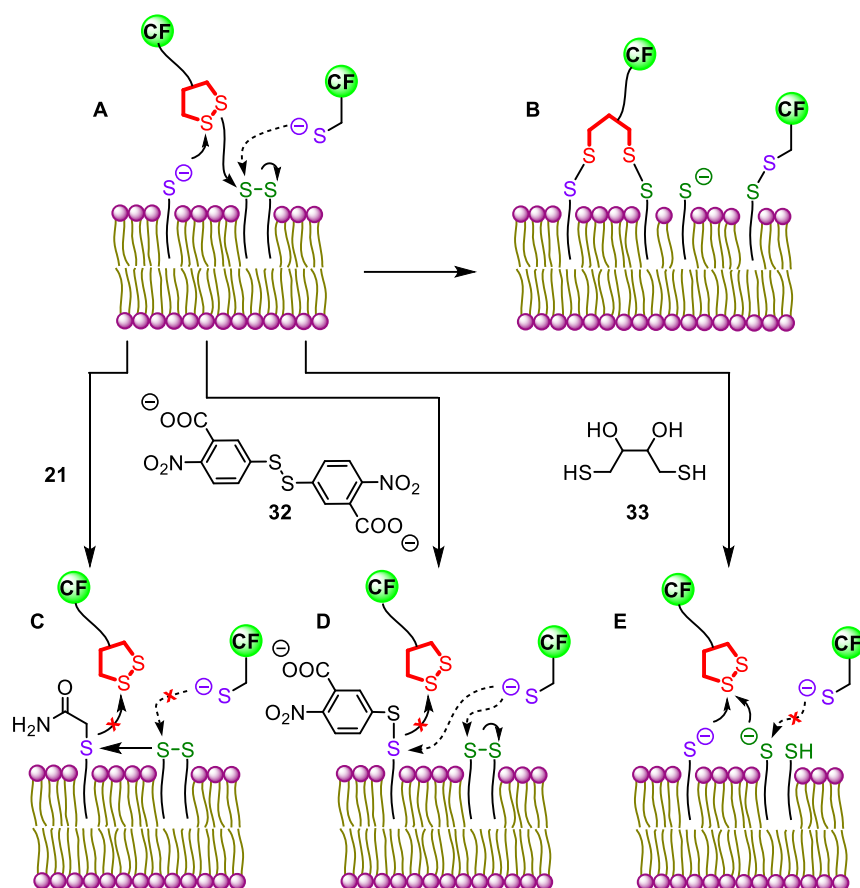


Figure 23. Thiol-disulfide exchange on the surface of (A) untreated cells with the corresponding anchored product (B), (C) cells pretreated with iodoacetamide **21**, (D) cells pretreated with DTNB **32** (Ellman reagent) or (E) cells pretreated with DTT **33**. Image adapted from reference.^[74]

bilayer, while the incubation with the fluorophore **31** alone showed negligible uptake.

The flow cytometry analysis gave the first evidence that thiol-mediated uptake occurs in which the disulfide on the transporter is attacked by thiol on the cell surface, but also the reverse is possible when thiolated substrate attacks

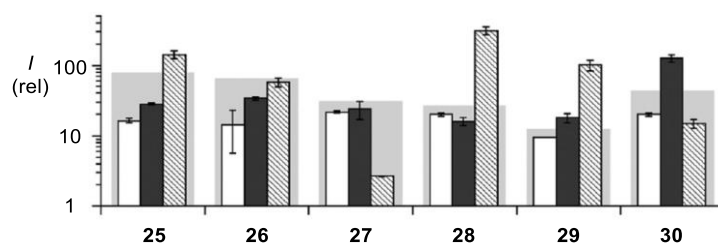


Figure 24. Flow cytometry data of HeLa Kyoto cells incubated with probes **25** – **30** after preincubation with **21** (blank bars), **32** (black bars) or **33** (hatched bars) compared to untreated cells (background grey bars). Image from reference.^[74]

disulfide present on the cell surface (Figure 23A to B) corroborating the results and scheme proposed by Torres and Gait.^[71-72] In order to further developed this theory, we decided to reduce the amount of free thiols on the cell surface by preincubation with iodoacetamide **21** (Figure 23C) or DTNB **32** (Figure 23D), or increase them using DTT **33** (Figure 23E).

The inhibition of exofacial thiol showed as expected a decreased in the cellular uptake for all the disulfide transporters but surprisingly also for the thiolated probe **30**, when the cells were preincubated with **21** (Figure 24, blank bars). We postulated that this is due to a rapid reduction of disulfides to thiols on the cell surface by the presence of control enzymes such as protein disulfide isomerases (Figure 23C), which would react instantly with **21** and blocked. The inhibition by **32** (Figure 24, black bars) showed a reduction of uptake for the disulfide containing probes particularly for those with ring tension and at the same time increased the uptake of thiol-containing **30**. This results was expected for overall the amount of reactive disulfide on the cell surface was increased (Figure 23D) even, if as postulated above, protein disulfide isomerase reduces part of the disulfide on the cell surface, they react with **32** to lead in reactive disulfides. Finally the reduction of disulfide on the cell membrane by **33** (Figure 24, hatched bars) demonstrated an increase in cellular uptake

particularly for linear disulfide **28** and **29** while it had nearly no effect on **25** probably because the initial uptake is already close to optimal. The uptake of **30** was reduced in this condition confirming the reduction of surface disulfide as proposed in Figure 23E.

Using confocal microscopy and colocalization dyes, we determined that the final localization in cells are in endosomes, demonstrating that the thiol-mediated uptake lead to an anchor of the transporter to cell membrane proteins before internalization of probably the whole complex by endocytosis. However the presence of positive charges as in CPDs, are essential to escape the endosomal pathway and get cytoplasmic release.

Encouraged by those results we decided to test the ability of small strained cyclic disulfide to deliver larger substrates than fluorophore, and turned toward small peptides in collaboration with the Adibekian group of the university of Geneva.^[81] Asparagusic acid was used as the best transporter identified so far and linked to the amine of lysine on peptides by reacting with the activated NHS ester asparagusic acid (AspA tag). Confocal images of HeLa Kyoto cells showed an increase of uptake of the peptide when the AspA tag was attached (**34**) with a release into the cytoplasm within 2 hours of incubation while the peptide without the tag (**35**) did not enter into cells for the same incubation time (Figure 25). Similarly, the proapoptotic BH3 peptides was delivered into different cell types and demonstrated activity by decreasing cell viability with increasing incubation concentration.

Proteomics studies were conducted to determine the proteins that react with the asparagusic acid and that are, by extension, involved in the thiol-mediated uptake. Among the different hits, one was particularly interesting: the transferrin receptor protein 1 (TFRC). It is a well-studied and abundant membrane protein^[82] that can bind transferrin when Fe is bond to it, before to get endocytosed by clathrin-mediated endocytosis. In early endosomes, the

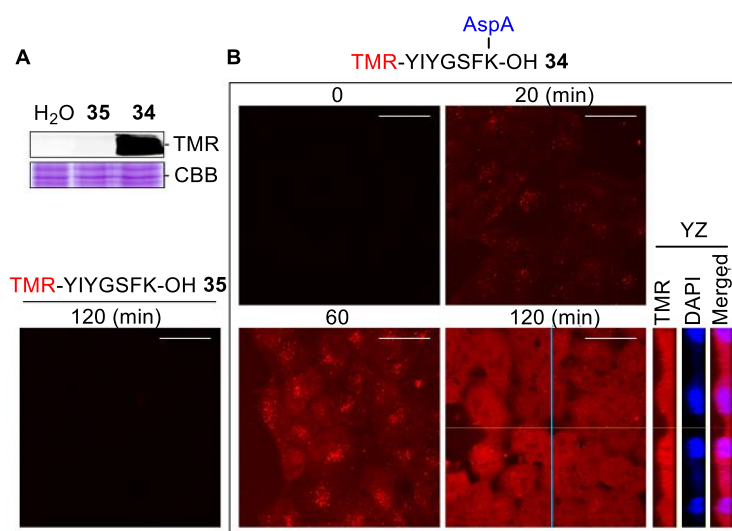


Figure 25. Cellular uptake of peptide **34** and **35**. (A) Fluorescent SDS-PAGE gel image showing the cellular uptake of **34** and **35** containing a fluorophore (TMR). (B) Confocal images of time dependence incubation in HeLa Kyoto cells of **34** and **35** with YZ projection and merged images with DAPI. Scale bar: 30 μm. Images from reference.^[81]

transferrin is released from the receptor due to the decrease in the pH and the receptor itself is recycled to the plasma membrane while the Fe is released into the cell.

By mutation in the TRFC the cysteine residues responsible for the thiol-mediated uptake were identified: C556 and C558. Interestingly those cysteines are not located into the transferrin-binding pocket explaining poor inhibition by competition with transferrin, and appear as thiol in the monomeric form of the receptor. Mutation of those two cysteines at the same time to serines was needed to decrease the uptake of the asparagusic acid probe.^[81]

Pursuing our research for cyclic disulfide with higher ring tension, we directed then our attention on epidithiodiketopiperazine (ETP). It is a naturally produced molecule found for example in lichens and fungi, with a broad variety

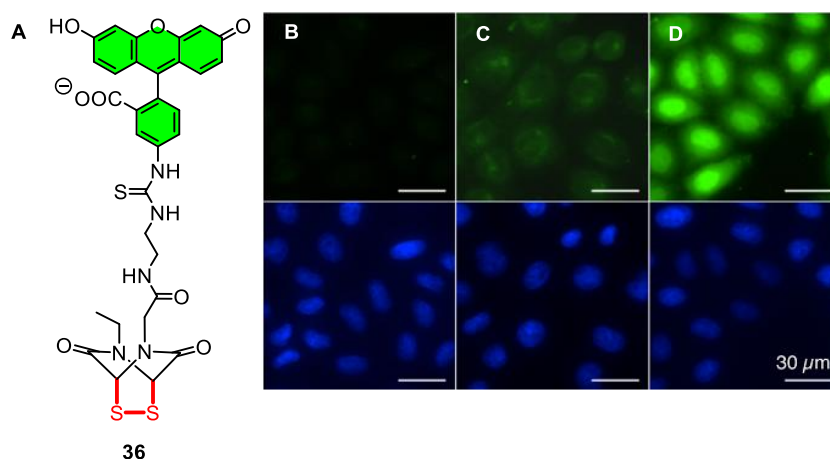


Figure 26. (A) Structure of ETP **36**. CLSM images of HeLa Kyoto cells incubated with **31** (B), **25** (C) and **36** (D). Top: CF channel, bottom: nuclei stained with Hoechst 33342. Images from reference.^[83]

of functions, mode of action and biosynthesis.^[84] According to the reported crystals structures,^[85-86] the CSSC dihedral angle is close to 0° which makes ETP a potential strained cyclic disulfide transporter with the highest ring tension possible.

We managed to synthesize the ETP derivative **36** (Figure 26A) with a CF fluorophore analogue to molecules **25** – **28** presented above and tested its cellular uptake in HeLa Kyoto cells, comparing it to asparagusic acid **25** and control **31**.^[83] As previously demonstrated, **31** did not enter into cell (Figure 26B) while **25** enter into cell but stay mainly trapped into endosomes (Figure 26C). ETP **36** was surprisingly active, escaping the endosomal pathway and accumulating into the nucleus (Figure 26D). Flow cytometry analysis demonstrated that the uptake of **36** is about 4 times higher than **25**. Further analysis demonstrated that **25** and **36** are not cytotoxic to the cell and that common endocytosis inhibitors are inactive in decreasing cellular activity with the exception of 4 °C experiments which indicated that active transport is needed for an efficient uptake. Modifications of surface thiols had only small

influence on the uptake except for DTNB **32** which was decreased down to 60% of the initial uptake pointing toward a thiol-mediated uptake.

Recently, the group of Wu started to take interest also in the thiol-mediated uptake and in the quantification of thiols on the cell surface using thioether-bonded fluorescent probes.^[87] They used thioether exchange to introduce directionality in the exchange compared to thiol-disulfide exchange (Figure 27). There is indeed only one possible product that result from the reaction of thiol with thioether (Figure 27A) while there are two possible products with asymmetric disulfide (Figure 27B). They were able to demonstrate the importance of both exofacial thiols and GSH export for reaction with their transporters.

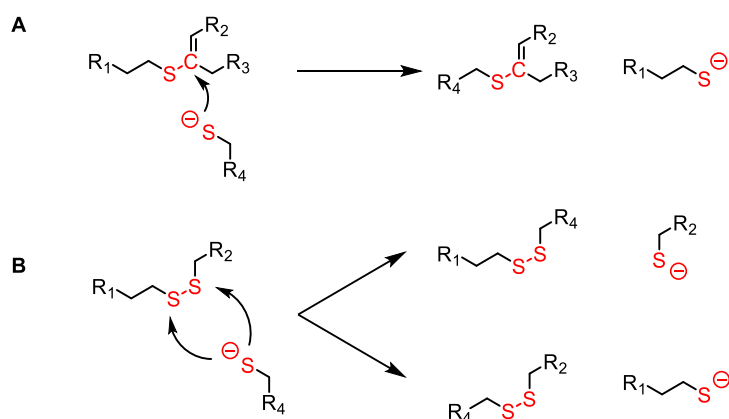


Figure 27. (A) Directed thiol attack on thioether leading in a single product. (B) Thiol-disulfide exchange with asymmetric disulfide leading in two different products. Image adapted from reference.^[87]

In a later report,^[88] they oxidized biscysteine-bearing peptide probe, studying the effect of the addition of amino acids in between the cysteines on the cellular uptake. The best motif they identified was a CXC meaning one amino acid spacing in between the two cysteine units. Once again, they showed the importance of the GSH export for the interaction of with the transporter.

1.4. Selenium in Cellular Uptake

Having discussed how disulfide and more specifically CPDs can be used in drug delivery system and pushing to the extreme the thiol-mediated uptake of strained cyclic disulfide with ETP scaffold, we wanted to investigate the possibility of using other elements from the chalcogen family for transport. Naturally we turned first to selenium as the next atom in the chalcogen column of the periodic table.

The human genome contains 25 genes encoding for selenoproteins^[89] where the selenium is taking the place of the sulfur atom in selenocysteine or selenomethionine amino acids. Those proteins are used mainly as oxidoreductase such as in glutathione peroxidases,^[90] thioredoxin reductases^[91] or deiodinase enzymes^[92] necessary in the thyroid cycle. Interestingly, 8 out of those 25 selenoproteins are located at the plasma membrane and therefore can be involved in a potential selenol-mediated uptake.^[93] Essential as trace element, concentration of selenium has to be carefully monitored because of its cytotoxicity at high concentration.^[94] Therefore only few examples are reported in the literature that used selenium in transporter and even less to use diselenide bonds.

1.4.1. Diselenide in Cellular Uptake

Many studies have been performed on the effect of diselenide compounds on cell or organism, the main one being the diphenyl diselenide^[95] and its derivatives which display cytotoxic effects in cancer cell lines and affect the nervous central system in different organisms. Particularly virulent in this area are the groups of Nogueira^[96] and Rocha^[97] from the Santa Maria University in Brazil.

However there are few examples where diselenides are used in the transporter to act as a redox sensitive bond to release a substrate into the cell. In

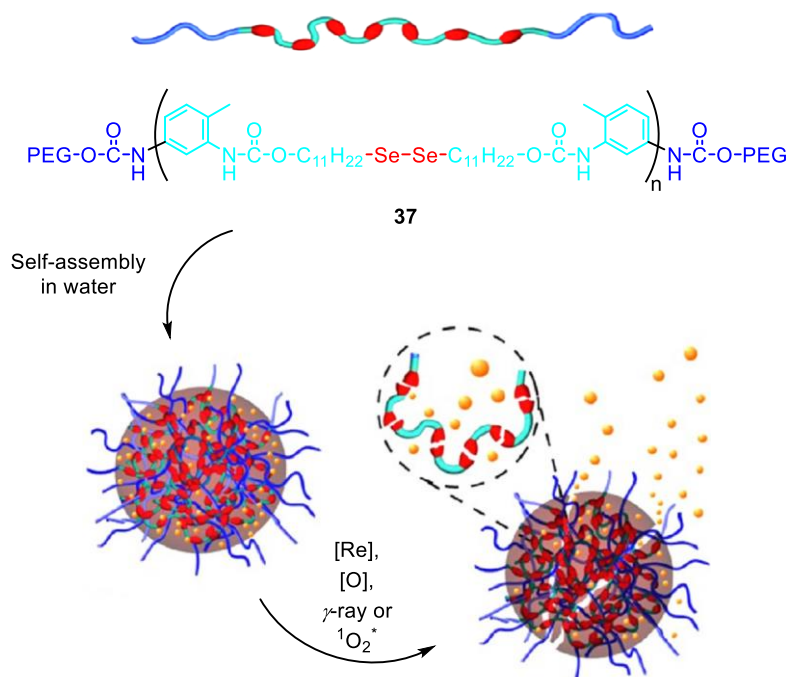


Figure 28. Schematic representation of diselenide-containing polymer **37** that forms micelles in water and can release their cargoes upon a reductive, oxidative, γ -radiation or singlet oxygen trigger. Adapted from reference.^[98]

those cases, the diselenides are incorporated into a polymer through different strategies like reported for the poly(disulfide)s (section 1.3.1, Figure 8). The main drawback for the synthesis of such polymers is the insertion of the diselenide bond which often leads to solubility issue. However the group of Zhang have developed a method in which the diselenide is already present in the monomeric unit with a diol after long alkyl chains to improve solubility in organic solvent.^[99] They were able to build diselenide-containing triblock copolymer **37** using such monomers which could form micelles in water in which a drug such as doxorubicin could be encapsulated (Figure 28). The micelles displayed response to reduction with glutathione by reducing the

diselenide bonds, to oxidation with H₂O₂ where the diselenides are transformed into selenic acids, to γ -radiation,^[100] or to red light irradiation through the generation of singlet oxygen species.^[101] Cytotoxic assays demonstrated that at low concentration such polymers are non-toxic to the cells.

Another example where diselenides were used in polymer to form micelles comes from the Xue group. In their design, a diselenide bond was inserted in the middle of two PEG units to form a copolymer which can form micelles in water.^[102] They were able to demonstrate that the micelles are sensitive to reduction by GSH and can release encapsulated drug when in the cytoplasm of cells.

The group of Park also studied the delivery of micelles containing diselenides in their core with PEG chains.^[103] However in their case they incorporated selenol on the side chain and oxidize by the ambient atmosphere to form crosslinkage between polymeric units leading to the formation of micelles. In their design, they focused on the oxidation of the diselenide to form selenic acid by reactive oxygen species particularly abundant in cancer tissue, to destroy the micelles and release the encapsulated drug.

The group of Jevševar was able to insert a PEG chain on a cysteine of the protein Neulasta (a recombinant human granulocyte colony-stimulating factor used in chemotherapy) by the reaction of the thiol on a diPEGylated diselenide to create a selenylsulfide adduct. The complex increased the *in vitro* biological activity of the protein compared to PEGylation of the cysteine through a reaction with a maleimide or disulfide polymer.^[104]

Hyperbranched polymers containing diselenides were also synthesized with different targets. For example the Smet group used an hyperbranched polymer^[105] while the Shen group used a dendrimer^[106] with a diselenide bond in the core, to mimic efficiently glutathione peroxidase. The group of Yan used hyperbranched polydiselenides as self-delivered polymer able to deliver doxorubicin inducing cytotoxicity into cancer cell lines.^[107]

The group of Gu very elegantly managed to deliver genes into cell by forming a ternary polyplexes composed of a nucleic acid sequence, a diselenide-conjugated oligoethylenimine and a disulfide-modified hyaluronic acid derivative to mimic viral invasion of the cell.^[108] The complex formed particles with a size between 85 nm and 200 nm in diameter depending on the ratio of the different compounds and the disulfide and diselenide polymers demonstrated different reduction kinetics toward GSH, leading to a temporal released of the nucleic acid only when the complex reached the cytoplasm. Transfection with luciferase or a DNA encoding EGFP reporter gene were successfully performed using this complex.

The groups of Qu used mesoporous silica nanoparticles containing Fe₃O₄ nanoparticles as magnetic-targeting core on which they grafted a diselenide-containing polymer as a redox sensitive bond to release the encapsulated doxorubicin.^[109]

Diselenide-rich amphiphilic block copolymer were also used by Xing and coworkers to entrap two different antitumor drugs: doxorubicin and camptothecin.^[110] Visible light was then used to form crosslinked micelles by dynamic exchange of the diselenide bonds. The efficiency of the system to reduce tumor growth was demonstrated in *in vivo* analysis in mice.

In all the examples reported here, the diselenide bond was used as a redox trigger to release a substrate which in most of the case was an apoptotic drug. Therefore the real contribution of the diselenide for the uptake itself was not investigated.

1.4.2. Diselenolane

Following the results obtained with strained cyclic disulfides, we wanted to investigate the diselenide analogues of dithiolanes: the diselenolanes. The five-membered rings analogues to the asparagusic acid **38** and lipoic acid **39**

containing diselenides in them **40**^[111] and **41**^[112] as well as the mixed thiaselenolane **42**^[113] (Figure 29) were already synthesized in the 1960s.

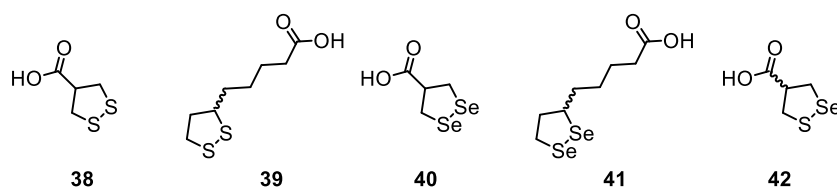


Figure 29. Structures of asparagusic (**38**) and lipoic (**39**) acids, diseleno asparagusic (**40**) and lipoic (**41**) acids, and mixed thio-selenol asparagusic acid (**42**).

However only few experiments were performed on them. Bergson and coworkers mainly focused on the comparison of the absorbance between disulfides, diselenides and mixed thio-seleno derivatives, and between linear and cyclic systems with some interesting differences despite the similar structures (Figure 30).^[114-115]

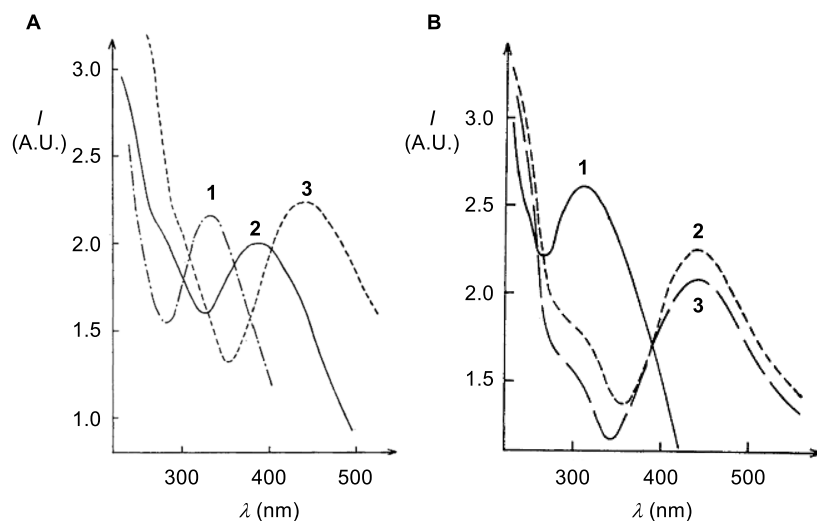


Figure 30. UV absorption spectra of: A) **38** (1), **42** (2), **40** (3). B) diethyldiselenide (1), 4,4-bis-hydroxymethyl-1,2-diselenolane (2), **41** (3).^[114]

There is a red shift going from disulfide to the mixed thio-seleno to the diselenide as shown in Figure 30A. The change from linear to cyclic diselenide resulted also in a red shift of the UV absorption band (Figure 30B), indicating tension in the ring cycle as in dithiolane, which is promising for the delivery of such compounds into cells. The shift from linear to cyclic diselenide is of about 100 nm which is similar to the shift observed between linear to cyclic disulfides.

In another study, Bergson demonstrated that diseleno asparagusic acid **40** cannot be oxidized to the selenoselenates but forms a mixture of the starting material and the corresponding selenic acid when treated with ammonium persulphate in aqueous ethanol.^[115] The selenoselenate could transiently be observed by absorbance, but not purified. In the same conditions, disulfide **38** was oxidized to the thiosulfonate.

More recently, reports showed that diseleno lipoic acid **41** could be used in biological assays. Packer group focused on the antioxidative properties of **39** and **41** on bovine serum albumin (BSA) and apo-B of human low density lipoprotein (LDL) when treated by hydroxyl radical or copper ions.^[116] The results demonstrated that the original lipoic acid **39** is a better scavenger for the hydroxyl radical oxidation compared to **40** with both BSA and LDL despite similar reactivity in the oxidation of salicylic acid as preliminary test. They explained this result by a difference in the partition coefficient of the two probes. Namely **41** prefers organic phase compared to **39**, making the probe buried into the hydrophobic part of BSA or LDL where it cannot prevent against hydroxyl radical. However **41** can prevent peroxidation of lipid alkyl tails of LDL by Cu²⁺.

In another study, Patel group demonstrated the ability of **41** to inhibit pyruvate dehydrogenase complex.^[117] This complex uses a lipoic acid moiety in one of its enzyme to convert pyruvate into acetyl-CoA. The results show that the diseleno lipoic acid is particularly efficient to inhibit the E1 enzyme which

is the pyruvate dehydrogenase while **39** is more efficient on the whole complex and in particular on E2 enzyme which is the dihydrolipoyl transacetylase in which the natural lipoic acid reacts.

Similarly the effect of **41** on the peroxynitrite-dependent inactivation of NADPH-cytochrome P450 reductase was studied by the Khrantsov group.^[118] This enzyme, located in the endoplasmic reticulum, is required to transfer an electron from NADPH to the cytochrome P450. It contains 7 thiols, one or two localized in the NADPH-binding center. It was reported that this enzyme can be irreversibly inhibited by peroxynitrate, but the addition of **41** increased the rate of inactivation probably by the formation of a selenoseleninate intermediate. However this inhibition was reversible by addition of thiols such as DTT or GSH demonstrating interaction between thiols and diselenolane.

More recently, the group of Weigand investigated asparagusic acid derivatives and their complexation with cytotoxic platinum(II).^[119] In this study, the authors report the crystal structures of **40** and **42** (Figure 31).

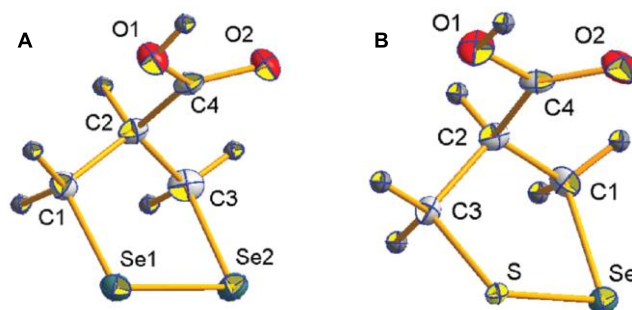


Figure 31. Crystal structures of diseleno **40** (A) and thio-seleno asparagusic acid **42** (B). Images from reference^[119]

The crystal structure of **40** showed that it forms dimer through hydrogen bonding between adjacent carboxylic groups. The CSeSeC dihedral angle is close to 0° (-0.28°) thus the ring can be described as a twist-free envelope structure. The Se–Se bond is of 2.3762 Å which is longer than the S–S in **38**

(2.096 Å)^[75] or the S–Se in **42** with a length of 2.2331 Å. The structure is more twisted in **42** with a CSSeC dihedral angle of -20.4° which stand in between **40** and **38** (27°).

In the same study, they investigated the cytotoxicity of platinum(II) complexes with **38**, **40** and **42** as analogues to cisplatin. Promising results were obtained with all derivatives in two ovarian carcinoma cell lines (SKOV3 and A2780). However no further investigations of the mode of action of those compounds was performed, nor on the effect of the compound without the platinum complexation.

Interestingly a computational study was performed on the nucleophilic substitution of cyclic diselenides by selenol or thiol.^[120] The gas-phase reactions were monitored using MP2/6-31+G(d) and B3LYP/6-31+G-(d). In the case of the attack of thiol or selenol on five- or six-member ring, the reaction proceed in a two steps mechanism: first an intermediate is formed when the nucleophile is bonded to one of selenium atom resulting in an hypercoordinated Se; then the diselenide bond is cleaved releasing a selenol. This addition-elimination mechanism with an hypercoordinated chalcogen was also found in a previous study for their disulfide counterpart.^[121] On the other hand, three- or four-member diselenide rings did not have an intermediate and the reaction goes through a one-step classical S_N2 mechanism in which the nucleophile attack occurs at the same time as the release of the leaving group. In order to explain this reactivity difference, the authors advance a higher tension in smaller ring compared to larger ones, making them more reactive.

This last study was particularly interesting since it demonstrated that, on a computational point of view, dithiolane and diselenolane react similarly toward thiol or selenol. Therefore **40** and **41** derivatives could potentially get uptaken by cell through thiol- or selenol-mediated uptake as for compounds **38** and **39**.

1.5. Vesicles in Cellular Uptake

In the previous sections, the focus was on polymers as delivery agents and how from cell-penetrating peptide, we developed our own cell-penetrating poly(disulfide)s before to focus on the use of small thiol-responsive molecules to extend the knowledge of the thiol-mediated uptake. However as shortly discuss in section 1.1, other transporters could be used to deliver compounds into the cells such as liposomes which will be briefly discussed in this section.

1.5.1. Liposomes Delivery

Discovered in the 1960s by Bangham,^[122] liposomes are spherical shape membrane bilayer constituted of phospholipids encapsulating an aqueous medium. There can be multiple layer of membrane or a single one, and their size can vary greatly from few nanometers to several micrometers. However the standard size for use as drug delivery system lies between 50 nm and 450 nm.^[123] One of their main advantage is that they can be used to deliver both hydrophilic and polar molecules in their aqueous space as well as lipophilic and apolar molecules in the core of their membrane bilayer.^[124] Moreover they display low toxicity, non-immunogenicity and biodegradability which make them powerful tools as therapeutic agents in organisms.^[125]

Different parameters of the liposomes can be tuned in order to obtain better delivery such as the vesicle size and the number of membrane bilayer. If the vesicle has more than one membrane bilayer, it is called multilamellar, while if it has only one it is called unilamellar and can be divided in different categories according to their size: small unilamellar vesicles (SUV) for a size smaller than 100 nm,^[126] or large unilamellar vesicles (LUV) for a size larger than 100 nm.^[127] Recently a new class has emerged: the giant unilamellar vesicles (GUV) corresponding to a size in micrometer range that can be used to study membrane properties under microscope,^[128] however GUVs are not used as delivery systems due to their instability.^[129-130]

Another tunable parameter is the lipid composition of the membrane bilayer. The lipids are natural or synthetic amphiphiles composed of a polar head and usually two hydrophobic alkyl tails. They can be zwitterionic, positively or negatively charged, or neutral depending on the head group. The most used lipids for liposomal formulation are phosphatidylcholine (zwitterionic), phosphatidylglycerol (negatively charged), phosphatidylethanolamine (zwitterionic) or phosphatidylserine (negatively charged). DOTMA and DOTAP are example of positively charged lipids that are widely used in gene delivery because of their electrostatic interactions with negatively charged oligomers such as DNA.^[131]

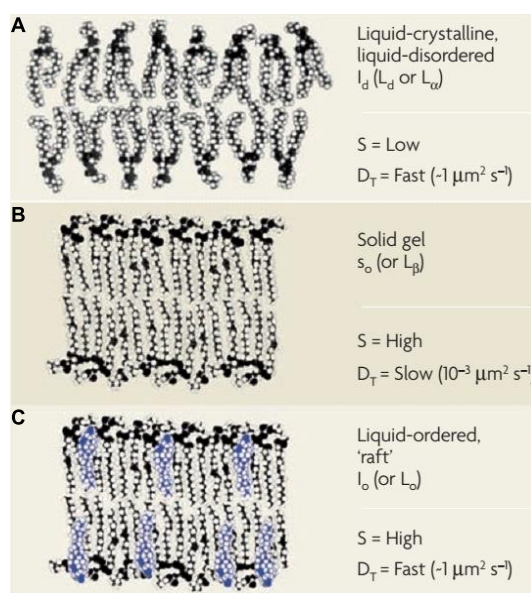


Figure 32. Different membrane phases and properties: (A) liquid-disordered, (B) solid-ordered, (C) liquid-ordered. S: lipid packing, D_T : translational diffusion coefficient. Image from reference.^[132]

The alkyl tail plays an important role in the fluidity and packing of the membrane. They can be fully saturated or contain one or more unsaturations. Depending on the composition and the temperature, the membrane can be in a

solid-ordered phase or in a liquid-disordered phase. A solid-ordered membrane can become liquid-disordered by increasing the temperature above the transition temperature (T_m) in a reversible process. Membranes enriched in unsaturated alkyl tail are usually in liquid-disordered (L_d) phase at room temperature characterized by low lipid packing, fluidic membrane and a fast translation diffusion coefficient (Figure 32A). When fully saturated lipids are used, the membrane will be more likely in a solid-ordered (S_o) phase at room temperature which is characterized by high lipid packing, low fluidity (slow translational diffusion coefficient) and high T_m (Figure 32B).^[132] When cholesterol is added to the membrane, a new phase can be observed with characteristics of both S_o and L_d : the liquid-ordered phase (L_o) (Figure 32C). It has a high lipid packing with a fast translational diffusion coefficient. This is the phase that is believed to constitute the “lipid rafts”.^[133]

In over 50 years of studies, liposomes have become one of the main tool for drug delivery and in order to stabilize the formulation and target specific cells, organelles or proteins, they have been functionalized with PEG tails,^[134] aptamers,^[135] antibody,^[136] proteins,^[137] etc. (Figure 33).^[138]

Interestingly, they are several examples in the literature where the thiol-mediated uptake was used in order to increase the delivery of liposomes inside cells. In all cases, maleimide was used to react with cell surface thiols. In 1995 already Schuber and coworker^[139] used modified dipalmitoylphosphatidylethanolamine (DPPE) lipids on which they introduced a maleimide, a bromide or an activated linear disulfide unit. They were able to demonstrate an increase in the uptake of liposomes when they introduced their modified lipids in 3T3 fibroblast cells and a normal uptake when the liposomes were pretreated with thiols. Unfortunately they did not investigate more the possibility of thiol-mediated uptake of vesicles, but focus more on the attachment of thiolated cargoes or targeting moieties using the maleimide lipid which is now commercially available.

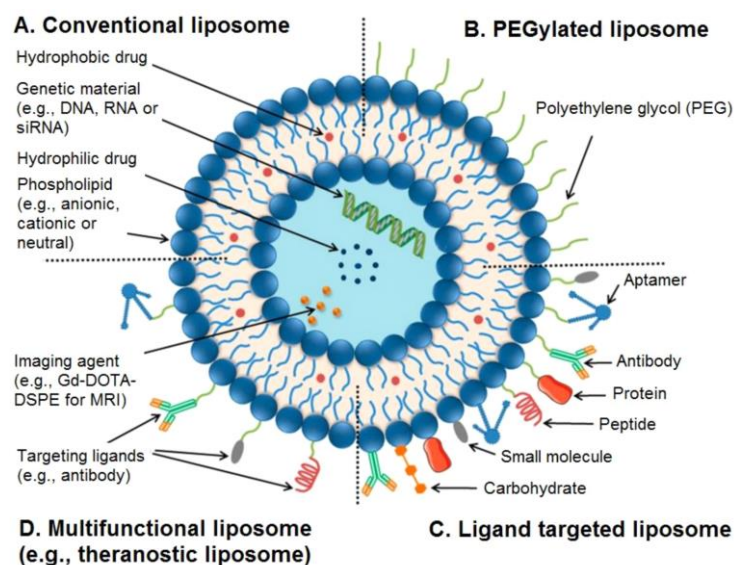


Figure 33. Structure of conventional and functionalized liposomes. (A) Conventional liposomes made from natural phospholipids; (B) PEGylated liposomes; (C) liposomes with a targeting unit; (D) multifunctional liposomes for diagnostic or tumor treatment. Image from reference.^[140]

It is only in 2013 that Li and Takeoka^[141] investigated more the thiol-mediated uptake of liposomes using once again a maleimide unit linked to distearoylphosphoethanolamine (DSPE) using a PEG linker. Their formulation displayed over 2-folds increase compared to liposomes without the maleimide in cellular uptake in HeLa, HCC1954 and MDA-MB-468 cell lines without toxicity (Figure 34A). They could deliver active doxorubicin (an anticancer drug) into those cell lines (Figure 34B) inducing apoptosis, and *in vivo* by intravenous injection in mice.

During their mechanistic investigations to determine the mechanism of entry of the maleimide-containing liposomes enter into cells,^[142] they observed

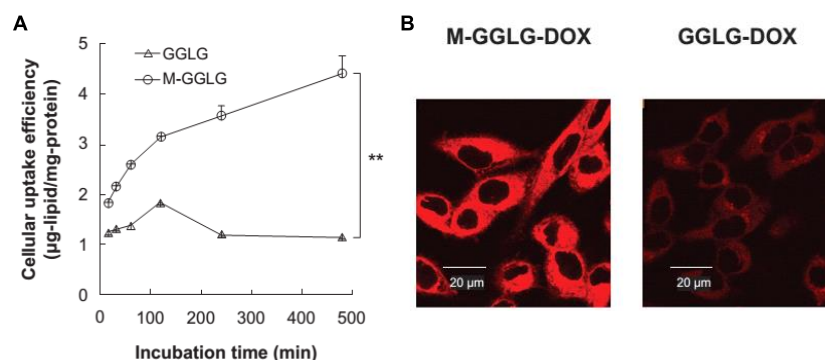


Figure 34. (A) Cellular uptake time dependence in HeLa cells of liposomes with (M-GGLG) or without (GGLG) the maleimide-modified lipid at pH 7.8. (B) Confocal images of HeLa cells incubated for 5 minutes with liposomes containing doxorubicin with (left) and without (right) the maleimide-modified lipid. Images from reference.^[141]

a decrease of 35% – 65% of the uptake at 4 °C depending on the cell line, a 40 – 60% decrease when incubated with serum, a 25% decrease when preincubated with maleimide *N*-ethylmaleimide and nearly no inhibition by common endocytosis inhibitors.

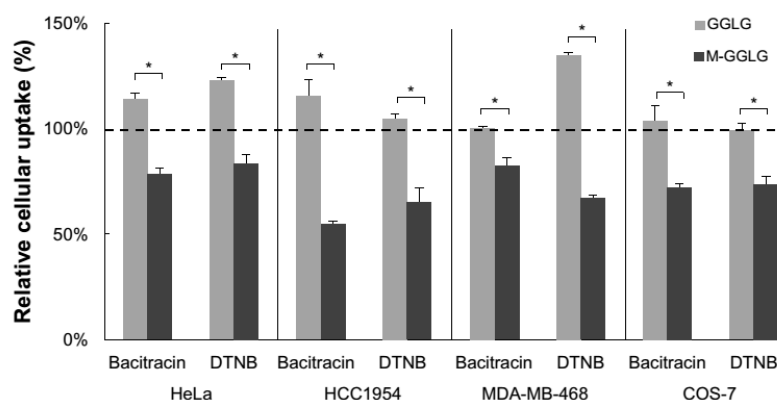


Figure 35. Cellular uptake of liposome with (black) and without (blank) maleimide-modified lipid in HeLa, HCC1954, MDA-MB-468 and COS-7 cells pretreated with Bacitracin and DTNB 32. Image from reference.^[142]

More specifically for the thiol-mediated uptake, preincubation with Bacitracin (a cyclic peptide with debated protein disulfide isomerase inhibitor abilities)^[143-144] or DTNB **32** to reduce or block thiols present on the cell surface, they observed a decrease of only 25% of the uptake of the liposomes containing the maleimide-modified lipid (Figure 35).

With all the evidences provided here, it remained difficult to identify if the maleimide-modified liposomes indeed react exclusively with cell surface thiols or if other membrane components help for the uptake of their liposomes. Moreover they postulated that there is a combination of passive diffusion and energy-dependent endocytosis occurring without more investigations.

1.5.2. Polymerized Vesicles and Polymersomes

In the previous section, liposomes were constituted of natural lipids with small alterations, forming spheres with a membrane bilayer. However modification in the membrane itself has been performed with an increase in the stability of the system as main advantage.

First examples aroused in the early 1980s with polymerized vesicles. Regen and coworkers^[145] introduced a modified lipid with a vinyl group on one of the alkyl tail, that could be polymerized after vesicle formation by radical polymerization keeping their spherical conformation. At the same time Ringsdorf,^[146] Chapman^[147] and O'Brien^[148] groups nearly simultaneously produced evidences of polymerized vesicles from lipids containing diacetylene units that could polymerize upon UV irradiation.

Those early examples of polymerized vesicles opened a new field in the delivery of liposomes with enhanced stability compared to the non-polymerized vesicles, leading to the development of the now called polymersomes. Polymersomes are vesicles composed of amphiphilic block copolymers instead of lipids that can form monolayer or bilayer depending on their assembly. The

Table 2. Common polymer blocks and their abbreviation from reference.^[149]

Abbreviation	Polymer
PAA	Poly(acrylic acid)
PB	Poly(butylene)
PBD	Poly(butadiene)
PBzMA	Poly(benzyl methacrylate)
PCL	Poly(caprolactone)
PDEAEM	Poly(2-(diethylamino)ethyl methacrylate)
PDMAEMA	Poly(2-(dimethylamino)ethyl methacrylate)
PDMIBM	Poly(3,4-dimethyl maleic imido butyl methacrylate)
PDMS	Poly(dimethylsiloxane)
PDPA	Poly(2-(diisopropylamino)-ethyl methacrylate)
PEG	Poly(ethylene glycol)
PEGMA	poly(ethylene glycol)methacrylate
PEO	Poly(ethylene oxide)
PEtOz	Poly(2-ethyl-2-oxazoline)
PFMMA	Poly(ferrocenylmethyl methacrylate)
PGA	Poly(glutamic acid)
PGMA	Poly(glycidyl methacrylate)
PHEMA	Poly(2-hydroxyethyl methacrylate)
PIAT	Poly(L-isocyanoalanine(2-thiophen-3-yl-ethyl)amide)
PLA	Poly(lactic)acid
PMA	Poly(4,5-dimethoxy-2-nitrobenzyl methyl methacrylate acid)
PMAA	Poly(methacrylic acid)
PMCL	Poly(γ -methyl- ϵ -caprolactone)
PMMA	Poly(methyl methacrylate)
PMOXA	Poly(2-methyl oxazoline)
PMPC	Poly(2-methacryloyloxyethyl phosphorylcholine)
PNBA	Poly(4,5-dimethoxy-2-nitrobenzyl methacrylate)
PnBMA	Poly(<i>n</i> -butylmethacrylate)
PNIPAM	Poly(<i>N</i> -isopropylacrylamide)
PNVP	Poly(<i>N</i> -vinyl-pyrrolidone)
PS	Poly(styrene)
PSA	Poly(sulfobetaine methacrylate)
PSBMA	Poly(11-mercaptoundecyl sulfonic acid)
PtBMA	Poly(<i>tert</i> -butyl methacrylate)
PTMC	Poly(trimethylene carbonate)
PVA	Poly(vinyl alcohol)
PVP	Poly(vinylpyridine)

block copolymers have indeed one or more hydrophobic and hydrophilic domains that mimic lipids and can form spherical structure depending on the solvent.^[150] The thickness of the formed membrane can easily be tuned between

3 nm^[151] to 40 nm^[152] by varying the copolymers used and the length of the different domains. In general the formed membrane displays higher stability than conventional lipids bilayer,^[153] making them at the same time less fluid.^[154]

Many different amphiphilic copolymers have been used to mimic membranes, some are summarized in Table 2. The most common hydrophilic copolymers are poly(acrylic acid) (PAA), poly(ethylene oxide) (PEO), poly(ethylene glycol) (PEG) or poly(2-methyl oxazoline) (PMOXA), while the most common hydrophobic copolymers are polystyrene (PS), poly(butadiene) (PB) or poly(dimethylsiloxane) (PDMS).

The surface of the membrane can also be functionalized as for the liposomes (Figure 33), pre- or post-formation of the vesicles, to introduce targeting unit or increase the stability of the whole complex. Examples of functionalization of polymersomes include attachment of polysaccharides,^[155] peptides^[156] or fluorescent probes.^[157]

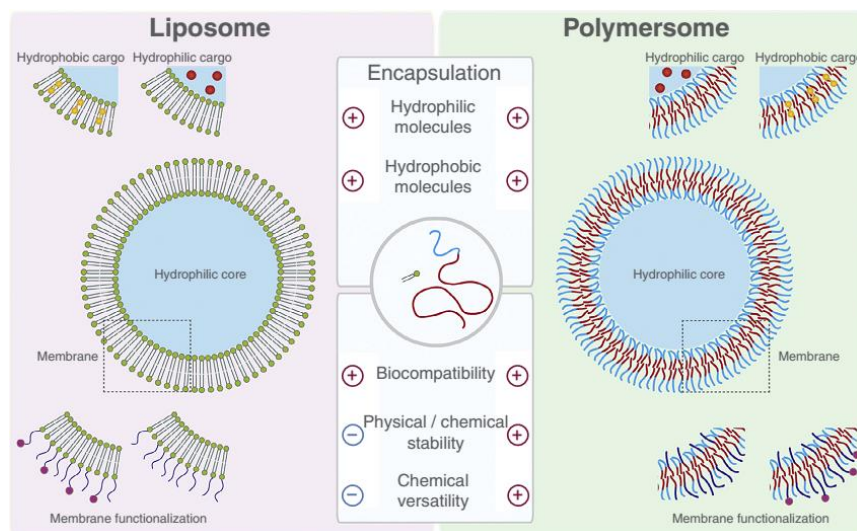


Figure 36. Schematic representation of liposomes and polymersomes with their advantages and disadvantages. Image from reference.^[158]

As for classical liposomes, polymersomes can vary in size from 50 nm to 10 μm depending on the composition of block copolymer and the formation conditions used.^[159] They display however low cytotoxicity and immunogenicity making them powerful for *in vivo* drug delivery.^[160] Both hydrophobic and hydrophilic molecules can be entrapped either in their membrane or internal aqueous compartment respectively (Figure 36).^[161-162]

Several examples of polymersomes containing disulfides can be found in the literature. However the disulfides bond were introduced in the core of the membrane copolymer and relatively shielded to be used in the thiol-mediated uptake. In those cases the disulfide bonds are used as a redox sensitive trigger to destroy the vesicle and release a drug contained in the hydrophilic core of the polymersomes.^[163] The release profile of such systems are usually slow indicating poor accessibility of the disulfide bond to the reductive environment in the cytoplasm.^[164] In order to increase the uptake and induce cell specificity an additional functionalization on the membrane is needed on such polymersomes.

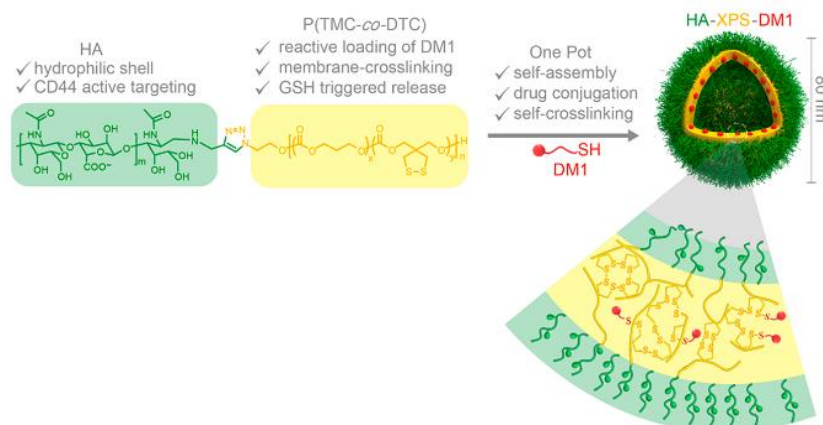


Figure 37. Schematic representation of polymersomes containing disulfide crosslinkage for redox-sensitive drug delivery. Image from reference.^[165]

In one example from the Zhong group,^[165] a derivative of asparagusic acid was introduced in the block copolymer to induce crosslinkage in the membrane core and attach thiolated cargo (Figure 37). The disulfide bonds formed were used as redox sensitive link to destroy the vesicle and release the drug while the cell specificity toward CD44 cells was induced by grafting hyaluronic acid to the membrane.

Chapter 2

OBJECTIVES

This thesis is centered on three different projects which have in common the delivery of substrates into cells.

The first goal will continue to explore the potency of the thiol-mediated uptake. After demonstrating the ability of asparagusic acid to deliver peptides in cells, we decided to investigate the delivery of liposomes and polymersomes. Therefore the synthesis of small amphiphiles containing a thiol-responsive head, a positive charge and an alkyl tail, will be presented. The effects of those compounds upon addition to preformed vesicles will be studied. The delivery of fluorescent probe encapsulated in the aqueous core of the vesicles into cells will be quantified in function of the thiol-responsive unit, the alkyl tail used and the vesicles properties to observe the best cellular uptake. The final localization of the probe in cells and the uptake mechanism will be presented.

In the second part, the delivery of fluorescent probes using small diselenide activators instead of disulfide will be introduced since the strained cyclic disulfide delivery systems have reached its full extend with the introduction of ETP. The reactivity of diselenolane toward thiols will be investigated. The incubation time and concentration dependences of the cellular uptake, the cytotoxicity and the entry mechanistic will be investigated for fluorescent diselenolane.

In the final project, a new type of activator for the uptake of polyarginine will be introduced. Screening of different alkyl tail attached to anionic polarized π -surface for ion-pairing and stabilization, and their efficiency in activation of polyarginine in model membrane and cells will be discussed.

In parallel, activation of polyarginine using perfluorinated fatty acid in model membrane and in cells, will be introduced. The importance of the fluorides adjacent to the carboxylic group will be investigated to determine the factors influencing the activation of polyarginine for those compounds.

Chapter 3

RESULTS AND DISCUSSION

3.1. Thiol-Mediated Uptake of Vesicles

Having demonstrated in the Matile group that it is possible to deliver small fluorophores^[74] or peptides^[81] into cells by thiol-mediated uptake using strained cyclic disulfides, we next focused our attention on the uptake of giant substrates which could be of great importance for biological purposes: liposomes and polymersomes.

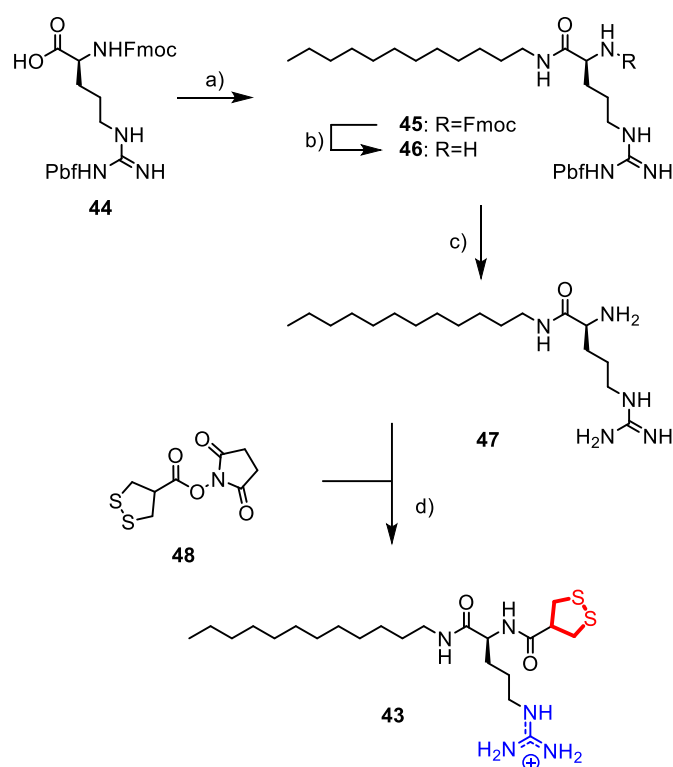
3.1.1. Design

In order to deliver liposomes and polymersomes, amphiphilic molecules were designed with three distinct parts: a hydrophobic alkyl tail in order to insert the compound into the vesicle membrane, a thiol responsive head to have a covalent anchor on the cell surface by thiol-disulfide exchange with exofacial thiols, and an arginine linker between the tail and the head. This linker has different functions: it ensures that the amphiphile remains at the surface of the vesicle membrane because of its hydrophilicity and by electrostatic repulsion with the choline head of the lipid used to form the liposomes; it keeps the thiol-responsive head at the surface of the membrane in order to interact with exofacial thiols; and the positive charge from the guanidinium cation of the arginine could help with uptake of the whole complex by conferring a counterion-mediated uptake to the system.

3.1.2. Thiol-Responsive Head Screening

3.1.2.1. Synthesis

The first alkyl tail chosen was a dodecyl chain which was shown to be one of the best for insertion into membranes in previous screening performed for the activation of CPPs (see section 3.3).^[166] Therefore, in order to obtain the best uptake in cells, we focused our attention on the screening of the thiol-responsive head.

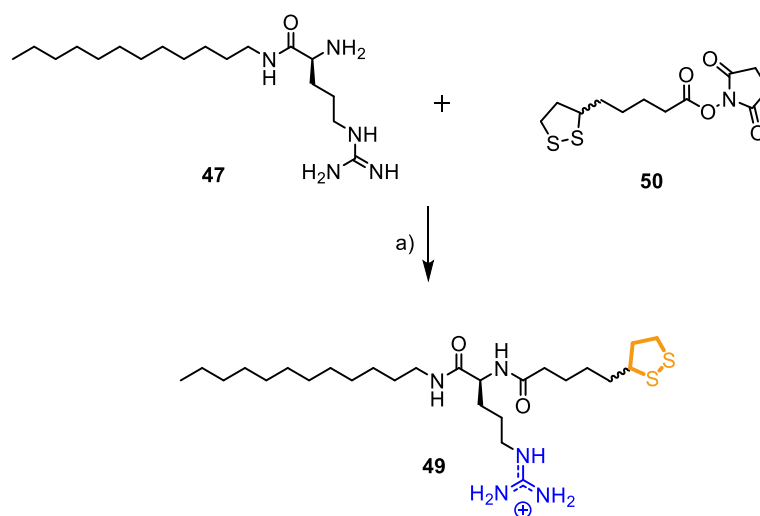


Scheme 1 a) DA, HATU, TEA, DMF, 4 h, 0 °C → rt, 78%; b) DBU, CH₂Cl₂, 3 h, rt, 94%; c) TFA, CHCl₃, 2 h, rt, 87%; d) TEA, CH₂Cl₂, DMF, 3 h, rt, 32%.

The first amphiphile synthesized contained an asparagusic acid as head derivative (**43**), which was the best performing strained cyclic disulfide

discovered from previous studies^[74] when we started this project. The synthesis of this compound is reported in Scheme 1.

In a first step, dodecylamine (DA), used as the hydrophobic alkyl tail, was connected to the C-terminus of the commercially available protected arginine **44** by peptide coupling using HATU as coupling reagent in basic conditions. Arginine **45** was then treated with 1,8-diazabiscyclo[5.4.0]undec-7-ene (DBU) to remove the fluorenylmethyloxycarbonyl (Fmoc) protecting group to give **46**, and subsequent treatment with trifluoroacetic acid (TFA) to remove the 2,2,4,6,7-pentamethyl-dihydrobensofuran-5-sulfonyl (Pbf) protecting group. The obtained dodecyl arginine **47** was then reacted with the *N*-hydroxysuccinimide (NHS) activated asparagusic acid **48** prepared according to previously published procedures,^[167–170] in basic conditions to give **43**.

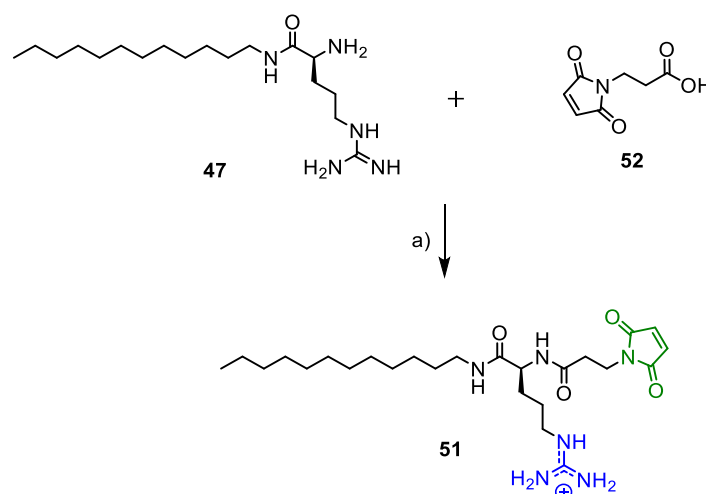


Scheme 2. a) TEA, CH₂Cl₂, DMF, 4 h, rt, 48%.

In order to compare the effect of ring tension on the uptake of vesicles, the lipoic acid derivative **49** was also synthesized, since it represented the second best performing strained cyclic disulfide identified so far from previous studies,^[74] following the procedure reported in Scheme 2.

The synthesis was straight-forward by reacting arginine **47** with the NHS activated lipoic acid **50** prepared according to previously published procedure,^[58] in basic condition to give **49**.

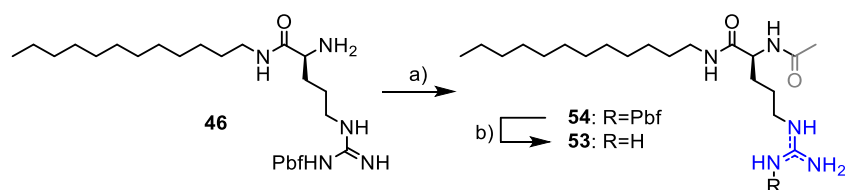
Since reports from Li and Takeoka^[141-142] showed that lipids containing maleimide residue were effective for the delivery of liposomes by thiol-mediated uptake, the maleimide derivative **51** was also synthesized following the procedure reported in Scheme 3.



Scheme 3. a) HBTU, TEA, DMF, CH₂Cl₂, 5 h, 0 °C → rt, 36%.

In this case the commercially available 3-(maleimido)propanoic acid **52** was coupled to the arginine **47** by peptide coupling using HBTU as coupling reagent in basic conditions to give **51**.

Finally, in order to evaluate the importance of the thiol-mediated uptake over the counterion-mediated uptake, we designed a control compound that was unable to interact with exofacial thiols, by simply acetylating the N-terminus of the arginine, and thus keeping the positive charge (**53**) as shown in Scheme 4.



Scheme 4. a) acetyl chloride, TEA, CH₂Cl₂, 2 h, rt, 94%; b) TFA, CHCl₃, 3.5 h, rt, 35%.

The acetylation with commercially available acetyl chloride was performed on the guanidinium-protected arginine **46** to avoid potential side reaction with in basic conditions. The fmoc protecting group on arginine **54** was then removed by treatment with TFA to yield compound **53**.

3.1.2.2. Flow Cytometry Assay

The different thiol-responsive heads were tested on 1,2-distearoyl-*sn*-glycero-3-phosphatidylcholine (DSPC) and 1,2-distearoyl-*sn*-glycero-3-phosphoethanolamine-N-[amino(polyethylene glycol)-2000] (DSPE-PEG₂₀₀₀) (95:5) 200 nm diameter liposomes, in which sulforhodamine (SRB, 30 mM) was entrapped. Size and composition of the vesicle were chosen since the Leblond group demonstrated that those liposomes were uptaken by cells through endocytosis, followed by subsequent release of the encapsulated probe by conformational change of a pH-sensitive lipid.^[171] The entrapped dye was also chosen according to their protocol. At this concentration, the fluorescence is slightly self-quenched as can be demonstrate by fluorescence recovery upon addition of Triton X-100 to destroy the liposomes.

The different probes were added to the preformed vesicles and incorporation into the liposome membrane was ensured by overnight incubation at 4 °C. The addition of the probes to the vesicles did not affect their stability demonstrated by no change in the fluorescence of the entrapped dye in the vesicle lumen. The vesicle solution was diluted in Leibovitz's medium shortly before addition to HeLa Kyoto cells, and subsequently incubated for 4 h at 37

°C as was reported in Leblond's procedure.^[171] Cellular uptake was quantified by flow cytometry at concentrations of 0 – 10 mol% of transporter compared to the amount of lipids in the vesicle solution, except for probe **43**, which was tested from 0 – 7.5 mol%, since at 10 mol% concentration, cytotoxicity was observed. The results obtained were normalized against the liposome uptake in absence of amphiphile.

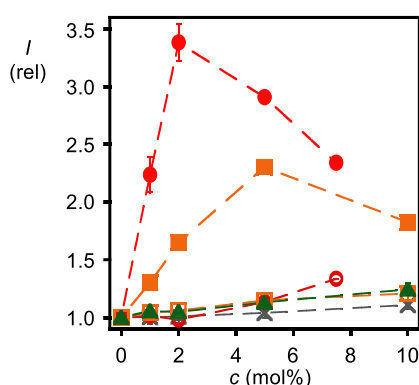


Figure 38. Dependence of liposome uptake efficiency on the concentration of amphiphile **43** (●, ○), **49** (■, □), **51** (▲) and **53** (×) without (●, ■, ▲, ×) and with (○, □) preincubation with DTNB (1.2 mM, 30 min). Data (average ± standard deviation from three experiments) are normalized against those obtained with liposomes in absence of transporter.

The asparagusic acid transporter **43** (Figure 38, ●) performed best with an increase in liposome uptake close to 3.5 times compared to the initial uptake of liposome without transporter. The bell shape curve observed is probably due to an increased incorporation of the amphiphile in the vesicle membrane up to a concentration where it starts forming micelles. If this is the case, the amount of compound **43** available for membrane insertion is reduced, leading to the observed decrease in uptake. The formation of micelles could also lead to the destruction of part of the liposome population, decreasing the amount available for uptake, and could also explain some cellular toxicity observed at high

concentration. Attempts to remove the excess of transporter by a Sephadex G-10 column were unsuccessful.

The lipoic acid derivative **49** showed also an increase in the uptake of liposomes close to 2.5 times compared to the reference at 5 mol% (Figure 38, ■). The difference of uptake between **43** and **49** is most likely due to the difference in the ring tension between the two transporters, as expected from previous studies.^[74] This difference in reactivity could also explain the higher concentration needed of transporter **49** to reach the maximum uptake along with a probable higher critical micellar concentration (CMC) compared to transporter **43**.

The addition of the acetylated probe **53** did not increase the uptake of the liposomes (Figure 38, ✕), demonstrating the importance of a thiol-responsive part on the head. This is an evidence that the vesicles are uptaken by cells through the thiol-mediated uptake and that the presence of a positive charge alone on the transporter is insufficient for the delivery of the substrate. With this specific result in hand, we decided that it was not necessary to investigate the replacement of the arginine and its positive charge since it is the thiol-reactive unit that is responsible for the uptake.

Further evidence that the liposomes are uptaken through the thiol-mediated uptake, came from experiments where cellular surface thiols were oxidized by DTNB **32** as reported in the literature.^[74] Preincubation of the cells with the Ellman reagent will block thiols on the cell surface by thiol-disulfide exchange with the activated disulfide making them unavailable for potential thiol-mediated uptake (Figure 23D). When cells were pretreated with **32** (1.2 mM) for 30 minutes, uptake of liposomes was shut down for transporters **43** and **49** (Figure 38, ○ and □ respectively) providing the involvement of thiol-mediated uptake for efficient cellular entry of the liposomes with those compounds.

Surprisingly the maleimide derivative **51** showed a response similar to transporter **53**, meaning no increase of the uptake of liposomes (Figure 38, ▲)

despite encouraging previous reports.^[141-142] This results was surprising considering the reactivity of thiols toward maleimide. It demonstrates however the power of a strained cyclic disulfide for the thiol-mediated uptake of liposomes.

3.1.2.3. Confocal Laser Scanning Microscopy

Having shown by flow cytometry that it was possible to increase the uptake of fluorescent liposomes upon addition of different transporters, we were interested where the vesicles would localized in the cell and to confirm qualitatively the results obtained by flow cytometry. Therefore confocal laser scanning microscopy (CLSM) was used to determine the fluorescence distribution inside the cell. The incubation was performed in the same conditions as for flow cytometry, namely incubation in Leibovitz's medium for 4 h at 37 °C. After washing with PBS, the cells were kept in Leibovitz's medium and the fluorescence distribution was analyzed without fixing the cells at 37 °C.

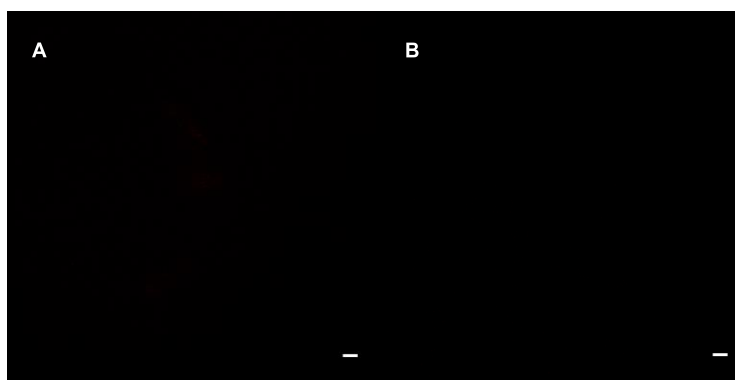


Figure 39. CLSM images of HeLa Kyoto cells alone (A) and after incubation with fluorescent liposomes without transporter (B). Scale bar: 10 μ m.

The first test performed were controls using the following setup on the microscope to observe the encapsulated SRB dye: $\lambda_{\text{ex}} = 514$ nm, $\lambda_{\text{em}} = 565 - 620$ nm and laser power (LP) = 4%. Even though SRB emits light in the red,

the color was artificially changed to green for better contrast with the remaining black picture unless stated otherwise.

As expected, the cells alone showed no fluorescence (Figure 39A) in the setup used. When the cells were incubated with the liposomes solution in the absence of transporter for 4 h, negligible uptake was observed (Figure 39B). Those observations are in agreement with flow cytometric data where the fluorescent response was low in those cases. Those two controls were encouraging since the difference in fluorescence distribution should be easily

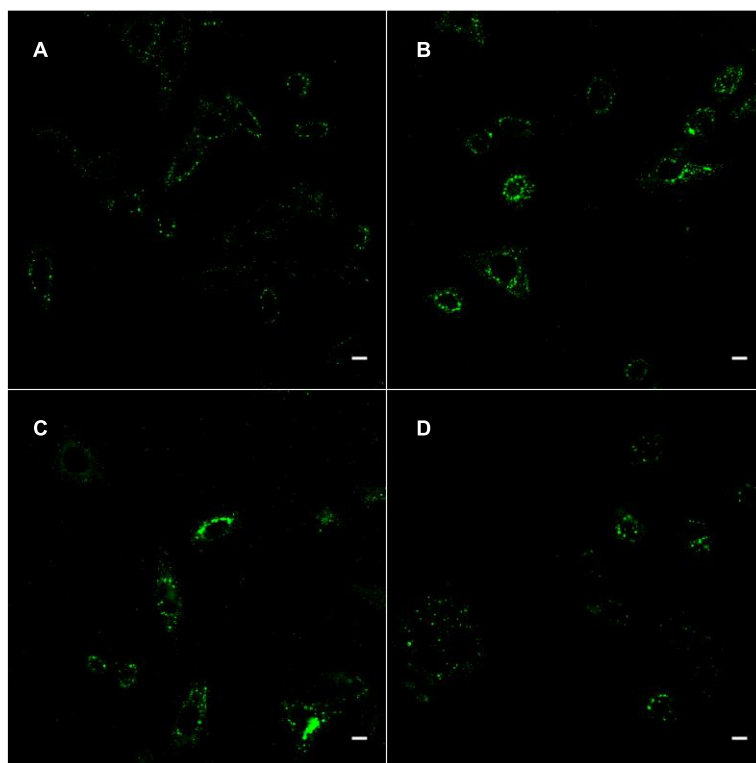


Figure 40. CLSM images of HeLa Kyoto cells after incubation with fluorescent liposomes containing transporter **43** at 1 (A), 2 (B), 5 (C) and 7.5 (D) mol%. Scale bar: 10 μ m.

observable upon addition of the transporter, if the liposomes are uptaken by cells.

Using the same setup, the distribution of fluorescence was determined for transporter **43** at concentrations from 1 – 7.5 mol%. As shown in Figure 40, the addition of transporter **43** to liposomes increased their uptake. Increasing the concentration of the amphiphile from 1 to 2 mol% (Figure 40A and B respectively) lead to a better uptake of the liposomes. The difference between 2 and 5 mol% (Figure 40C) was not evident from the CLSM images and was in

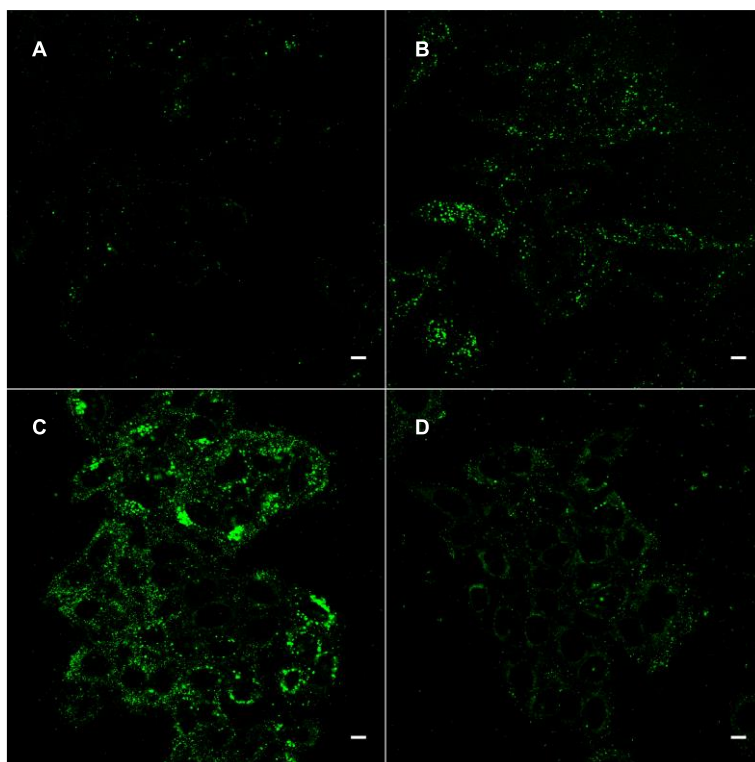


Figure 41. CLSM images of HeLa Kyoto cells after incubation with fluorescent liposomes containing transporter **49** at 1 (A), 2 (B), 5 (C) and 10 (D) mol%. Scale bar: 10 μ m.

accordance with the flow cytometric data where 2 mol% was slightly better than 5 mol% (3.5 compared to 3 respectively, relative to the liposome uptake in absence of transporters. Figure 38, ●). The uptake at 7.5 mol% (Figure 40D) was clearly reduced compared to 2 or 5 mol%, corroborating the bell shape curve observed from flow cytometry data (Figure 38, ●).

CLSM images demonstrated also an increase of uptake with increasing the concentration of transporter **49** (Figure 41), with a maximum at 5 mol% (Figure 41C), while at 10 mol% the fluorescence was attenuated (Figure 41D). Once again this result was in excellent agreement with the data obtained from the flow cytometry measurements (Figure 38, ■).

For both transporters **43** and **49**, the fluorescence is mainly in punctate localization and not diffuse through the cytoplasm as it was the case for the adjunction of pH-sensitive lipid in the study of Leblond.^[171] Colocalization studies were performed to determine the fate of the liposome content (see section 3.1.5).

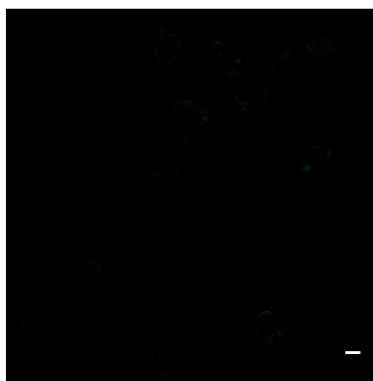


Figure 42. CLSM images of HeLa Kyoto cells after incubation with fluorescent liposomes containing transporter **53** at 5 mol%. Scale bar: 10 μ m.

The flow cytometric data were also in good agreement with the CLSM images for transporter **51** and **53**. In the absence of the thiol responsive unit, there was no increased uptake of liposomes, as shown with transporter **53** in

Figure 42, while **51** with its maleimide head, was indeed less reactive than strained cyclic disulfide, with no visible increase of cellular uptake in CLSM images at different concentrations (Figure 43).

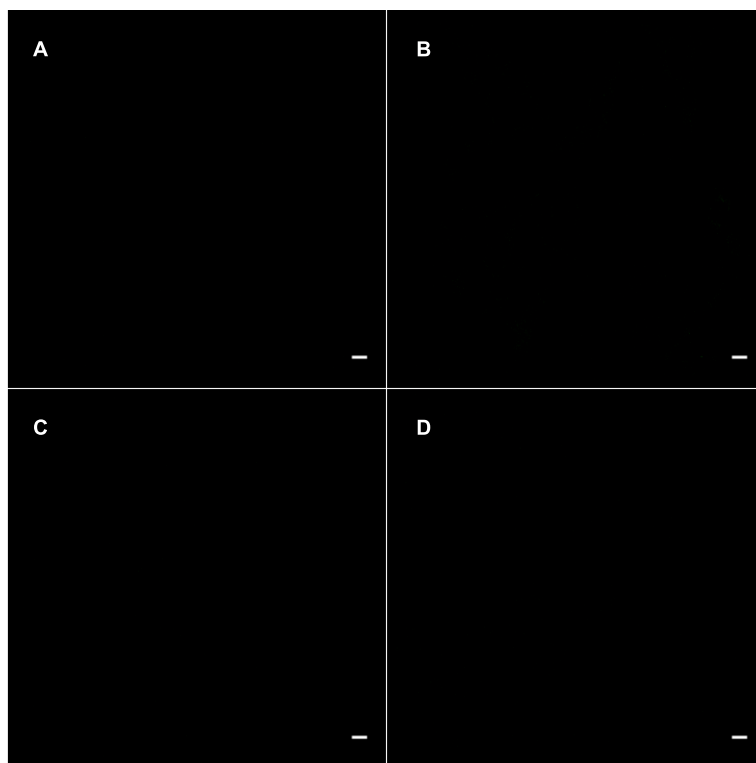


Figure 43. CLSM images of HeLa Kyoto cells after incubation with fluorescent liposomes containing transporter **51** at 1 (A), 2 (B), 5 (C) and 10 (D) mol%. Scale bar: 10 μ m.

Overall the screening of thiol-responsive head demonstrated that the two amphiphiles **43** and **49** were able to increase the uptake of liposomes in the conditions used. The asparagusic acid behaved slightly better than the lipoic acid both in term of maximal uptake and concentration needed to reach it, as expected from a previous study.^[74] Surprisingly the maleimide transporter did not increase the uptake, despite the promising results from Li and

Takeoka.^[141-142] This difference could be due to many aspects such as the different lipid composition to form the liposomes, the position and concentration of the maleimide unit, or the reactivity between strained cyclic disulfide and maleimide toward surface thiols. To continue with the optimization of liposomal uptake, transporter **43** was selected, as the best performing head identified so far.

3.1.3. Liposome Influence on Uptake

Having identified **43** as the best thiol-responsive head for transport, we decided as the next step to investigate the influence of lipid composition and size of the vesicles on cellular uptake.

3.1.3.1. Lipid Composition Screening

For the head screening experiments, liposomes were composed of DSPC/DSPE-PEG₂₀₀₀ (95:5). We decided to test the importance of the PEGylated lipid on the uptake. Therefore LUVs composed of only DSPC were generated. CLSM images showed that such liposomes even in the presence of transporter **43** at 5 mol%, did not enter into cells but remained mainly at the surface of the membrane (Figure 44A) demonstrating the importance of the PEG unit for the uptake of liposomes.

Changing drastically the lipid composition to egg yolk phosphatidylcholine (EYPC) generated instable vesicles, releasing the fluorescent dye from their core in less than a day. Therefore such vesicles were not tested for cellular uptake.

Empty liposomes constituted from brain phosphatidylserine (PS) and 1,2-dipalmitoyl-*sn*-glycero-3-phosphoethanolamine-N-(lissamine rhodamine B sulfonyl) (Rhod-PE) (98:2) with transporter **43** at 5 mol% were also disappointing regarding cellular uptake, leading to aggregation outside of the cell with poor cellular entry (Figure 44B).

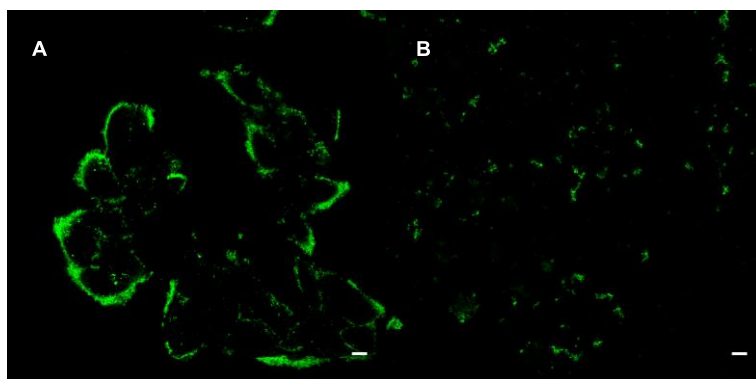


Figure 44. CLSM images of DSPC LUVs (A) and brain PS LUVs (B) in the presence of transporter **43** at 5 mol%. Scale bar: 10 μ m.

Changing the lipid packing of the initial liposomes from solid-ordered to liquid-disordered phase by warming the vesicles to 65 °C (the transition temperature for DSPC vesicles is of 55 °C) did not influence the incorporation of the probe into the liposome membrane as demonstrated no significant increase of uptake of liposomes by flow cytometry.

Therefore the initial membrane composition (DSPC/DSPE-PEG₂₀₀₀ 95:5) was kept for the following experiments.

3.1.3.2. *Size Dependence*

Liposomes of different sizes were easily produced by changing the pore size of the polycarbonate membrane during extrusion (50, 100, 200 and 400 nm). In order to test and compare all the different sizes in the same experimental setup, the dependences of size and concentration of transporter **43** on uptake were studied by automated microscopy, which enabled testing of many different conditions in a single assay. Statistical analysis of liposomes uptake by HeLa Kyoto cells was performed by Dr. Dimitri Moreau from the University of Geneva, following the procedure described in reference.^[172]

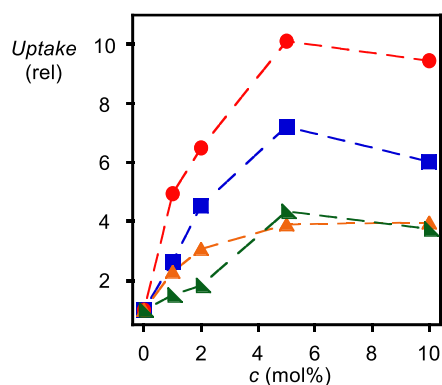


Figure 45. Automated microscopy results for the dependence of uptake efficiency on the concentration of **43** in liposomes with $d = 50$ nm (▲), 100 nm (●), 200 nm (■) and 400 nm (▼).

The normalized uptake of liposomes with a diameter of 50 nm was lower than the uptake with 200 nm (Figure 45, ▲ compared to ■) with a decrease of about 50% at 5 mol% of transporter **43**. This difference is due to a non-negligible uptake of 50 nm liposomes in absence of transporter as shown by the CLSM images (Figure 46A). It was indeed demonstrated that smaller liposomes

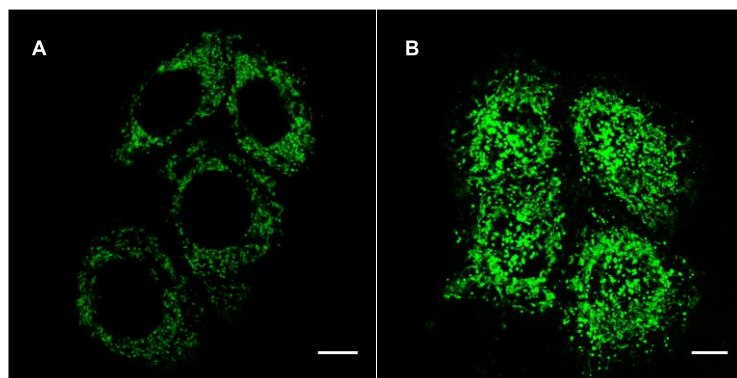


Figure 46. CLSM images of HeLa Kyoto cells after incubation with fluorescent liposomes of 50 nm diameter without (A) and with (B) transporter **43** at 5 mol%. Scale bar: 10 μ m.

are more easily uptaken by cells in the absence of transporter,^[173] probably due to an easier uptake by cells through normal endocytic pathways. Therefore the normalization by the uptake of 50 nm liposomes in absence of transporter lead to a lower response compared to what was expected from the CLSM images in Figure 46B.

On the other hand, a diameter size of 100 nm lead to an increase of uptake of 40% compared to 200 nm diameter at 5 mol% of transporter **43** (Figure 45, ● compared to ■). In this case the initial uptake without addition of transporter was negligible as demonstrated in Figure 47A. The distribution of the fluorescence is similar to the 200 nm vesicles (Figure 40C) when activated with 5 mol% of **43** (Figure 47B).

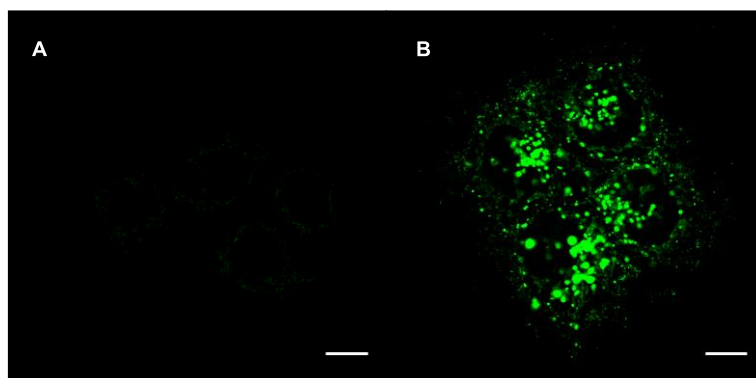


Figure 47. CLSM images of HeLa Kyoto cells after incubation with fluorescent liposomes of 100 nm diameter without (A) and with (B) transporter **43** at 5 mol%. Scale bar: 10 μ m.

Finally, further increasing the diameter to 400 nm lead again to a reduction of the cellular uptake compared to 200 nm (Figure 45, ▲ compared to ■). Once again this reduction is due to a non-negligible uptake of the liposome without transporter (Figure 48A). Considering their size, those vesicles are probably uptaken through a different uptake mechanism compared to the other vesicle

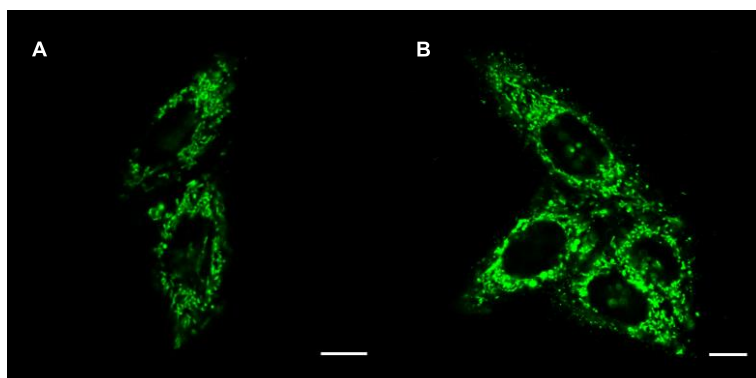


Figure 48. CLSM images of HeLa Kyoto cells after incubation with fluorescent liposomes of 400 nm diameter without (A) and with (B) transporter **43** at 5 mol%. Scale bar: 10 μ m.

sizes, such as macropinocytosis.^[10] Furthermore even upon the addition of compound **43**, the increase of uptake seemed smaller and the final localization of the fluorescence seemed different compared to the other vesicles (Figure 48B).

Considering the results obtained in this section, the final liposomal composition selected for the rest of the study was DSPC/DSPE-PEG₂₀₀₀ (95:5) and a diameter of 100 nm.

3.1.4. Uptake Kinetics

The incubation time used in the experiments so far was fixed at 4 h, according to the procedure described by Leblond.^[171] However, since our system is different, we decided to study the uptake kinetics qualitatively, using CLSM, in order to determine the optimal incubation time. Liposomes of 100 nm diameter were used with transporter **43** at 5 mol%. The cells were kept at 37 °C under the microscope without washing before taking images.

After 30 min incubation, some diffuse fluorescence could be observed at the membrane which accumulate clearly until 1 h, without any detection inside the cells (Figure 49A). After 2.5 h of incubation, some faintly fluorescent dots

could be observed inside the cells but the main localization remained on the membrane (Figure 49B). After 4 h incubation, the fluorescence was distributed between the membrane and inside the cell (Figure 49C). The membrane localization was present since no washing steps were performed before imaging. However, the fluorescence intensity and distribution inside the cells was similar to what was observed previously (Figure 47B). After 6 h incubation, the membrane was not stained anymore and only dotted localization of the fluorescence inside the cells (Figure 49D) could be observed. Some cellular toxicity could already be detected at this time point. The uptake

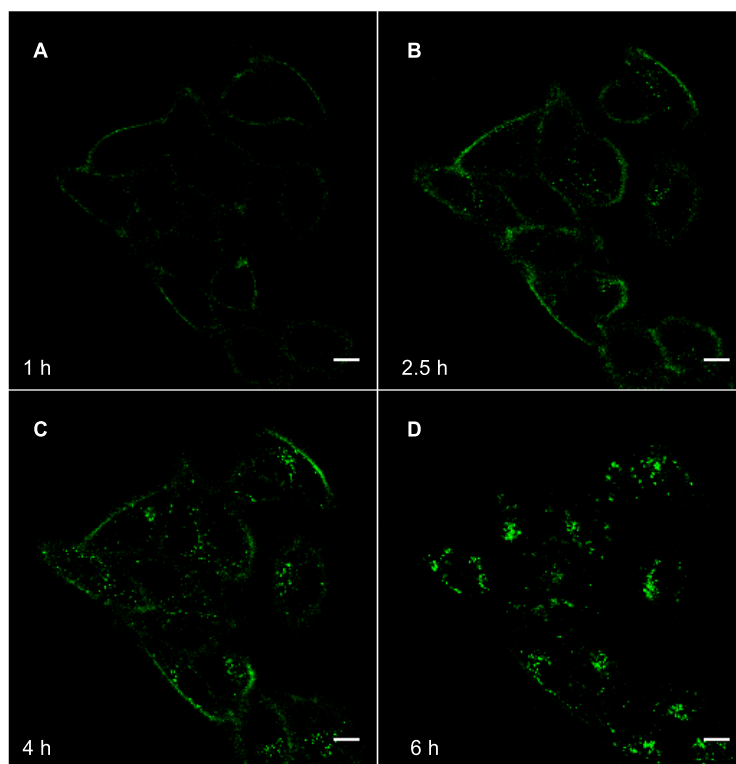


Figure 49. Representative CLSM images of HeLa Kyoto cells after incubation for 1 (A), 2.5 (B), 4 (C) and 6 (D) h with fluorescent liposomes containing transporter **43** at 5 mol%. Scale bar: 10 μ m.

kinetics was monitored until 8 h, however in the conditions used, most of the cells were dead or dying.

Overall this experiment demonstrated that initially the liposomes attach to the cell membrane probably by thiol-disulfide exchange on the surface of the cell membrane, before being slowly uptaken. Even if no quantitative analysis was performed in this case, the maximal uptake should occur around 6 h incubation, at which point no membrane staining could be observed anymore. However, since at this point some cellular toxicity was observed, the 4 h

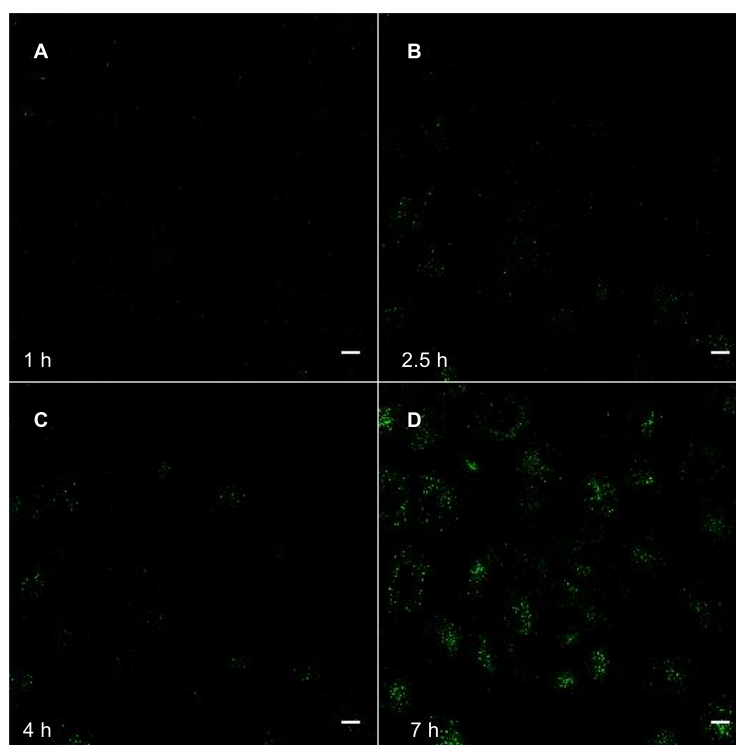


Figure 50. Representative CLSM images of HeLa Kyoto cells after incubation for 1 (A), 2.5 (B), 4 (C) and 7 (D) h with fluorescent liposomes containing transporter **43** at 5 mol% in presence of 10% FBS in the medium. Scale bar: 10 μm .

incubation time was kept for next experiments, as a good compromise between good cellular uptake and low cellular death.

Since previous reports showed that the presence of serum in the incubation medium could decrease^[83] or slow down^[81] the uptake of strained cyclic disulfides, we were interested to study the effect of the presence of 10% fetal bovine serum (FBS) on the uptake kinetics of liposomes.

Compared to the uptake of liposomes in the absence of FBS, there are some significant differences when serum was present in the medium. The first one being that during the 8 h incubation studied, the membrane of the cell was never stained such as in Figure 49 especially significant after 1 and 2 h incubation (Figure 50A and B). After 2.5 h some faint fluorescence could be observed inside the cells. However even after 4 h the uptake efficiency remained clearly lower than in the absence of serum (Figure 50C compared to Figure 49C). In order to have substantial uptake of liposomes, 7 h incubation was needed (Figure 50D). In this case, the cells are less suffering from the long incubation probably due to the lower uptake of the liposomes.

In order to quantify the decrease of uptake in presence of 10% FBS, flow cytometry was measured after 4 h incubation in function of the concentration of transporter **43** in presence or absence of serum. Figure 51 represents the relative uptake of liposomes in the presence of FBS compared to the uptake in its absence. There is already a 10% reduction of liposome uptake in the absence of transporter when incubated in a serum-containing medium. At a concentration of 1 mol% of **43**, the decrease in cellular uptake is of 25% after 4 h incubation, while from 2 to 10 mol% the reduction remained constant with a 45% decrease compared to the uptake in the absence of serum.

Overall the CLSM images demonstrated that in the presence of 10% of FBS, the uptake kinetic is slowed down. Longer incubation time such as 7 h is needed to obtain a fluorescence response similar to 4 h incubation in absence of

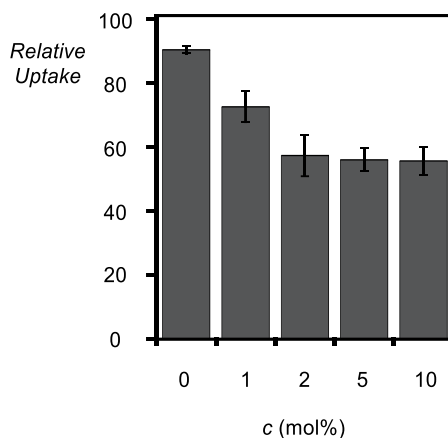


Figure 51. Dependence of liposomes uptake efficiency in presence of 10% FBS in the medium, in function of the concentration of amphiphile **43**. Data (average \pm standard deviation from three experiments) are normalized against those obtained with liposomes in the absence of FBS in the medium at the same concentration of **43**.

serum. Moreover the flow cytometry measurements demonstrated that there is indeed a reduction of the uptake of liposome when 10% FBS was present in the incubation medium. The exact reason of this decrease is not known but probably the serum interacts with the liposomes or with the proteins of the cellular membrane involved in the thiol-mediated uptake, decreasing the interaction between the liposomes and the cell surface.

3.1.5. Colocalization Assay

So far, the best thiol-responsive head group, membrane composition, liposome size and incubation time were determined in order to obtain the best cellular uptake. The CLSM images showed that the fluorescence from the liposomes was located in punctate location, but the subcellular compartment it was in, was still unknown. Therefore we investigated different organelles possibly targeted by the uptake, by colocalization. In a first assay, we tried using automated microscope to determine their localization by immunostaining. However this method needed fixing the cells before their permeabilization, and

during the permeabilization process, SRB fluorescence was lost. Therefore we decided to use colocalization dyes to determine the final localization of the SRB fluorescence inside the cell by co-incubation.

The first hypothesis considered was that liposomes were trapped into the endocytic pathway, therefore we tested the colocalization with early endosomes (Figure 52). The following test was the colocalization with lysosomes as the final stage of the endocytosis pathway (Figure 53). Finally mitochondria were tested not only for 100 nm size vesicles (Figure 54), but also for all the different size studied in 3.1.3.2 since the CLSM images suggested a different localization according to the size of the liposomes (Figure 55).

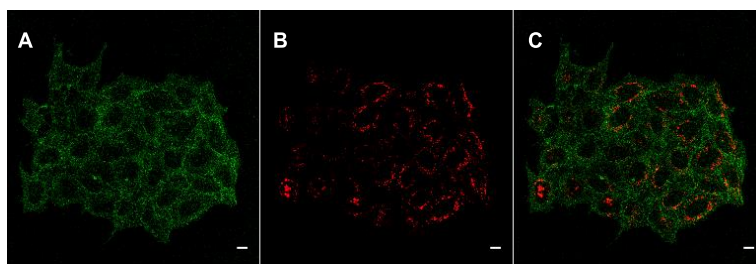


Figure 52. CLSM images of HeLa Kyoto cells after 4 h incubation of 100 nm liposomes with the last 20 min co-incubation with FITC-dextran (40 kDa) at 37 °C in Leibovitz's medium. (A) FITC-dextran, LP = 10%; (B) liposomes containing 5 mol% transporter **43**, LP = 4%; (C) merged. Scale bar: 10 μ m.

CLSM images were analyzed for colocalization and the Pearson correlation coefficient (PCC) was calculated on at least 3 images containing at least 5 cells, using the coloc2 plugin of ImageJ software. According to literature,^[174] a correlation value between -1 to -0.5 indicates segregation, a value between -0.5 to 0.5 indicates no correlation while a value between 0.5 and 1 indicates correlation, meaning in our case colocalization. The values calculated for all the experiments are reported in Figure 56.

The colocalization with endosomes was performed using dextran (40 kDa) labelled with FITC. The dye was added to the incubation medium for the last

20 min before washing the cells and taking the CLSM images. The merge image between FITC (Figure 52A) and SRB fluorescence (Figure 52B) showed no colocalization (Figure 52C) which was confirmed by a PCC value calculated of 0.27 ± 0.06 (Figure 56A, E).

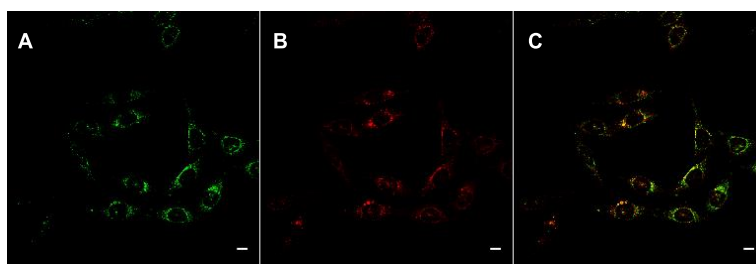


Figure 53. CLSM images of HeLa Kyoto cells after 4 h incubation of 100 nm liposomes with the last 40 min co-incubation with LysoTracker Green at 37 °C in Leibovitz's medium. (A) LysoTracker, LP = 10%; (B) liposomes containing 5 mol% transporter **43**, LP = 4%; (C) merged. Scale bar: 10 μ m.

The lysosomes was localized using LysoTracker Green. The dye was added to the incubation medium for the last 40 min of incubation before to wash the cells and take the CLSM images. Once again the merge image between the colocalization dye (Figure 53A) and the fluorescent vesicles (Figure 53B) showed only few yellow superpositions (Figure 53C). The PCC value

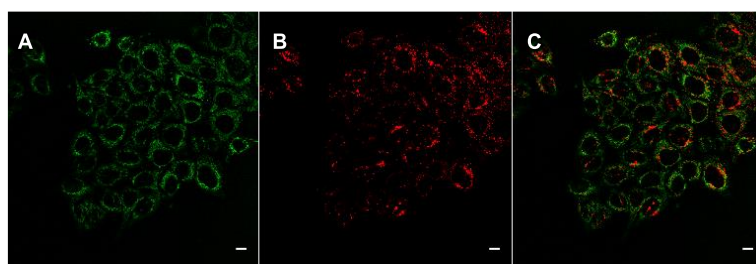


Figure 54. CLSM images of HeLa Kyoto cells after 4 h incubation of 100 nm liposomes with the last 15 min co-incubation with MitoTracker Green at 37 °C in Leibovitz's medium. (A) MitoTracker, LP = 10%; (B) liposomes containing 5 mol% transporter **43**, LP = 4%; (C) merged. Scale bar: 10 μ m.

calculated was of 0.41 ± 0.05 confirming that the liposomes do not colocalize with lysosomes (Figure 56A, L).

Finally mitochondria were targeted using MitoTracker Green as colocalization dye. The dye was added to the incubation medium for the last 15 min before to wash the cells and take the CLSM images. The merge image (Figure 54C) showed that MitoTracker (Figure 54A) and SRB fluorescence (Figure 54B) are not colocalized which was confirmed by a PCC value calculated of 0.26 ± 0.06 (Figure 56A, M).

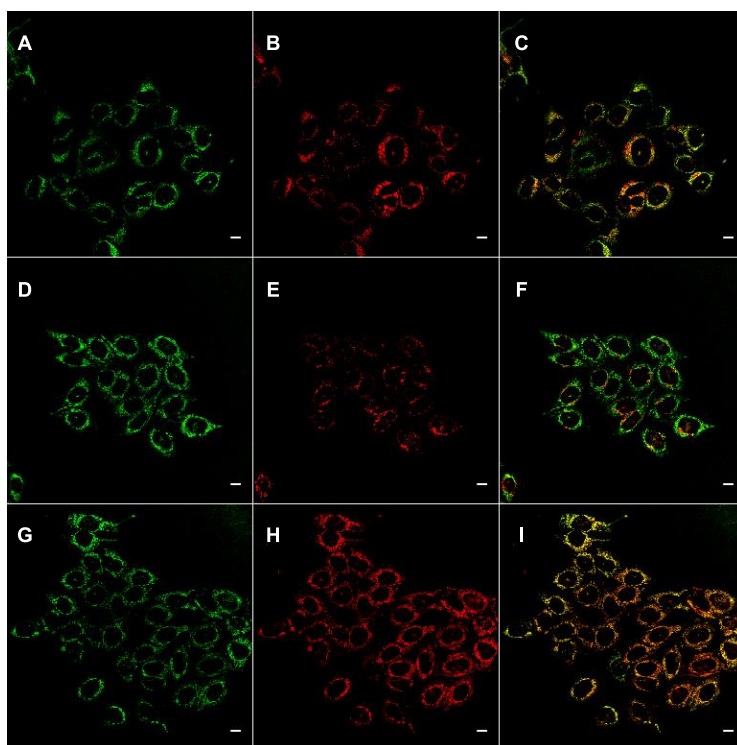


Figure 55. CLSM images of HeLa Kyoto cells after 4 h incubation of 100 nm liposomes with the last 15 min co-incubation with MitoTracker Green at 37 °C in Leibovitz's medium. (A, D, G) MitoTracker, LP = 10%; (B) 50 nm liposomes, (E) 200 nm liposomes and (H) 400 nm liposomes containing 5 mol% transporter **43**, LP = 4%; (C, F, I) merged. Scale bar: 10 μ m.

The colocalization of MitoTracker Green (Figure 55A, D, G) with liposomes of different sizes (Figure 55, B: 50 nm, E: 100 nm, H: 400 nm) showed that for 50 nm and 200 nm diameter the vesicles are not in mitochondria with a calculated PCC value of 0.29 ± 0.03 and 0.42 ± 0.08 respectively. However at 400 nm, the fluorescence are mainly located in mitochondria as can be observed in Figure 55I by the yellow superposition of the two fluorescent dyes, and confirmed by a PCC value of 0.68 ± 0.03 . This result explains the difference in localization observed by CLSM (Figure 48) but might not be due to the thiol-mediated uptake since the liposomes alone showed already good uptake with probable localization into mitochondria.

Since 100 nm liposomes do not colocalize with endosomes, lysosomes nor mitochondria, we postulated that they should be in the cytoplasm. We can however not exclude nor prove that the fluorescence remained in the original liposomal formulation.

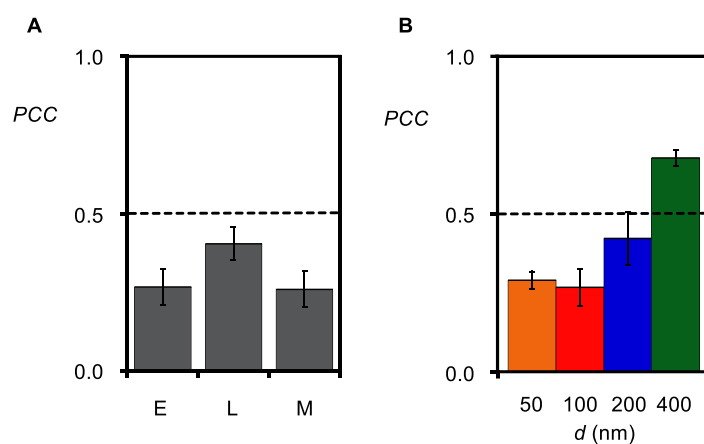


Figure 56. (A) Colocalization of liposomes ($d = 100$ nm, 5 mol% **43**) with endosomes (E, FITC-dextran), lysosomes (L, LysoTracker Green) and mitochondria (M, MitoTracker Green), quantified by PCC. (B) Colocalization of liposomes (5 mol% **43**) of $d = 50$, 100, 200 and 400 nm diameter with mitochondria (MitoTracker Green), quantified by PCC.

3.1.6. Tail Screening

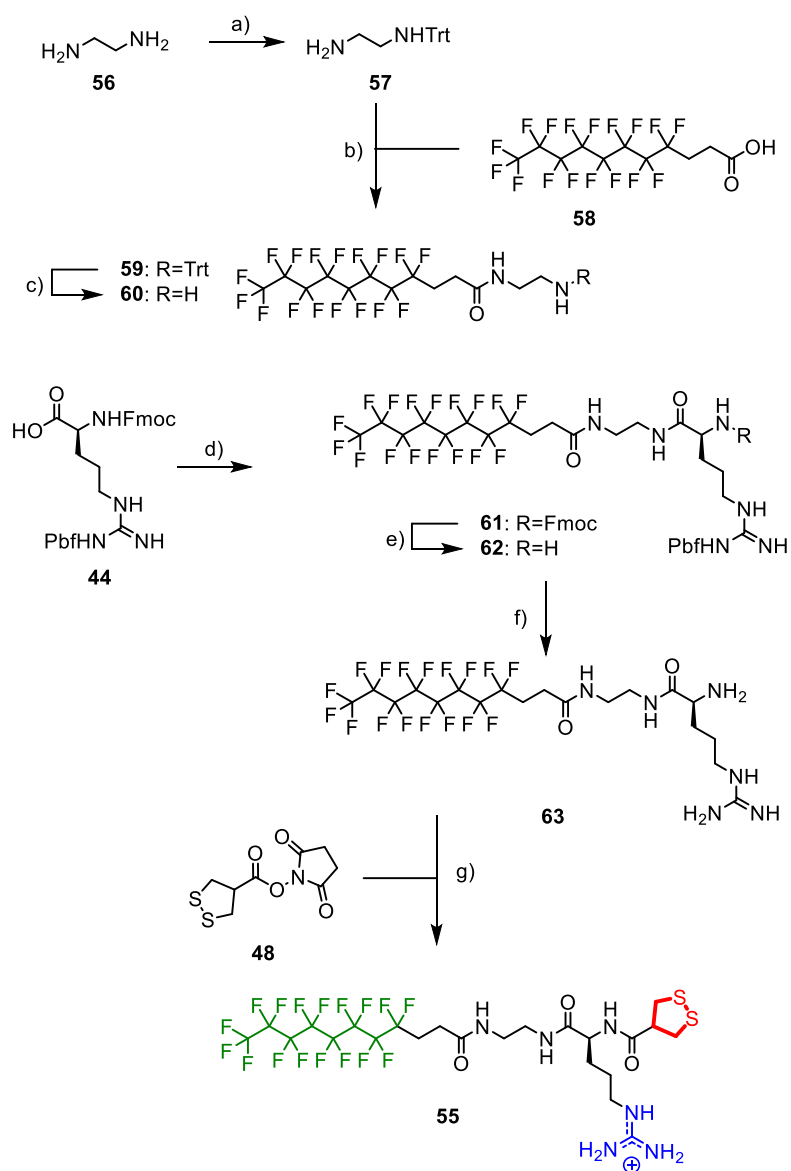
Having identified asparagusic acid as the best performing head and a diameter of 100 nm as the optimal liposome size for the best cellular uptake, we screened the tail to further increase the uptake.

3.1.6.1. Synthesis

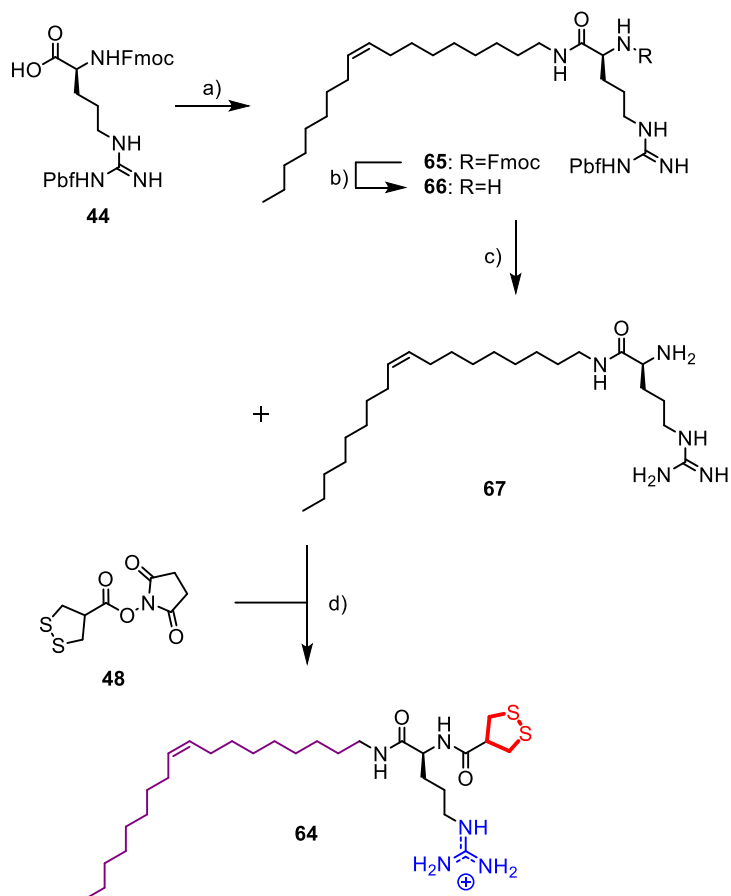
Since perfluorinated alkyl chain could enhance the uptake of CPPs compared to carbohydrate chain (see chapter 3.3),^[166] transporter **55** was designed to use the unique properties of fluorocarbon. The synthesis plan is presented in Scheme 5.

Commercially available ethylenediamine **56** was first monoprotected with a trityl group (Trt) following reported procedures from Kozielski^[175] and Papaioannou,^[176] to obtain **57**, before to be coupled with perfluorinated fatty acid **58** provided by Prof. Pierangelo Metrangolo and Prof. Giuseppe Resnati from Politecnico di Milano. This peptide coupling was performed in basic conditions using HBTU to gives **59**. After deprotection of the trt group by treatment with TFA, amine **60** was obtained and reacted with the protected arginine **44** by peptide coupling in basic conditions using HBTU to give **61**. The fmoc protecting group was removed by treatment with DBU to give **62**, before deprotection of the pbf group by treatment with TFA. Arginine **63** was coupled with NHS activated asparagusic acid **48** in basic conditions to give **55**.

Since the alkyl chain should be inserted in the vesicle membrane, we were interested to determine the effect that an unsaturated alkyl tail would have on the uptake of liposomes. The presence of unsaturated tails in natural membranes helps indeed to fluidify them from solid-order phase to liquid-disorder phase (see section 1.5.1).^[132] Therefore the dodecyl tail was replaced by an oleyl tail in transporter **64**. Its synthesis is reported in Scheme 6.



Scheme 5. a) Trt-Cl, CH_2Cl_2 , 4.5 h, $0\text{ }^\circ\text{C} \rightarrow \text{rt}$, 33%; b) HBTU, TEA, DMF, 3 h, $0\text{ }^\circ\text{C} \rightarrow \text{rt}$, 78%; c) TFA, CH_2Cl_2 , 1 h, rt, 61%; d) **60**, HBTU, TEA, DMF, 3 h, $0\text{ }^\circ\text{C} \rightarrow \text{rt}$, quant.; e) DBU, CH_2Cl_2 , MeOH, 3 h, rt, 81%; f) TFA, CH_2Cl_2 , 2 h, rt, 47%; g) TEA, CH_2Cl_2 , DMF, 48 h, rt, 79%.



Scheme 6. a) OA, HATU, TEA, DMF, 2.5 h, 0 °C → rt, 79%; b) DBU, CH₂Cl₂, 1 h, rt, 81%; c) TFA, CHCl₃, 2.5 h, rt, quant.; d) TEA, CH₂Cl₂, MeOH, 3 h, rt, 14%.

Commercially available oleylamine (OA) was reacted with the C-terminus of protected arginine **44** by peptide coupling using HATU as coupling reagent in basic conditions. Arginine **65** was then deprotected by DBU treatment to remove the fmoc yielding in **66**, followed by TFA treatment to remove the pbf group. The obtained arginine **67** was then reacted in basic conditions with NHS activated asparagusic acid **48** to give **64**.

3.1.6.2. Flow Cytometry Assay

In order to compare the uptake response for those compounds with the results obtained for **43**, **49**, **51** and **53** with 200 nm liposome size (see section 3.1.2.2), the best performing transporter (**43**) was also used in this section as benchmark. Quantification of liposomes cellular uptake for transporters **55** and **64** was performed by flow cytometry.

As demonstrated by automated microscopy in section 3.1.3.2, the switch from 200 nm to 100 nm LUVs diameter, lead to an increase in the liposome uptake for compound **43** from about 3.5 (Figure 38, ●) to more than 4 times the uptake of liposomes without transporter (Figure 57, ●).

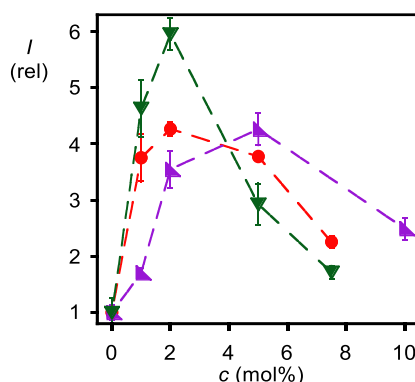
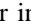
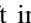
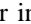


Figure 57. Dependence of liposomes uptake in function of the concentration of **43** (●), **55** (▼) and **64** (▲). Data (average \pm standard deviation from three experiments) are normalized against those obtained with liposomes in absence of transporter.

The change from a carbohydrate tail to a fluorocarbon tail enhanced impressively of the uptake of liposome to about 6 times at 2 mol% of transporter **55** compared to the liposomes uptake in absence of transporter (Figure 57, ▼). Knowing that perfluorinated alkyl chains tend to form domain of their own in hydrophobic and/or hydrophilic environment (phenomena called the “fluorous effect”),^[177–178] the increase of uptake with fluorocarbon is probably due to formation of specific microdomains in the vesicle membrane

where the amphiphile is more concentrated leading to an increase in the uptake. This result showed that the choice of the membrane interacting part on the transporter is also of crucial importance and can greatly influence the amount of liposomes uptaken, despite not being directly involved in the uptake mechanism.

Transporter **64** with its unsaturated alkyl tail did not change the maximal uptake of the vesicle compared to **43** which remained at about 4 times the initial liposome uptake in the transporter absence (Figure 57, ). However in this case, the concentration needed to reach this maximal uptake shifted from 2 mol% for **43** to 5 mol% for **64** (Figure 57,  compared to ). This shift in maximal uptake is probably due to longer chain length in **64** compared to **43**, leading in an increase of the CMC. This experiment would indicate that the change in the membrane phase is of minor importance on the maximal uptake of the liposomes.

3.1.6.3. *Confocal Laser Scanning Microscopy*

We have demonstrated in section 3.1.3.2 that the reduction of liposomes diameter from 200 nm to 100 nm did not influence the cellular fluorescence distribution for transporter **43** which remained in the punctate location (Figure 47B) probably in the cytoplasm. In order to compare the results obtained here for transporter **51** and **53** with the previous ones, the same setup as described before was used in order to test the influence of the tail.

The CLSM images of liposomes uptake in function of the concentration of **55** showed that already at 1 mol% (Figure 58A), the increase was substantial, especially when compared to 1 mol% of **43** (Figure 40A). The maximal uptake was clearly reached with a concentration of 2 mol% (Figure 58B), while it decreased at higher concentration such as 5 or 7.5 mol% (Figure 58C and D respectively). Those CLSM images are in agreement with the flow cytometry

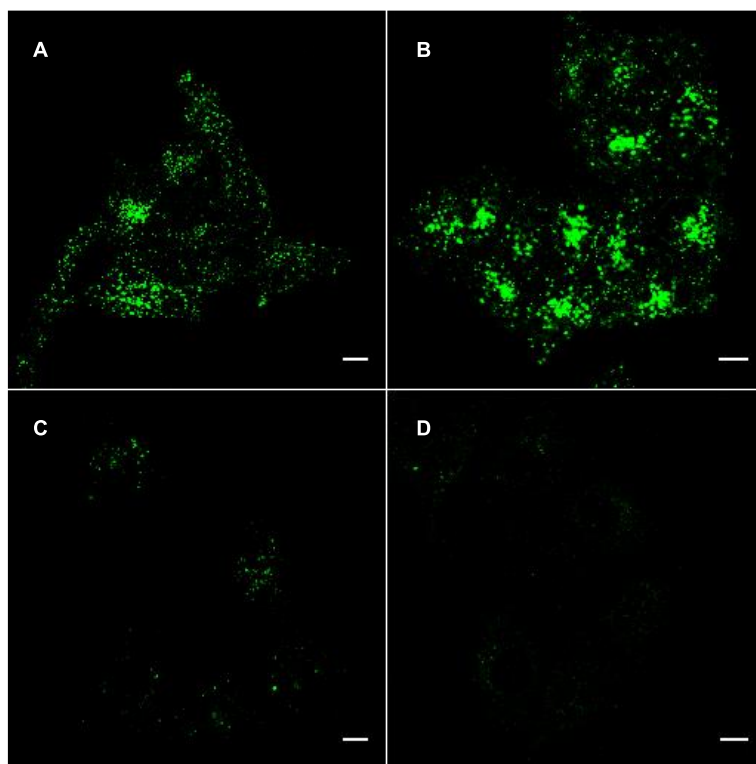


Figure 58. CLSM images of HeLa Kyoto cells after incubation with fluorescent liposomes containing transporter **55** at 1 (A), 2 (B), 5 (C) and 7.5 (D) mol%. Scale bar: 10 μ m.

measurements (Figure 57) both in term of maximal liposome uptake in comparison with the transporter **43** and the concentration of transporter needed to reach it.

The CLSM images for transporter **64** showed a really low uptake for 1 and 2 mol% (Figure 59A and B respectively), while the maximum was reached with a concentration of 5 mol% (Figure 59C). As observed previously with all transporters, at higher concentration (7.5 mol%), the uptake of vesicles was reduced (Figure 59D). Those images are in agreement with the trend observed

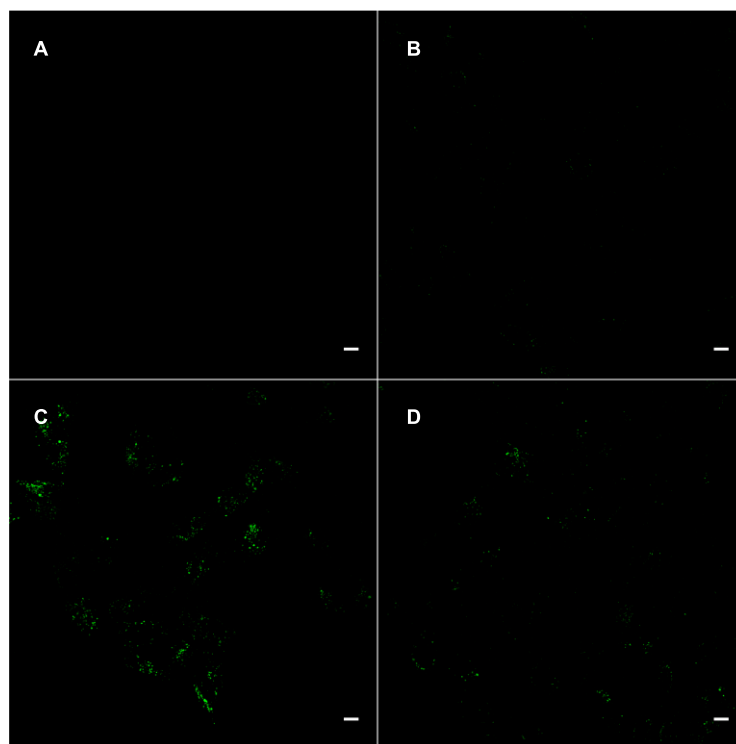


Figure 59. CLSM images of HeLa Kyoto cells after incubation with fluorescent liposomes containing transporter **64** at 1 (A), 2 (B), 5 (C) and 7.5 (D) mol%. Scale bar: 10 μ m.

by flow cytometry with a maximal uptake at 5 mol%. The comparison in cellular uptake between **64** and **43** was difficult from the CLSM images. According to the flow cytometric data, the uptake should be similar between 2 mol% for **43** and 5 mol% for **64**, while it seemed higher for **43** (Figure 47B) compared to **64** (Figure 59C) on the CLSM images.. However the CLSM should be taken as qualitative and the flow cytometry as quantitative, so the uptake at 5 mol% for **64** is similar to the one at 2 mol% for **43**.

As for previous experiments, the fluorescence from the liposomes was in punctate location confirming that the change in alkyl tail does not influence the liposomes stability. No colocalization assays were performed with those

transporters, but the fluorescence are probably in endosomes-like compartment in the cytoplasm as postulated from previous experiments.

We decided not to screen for other alkyl chains of different sized based on the results presented in this section. We figured out indeed that shorter alkyl chain should lead in a decrease of the CMC, and therefore have a maximal uptake equal or lower than in the case of the dodecyl chain. On the other hand, the increase in the tail length should lead in an increase of the CMC but would probably shift the maximal uptake toward higher concentration as in the case of transporter **64**.

3.1.7. Polymersomes Uptake

In order to test the delivery of other giant substrates, we investigated polymersomes. We collaborated with the Palivan and Meier groups from the University of Basel, who synthesized the building blocks^[179] and formed the polymersomes with SRB encapsulated inside.^[172] The membrane of the polymersomes was constituted of poly(2-methyl-2-oxazoline)-block-poly(dimethylsiloxan)-block-poly(2-methyl-2-oxazoline) (PMOXA-PDMS-PMOXA) block copolymers (Figure 60) leading to a monolayer membrane. Different length of PMOXA-PDMS-PMOXA were tested in order to determine the influence of the thickness of the monolayer on the uptake of vesicles. All the polymersomes size had a constant diameter of circa 160 nm.

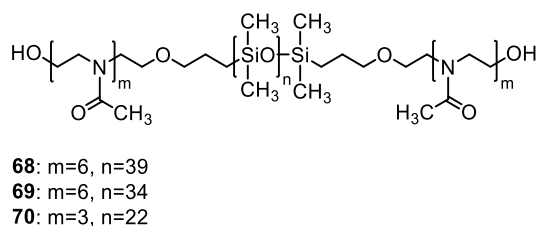


Figure 60. Chemical structure of PMOXA-PDMS-PMOXA and ratio of block copolymer to form polymersomes **68**, **69** and **70**.

Polymersomes **68** have the thickest membrane of the series studied here with a thickness of 10.7 ± 0.7 nm. **69** have a membrane thickness of 9.2 ± 0.5 nm, while **70** have the thinnest membrane with 6.0 ± 0.5 nm. The thickness of the membrane was determined by electron microscopy in a previous study.^[180]

3.1.7.1. Confocal Laser Scanning Microscopy

The uptake efficiency was determined first by CLSM in the absence or presence of the transporter **43** at 5 mol%. The procedure was exactly the same as described above (section 3.1.1.2) for the liposomes, meaning 4 h incubation at 37 °C in Leibovitz's medium.

In the absence of transporter, polymersomes **68** had negligible uptake (Figure 61A), while when amphiphile **43** was incorporated at 5 mol% into the polymersomes membrane (Figure 61B), the increase of uptake was spectacular.

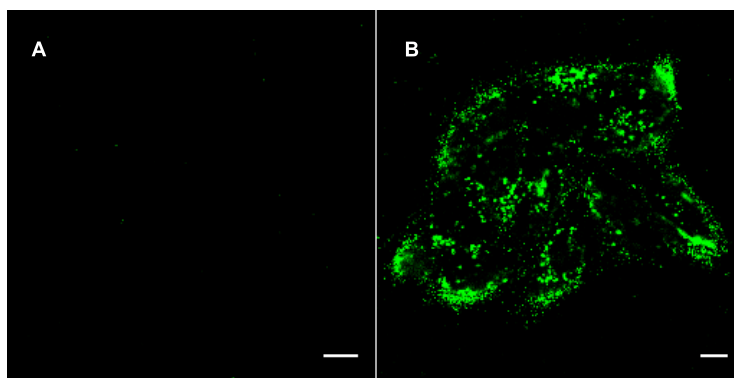


Figure 61. CLSM images of HeLa Kyoto cells after incubation with fluorescent polymersomes **68** without (A) and with (B) transporter **43** at 5 mol%. Scale bar: 10 μ m.

Surprisingly with polymersomes **69**, the uptake in the absence of transporter was weak but none totally negligible (Figure 62A) as for **68**. The main difference with **68** polymersomes being a thinner membrane thickness, it

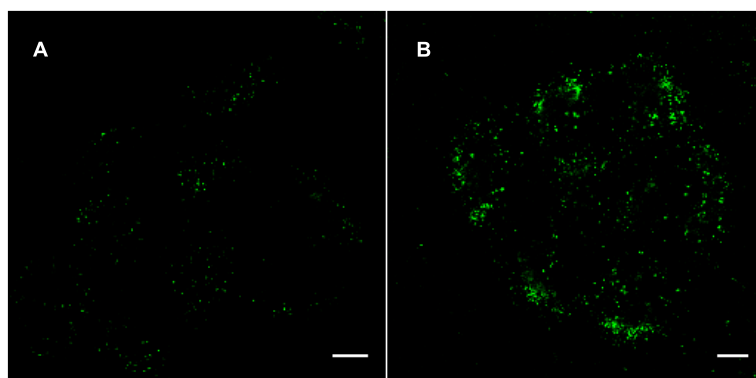


Figure 62. CLSM images of HeLa Kyoto cells after incubation with fluorescent polymersomes **69** without (A) and with (B) transporter **43** at 5 mol%. Scale bar: 10 μ m.

indicates that the membrane thickness plays a role in the transport of polymersomes. The addition of transporter **43** to polymersomes **69** increased their uptake (Figure 62B) as for **68**.

As for polymersomes **69**, **70** with the thinnest membrane of the present polymersomes series had a reasonable uptake in the absence of transporter (Figure 63A). However adding **43** did not increase the uptake of those polymersomes (Figure 63B). On the contrary, the fluorescence distribution inside the cells was totally absent. A possible explanation is that the addition of the amphiphile to the polymersome membrane creates a perturbation such that the very thin polymersome membrane was not stable in this condition, yielding in a destruction of the vesicle population and the release of the encapsulated dye, which cannot then be uptaken by cells. As for liposomes delivery, the addition of transporter **43** led to an increase in the uptake for polymersomes **68** and **69**. The fluorescence distribution was in punctate localization which was probably, as for liposomes, located in the cell cytoplasm. However no colocalization experiments were performed to confirm this hypothesis with polymersomes.

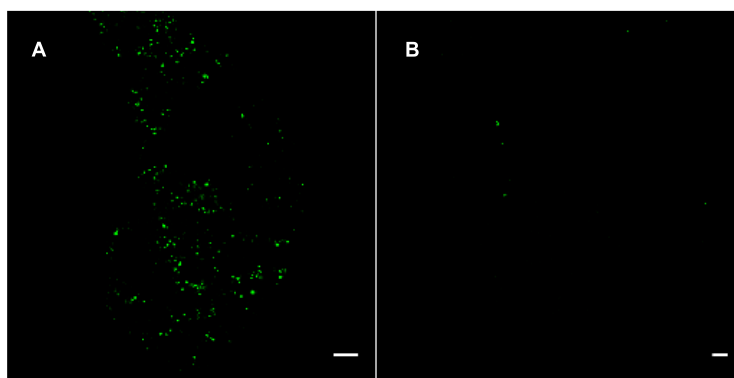


Figure 63. CLSM images of HeLa Kyoto cells after incubation with the fluorescent polymersome **70** without (A) and with (B) transporter **43** at 5 mol%. Scale bar: 10 μ m.

Since there was no increase of fluorescence upon addition of transporter **43** for polymersomes **70**, the quantification of the cellular uptake was performed by flow cytometry only on the two other polymersome (**68** and **69**).

3.1.7.2. Flow Cytometry Assay

The CLSM images for the different polymersomes showed that **68** and **69** had an increase of uptake upon addition of transporter **43** whereas **70** did not probably due to instability of the vesicle membrane under the same conditions. In order to quantify the increase of uptake, flow cytometry measurements were performed at different concentration of **43** for **68** and **69** only.

The flow cytometric measurements indicated indeed that there is an increase of uptake for both polymersomes upon increasing concentration of **43**. The increase is larger for polymersomes **68** with a maximal uptake at 5 mol% more than 5 times the uptake of polymersomes alone (Figure 64, ●). The increase is similar as for the best liposomal uptake increase with transporter **43** (Figure 57, ●). On the other hand, the increase of uptake was smaller for polymersomes **69**

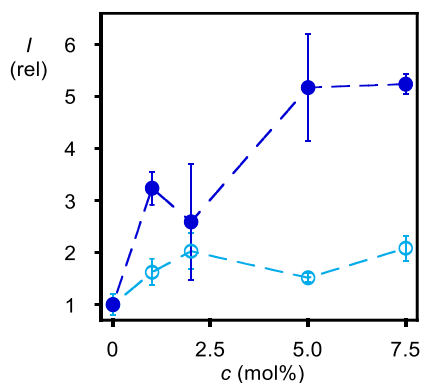


Figure 64. Dependence of polymersome **68** (●) and **69** (○) uptake efficiency in function of the concentration of amphiphile **43**. Data (average \pm standard deviation from three experiments) are normalized against those obtained with polymersomes in absence of transporter.

with a maximal increase at 2 times the initial polymersome uptake (Figure 64, ○). This is probably due to the non-negligible initial uptake of vesicles in absence of transporter (Figure 62A).

Unlike for liposome dose response curves, the flow cytometric data for polymersomes did not represent a bell shape curve. A possible explanation is the increased stability of the polymersome monolayer compared to the liposome bilayer: when compound **43** reaches the CMC and start forming micelles, it does not destroy the polymersomes population.

3.1.8. Additional Transporters and Assays

3.1.8.1. Epidithiodiketopiperazine Transporter

When we started the study of liposomes uptake using strained cyclic disulfides, the best compound in our hand was the asparagusic acid.^[74] However in parallel to this work, we continued in our group to work on the development of more powerful strained cyclic disulfide with higher ring tension for increased uptake of substrates. We found that the epidithiodiketopiperazine (ETP) scaffold was better for both the maximal

uptake and the localization in cells compared to asparagusic acid with a final nuclei location.^[83] Therefore we decided to test ETP in the delivery of liposomes and developed the new transporter **71**. This compound was synthesized by Dr. Lili Zong in our group.

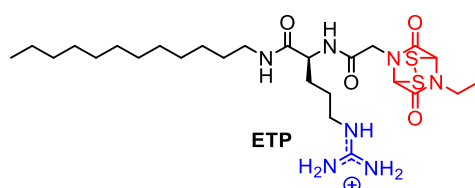


Figure 65. Structure of transporter **71** for the delivery of liposomes.

Transporter **71** was tested for cellular delivery in HeLa Kyoto cells with 100 nm liposomes in Leibovitz's medium at 37 °C for 4 h incubation by CLSM and flow cytometry (Figure 66).

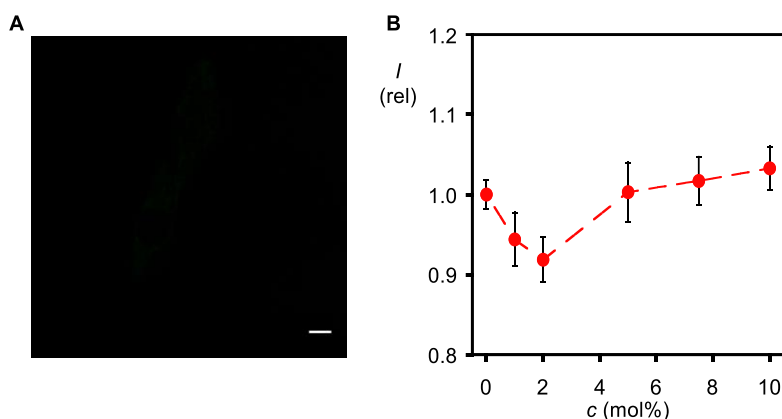


Figure 66. Cellular uptake in HeLa Kyoto cells incubated for 4 h with fluorescent liposomes. (A) CLSM images at 5 mol% of **71**. Scale bar: 10 μ m. (B) Flow cytometric measurements with different concentration of **71**.

Unfortunately over the range of concentration (1 – 10 mol%) and incubation time (1 – 8 h) tested by CLSM, no trace of fluorescence could be observed inside the cells upon addition of **71** (Figure 66A). This result was corroborate with flow cytometric measurements performed with an incubation of 4 h at

concentrations of **71** of 1 – 10 mol% (Figure 66B). There was no increase of liposomes uptake in the presence of **71** compared to the uptake of liposomes in absence of transporter.

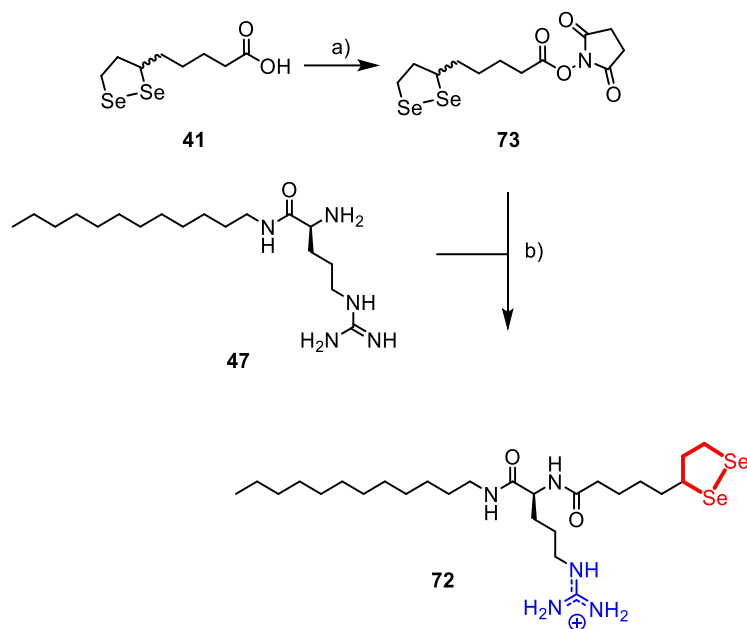
The inactivity of **71** was surprising and could be explained by the instability observed of the ETP scaffold depending on the solvent it is stored in. It was indeed shown in our group that oxidation is possible on the sulfur atom to give thiosulfinate or thiosulfonate when stored in DMSO. This change in structure could reduce the cellular uptake activity of ETP. Taking into account the low response of liposome uptake with **71**, no additional experiments were performed with this compound.

3.1.8.2. *Diseleno Lipoic Acid Transporter*

Pushed by the results we obtained with diseleno lipoic acid as transporter for small fluorophore (section 3.2),^[181] we decided to test the ability of diselenolane to deliver giant substrates. Therefore the new transporter **72** was synthesized following Scheme 7.

The diseleno asparagusic acid **41**, synthesized in our lab by Dr. Xavier Martin-Benlloch following published procedure,^[182] was coupled with NHS using *N,N'*-dicyclohexylcarbodiimide (DCC) as coupling reagent to obtain the activated ester **73**. It was then reacted with arginine **47** in basic conditions to lead in **72**.

The uptake of 100 nm liposomes upon addition of **72** was determined by CLSM and quantified by flow cytometry. The CLSM images at different concentration of **72** (1 – 10 mol%) and different incubation time (1 – 8 h) displayed only weak uptake by HeLa Kyoto cells as shown in Figure 67A for 5 mol% of **72** after 4 h incubation. The quantification of the uptake by flow cytometry corroborates this observation with a very low increase at 5 mol% of



Scheme 7. a) NHS, DCC, THF, 18 h, rt, 53%; b) TEA, DMF, 5 h, rt, 21%.

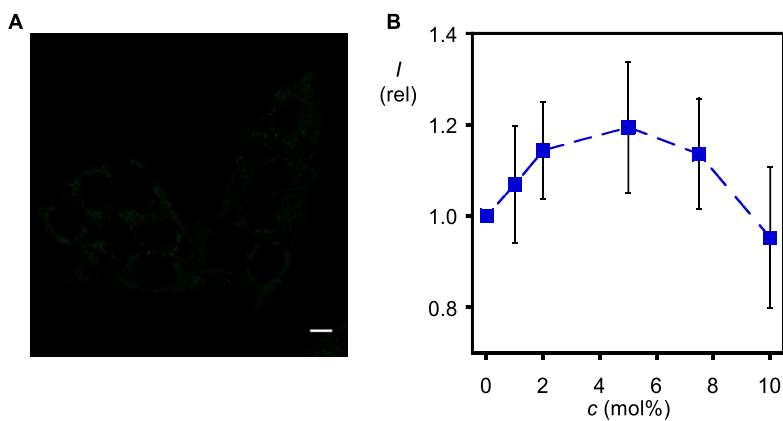


Figure 67. Cellular uptake in HeLa Kyoto cells. (A) CLSM images after 4 h incubation with fluorescent liposomes containing 5 mol% of **72**. Scale bar: 10 μm . (B) Flow cytometric measurements after 4 h incubation with different concentration of **72**.

72 after 4 h incubation of 1.2 times compared to the uptake of liposomes in absence of transporter (Figure 67B). As previously observed, the curve is bell-shaped indicating probable micelles formation at high concentration.

The poor uptake observed upon the addition **72** is not well understood. A possible explanation could be a difference in the uptake mechanism between diselenolane and dithiolane incompatible with the delivery of giant substrate such as liposomes. Another possibility would be that after the thiol-diselenide exchange, the ring closure to reform the diselenolane is so fast that the whole liposome does not have the time to be uptaken (see chapter 3.2). Due to the poor uptake of liposomes, no additional assay was performed with this transporter.

3.1.8.3. Addition of Positive Charges

Based on the results observed on the functionalization of cell-penetrating poly(disulfide)s with additional positive charges leading in a good uptake at low concentration,^[67] we decided to increase the amount of positive charges by adding **53** to our working system hoping to increase the uptake of liposomes by activating the CPPs uptake mechanism (section 1.2). Therefore we decided to incubate HeLa Kyoto cells for 4 h with 100 nm liposomes, 5 mol% of **43** and increasing concentrations of **53** (0 – 20 mol%).

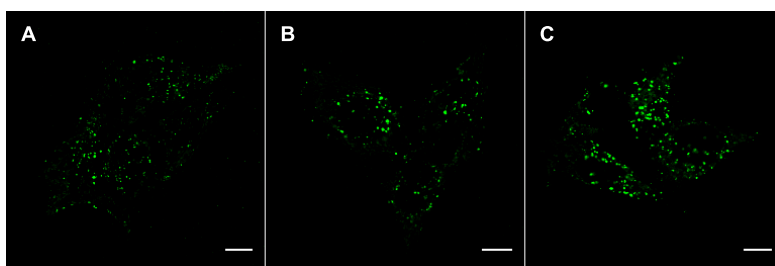


Figure 68. CLSM images of HeLa Kyoto cells incubated for 4 h with fluorescent liposomes containing 5 mol% of **43** and 0 (A), 5 (B) or 10 (C) mol% of **53**. Scale bar: 10 μ m.

The difference in uptake was determined qualitatively by CLSM. Surprisingly, the presence of **43** at 5 mol% and addition of **53** at a concentration of as high as 20 mol% to the system did not lead to observable cytotoxic effects on cells. However the general fluorescence response and cellular localization did not change significantly. This observation was consistent with the results obtained previously in which transporter **53** did not increase the uptake of liposomes (section 3.1.2). Therefore no additional assay was performed with increasing amount of positive charges.

In conclusion, the delivery into cells of giant substrates such as liposomes and polymersomes by thiol-mediated uptake is possible using strained cyclic disulfides. Several thiol-responsive heads and alkyl tails were screened to obtain the best cellular uptake. Finally the best performing transporter contains an asparagusic acid head and a perfluorinated alkyl tail with an arginine in between. The composition of the liposome membrane and diameter size influence greatly the uptake and final localization of the substrate entrapped in the aqueous core. The best cellular uptake response quantified by flow cytometry was of more than 6 times the uptake of liposomes in absence of transporter, after 4 h incubation with **55** at 2 mol% in 100 nm DSPC/DSPE-PEG₂₀₀₀ liposomes. The fluorescent probe contained inside the vesicles was efficiently delivered inside the cell in punctate location that does not colocalize with endosomes, lysosomes nor mitochondria. Therefore we postulated that they are probably in the cytoplasm. This delivery is not only valid for liposomes but also for polymersomes with which the influence of the membrane monolayer thickness was demonstrated. With thicker membrane, the uptake was increased compared to thinner ones.

3.2. Delivery of Diselenides

We have efficiently demonstrated in the Matile group that the thiol-mediated uptake is a powerful method to deliver various cargoes inside cells,

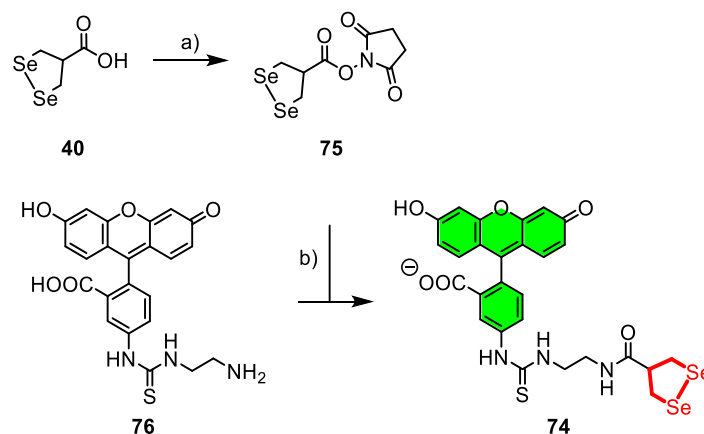
ranging from small fluorophores^{[74],[83]} to peptides^[81] or entire vesicles (section 3.1).^[172] The uptake is increased with higher ring tension correlated with smaller CSSC dihedral angle. Having pushed it to the extreme with the epidithiodiketopiperazine (ETP) scaffold with a dihedral angle close to 0°, ^[83] we decided to move from disulfides to diselenides.

Computational studies performed by Dr. Amalia I. Poblador-Bahamonde from the University of Geneva, showed that unlike for 1,2-dithiolane **38** and **41** where the CSSC dihedral angle is of 27° and 35° respectively, the diseleno asparagusic acid **40** have a minimized energy with a CSeSeC dihedral angle of 0° confirming the 0.2° angle found in the cristal structure^[119] which correspond to a twist-free envelope structure for this five member ring. The decrease in energy maxima for a 0° dihedral angle between peroxide, disulfide and diselenide, predicts a ring tension reduced in selenolane compared to dithiolane or dioxolane.^[181] Despite this predicted reduced ring tension, we decided to investigated the delivery of small fluorophore covalently linked to diselenolane in cellular uptake.

3.2.1. Synthesis

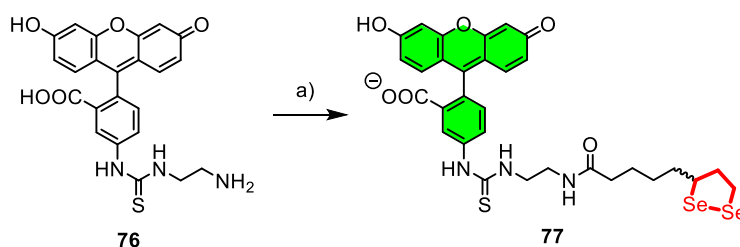
In order to compare the uptake of diselenides with the one of disulfides, similar compounds were synthesized. Fortunately the diseleno asparagusic and lipoic acids, **40** and **41** respectively, were already reported in literature by reacting the 3-bromo-2-(bromoethyl)-propanoic acid or the 6,8-dichlorooctanoic acid with sodium diselenide.^[111-112] Therefore only functionalization with FITC from those compounds was needed to obtain similar compounds as in previous studies.^[74]

The fluorescent diseleno asparagusic acid **74** was synthesized as described in Scheme 8. **40** was synthesized and provided by Jana Hildebrandt from Prof. Wolfgang Weigand group in the University of Jena, following published



Scheme 8. a) NHS, DCC, THF, 22 h, rt, 49%; b) DMF, 3 h, rt, 12%.

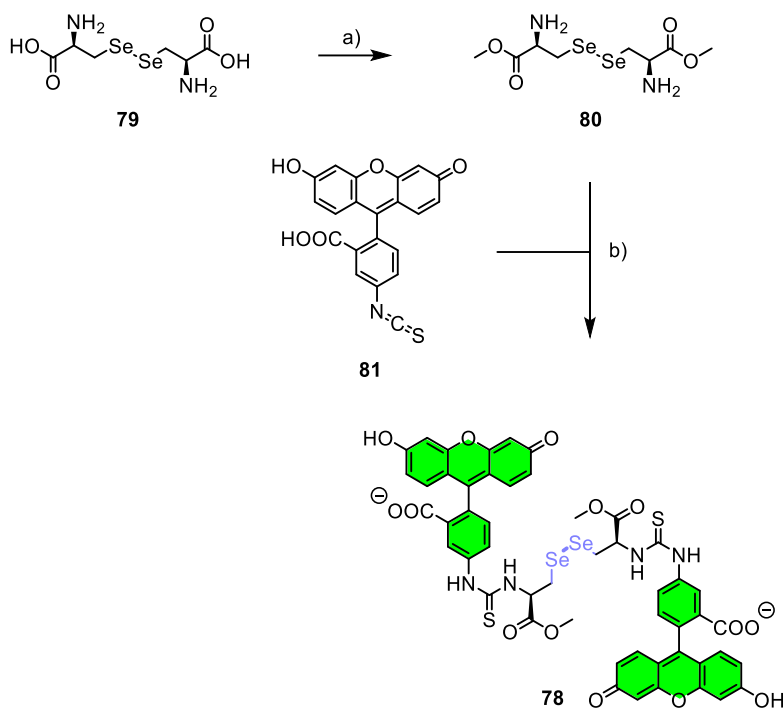
procedures.^{[111],[183]} It was functionalized with NHS by using DCC to give **75**. The activated ester was then reacted with FITC functionalized with ethylenediamine **76** prepared as previously described,^[74] to give **74**.



Scheme 9. a) **73**, DMF, 3 h, rt, 14%.

The activated ester **73** was reacted with the functionalized FITC **76** to give the fluorescent diseleno lipoic acid **77** as reported in Scheme 9.

In order to compare the uptake of not only cyclic diselenide but also of linear one as in previous studies,^[74] compound **78** was synthesized as described in Scheme 10. The diseleno cystine **79** was methylated by Fischer esterification



Scheme 10. a) PTSA, MeOH, 45 h, reflux, quant; b) TEA, DMF, 3 h, rt, 44%.

following the procedure from the Nakayama group.^[184] Compound **80** was then directly reacted with commercially available FITC **81** to give **78**.

3.2.2. Reactivity Toward Thiols

It has been demonstrated that linear diselenides react easily with thiols. Prof. Michael Pittelkow group for example uses the dynamicity of the disulfide and diselenide bonds in order to achieve combinatorial libraries.^[185] However it was not yet demonstrated that diselenolanes could react with thiols. Already in 1967, Wolfgang Günther showed by absorbance that DTT **33** could reduce several linear diselenides by showing the disappearance of diselenide band (around 300 nm). However no change in the absorbance spectrum was observed for the diseleno asparagusic acid **40**.^[186]

We decided to investigate the reactivity of the cyclic diselenides toward different thiols such as octanthiol, DTT or GSH, in different conditions. However no change in the characteristic 430 nm absorbance band nor in the proton NMR corresponding to **40** could be observed. There are two possible explanations to those observations: either the diselenolanes do not react with thiols, or the proximity of the released selenol from the thiol-diselenide exchange is so reactive that it reacts with the formed thiol-selenol bond, closing the ring by selenol-selenosulfide exchange. This back reaction is so fast that it cannot be observed in our conditions. It was indeed demonstrated that the diselenide is favored over the mixed thiol-selenol bond.^[187] Therefore we decided to investigate the thiol-diselenide exchange with diselenolane indirectly by thiol-exchange affinity column and by studying the oxidation kinetic of DTT **33**.

3.2.2.1. *Thiol-Exchange Affinity Column*

The first evidence for the exchange between thiols and diselenolane was provided by the use of a thiol-exchange affinity column in which the solid phase exposes reactive thiols on its surface. This experiment was performed by Dr. Naomi Sakai in our lab. In order to compare the reactivity with thiols, not only diselenides **74**, **77** and **78**, were tested but also different disulfides from previous studies: the original asparagusic acid **25**^[74] and ETP **36**^[83]. The retention time was measured by detection of the fluorescence from the CF dye present on all compounds.

In this experiment, the reactivity of the thiol toward disulfides and diselenides was tested. To calibrate the instrument, CF **31** as a standard without disulfide nor diselenide, was eluted through the column in order to determine the dead time (Figure 69A). All the disulfides and diselenides tested showed some delayed retention time compared to **31** supporting probable dynamic and

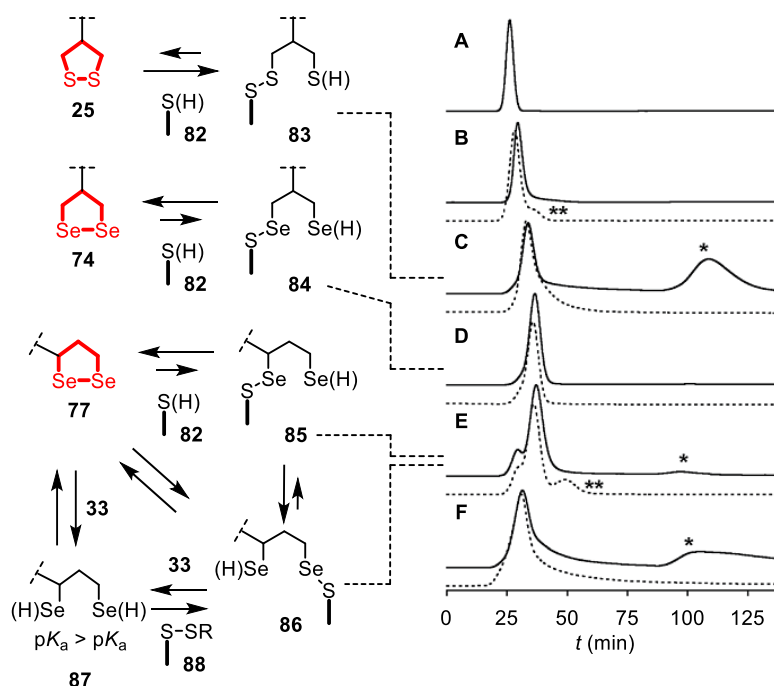


Figure 69. Thiol-exchange affinity chromatograms of CF **31** (A), ETP **36** (B), asparagusic acid **25** (C), **74** (D), **77** (E) and **78** (F) in 10 mM Tris, 0.1 M NaCl, 1 mM EDTA, pH 7.5 with a 0 – 50 mM DTT gradient at $t = 60 - 70$ min (solid) and constant 50 mM DTT from $t = 0$ (dashed). * = Peaks indicative for inert binding of **25**, **77** and **78** to thiols on the stationary phase by strain-releasing thiol-disulfide/diselenide exchange in the absence of DTT. ** = Peaks indicative for labile binding of reduced forms (e.g. **87**) to disulfides on the stationary phase by thiol/selenol-disulfide exchange in the presence of DTT.

temporal covalent bonding with thiols **82** exposed from the solid phase (Figure 69, solid lines). With the presence of DTT in the eluent, the retention times were slightly reduced by about 1 min (Figure 69 dashed lines).

However some significant differences between the different compounds tested, could be observed. For compounds **25**, **77** and **78** (Figure 69C, E and F respectively), a second elution peak could be observed upon the addition of DTT in the eluent (Figure 69, *). This proves that those compounds did interact and were covalently trapped by the solid phase, needing the addition of DTT in

the eluent to get released. It was expected from previous studies^[83] that **25** should react with thiols by ring-opening strain-released disulfide exchange to form **83**. The absence of such a peak for **74** indicates that if the mixed S–Se **84** is formed, it is quickly cleaved by ring closure (Figure 69D). From all the thiol-diselenide exchange present in the literature, it was also expected that linear **78** should be trapped by the thiolated column. The presence of the second peak for compound **77** is a first proof that the mixed S–Se compound can be formed. Upon the thiol attack, two possible products can be formed with chiral diseleno lipoic acid: exchange to form **85** is more probable compared to its isomer **86** due to the difference in pK_a between primary and secondary selenol (about 0.15)^[188] making the primary selenol a better and thus more reactive leaving group compared to the secondary selenol. However an intramolecular exchange between the two isomers is possible since the primary selenol with a lower pK_a is a better nucleophile and after the thiol-diselenide exchange, **86** should be preferentially formed because it should be less reactive than **85**. This exchange could also provide an explanation for the split of the first elution peak.

Surprisingly ETP **36** and the diseleno asparagusic acid **74** did not showed a second elution peak upon addition of DTT to the eluent (Figure 69B and D respectively). This demonstrate that there is not a stable covalent anchorage of those compounds on the thiolated column. However some transient reaction should occur since there is a delay in the retention time compared to reference **33**. It was observed that for **36**, the ring can close even in the presence of thiols^[83] which would explain its low interaction with the stationary phase of the column and thus the absence of the second elution peak. Similar explanation could be provided for **74**. The delayed retention time for the first peak prove a transient thiol-diselenide exchange, but in this case only primary selenol are released which could undergo rapid ring closure to form again the diselenolane.

Finally an interesting observation was made when DTT was present in the eluent from the beginning (Figure 69 dashed line). A second peak could be observed after the initial one for **36** and **77** (Figure 69B and E respectively, **). This behavior could be explained by a reaction between the compounds and DTT, opening their ring and exposing a reactive thiol or primary selenol such as **87** that could react with “hidden” disulfide **88** on the stationary phase surface unreduced by DTT.

Overall the thiol affinity column provides a first indirect evidence of thiol-cyclic diselenide exchange proven by the delayed retention time compared to the dead time measured with **33** and the presence of the second elution peak for **77** when DTT was added to the eluent.

3.2.2.2. *Oxidation of DTT*

As mentioned before, it was not possible to demonstrate the ring-opening of the diselenolane using DTT by absorbance^[186] nor by ¹H NMR as in the case of **25** and **36**.^[83] However a second evidence of thiol-diselenide exchange can be provided by determining the oxidation rate constant of DTT in the presence or absence of diselenolane. A difference in rate would indeed indicate an attack from DTT **33** on the diselenide compound to form transiently the mixed specie **89** before ring closure to **90**, while the resulting diselenol **87** would reoxidize into the five member ring due to the presence of ambient oxygen in the system (Figure 70).

Therefore, a solution **33** was prepared in a deuterated sodium phosphate buffer (100 mM, pD 8.0) at a concentration of 1 mM. The evolution of the oxidation of DTT was monitored by ¹H NMR in the presence or absence of the **40** or **41** at different concentration to obtain DTT/diselenolane ratio of 1:1, 1:2, 1:5 or 1:10. The significant NMR spectra recorded for different concentration of diselenolane are reported in section 5.3.3.

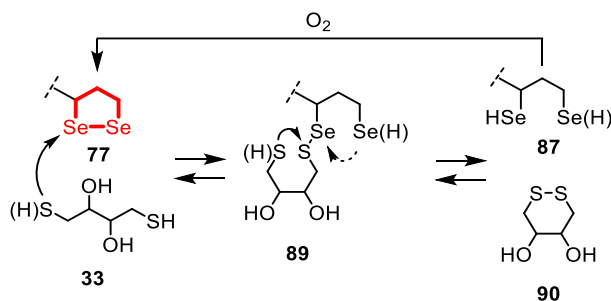


Figure 70. Schematic representation of the oxidation of DTT in presence of **77** and reoxidation of **87** into **77** by ambient oxygen. Structures are shown in neutral form, acidic protons are indicated in parenthesis. Competing ring closures in reactive intermediate **89** are indicated with solid (preferred) and dashed arrows.

With time, **33** oxidized slowly into **90**. It took more than 35 hours in those conditions to have a complete oxidation (Figure 71) with a half-time of 16 hours calculated from the linear fit (Table 3, entry 5).

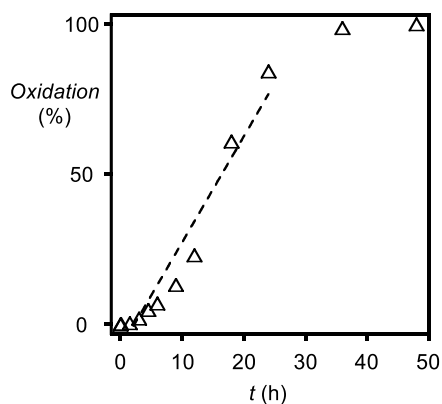


Figure 71. Oxidation kinetic of DTT (0.5 mM) in absence of diselenolane with linear fit.

In the presence of the seleno asparagusic acid **40**, the oxidation kinetic was impressively accelerated (Figure 72A). At a 1 to 1 ratio already, it took about 8 hours to reach the full oxidation of DTT with a half-time around 4 h (Table 3, entry 4). With increasing concentration of **40**, the rate was further accelerated.

At a 5 to 1 ratio, the conversion into the oxidized DTT was so fast that it was not possible to determine a half-time. The reaction was indeed complete in less than 33 minutes.

With the seleno lipoic acid **41**, the oxidation was also accelerated compared to the oxidation in the absence of diselenolane (Figure 72B). It was however slower than with **40** at the same concentration. At a 1 to 1 and 2 to 1 ratio, the oxidation half-time was shortened by half (Table 3, entry 4 and 3 respectively) compared to the oxidation in absence of **41** and the full conversion was achieved in about 20 hours. From the calculated half-time, it seems that the 1 to 1 ratio is faster than the 2 to 1 ratio. This observation could be explained by the minimum acceleration due to the presence of the catalyst. However the oxidation was further increased by increasing the concentration of the **41**, with the fastest oxidation reached with a 10-fold excess of the diselenide compared to DTT.

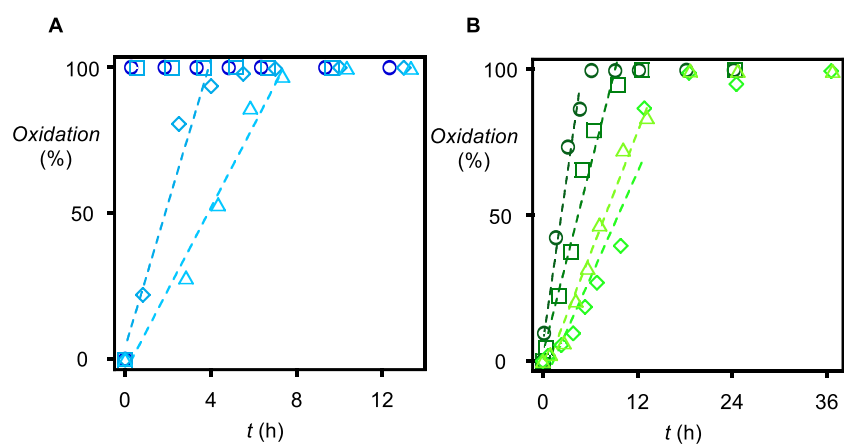


Figure 72. DTT (0.5 mM) oxidation kinetics, catalyzed by **40** (A) and **41** (B) with linear fits. Concentration of catalysts: 5.0 (○), 2.5 (□), 1.0 (◇) and 0.5 (△) mM.

The half-times (t_{50}) for every concentration of catalyst were determined by plotting the time as a function of the oxidation ratio and equaling the linear fit

of the points before to reach the full oxidation conversion to 50% (Figure 71 and Figure 72). The values obtained are summarized in Table 3.

Table 3. Half-time t_{50} (h) of DTT oxidation as a function of the concentration of diselenide.

Entry	Concentration (mM) ^a	t_{50} with 40 ^b (h)	t_{50} with 41 ^b (h)
1	5.0	<0.28	2.3 ± 0.2
2	2.5	<0.55	4.5 ± 0.3
3	1.0	1.9 ± 0.3	9.0 ± 1.0
4	0.5	3.9 ± 0.4	6.9 ± 0.9
5	0.0	16.0 ± 2.0	16.0 ± 2.0

^aConcentration of diselenides **40** or **41** in NMR tube. DTT concentration was 0.5 mM. ^bSee Figure 29.

The oxidation rate constant k for different concentration of catalyst was calculated using Equation 1 valid for pseudo-first order rate constant. This approximation can be used when one of the reactant is in excess and its concentration does not change significantly during the reaction.^[189] In this case, since the diselenolane is reformed by ambient oxygen (Figure 70, **87** to **77**), its concentration remained constant during the reaction.

$$k = 0.693/t_{50} \quad \text{Eq. 1.}$$

The oxidation rate constant k_{ox} was determined by plotting the calculated k in function of the concentration of the catalyst and fitting with the linear regression corresponding to Equation 2 (Figure 73).

$$k = k_0 + k_{ox}c \quad \text{Eq. 2.}$$

From the slope of the linear regression an oxidation rate constant k_{ox} of $8.9 \times 10^{-2} \text{ M}^{-1}\text{s}^{-1}$ for **40** and $1.4 \times 10^{-2} \text{ M}^{-1}\text{s}^{-1}$ for **41** were determined.

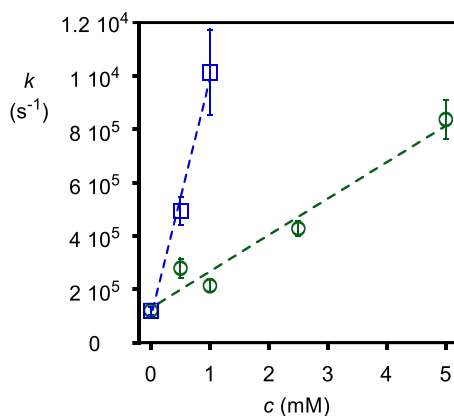


Figure 73. Linear correlations between the rate constant k and the concentration c of **40** (□) and **41** (○).

This experiment provide a second evidence that diselenolane can react with thiols and thus could potentially enter into cells by thiol-mediated uptake.

3.2.3. Solutions Studies

In order to quantify the cellular uptake of the diselenolane, the fluorescence of the CF attached to the diselenolane was measured. It was indeed demonstrated in previous experiment that when linked to dithiolane, the fluorescence was non-negligibly quenched.^[74] Therefore we investigated the potential reduction of fluorescence due to the presence of the nearby ring in **74** and **77**. Since it was possible that the diselenide bond did not survive the entry nor the reductive environment inside the cell cytoplasm, we needed to find an efficient way to reduce the bond without affecting the fluorescence of CF.

3.2.3.1. Reduction of the Diselenide Bond

As mentioned before, the first test to reduce the diselenide bond was performed using thiols such as DTT in PBS buffer or in octanthiol directly as solvent. However no evidence of the reduction was detected by checking the absorbance at 430 nm nor by ¹H NMR. The addition of disulfide into the

solution to trap the released selenol, nor the addition of base in the reaction mixture changed the outcome of the experiment. However as control experiments, evidences of reduction of linear diphenyl diselenide and dimethyl diselenide by DTT were obtained by ^1H NMR. Those results were in accordance with already published results^[186] showing that linear diselenide are more reactive toward thiols than diselenolane and that the absence of reduction of diselenolane is due to the stability of the ring.

Further experiments were performed following literature procedures. The addition of NaBH_4 ^[190] or H_3PO_4 ^[191] reduced the diselenide bond but also quenched the fluorescence from CF. On the other hand, the addition of Zn in a $\text{HCl}/\text{CH}_3\text{CN}$ mixture^[192] did not reduced the diselenide bond.

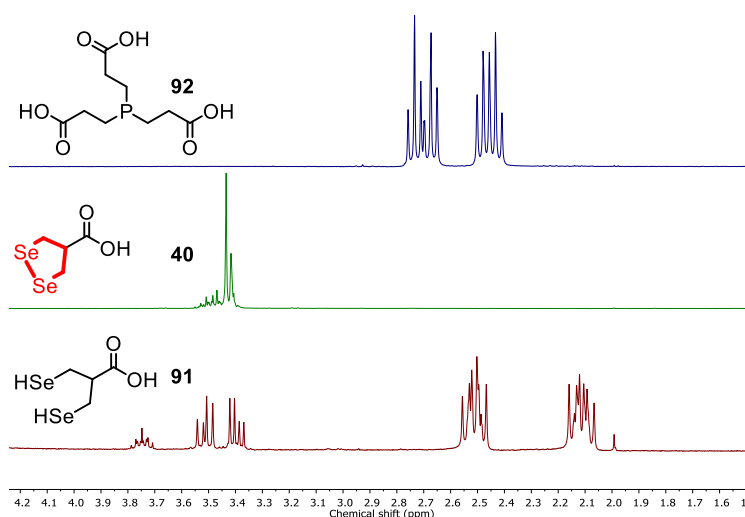


Figure 74. ^1H NMR spectra of TCEP **92**, **40**, and reduced diseleno asparagusic acid **91** by TCEP, in D_2O at pD 8.0.

Finally **40** was successfully reduced to diselenol **91** using Tris(2-carboxyethyl)phosphine **92** (TCEP) as reducing agent as shown by ^1H NMR

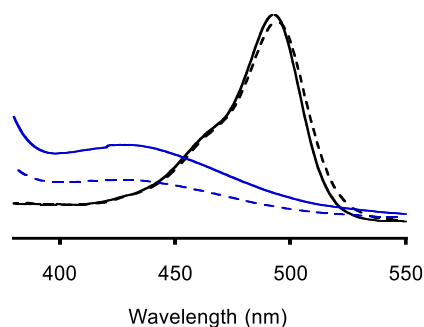


Figure 75. Absorption spectra of the isolated motifs FITC (black) and **40** (blue) before (solid) and after treatment with TCEP (dashed).

(Figure 74) and absorbance (Figure 75) while the fluorescence of CF in the presence of TCEP was not affected. Dilution of the obtained diselenol with water demonstrated a reformation of the diselenolane.

3.2.3.2. Fluorescence Quenching Effect

It was reported that for the original asparagusic and lipoic acids, **40** and **41**, the fluorescence of CF was quenched compared to the free FITC motif by a factor of 3.36 and 5.62 respectively.^[74] In order to calibrate and compare the quantification of the cellular uptake with previous results, we investigated the influence of the cyclic diselenide and their reduced form on the fluorescence of CF.

The comparison of the fluorescence response for **74** and **77** with **25** demonstrated a clear quenching effect of the diselenolane ring (Figure 76, solid lines). The correction factor was of 3.29 for **74** and 4.59 for **77**, compared to **25** (Table 4, columns 2 and 3) for the closed rings. Taken into account the fluorescence quenching for **25** compared to FITC reported above, the overall quenching was up to a factor of 15.6 for **77** compared to the free FITC motif.

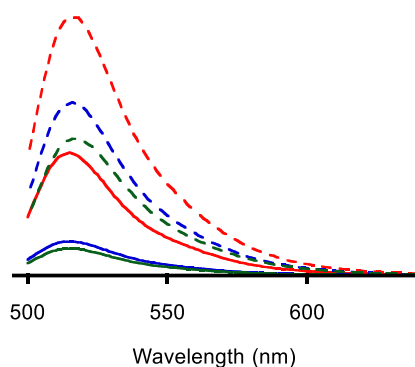


Figure 76. FITC emission from conjugates **25** (red), **74** (blue) and **77** (green, 100 μ M, PBS) before (solid) and after (dashed) reduction with TCEP.

The quenching effect was lower when the compounds were treated with **92** to obtain the reduced disulfide and diselenides. The reduced form of asparagusic acid **25** was about 2.11 times brighter than its closed form (Figure 76, red dotted lines) which is 1.60 less fluorescent compared to the free FITC motif. The fluorescence of **91** and **87** was quenched by a factor of 1.51 and 1.89 respectively, compared to reduced **25** (Table 4, columns 4 and 5).

Table 4. Fluorescence intensity and correction factors for compounds **25**, **74**, and **77**.

Compound ^a	Emission Intensity ^{b,c}	Correction factors ^{b,d}	Emission Intensity ^{c,e}	Correction factors ^{d,e}
25	3.09 10 ⁶	1.00	1.80 10 ⁶	1.00
74	9.40 10 ⁵	3.29	1.21 10 ⁶	1.51
77	6.73 10 ⁵	4.59	9.54 10 ⁵	1.89

^aSee Figure 21, Schemes 8 and 9. ^bExperiment in the absence of **92**. ^cEmission intensity recorded from 500 nm to 700 nm upon excitation at 488 nm.

^dCorrection factors calculated by dividing the integrated emission intensity through the recorded spectral region of compound **25** by that of **74** or **77**.

^eExperiment in the presence of **92**.

Based on the results presented in section 3.2.2, it is more likely that **74** and **77** end up in a closed form into cells even if during the transport, they might transiently get reduced by reacting with thiols to enter by the thiol-mediated uptake mechanism. Therefore the closed correction factors (Table 4, column 3) were applied for the quantification of the fluorescence inside cells. Considering the thiol-mediated uptake as entry mechanism, **25** should be present under its reduced form. Therefore the real correction factor between **25** and **74** or **77** should be actually 2.11 times the close correction factor. However since the fate of both disulfide and diselenide bonds cannot accurately be determined in cells, we decided to keep the correction factors as presented in Table 4, column 3.

3.2.4. Cellular Uptake Studies

With the fluorescent correction factor in hand, we turn toward cellular experiment assays using flow cytometry to quantify the amount of probe uptaken by the cells, and CLSM to determine the final localization of the probe inside cells.

3.2.4.1. Flow Cytometry Assay

The quantification of cellular uptake was performed by flow cytometry. Therefore solutions of probes **74** and **77** (10 μ M) in Leibovitz's medium were prepared and added to cells for 1 – 4 h incubation. The experiment was performed using **25** as a reference in order to compare the uptake of diselenides to previous studies.^{[74],[83]} The results were normalized to the fluorescence of **25** after 1 h incubation and the closed correction factors (Table 4, column 3) were applied to overcome the fluorescence quenching effect and obtain results closer to reality (Figure 77).

As a control the fluorescence of the cell incubated without any compound was recorded and, as expected, showed really weak fluorescent signal

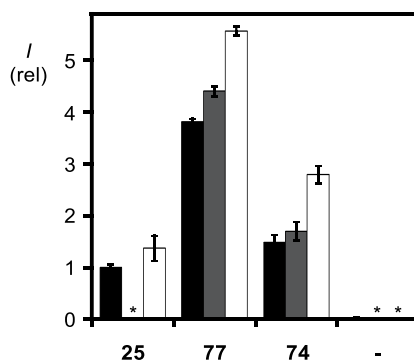


Figure 77. Flow cytometry results (mean \pm error of three independent measurements) for uptake of 10 μ M **25**, **74** and **77** and untreated (-) HeLa Kyoto cells after incubation for 1 h (black), 2 h (grey) and 4 h (white), corrected for emission in closed form (Table 4, column 3). *Not determined.

(Figure 77, -). For all the compounds, increasing incubation time lead to an increase of the cellular uptake. The uptake of diseleno asparagusic acid **74** was increased compared to the uptake of disulfide **25**, especially for long incubation time. To our surprise, the uptake of the diseleno lipoic acid **77** was really good with an increase close to 4 times the uptake of **25** after an incubation of 1 h. This result was in contrast to results obtained with lipoic acid **26** where the cellular uptake was about 20% lower than the uptake of **25** after 1 h incubation.^[74] In the case of diselenolane, the uptake of **77** was more than 2.5 times higher than for **74** after 1 h incubation, making **77** the best 5-member ring transporter identified so far.

3.2.4.2. Concentration and Time Dependences on Cellular Uptake

The final localization of the fluorescence in the cells was determined by CLSM. Therefore the cells were incubated with **74**, **77** and **78** at different concentrations and incubation times to monitor the influence of those parameters on the uptake. As a benchmark, the concentration and time dependences uptake for probe **25** was repeated in order to compare the results obtained here to previously published data.^{[74],[83]}

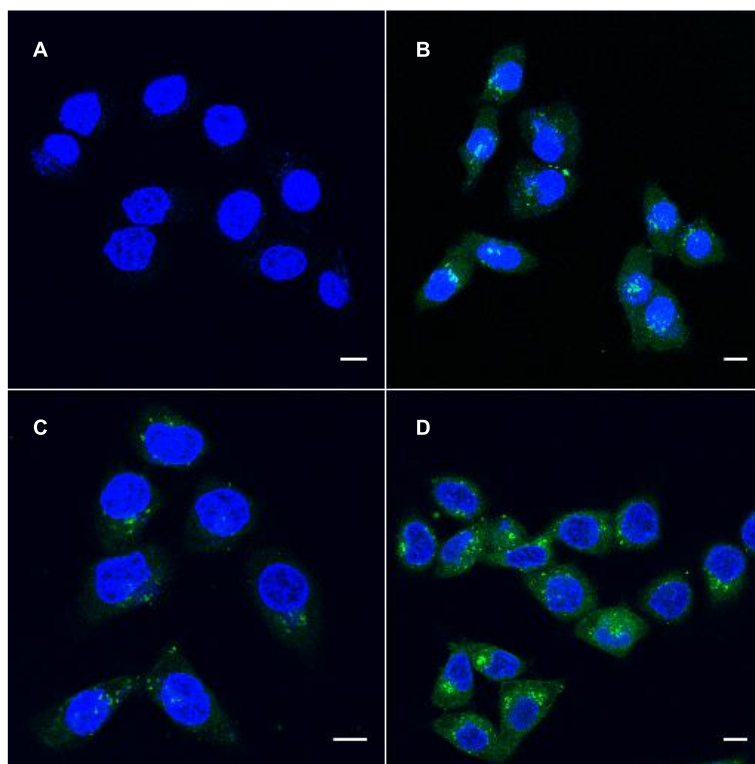


Figure 78. CLSM images of HeLa Kyoto cells incubated for 1 h with **25** (green) at 1 (A), 10 (B), 50 (C) and 100 (D) μM . Nuclei were stained in blue by Hoechst 33342. Scale bar: 10 μm .

The concentration dependence CLSM images for compound **25** after 1 h incubation (Figure 78) showed that at a concentration of 1 μM , no evident uptake of the compound was observable. At 10 μM and higher concentrations fluorescence distribution was observed inside the cells. The fluorescence intensity was similar between 10 and 50 μM , while at 100 μM cytoplasmic delivery was increased.

The incubation time dependence uptake for **25** (Figure 79) at a fix concentration of 10 μM , showed that after 15 min incubation, no fluorescence

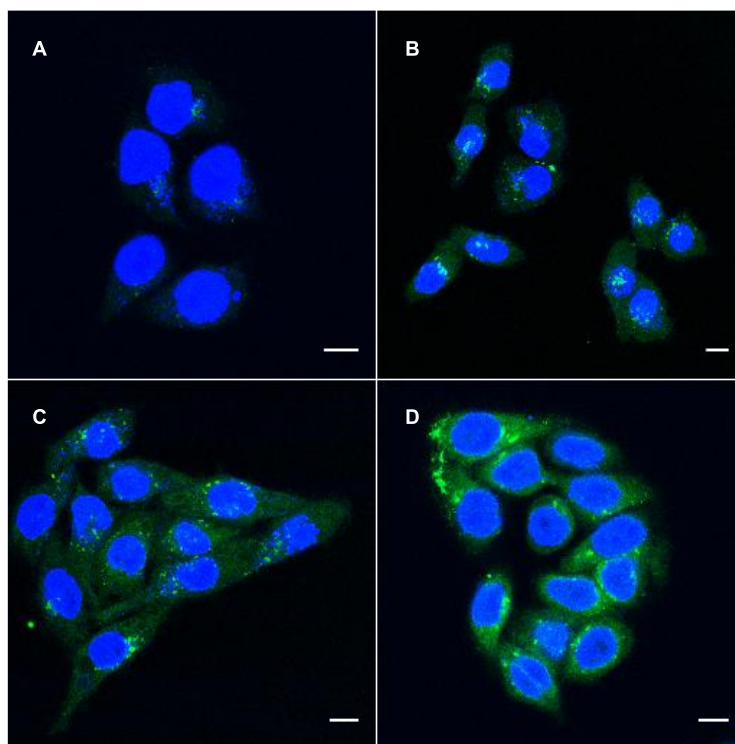


Figure 79. CLSM images of HeLa Kyoto cells incubated for 15 min (A), 1 (B), 2 (C) and 4 (D) h with **25** (green) 10 μ M. Nuclei were stained in blue by Hoechst 33342. Scale bar: 10 μ m.

was detectable inside cells. A minimum 1 h incubation was needed to observe cellular uptake with an increasing fluorescence in the cytoplasm especially after 4 h incubation.

Overall in the concentration and time dependences CLSM images for **25**, the fluorescence was mainly located in punctate dots which according to previously reported experiments,^[74] are endosomes.

For compound **77**, only faint fluorescence was observed at a concentration of 1 μ M (Figure 80A) but the fluorescence increased with increasing concentration (Figure 80D, G, J). Similarly, after 15 min incubation

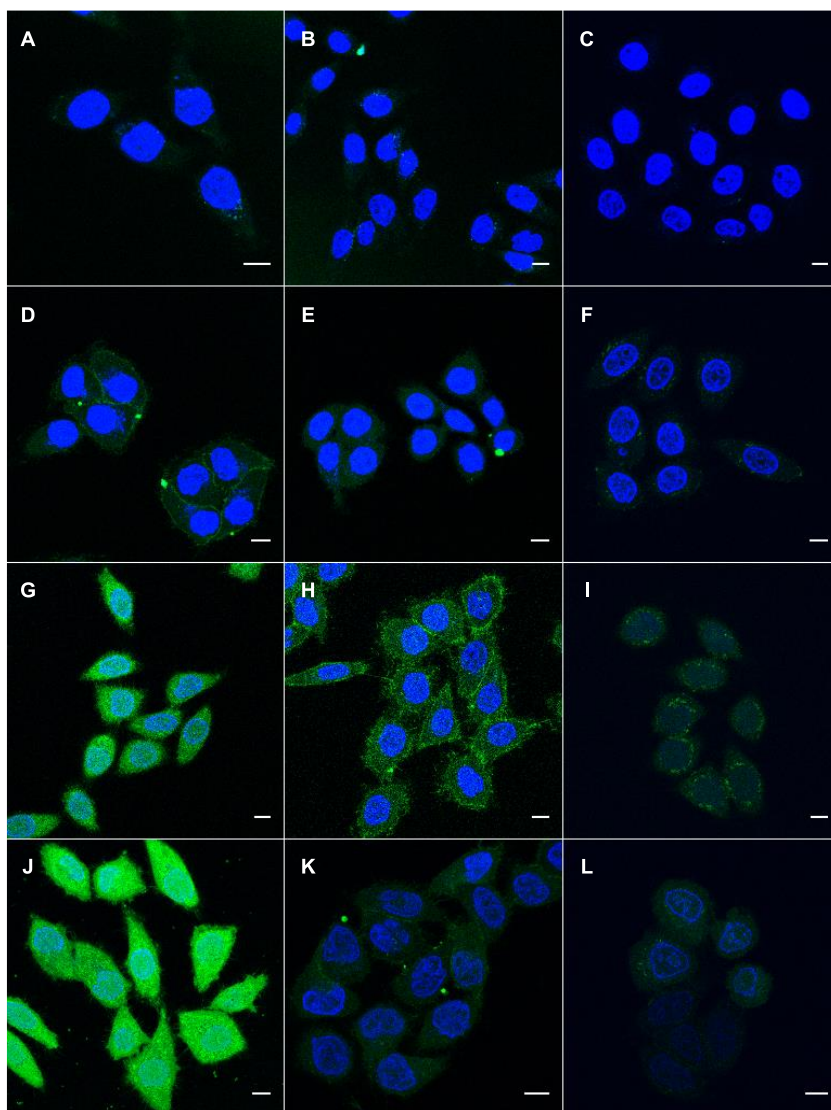


Figure 80. CLSM images of HeLa Kyoto cells incubated for 1 h with **77** (A, D, G and J), **74** (B, E, H and K) and **78** (C, F, I and L) at 1 (A – C), 10 (D – F), 50 (G – I) and 100 (J – L) μM . Nuclei were stained in blue by Hoechst 33342. Scale bar: 10 μm .

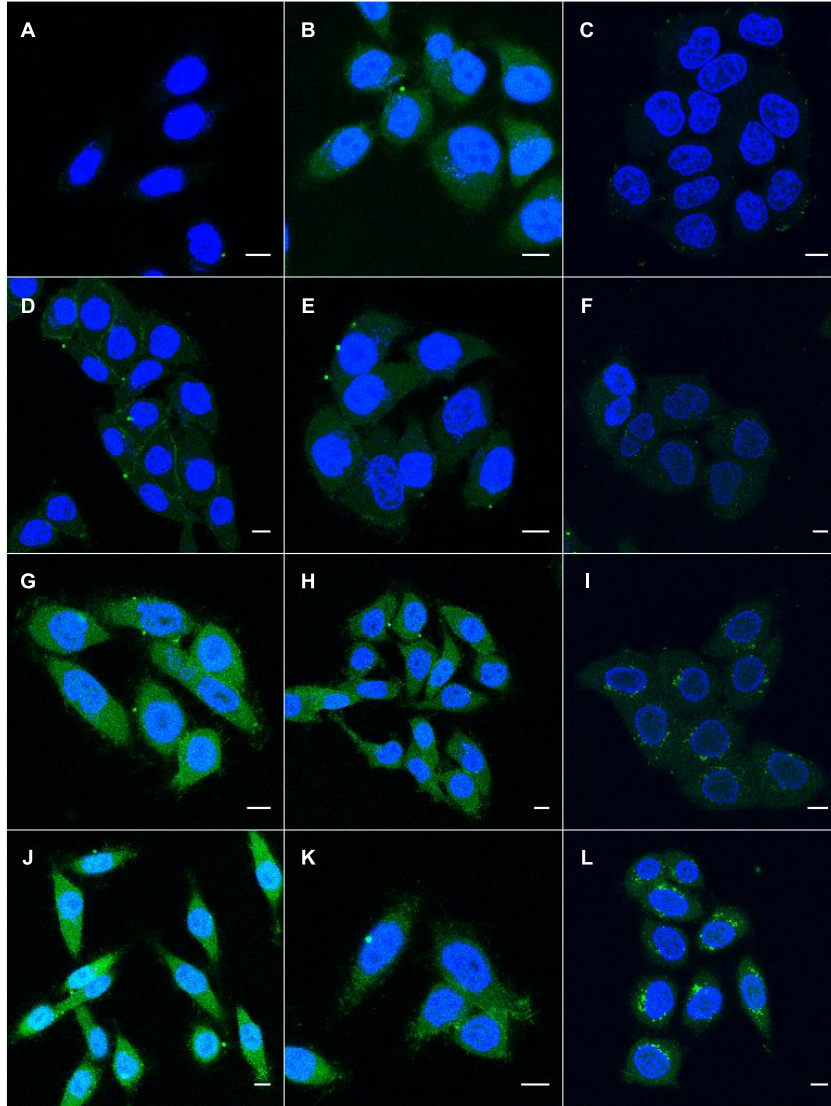


Figure 81. CLSM images of HeLa Kyoto cells incubated for 15 min (A – C), 1 (D – F), 2 (G – I) and 4 (J – L) h with **77** (A, D, G and J), **74** (B, E, H and K) and **78** (C, F, I and L) at 10 μ M. Nuclei were stained in blue by Hoechst 33342. Scale bar: 10 μ m.

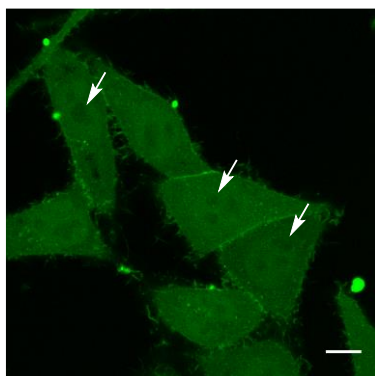


Figure 82. CLSM images of HeLa Kyoto cells after for 4 h incubation with 10 μM of **77**, arrows indicate selected nucleoli. Scale bar: 10 μm .

(Figure 81A), the fluorescence was totally absent in cells, showing no uptake. However increasing the incubation time lead to an increase of uptake as expected (Figure 81D, G, J).

For compound **74**, no fluorescence was detected at a concentration of 1 μM and only faint cellular distribution at 10 μM (Figure 80B and E respectively). For this probe, the best uptake was observed at a concentration of 50 μM (Figure 80H) with the cells starting to suffer from the incubation conditions. At 100 μM (Figure 80K) the overall fluorescence intensity was lower for most of the cells compared to the uptake at 50 μM and visible cytotoxicity was observed. Surprisingly after 15 min incubation at 10 μM (Figure 81B), some fluorescence distribution could be observed inside the cell. The optimal incubation time for this compound at 10 μM was of 2 h (Figure 81H) without significant changes after 4 h incubation (Figure 81K).

The fluorescence cellular distribution for both probes **74** and **77** showed homogenous staining of the whole cells with the exception of the nucleoli when the nuclei are not stained by Hoechst 33342 (Figure 82) and without obvious organelle specificity otherwise. This cellular distribution is interesting compared to the delivery agent we developed previously in our lab: asparagusic

acid **25** was indeed trapped in the endocytic pathway not able to escape efficiently to the cytoplasm (Figure 78 and 79) whereas the ETP **36** accumulated in nuclei staining it all. If the diselenolanes are uptaken through endocytosis pathway, they can efficiently escape them by themselves.

In the case of linear diselenide **78**, the uptake was lower compared to the cyclic diselenides: a concentration of 50 μM was needed to observe cellular uptake after 1 h incubation (Figure 80I) or an incubation of 2 h at a concentration of 10 μM (Figure 81I). However after 4 h incubation, punctate localization of fluorescence inside the cell could be observed, coming probably from endosomal capture. This observation is in accordance with the observation coming from the thiol-exchange affinity column experiment: when compound **78** reacts with thiols the released selenolate does not stay in close proximity to reform the diselenide bond as it is the case with cycle diselenide **74** or **77**. Therefore the reactivity of **78** is similar than the one of **25** toward thiols and the final localization inside the cell is probably also the same, i.e. endosomes.

Attempts to determine the final localization of the fluorescent probes was performed by colocalization with fluorescent trackers for early endosomes (Figure 83), lysosomes (Figure 84) and mitochondria (Figure 85). However no specific localization of probe **77** could be determined as expected from the CLSM images shown above (Figure 86).

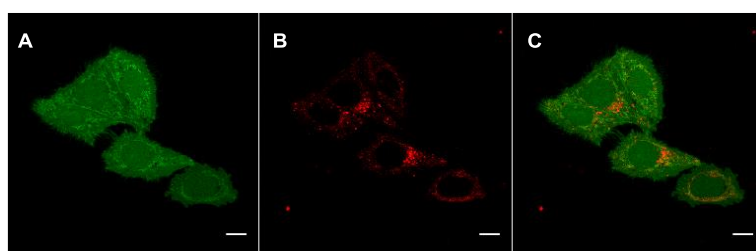


Figure 83. CLSM images of HeLa Kyoto cells incubated with **77** (100 μM) for 2 h and for the last 20 min with Dextran Red (10 μM). Scale bar: 10 μm .

The colocalization with early endosomes was performed using Dextran Red (70 kDa). The tracker was added to the incubation medium for the last 20 min of incubation before washing the cells and taking the CLSM images without fixation. The merge images between **77** (Figure 83A) and dextran (Figure 83B) showed no colocalization (Figure 83C) which was confirmed by a PCC value calculated of 0.38 ± 0.04 (Figure 86, E).

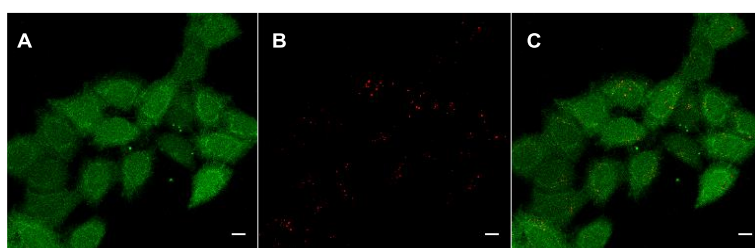


Figure 84. CLSM images of HeLa Kyoto cells incubated with **77** (100 μ M) for 2 h and for the last 40 min with LysoTracker Red (100 nM). Scale bar: 10 μ m.

The lysosomes were localized using LysoTracker Red. The dye was added to the incubation medium for the last 40 min of incubation before to wash the cells and take the CLSM images without fixation. Once again the merge images between **77** (Figure 84A) and fluorescent tracker (Figure 84B) showed no colocalization (Figure 84C). The PCC value calculated was of 0.123 ± 0.005 confirming that **77** is not localized into lysosomes (Figure 86, L).

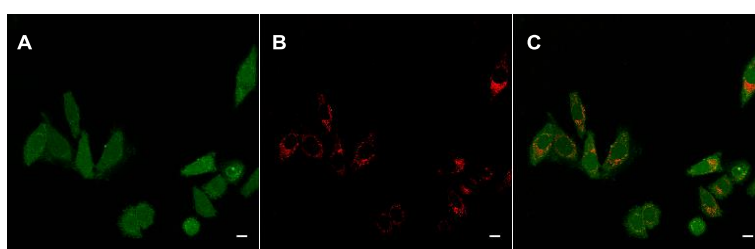


Figure 85. CLSM images of HeLa Kyoto cells incubated with **77** (100 μ M) for 2 h and for the last 20 min with MitoTracker Red (500 nM). Scale bar: 10 μ m.

Finally mitochondria were targeted using MitoTracker Red as colocalization dye. The dye was added to the incubation medium for the last 20 min of incubation before to wash the cells and take the CLSM images without fixation. The merge images (Figure 85C) showed that **77** (Figure 85A) and the fluorescent tracker (Figure 85B) are not colocalized which was confirmed by a PCC value calculated of 0.38 ± 0.02 (Figure 86, M).

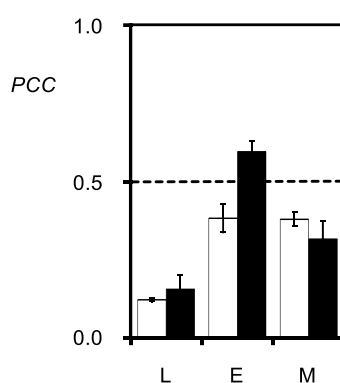


Figure 86. Colocalization of compounds **77** (white) and **74** (black) with lysosomes (L, LysoTracker Red), endosomes (E, Dextran Red) and mitochondria (M, MitoTracker Red), quantified by PCC.

As expected from the CLSM images presented above, the fluorescent probes do not target any specific organelles inside the cell. The only positive response to colocalization was obtained between **74** and early endosomes (Figure 86, E), however the CLSM images tend to demonstrate random localization of the probe.

3.2.4.3. Cytotoxicity Assay

Knowing that the concentration of selenium as to be carefully monitored in cells to avoid cytotoxicity, we decided to determine the cell viability upon incubation with diselenolane probes, especially at high concentration. Therefore the MTT assay was performed to determine the cytotoxicity of **74** and **77**. This assay is based on the transformation of the yellow 3-(4,5-

dimethylthiazol-2-yl)-2,5-diphenyltetrazolium bromide (MTT) into the purple (E,Z)-5-(4,5-dimethylthiazol-2-yl)-1,3-diphenylformazan by mitochondrial reductase (Figure 87). Only cells with a working metabolism can perform this transformation and thus give a read out of the amount of living cells by detecting the formazan product by absorbance at 570 nm.

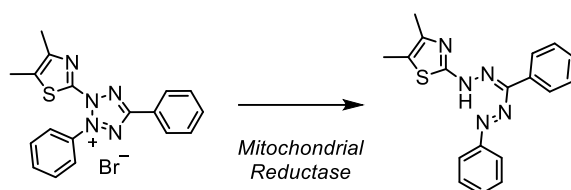


Figure 87. Transformation of MTT into its corresponding formazan by mitochondrial reductase.

After incubation of the probes at different concentrations, the MTT was added to the cell and incubated for 4 h. Then a solution of sodium dodecylsulfate (SDS) in HCl was added to the cell to solubilize the formazan product and incubate for 2 h in the dark. The quantification of the formation of the product was monitored by measuring the absorbance at 570 nm.

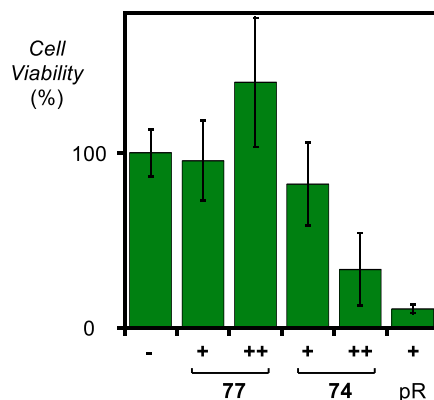


Figure 88. Cell viability from MTT assay with 0 (-, normalized to 100), 10 (+) and 100 μM (++) of **77**, **74** or polyarginine (pR) in HeLa Kyoto cells (mean ± error of five independent measurements).

In order to normalize the results, cells were incubated without any probe and the mean of the absorbance measurements was normalized to a cell viability of 100% (Figure 87, -). Incubation with **77** did not influence the cell viability at a concentration of 10 or 100 μ M. On the other hand with **74**, cytotoxicity was demonstrated with a cell viability around 80% at 10 μ M and only 33% at 100 μ M. Polyarginine (pR) at 10 μ M was incubated with cells as positive control, since it was known to be cytotoxic at this concentration.^[39]

Due to the cytotoxic observed with **74**, further experiments were performed only with probe **77**.

3.2.4.4. *Uptake Inhibition Assay*

As previously demonstrated, **77** can enter into cells and the fluorescence distribution is spread throughout the cell without organelle specificity. In order to understand the exact uptake mechanism, common inhibitors of endocytic pathways were used, in order to determine if an energy-dependent mechanism is required for its uptake. In parallel, oxidation of the thiols of the cell surface using the Ellman reagent **32** was used to determine if the uptake mechanism was thiol-mediated dependent. The fluorescence upon addition of the inhibitors was quantified by flow cytometry (Figure 89).

The uptake inhibitions were normalized against 1 h incubation at 37 °C of **77** at 10 μ M in the absence of inhibitors. When the experiment was performed at 4 °C, a reduction of 65% of the uptake was observed. At this temperature, all the energy-dependent uptake mechanism are turned off.^[193] Therefore it seems that **77** need an energy-dependent pathway in order to enter into cells. However at this temperature, the plasma membrane is rigidified which could influence cellular uptake by passive diffusion as well.^[194] Considering an uptake inhibition up to 80% for dithiolane probes at 4 °C,^[83] passive diffusion of **77** into the cells cannot be totally excluded.

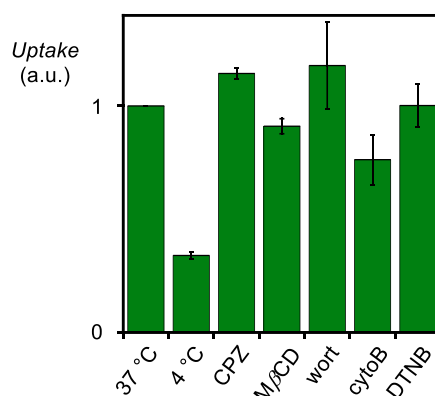


Figure 89. Flow cytometry data for HeLa Kyoto cells that were incubated with **77** (10 μ M) at 37 °C (normalized to 1.0) and 4 °C, and cells that were preincubated with inhibitors of endocytosis (CPZ, m β CD, wort, cytoB) and thiol-mediated uptake (DTNB, 1.2 mM), followed by incubation with **77** at 37 °C. Shown are average values \pm error from three independent measurements.

Common inhibitors of endocytosis such as chlorpromazine (CPZ, clathrin-mediated endocytosis),^[195] methyl- β -cyclodextrin (M β CD, caveola-mediated endocytosis),^[196] wortmannin (wort, receptor-mediated endocytosis)^[197-198] or cytochalasin B (cytoB, actin-dependent phagocytosis and macropinocytosis)^[199] were used in order to determine by which endocytic pathway diselenide **77** is taken up (Figure 89). Unfortunately none of those inhibitors displayed a clear decrease of the uptake of **77**, therefore it remains unclear how the compound is taken up by cell. It is also possible that several pathways are involved at the same time. Therefore inhibition of one pathway can be compensated by the uptake through another.

Using DTNB **32** to oxidize all the exofacial thiols on the cell surface did not decrease the cellular uptake of **77** (Figure 89). This result would point toward a mechanism different than thiol-mediated uptake. However considering the result obtained with the thiol-exchange affinity column (section 3.2.2.1), it is possible that diselenolane **77** and ETP **36** are able to interact with thiols that are

not reactive enough to be blocked by DTNB, explaining the poor inhibition observed for those two compounds in this condition.^[83]

As previously shown, the addition of serum in the incubation medium could delay or reduce the cellular uptake of different probes. We decided to investigate the effect that 10% of FBS in the incubation medium would have on the uptake of **77** (Figure 90).

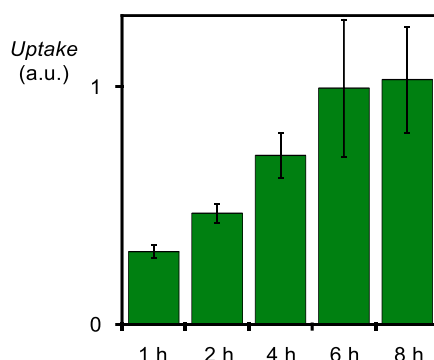


Figure 90. Flow cytometry data for HeLa Kyoto cells that were incubated with **77** (10 μ M) in the presence of 10% serum at 37 °C normalized against 1 h incubation in the absence of serum. Shown are average values \pm error from three independent measurements.

In this case, the uptake was normalized after 1 h incubation of **77** (10 μ M) in the absence of serum in the medium. There was a decreased of the uptake of 70% after 1 h in the presence of serum in the incubation medium. However with increasing incubation time, the uptake increased to reach after 6 h incubation a similar response to 1 h incubation in absence of FBS. Presence of serum in the incubation medium influences once again the uptake kinetic, but with longer incubation time, normal uptake could be observed.

In conclusion, based on the result presented in this section, we can say that diselenolane reacts differently compared to dithiolane previously studied in the Matile group. It was demonstrated indirectly that diselenolanes react with thiols by thiol-affinity column and studying the oxidation rate constant of DTT in

presence of diselenides. However when the mixed thioselenol compound is formed the released selenolate can attack back reforming the ring easily or if the diselenolate compound is released, it can reoxidize by ambient oxygen. In both cases, the diselenolane is reformed after reaction with thiols. The ring closure is so fast that it cannot be observed by absorbance nor by fluorescence.

The diseleno lipoic acid **77** performed better in cellular uptake than the diseleno and dithio asparagusic acids **74** and **25**, making it the best 5-member ring identified so far. The fluorescence was distributed through the whole cell without specific organelle targeting and it displayed a low cytotoxicity even at a concentration as high as 100 μ M. The exact uptake mechanism uptake is not clear for the moment. Common endocytosis inhibitors did not reduce the uptake, but incubation at 4 °C inhibited it to 35% of its value at 37 °C pointing toward an energy-dependent pathway. Oxidation of exofacial thiols by DTNB did not decrease the uptake of **77**. A possible hypothesis would be that the probe can react with thiols on the cell surface that are beyond the reach of the Ellman reagent, and therefore are not inhibited in this condition. The linear diselenide **78** showed a very similar uptake as **25**, with punctate localization inside the cells, probably endosomes. This observation was in agreement with the results observed from the thiol-exchange affinity column: once the compound react with thiols, the selenol is released without staying in close proximity to reform the diselenide bond which appears essential to escape endosomal capture.

3.3. Activation of Polyarginine

Polyarginine (pR) are part of the cell-penetrating peptides (CPPs). Those polymers have the ability to cross the plasma membrane with cargoes and are extensively studied since their discovery in the late 1980's. However it has been demonstrated that small pR such as octaarginine cannot escape the endosomal pathway when they are incubated alone.^[36] In order to get

cytoplasmic release of such kind of polymers, activators are needed. The only potent activator successfully discovered is the 4-(1-pyrenyl)-butyric acid in its deprotonated form (**1**) and is nowadays known as the pyrenebutyrate trick.^{[34],[36]} The preincubation of membrane with **1** lead to an increase in activity of pR in model membrane and ensure cytoplasmic delivery into HeLa Kyoto cells. This method showed also some promising results for protein transduction in transdermal activity.^[38]

Originally, we wanted to determine if the pyrenebutyrate trick could be applied to short cell-penetrating poly(disulfide)s (CPDs) that have been demonstrated to get mainly trapped into endosomes (Figure 16).^[59] Since small polyarginine could escape endosomal capture using this trick, we thought it would be the same for small CPDs, and have ultimately cytoplasmic delivery. However this method showed to be unsuccessful to increase the uptake and localization in the cells for our CPDs.

Therefore we turn again to the delivery of polyarginine but this time optimizing the activator so that it could stabilized both the positive and the negative charges at the same time on the same surface.

3.3.1. Design

Pyrenebutyrate is simply a carboxylate group that can interact with the guanidinium group of the arginine, linked to an aromatic surface. This π -surface could probably be involved to stabilize the cation by the well-known cation- π interaction^[200] and increase the hydrophobicity of the whole system to enable it to pass through the membrane by passive diffusion. More recently it was successfully demonstrated that by using electron poor aromatic surface, anion could be stabilized: the now called anion- π interaction.^[201] This new exotic interaction have been successfully applied in transport of halogen^[202] and catalysis involving an anionic transition state such as enamine addition to nitroolefins^[203-204] or iminium/nitroaldol cascades.^[205]

In order to stabilize both the positive and negative charges on the same π -surface, it has to be tuned to have a part π -basic and another π -acid at the same time. Therefore we decide to use the 4-amino-1,8-naphthalimide (ANI) scaffold where the amine in the 4 position act as an electron donor while the imide as an electron acceptor, creating a push-pull system which leads in a polarization of the π -electron above the surface and a dipole moment (Figure 91). This type of

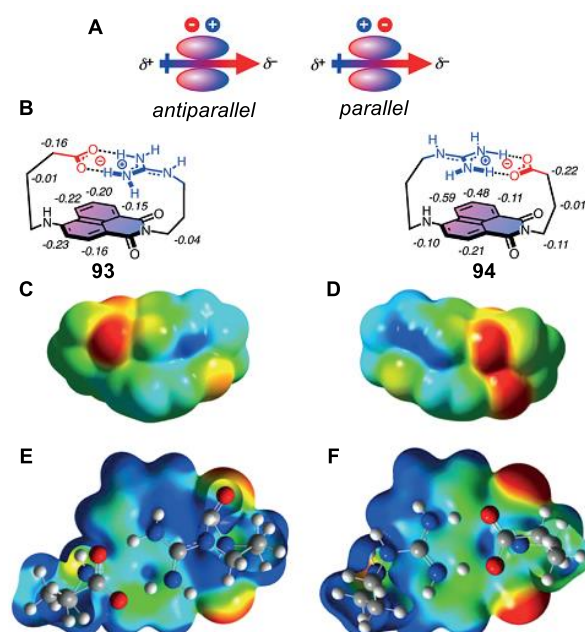


Figure 91. Schematic representation of the ion pair- π interaction on push-pull chromophores. (A) Definition of antiparallel or parallel ion pair- π interactions in comparison to the push-pull component of the ground-state dipole moment (arrows). (B) Covalent positioning of antiparallel or parallel ion pair- π interactions in **93** and **94**, with indication of changes in chemical shifts ($\Delta\delta$, in ppm) in the ^1H NMR spectra in response to deprotonation of the conjugate carboxylic acids (DMSO- d_6 , 25 °C). (C – F) Electrostatic potential surfaces of complete ground state structures (C, D) and π -surfaces only (E, F) for antiparallel ion pair- π interactions in **93** (C, E) and parallel ion pair- π interactions in **94** (D, F). Red: negative, blue: positive, isovalue 0.0004 au/ \pm 30 kcal mol $^{-1}$. Images from reference.^[206]

surface have been shown to have the ability to stabilize ion-pairing on the top of their surface by computational and NMR studies.^[206-207]

To compare the effect of the stabilization of the ion-pairing on the π -surface, the two possible orientations have been synthesized. The first is the antiparallel version **93** (Figure 91) where the dipole moment of the surface is in the antiparallel orientation compared the ion-pairing, meaning that the anion is sitting on the π -electron rich part of the surface and the guanidinium on the π -electron poor part of the surface; and the parallel version **94** (Figure 91) where the dipole moment of the surface is in the same direction as the ion-pairing orientation, meaning that the carboxylate sit on the top of the π -acidic part of the surface while the guanidinium sit on the π -basic part of the surface.

According to NMR and computational studies, the parallel orientation **94** have the perfect orientation for the stabilization of the ion-pairing on the top of the surface while the stabilization is weaker in the antiparallel configuration **93** due to probable repulsion from the π -surface.^[206]

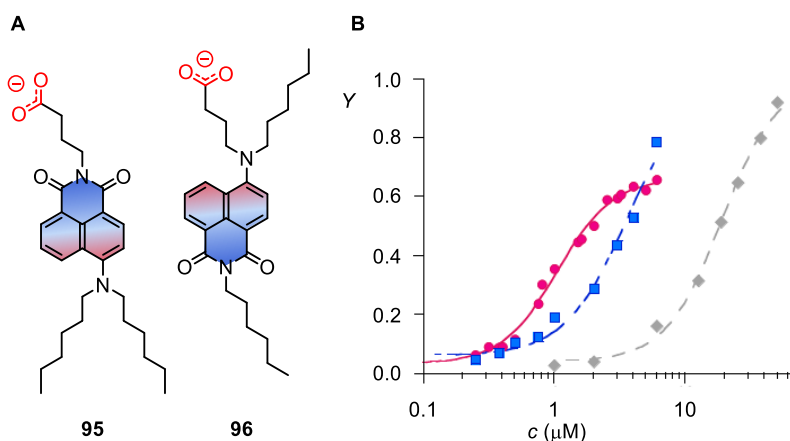


Figure 92. (A) Structures of transporters **95** and **96** developed for activation of polyarginine. (B) Dependence of transport activity Y on the concentration (c) of **95** (●), **96** (■) and **1** (◆) in the presence of pR (250 nM) and fitted with Hill equation. Image from reference.^[207]

By changing slightly compound **93** or **94** to have only the carboxylate directly linked to the ANI surface, it was demonstrated by NMR that the system could bind free guanidinium and stabilize the ion-pairing on the π -surface.^[207] Moreover preliminary results showed that compound **95** and **96** (Figure 92A) could act as activators for the transport of pR into model membrane with the parallel orientation **95** being more active than the antiparallel **96**. The effective concentration to reach 50% activity (EC_{50}) calculated was lower than for the pyrenebutric acid **1** for both transporters.

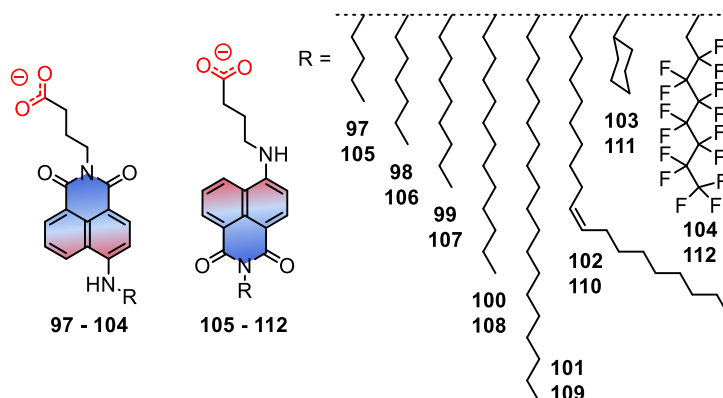


Figure 93. Structures of amphiphiles tested as activators of pR with different alkyl tails used.

Encouraged by those results, we decided to investigate deeper into the ANI core as activator and optimize the transporter to achieve the best membrane activity for pR. In order to have a better push-pull system, we turned toward a secondary amine instead of the tertiary amine in **95** and **96**. In addition, the presence of only one alkyl chain would help for a better incorporation of the probe into the membrane, and the comparison between parallel (**97 – 104**) and antiparallel (**105 – 112**) orientations would be more evident (Figure 93). The influence of the alkyl tail was tested by changing its length, ranging from a 4-carbons to 18-carbons alkyl chains (**97 – 101**, **105 – 109**), introducing an

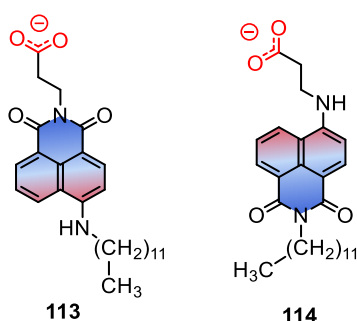


Figure 94. Structures of amphiphiles **113** and **114** with a shorter carboxylate linker tested as activators of pR.

unsaturation (**102**, **110**), a cyclic alkane (**103**, **111**) or a perfluorinated alkyl chain (**104**, **112**). The different amphiphiles were synthesized by Dr. Kaori Fujisawa in our group starting from the commercially available 4-bromo-1,8-naphthalene anhydride. The detail of the synthetic procedures is reported in reference.^[166]

It has been reported that a four atom linker between the ANI and the carboxylic group could form an ideal Leonard turn to place the anion on the top of the π -surface.^[208] In order to control the influence of the linker, analogues of **100** and **108** were synthesized with a three atom linker **113** and **114** respectively (Figure 94).

In addition to the ANI derivatives presented above, we decided to look at the activation of pR using fatty acid derivatives since a report from Cardoso and co-workers studied the importance of fatty acids and pH dependence for the cellular uptake of guanidinium-rich molecules.^[209] They demonstrated that adding fatty acids on cells and incubation in slightly basic conditions, the polyarginine are better uptaken by cells due to a forced ion-pairing of the carboxylate with cations of the peptide. Therefore we decided to investigate the influence that would have the addition of perfluorinated fatty acid on the uptake of pR.

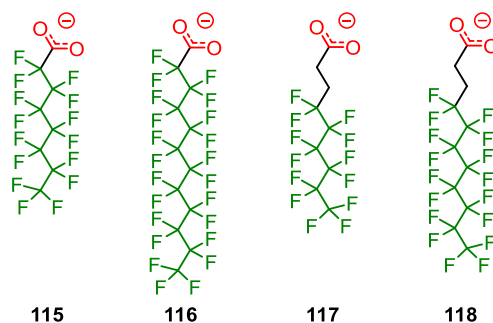


Figure 95. Structures of the perfluorinated fatty acids **115** – **118** tested as activators of pR.

For this experiment, we collaborated with Prof. Metrangolo and Prof. Resnati from Politecnico di Milano, who provided the perfluorinated fatty acids **115** – **118**. We investigated two different sizes of alkyl tail, an octanoic acid (**115**) and a dodecanoic acid (**116**), to test the difference in membrane insertion. In addition perfluorinated alkyl tail lacking the fluoride on two carbons adjacent to the carboxylic acid (**117** and **118**) were tested to determine if the potential increase of uptake of pR is due to a difference in pK_a of the acidic protons.

3.3.2. Solution Studies

The ability of compounds **105** – **118** to activate pR was tested first on model vesicles by the CF-efflux assay. In parallel, the absorbance of the ANI probes in membrane was tested because this scaffold have been shown to be solvatochromic.^[206-207] Therefore a shift in the absorbance of the different probes should be related to the insertion of the activator into the membrane.

3.3.2.1. CF-Efflux Assay

In the CF-efflux assay, carboxyfluorescein (CF) is encapsulated inside EYPC large unilamellar vesicles (LUVs) at a concentration of 50 mM which is high enough to ensure self-quenching of the dye. Upon the addition of an

efficient transporter and pR ($M_w = 5 - 15$ kDa), there is a transport a CF from inside the LUVs to its surrounding solution which reduces the local concentration of the dye, leading to an increase of the fluorescence.

The fluorescence recovery was monitored as a function of time. The baseline corresponds to the initial fluorescence of LUVs alone in solution, followed by the additions of the activator after 50 s, pR after 100 s and finally destruction of the vesicles for calibration using detergent after 500 s (Figure 96A). The increase of fluorescence upon addition of the activator without the CPP signicate that the probe acts as a detergent which was the case for most of them at high concentration. Therefore the concentration dependence was monitored at sublytic concentration.

The intensity $I(t)$ of an activator at a given concentration was determined by normalizing the time dependent curve I_t between the baseline I_0 of the initial

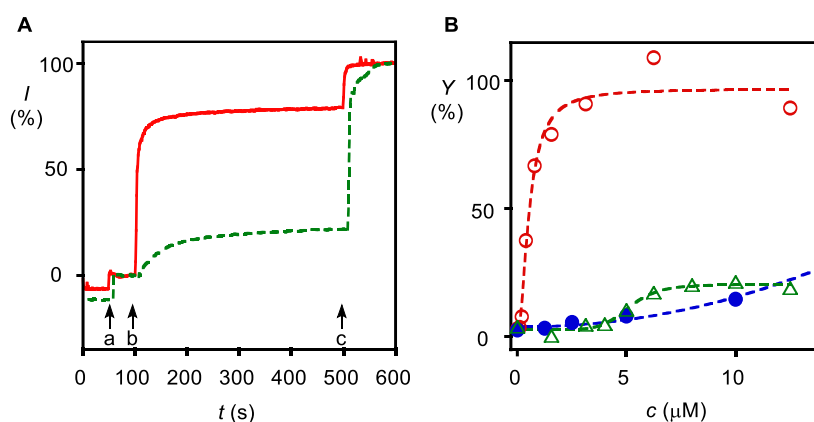


Figure 96. (A) Example of CF-efflux assay fluorescence recovery upon addition of activators **100** (red, solid) and **116** (green, dashed) after 50 s (a), and pR (250 nM) after 100 s (b), before lysis of LUV by excess of Triton X-100 after 500 s (c) for final calibration. (B) Dependence of the final activity Y of pR before LUVs lysis in function of the concentration of **100** (\circ), **108** (\bullet) or **116** (Δ) with curve fit to Hill Equation 4.

LUVs fluorescence and the maximal fluorescence obtained upon lysis of the vesicles I_{∞} using Equation 3.

$$I(t) = \frac{(I_t - I_0)}{(I_{\infty} - I_0)} \quad \text{Eq. 3.}$$

By taking the $I(t)$ value before the addition of the detergent which corresponds to the activity Y_{\max} and by varying the concentration (c) of the activator, the Hill analysis can be applied to determine the EC_{50} and Hill coefficient (n) of each activators using Equation 4 (Figure 96B).

$$Y = Y_0 + \frac{Y_{\max} - Y_0}{1 + (EC_{50}/c)^n} \quad \text{Eq. 4.}$$

The different curves of activity in function of the concentration of activator are reported in section 5.3.1.7 along with their Hill curve fits. The values of the Hill analysis are reported in Table 5 and a graphical representation of the maximal activity and the EC_{50} of each activator in function of the hydrophobicity of the probe ($\log P$, estimated from ChemDraw software) are represented in Figure 97.

Table 5. Characteristic parameters for pR activators in model membrane determined by Hill analysis.^a

Activators ^b	Y_{\max} (%) ^c	EC_{50} (μM) ^d	n ^e	$\log P$ ^f
1^g	78 ± 2	44 ± 2	2.2 ± 0.2	4.68
95^h	61 ± 4	1.05 ± 0.05	2.1 ± 0.2	6.26
96^h	75^i	3.6 ± 0.2	1.8 ± 0.2	6.26
97	9	inactive		2.56
98	87 ± 3	6.2 ± 0.2	3.8 ± 0.6	3.40
99	66 ± 2	1.18 ± 0.07	2.4 ± 0.3	4.23
100	97 ± 5	0.54 ± 0.09	1.8 ± 0.5	5.90
101	21 ± 3	6 ± 1	1.3 ± 0.2	8.40
102	27 ± 1	2.6 ± 0.2	1.9 ± 0.2	8.08

103	59 ± 3	30 ± 1	4.4 ± 0.7	2.87
104	70 ± 10	0.31 ± 0.08	1.8 ± 0.7	5.92
105	3	inactive		2.56
106	58 ⁱ	19 ± 1	3.0 ± 0.6	3.40
107	36 ⁱ	15 ± 3	1.9 ± 0.7	4.23
108	14	inactive		5.90
109	19 ± 1	3.5 ± 0.1	2.8 ± 0.2	8.40
110	33 ± 9	30 ± 8	4 ± 3	8.08
111	12	inactive		2.87
112	25	inactive		5.92
113	68 ± 4	1.2 ± 0.2	4 ± 1	5.62
114	32 ⁱ	28 ± 1	2.3 ± 0.2	5.62
115	21 ± 1	61 ± 8	5 ± 4	4.46
116	21 ± 1	5.1 ± 0.3	8 ± 2	6.87
117	7	inactive		3.90
118	14	inactive		5.11

^aDetermined using Equation 4. Hill analysis were not applied to those with low Y_{\max} values. Errors are from curve fit. ^bSee Figures 5, 92 – 95. ^cMaximal activity. ^dEffective concentration to reach 50% activity of Y_{\max} . ^eHill coefficient. ^fEstimated by ChemDraw Professional software (16.0.1.4). ^gFrom reference.^[34] ^hFrom reference.^[207] ⁱMaximum observed Y before onset of the detergent effect. Hill analysis were made assuming $Y_{\max} = 100\%$.

For most activators, their EC_{50} value could be determined however for some of them, no recovery in fluorescence in the CF-efflux assay was measured and they were therefore set as inactive. However the EC_{50} is not the only parameter that has to be taken into account to determine if an activator is potent. It needs to have also a reasonable maximal activity Y_{\max} . For example activator **116** have a relatively good $EC_{50} = 5.1 \pm 0.3 \mu\text{M}$ whereas the Y_{\max} was only of 21%. Therefore this activator cannot be considered as potent in this experiment. An

$Y_{\max} \geq 50\%$ (Figure 97A, grey line) and an $EC_{50} \leq 10 \mu\text{M}$ (Figure 97B, grey line) were arbitrarily defined as the minimum values for potent activity.

Pyrenebutyrate **1** was taken as a benchmark with an excellent $Y_{\max} = 78 \pm 2\%$ and a relatively high $EC_{50} = 44 \pm 2 \mu\text{M}$ (Figure 97, \diamond).^[34] Most of the parallel activator had a good Y_{\max} (Figure 97A, \circ) except for the extremely short (**97**) or long alkyl tail (**101** and **102**) making a bell shaped curve in function of the hydrophobicity of the compound. An exceptional $Y_{\max} = 97 \pm 5\%$ was found for **114** while all other are around 70%. The EC_{50} for the parallel series (Figure 97B, \circ) showed that most of the activator are active except for the smaller alkyl tail in **95** and **97**. The general trend is also a bell shaped curve with the EC_{50} increasing again for longer alkyl tail. **102** and **104** displayed an impressive submicromolar EC_{50} for the activation of pR.

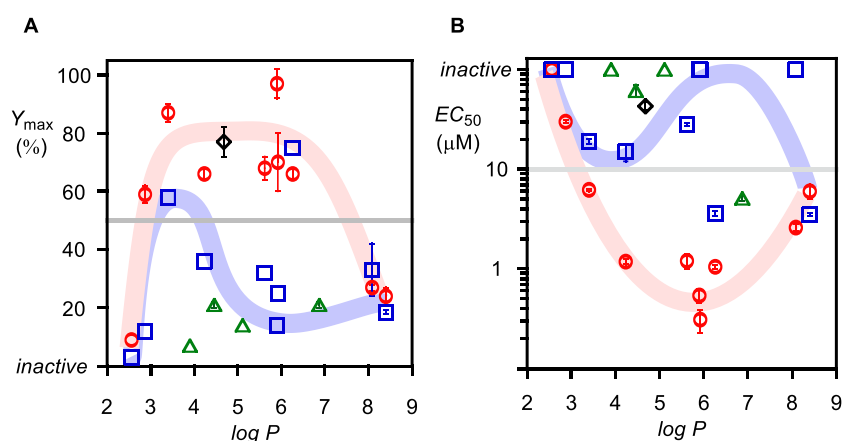


Figure 97. (A) Maximal activity Y_{\max} and (B) effective concentration EC_{50} in model membrane as a function of the hydrophobicity of the pR activators from Hill analysis of dose response curves. Antiparallel series: \square , parallel series: \circ , perfluorinated fatty acids: \triangle , pyrenebutyrate: \diamond .

On the other hand, the antiparallel series were essentially inactive. Nearly all the Y_{\max} were under the 50% limit for good activity (Figure 97A, \square) except **96** and **106** with calculated values of 75% and 58% respectively. These exception may be explained considering the structure of the two activators. **96**

contains an alkyl chain at each end of the ANI core which disturbs its amphiphilicity and have a weakened push-pull system due to the presence of the tertiary amine. Despite its relatively good Y_{\max} , **106** showed a poor EC_{50} of $19 \pm 1 \mu\text{M}$ as all the antiparallel activators with the exception of **96** (Figure 97B, \square).

Those results are in accordance with a stabilization of the ion-pairing above the π -surface in the case of the parallel orientation of the dipoles while ionpair- π interaction is absent in the antiparallel version leading to a poorer activity in transport of pR. The control activator **113**, with a shorter linker, displayed a smaller activity than expected from its hydrophobicity with an EC_{50} of $1.2 \pm 0.2 \mu\text{M}$ consistent with a mismatch of the ion-pairing on the π -surface.

The perfluorinated fatty acid **115** – **118** all showed poor activities in the CF-efflux assay independent of their chain length and carboxylate basicity, with Y_{\max} far from the 50% threshold (Figure 97A, Δ) and high EC_{50} (Figure 97, Δ) except in the case of **116**. This indicates that the hybrid **104** behave more like ionpair- π activator than fluorous activator in this assay.

The Hill coefficient were more difficult to interpret since it should demonstrate the cooperativity of the system but depends also on the stability of the formed complex. Overall the Hill coefficients are smaller than expected considering the number of guanidinium cations that are present on the pR. They are higher with smaller alkyl tail (**98**, **103**) or shorter linker (**113**).

3.3.2.2. Absorbance of the ANI in presence of vesicles

Since the ANI core unit has a specific absorbance and it was shown that the maximal wavelength of absorbance shifted in the function of the polarity of the solvent,^[206–207] we were interested to see if the burial of the probe into vesicles membrane could be determined by absorption. To do this, we tested the library of compounds with different alkyl chain lengths which should make the ANI

more or less buried into the hydrophobic lipid membrane in function of the predicted $\log P$ of the system.

EYPC-LUVs were formed with exactly the same buffer in and outside of their membrane, and without the presence of any encapsulated dye. The activator was added at a fix concentration (3 μM) to a fix amount of LUVs, and the absorbance was recorded. The maximal absorbance wavelengths for each activator are reported in Figure 98 as a function of their $\log P$ (Table 5). The absorbance and fluorescence spectra can be found in section 5.3.5.

The absorption maxima did not vary greatly with increasing hydrophobicity, however a clear trend can be observed. With increasing $\log P$, the absorption wavelength shifted from about 460 nm to 430 nm. This blue shift suggests a deeper burial of the ANI core into the membrane of the vesicle.^[207] The parallel and antiparallel series displayed similar trends showing that the difference observed in the previous section is not due to a difference in the partition of the probe into the vesicular membrane, but because of the orientation of the dipole moment.

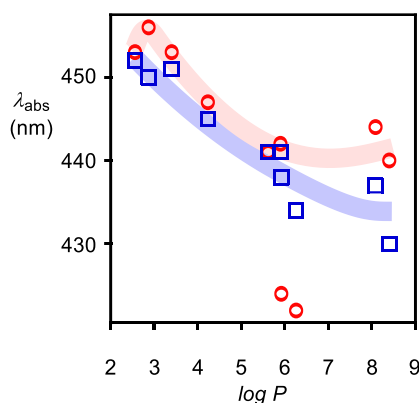


Figure 98. Maxima in absorption spectra of ANI activators in empty EYPC-LUVs. Antiparallel series: □, parallel series: ○.

Two significant exceptions were observed with **95** and **104**. There is a hypochromic effect of about 20 nm from the value expected according to their log *P*. This shift probably originates from a twisted push-pull system in the case of **95**; whereas for **104** it may be due to self-assembly of the perfluorinated alkyl chain rather than a deeper partitioning into the membrane lumen.

3.3.3. Cellular Uptake

The cellular uptake was then assessed. In this case, an octaarginine was synthesized by solid-phase peptide synthesis with the help of Jacques Saebach from the group of Prof. Nicolas Winssinger of the University of Geneva. The peptide was then labelled with a cyanine 5 dye (Cy5) to lead to **119**. This fluorophore was chosen to track the final localization of the peptide inside the cells instead of CF as in previous studies, because of its absorbance and fluorescence (λ_{ex} : ~650 nm, λ_{em} : ~670 nm) are far red shifted compared to the ANI core (λ_{ex} : ~450 nm, λ_{em} : ~520 nm).

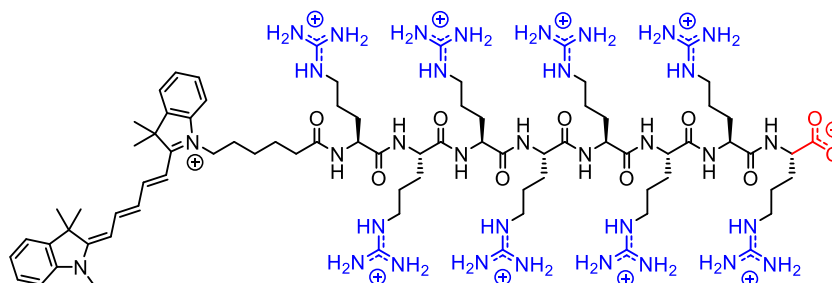


Figure 99. Structure of the Cy5-R₈ **119** used in cellular uptake experiments.

Cellular uptake was evaluated by CLSM with the most promising activators identified in the CF-efflux assay: **100** and **104**. As a control their antiparallel version **108** and **112** were also tested as well as Cy5-R₈ **119** alone. The concentration of **119** was fixed at 1 μM , a concentration low enough to avoid cell apoptosis.^[39] The cells were first treated with the activator solution in Leibovitz's medium for 5 min before the addition of **119** and incubated for

further 15 min at 37 °C. The concentration of activator used was 10 μ M since at 20 μ M cellular toxicity could be observed. The cells were washed with a heparin solution to remove potential electrostatic binding of the peptide on the mainly negatively charged cell membrane.

When the cells were treated with **119** in the absence of activator, the fluorescence was localized in punctate location, characteristic of endosomal capture (Figure 100) as expected from previous studies.^[36] The overall fluorescence intensity was rather weak with nearly no cytoplasmic release.

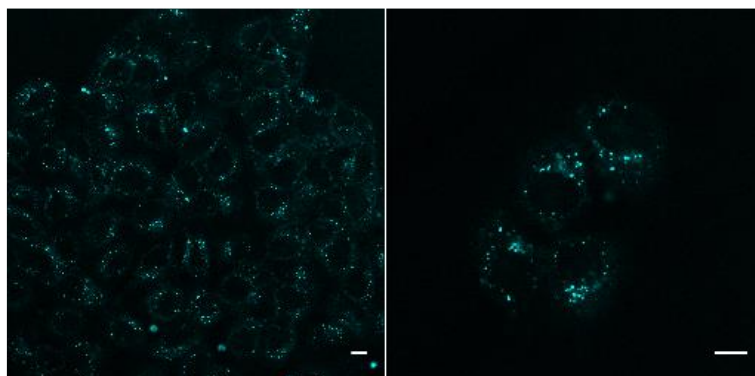


Figure 100. CLSM images of HeLa Kyoto cells incubated with **119** (1 μ M) for 15 min. Scale bar: 10 μ m.

When cells were preincubated with **100**, different populations were observed (Figure 101A). In the first population, only punctate location was observed as if the presence of the activator did not influence the uptake of peptide **119**. On the other hand, in the second population, there was a strong increase of fluorescence in the whole cell with the exception of the nucleus (Figure 101A). There was also an in-between population where the fluorescence inside cells was increased with some cytoplasmic delivery, but otherwise mainly in dotted localization, probably endosomes. In the presence of the antiparallel activator **108** (Figure 101B), only punctate endosomal capture

fluorescence was observed, like in control experiment with peptide **119** alone (Figure 100).

Similar cellular distribution was observed with probes **104** and **112** (Figure 102). The parallel perfluorinated ANI displayed the two population types: one with a strong uptake and a stain of the whole cell, a second one similar to the uptake of the peptide alone. On the other hand, the uptake with the antiparallel version was nearly exclusively as the one displayed by the peptide **119** in the absence of transporter.

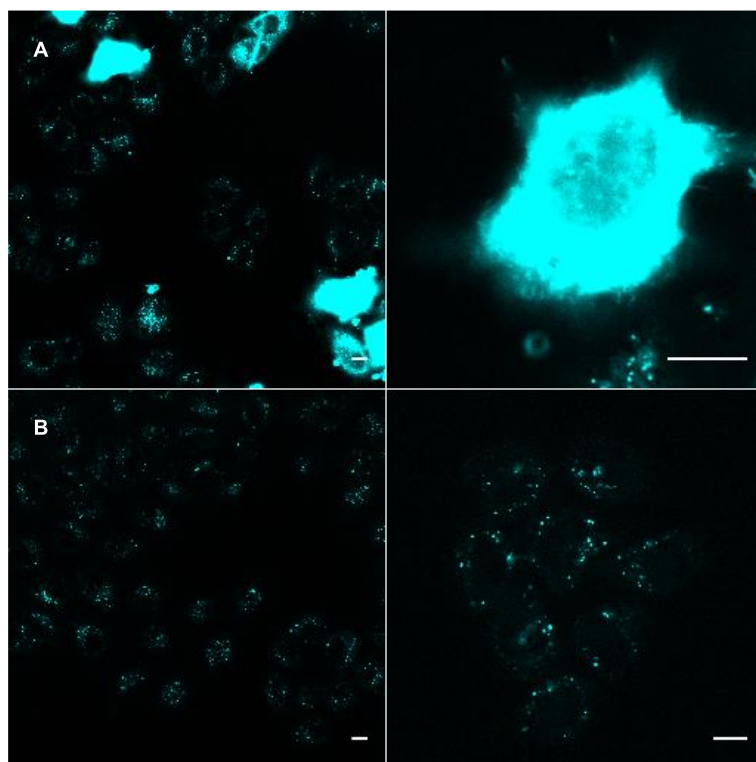


Figure 101. CLSM images of HeLa Kyoto cells incubated with **119** (1 μ M) for 15 min with preincubation with **100** (A) and **108** (B, 10 μ M each) for 5 min. Scale bar: 10 μ m.

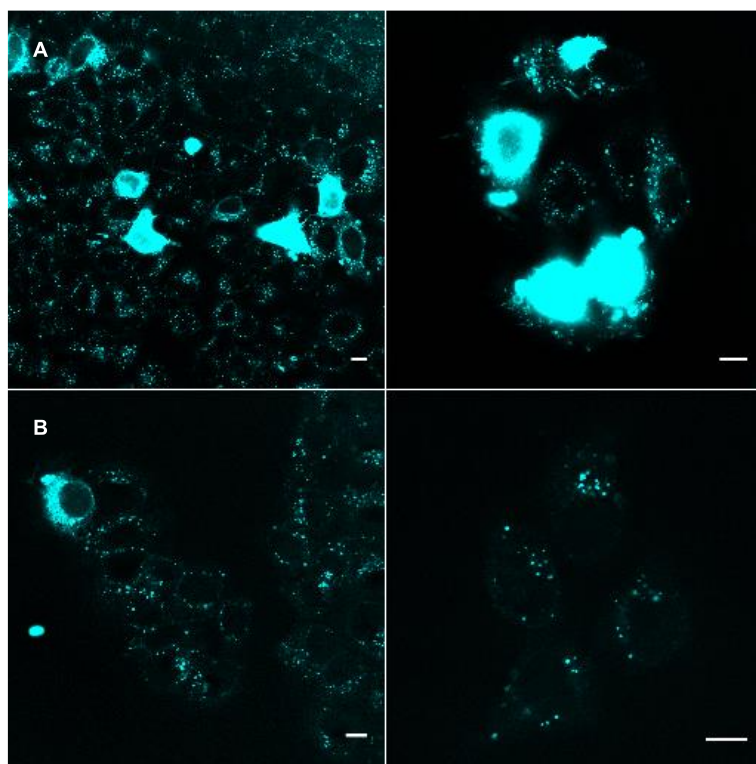


Figure 102. CLSM images of HeLa Kyoto cells incubated with **119** (1 μ M) for 15 min with preincubation with **104** (A) and **112** (B, 10 μ M each) for 5 min. Scale bar: 10 μ m.

Those results confirm the ones obtained with the CF-efflux assay. The uptake of the Cy5-R₈ **119** is higher with a parallel orientation of the dipole moment whereas the antiparallel ionpair- π activator does not increase the uptake and thus stabilize in a less effective manner the electrostatic interaction.

Controls experiments were performed to demonstrate that the observed fluorescence is indeed due to the fluorophore on the peptide and not due to the ANI core (Figure 103). Therefore, the different activators were incubated in Leibovitz's medium for 20 minutes at 37 °C without the addition of **119**, and

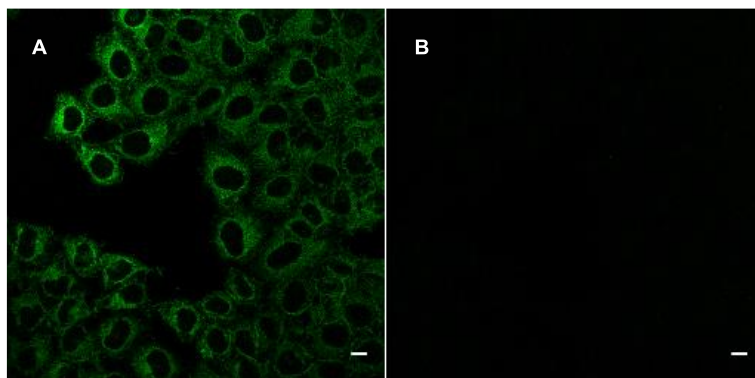


Figure 103. CLSM images of HeLa Kyoto cells after 20 min incubation with activator **108** (10 μ M) in Leibovitz's medium at 37 °C. (A) λ_{ex} 458 nm and λ_{em} 500 – 541 nm, (B) λ_{ex} 633 nm and λ_{em} 650 – 700 nm. Scale bar: 10 μ m.

the fluorescence was checked between 500 nm and 541 nm upon excitation at 458 nm for the ANI core, and between 650 nm and 700 nm upon excitation at 633 nm for the Cy5 channel (Figure 103). Weak fluorescence for the ANI was observed indicating that the activator can indeed insert into the cellular membrane and get internalized probably by endocytosis (Figure 103A). However no fluorescence was detected in the Cy5 channel indicating that the fluorescence observed above is indeed due to the uptake of **119** into cells and not from residual fluorescence of the transporter itself.

The presence of the two populations is not well understood yet. A possible explanation could be a difference in the cell cycle which could influence the uptake. However no additional experiment has been performed to issue this observation.

Additional experiments were performed with decreasing the concentration of activator to 5 μ M leading to CLSM images similar to the control (Figure 100), or with increasing the concentration of **119** to 5 μ M leading to cellular death confirming previous studies on cytotoxicity of pR.^[39] Therefore the

concentrations were fixed for further experiments at 10 μM of activator and 1 μM of Cy5-R₈ **119**.

Based on the results with perfluorinated ANI **104** and the increased population with good uptake compared to **100**, we decided to investigate also the cellular activity of the perfluorinated fatty acids **115** – **118** despite their poor efficiency in the CF-efflux assay (Figure 104). The two types of perfluorinated fatty acids were studied to determine if the potential efficiency in cellular uptake originated from a self-assembly of the activator in the

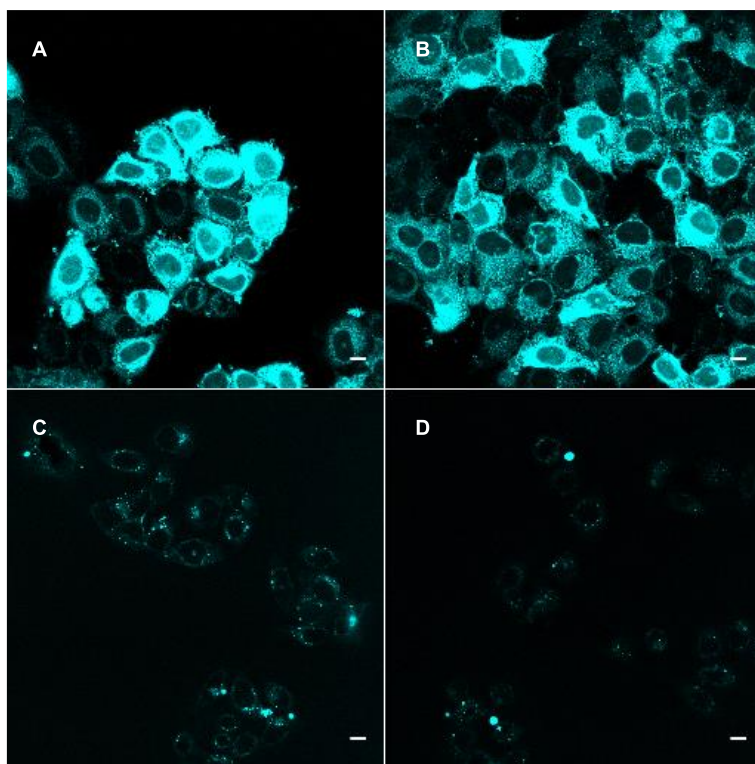


Figure 104. CLSM images of HeLa Kyoto cells incubated with **119** (1 μM) for 15 min with preincubation with **115** (A), **116** (B), **117** (C) and **118** (D, 10 μM each) for 5 min. Scale bar: 10 μm .

membrane increasing their local concentration, or a difference in the pK_a of the acidic proton.

Two very distinct uptake behaviors were observed between the fully perfluorinated fatty acids **115** and **116**, and the polyfluorinated acid **117** and **118**. Activators **115** (Figure 104A) and **116** (Figure 104B) provided a clear increase in cellular uptake of **119** compared to the peptide alone. The CPPs remained mainly in the cytoplasm or in punctate locations that are probably endosomes excluding totally the nucleus of the cells. In the case of activator **117** (Figure 104C) and **118** (Figure 104D), the peptide remained only in punctate location as in control experiment in absence of activator.

This observation was rather unexpected from the CF-efflux assay since all the perfluorinated fatty acids showed only poor pR activation. In order to explain this result, we postulated that the mechanism by which the perfluorinated fatty acids activate CPPs in cellular uptake, is not only due by self-assembly into the membrane of the cell but also by a repulsion-driven ion-pairing interaction.

In this theory, the unique propriety of the perfluorinated alkyl chain to form self-assembly will bring the negatives charges of the acid in close proximity. In order to avoid charge repulsion, protonation could occur on strongly basic bundles of anion (Figure 105A). However for more acidic bundle of anion, the charge-repulsion has to be overcome by binding with counterions (Figure 105B). It is exactly the same as comparing polylysine with polyarginine: the proximity of ammonium groups in polylysine decrease their pK_a for charge neutralization by protonation while the more basic guanidinium groups in pR remain charged despite charge proximity and need electrostatic interaction with counterion for charge neutralization. This phenomenon is known as the “arginine-magic” (see section 1.2.1).^[210] There are already numerous examples

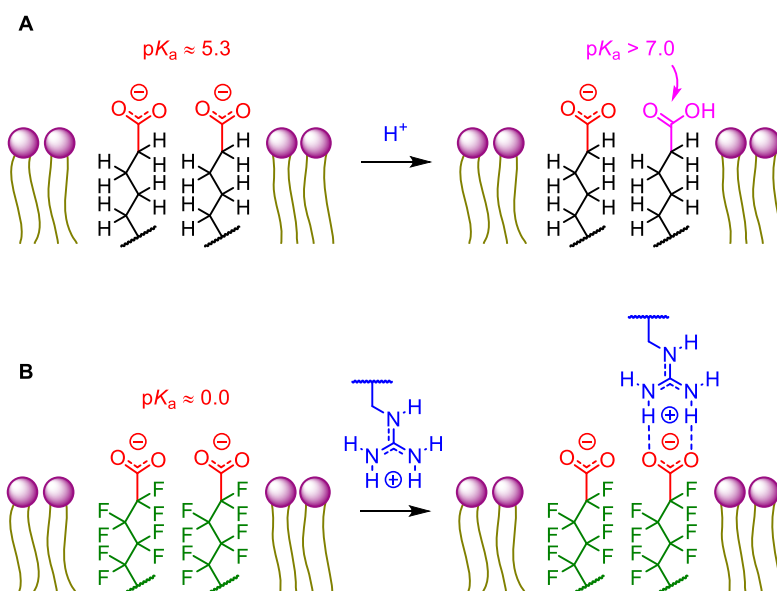


Figure 105. Schematic representation of the protonation of strongly basic anionic bundle by increase of nearby pK_a (A) and repulsion-driven ion-pairing of weakly basic anionic bundle (B) to compensate charge repulsion.

in the literature of this kind of interaction. It is indeed the basic principle of DNA and RNA delivery where the oligophosphodiester bind to cationic transporter to form lipoplexes.^[211-212]

In our case the lack of fluorine on the proximal carbon next to the carboxylic acid in **117** and **118** increase the basicity of the carboxylate making them prone to protonation (Figure 105A), which decrease their ability to activate CPPs in cellular uptake. This is consistent with the observation of Cardoso and co-workers, in which they demonstrate higher uptake in basic conditions upon addition of fatty acid.^[209] By raising the pH in the incubation medium, fatty acids cannot undergo protonation but avoid charge repulsion by ion-pairing with the CPPs, leading to their uptake into cells.

On the other hand, the fully perfluorinated fatty acids **115** and **116** display the perfect combination between self-assembly and acidity of the carboxylic

acid, which makes them perfect candidates to transport CPPs by repulsion-driven ion-pairing (Figure 105B), through plasma membrane even at physiological pH. The drawback might be that such a strong interaction would make difficult the release of the cationic peptide even inside the cell despite the abundance of polyanions in the cytoplasm. This would explain why in the cellular experiment, it is mainly membranes that are stained, and also the poor activity of those probe in the CF-efflux assay. In this experiment it is indeed the CF-efflux that is monitored. However it was shown that the efflux occurs via counterion exchange between the anionic CF and the pR-activator complexes.^{[28],[213]} While it is unproblematic with ANI probes due to weaker ion-pairing between the guanidinium and the carboxylate group, the problem arise with the perfluorinated fatty acid since the electrostatic interaction is so strong that the exchange is difficult to occur with the intravesicular CF. Therefore the efflux does not occur in this case and the activators seem inactive.

Encouraged by the results presented here, we decided to try to increase the uptake of short CPDs with activators **100**, **104**, **115** and **116** as previously attempted with pyrenebutyrate **1**. However no increase in activity nor different cellular localization were observed in model membrane or in cellular uptake.

In conclusion, two different types of activators were found in this study. The first activators are based on an ANI core for the stabilization of the ion-pairing on the top of its surface. The influence of the alkyl chain for membrane insertion was studied to find the best hydrophobicity for activation of pR in model membrane: the dodecyl chain and a perfluorinated alkyl tail. In model membrane, it was determined that the parallel orientation of the dipole is necessary to have good activity while the antiparallel one where the ion-pairing is not stabilized, are essentially inactive. Cellular uptake of **119** with **100** and **104** showed mainly two populations: one where the whole cell is stained with

the exception of the nucleus, the other were the distribution is similar to the one with the peptide alone.

The second activators are based on perfluorinated fatty acids. The activity in model membrane was low for all probes tested. However cellular uptake demonstrated a large increase of the uptake of **119** for fully perfluorinated fatty acids **115** and **116**. In the case of **117** and **118** where the fluorine are missing next to the carboxylate, no increase of the uptake was noticed. Those results lead us to postulate that **115** and **116** activate **119** by a strong repulsion-driven ion-pairing interaction to deliver the peptide inside the cell staining mainly the membrane, and explaining the poor activity observed in model membrane.

Chapter 4

PERSPECTIVES and CONCLUSION

In the first part of this thesis, the strained cyclic disulfides developed in our group were successfully adapted from the delivery of small fluorophores and peptides, to the delivery of liposomes and polymersomes. Small amphiphilic molecules could be directly added to preformed vesicles to increase successfully their cellular uptake.

Other thiol responsive heads currently investigate in our group could be interfaced with the delivery of vesicles such as thiosulfi(o)nate **120** or *o*-benzopolysulfanes **121** (Figure 106).

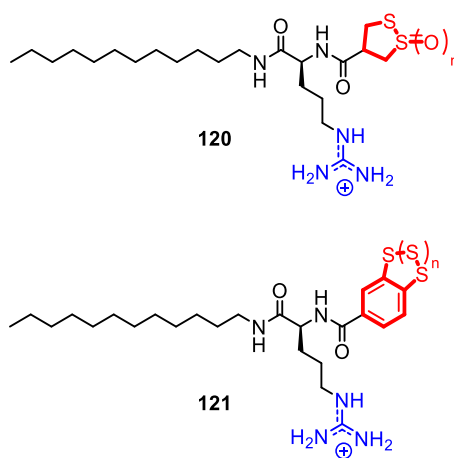


Figure 106. New transporters for thiol-mediated uptake of vesicles: thiosulfi(o)nate **120** and *o*-benzopolysulfanes **121**.

The delivery of liposomes by the thiol-mediated uptake have been only tested on HeLa Kyoto cells until now. It would be interesting to test the uptake on different cell lines or even in different organism to test if this entry

mechanism is conserved through evolution. A challenging perspective would be next to induce cell type specificity for therapeutic use.

Having demonstrated that the liposomal content does not leak into the cell cytoplasm, and colocalization studies demonstrated that they are not in endosomes, lysosomes nor mitochondria, it would be interesting to deliver vesicles with unnatural function. By encapsulating specific enzymes and introducing pores into the vesicles membrane, new synthetic organelles could be developed which would perform endogenous reaction inside the cell cytoplasm in a confine compartment. It has already been proven that polymersomes could act as artificial organelles^[214] or nanoreactor^[215] but only in solution so far. Moreover it could be interesting to stain cellular membrane directly in cells to determine if the liposomes are coated by another membrane in the cytoplasm in an endosome-like compartment.

Considering that proteomic studies performed for the uptake of asparagusic acid enlightened the transferrin receptor as one of the proteins responsible for the thiol-mediated uptake, it would be interesting to test the permeability of such transporter across the blood brain barrier. It has been demonstrated indeed that there is an over expression of this receptor on the surface of this barrier.^[216] Therefore our small transporter could potentially transport substrate and ultimately liposomes to the brain for therapeutic purposes.

Concerning the diselenide project, the logical next step would be the delivery of other substrate than small fluorophores. As with the asparagusic acid, the diseleno lipoic acid tag **73** could be used to bind small peptides on a lysine residue and test for cellular uptake, and going for bigger substrate such as streptavidin once the procedure and cellular uptake is established.

Based on the results obtained with ETP,^[83] it would be interesting to test the epidiselenodiketopiperazine probe **122**. The synthesis of ETP analogue has

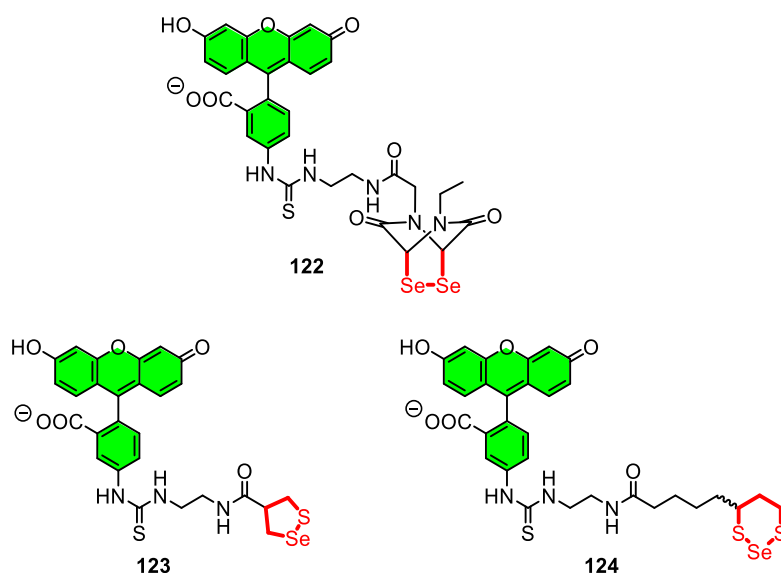


Figure 107. Structure of epidiselenodiketopiperazine **122**, thioseleno asparagusic acid **123** and selenotrisulfide **124** to test for thiol-mediated uptake.

been established recently.^[217] It would also be interesting to investigate mixed thioseleno compounds such as the thioseleno asparagusic acid^[113] **123** or the selenotrisulfide^[218] **124** (Figure 107).

Another goal would be to form cell-penetrating poly(diselenide)s to be used as CPDs. However considering the stability displayed by the diselenolane ring, the conditions developed to form CPDs will probably not be strong enough to induce ring-opening polymerization. A potential strategy would be to have template-assisted polymerization using for example anionic micelles to increase locally the concentration of the monomer.^[219] If monomers are in close proximity, the chance to have intermolecular crosslinkage should be increased.

The switch from disulfide to diselenide improved greatly the uptake and a different cellular distribution was found. Therefore it could be also interesting to push the comparison forward and try to deliver ditelluride. Several studies have been conducted on the toxicity of diphenyl ditelluride, but only one

studied ditelluride-containing polymer as redox sensitive drug delivery system.^[220] The ditelluro asparagusic and lipoic acids have however not been synthesized yet.

Finally concerning the activation of CPPs by ion-pairing stabilized on polarized π -surface, only few additional experiments were thought of, such as trying to determine in cellular experiment, if a specific membrane is stained with perfluorinated fatty acids. Cytotoxicity of the different activators could also be tested to determine the maximal concentration that could be added to cells for increased uptake.

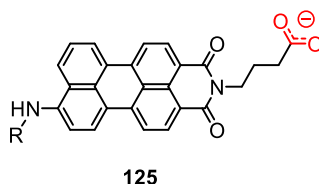


Figure 108. Potential activator of CPPs based on perylene monoimide core **125**.

On the optimization of the stabilizing surface, it could be interesting to test a larger π -surface such as a perylene monoimide core **125**. This larger surface could stabilize additional positive charges on their surface. However some concerns can be attributed to the strength of the push-pull system for such a large complex.

Chapter 5

EXPERIMENTAL SECTION

5.1. General

5.1.1. Reagents, Solvents, Medium and Equipment

Reagents for synthesis were purchased from Fluka, Sigma-Aldrich, Brunschwig, Bachem, Apollo Scientific, Alfa Aesar and Acros, buffers and salts of the best grade available from Fluka or Sigma-Aldrich and used as received. Egg yolk phosphatidylcholine (EYPC), 1,2-distearoyl-*sn*-glycero-3-phosphatidylcholine (DSPC), 1,2-distearoyl-*sn*-glycero-3-phosphoethanolamine-N-[amino(polyethylene glycol)-2000] (DSPE-PEG₂₀₀₀), brain phosphatidylserine (PS) and 1,2-dipalmitoyl-*sn*-glycero-3-phosphoethanolamine-N-(lissamine rhodamine B sulfonyl) were purchased from Avanti Polar Lipids. Sulforhodamine B (SRB) was purchased from Acros. Fluorescein isothiocyanate (FITC) was purchased from Apollo Scientific. LysoTracker green DND-26, LysoTracker Red DND-99, MitoTracker Green FM, MitoTracker Red CMXRos, Dextran Red 70 kDa and Hoechst H3570 were purchased from Life Technology. FITC-dextran 40 kDa was purchased from Sigma-Aldrich. Cy5-NHS was purchased from Lumiprobe. Poly-L-arginine ($M_w = 5 - 15$ kDa) was purchased from Sigma-Aldrich.

Organic solvent used for synthesis were of HPLC or reagent grade. Organic solvents like acetonitrile, dichloromethane or tetrahydrofuran were purified using a solvent purification system from Solv-Tek. Buffer were prepared using bidistilled water.

All reaction were carried out with magnetic stirring and under inert gas (Ar) when specified. Solvents were evaporated using a rotavapor R-210 from Büchi equipped with a vacuum controller V-850, a pump V-700 and a heating bath B-491 from Büchi.

All the glassware used for synthesis and experiments was washed with soap solution, demineralized water and acetone, and dried in oven. Bidistilled water was used for vesicle formation, experiments and cleaning.

For cell experiments, minimum essential medium (MEM) alpha without nucleoside, Leibovitz's L-15, fetal bovine serum (FBS) South American (CE), phosphate buffered saline (PBS) tablets, penicillin-streptomycin solution (10000 U/mL) and tryPLE express with phenol red were purchased from Thermo Fisher Scientific. L-glutamine were purchased from Brunschwig.

NovaPEG Rink Amide Resin was purchased from Novabiochem®, and was swollen in CH₂Cl₂ before each reaction. Solid phase reactions were carried in SPE tubes fitted with a frit and a tap. Automated solid phase synthesis was carried out on an Intavis AG MultiPep RS instrument.

5.1.2. Chromatographic Equipment and Methods

Column chromatography was carried out on silica gel (SiliaFlash® P60, 230 – 400 mesh) from SiliCycle. Analytical thin layer chromatography (TLC) were performed on silica gel 60 F254 from Merck. Description of the results in the text are reported as retention factor R_f with eluent. Detection of the compounds was done with a UV-lamp (CAMAG) at a wavelength of $\lambda = 254$ nm or 366 nm or with appropriate staining.

Semi-preparative HPLC was performed using JASCO LC-2000 Plus system equipped with quaternary pump (JASCO PU-2089) and UV/Vis detector (JASCO UV-2077 Plus). The chromatographic column used was a Phenomenex Jupiter Proteo (250 x 10 mm, 4.0 μ m particles size, flow 3.0

mL/min with a linear elution gradient from 90% H₂O / 10% CH₃CN + 0.1% TFA to 10% H₂O / 90% CH₃CN + 0.1% TFA in 15 min or 30 min).

Reverse phase flash chromatography was performed on Biotage Isolera™ Four (column: SNAP Cartridge, KP-C18-HS-60g, eluents: CH₃CN and H₂O with 0.1% TFA).

UHPLC-MS (ESI) were recorded using a Thermo Scientific Accela HPLC with a LCQ Fleet three-dimensional ion trap mass spectrometer (Thermo scientific) and a diode array detector. The chromatographic column used was a Thermo C18 Hypersil gold column 1.9 µm, 5 cm x 2.1 mm, using an eluent gradient CH₃CN and H₂O with TFA 0.01% in 4 min at a flow rate 0.75 mL/min. The characterization of new compounds are reported as mass-per-charge ratio *m/z* (intensity in %, [assignment]). Only the most intense ones among isotopic peaks are reported.

5.1.3. Equipment for Characterization

Melting points (Mp) were measured on a Melting Point M-565 from Büchi and are reported in degrees Celsius.

[α]_D²⁰ values were recorded on a Jasco P-1030 polarimeter using a sodium lamp (λ = 587 nm) in a quartz cell of 10 cm length at 20 °C and are reported as degree ° (concentration, solvent).

IR spectra were recorded on a Perkin Elmer Spectrum One FT-IR spectrometer (ATR, Golden Gate) and are reported as wavenumbers ν in cm⁻¹ with band intensities indicated as s (strong), m (medium) or w (weak).

¹H and ¹³C{¹H} NMR spectra were recorded (as indicated) either on a Bruker 300 MHz, 400 MHz or 500 MHz spectrometer and are reported as chemical shifts (δ) in ppm relative to TMS (δ = 0). Proton spin multiplicities are reported as a singlet (s), doublet (d), triplet (t), quartet (q), quintet (quint) and sextuplet (sext) with coupling constants (*J*) given in Hz, or multiplet (m).

^1H and $^{13}\text{C}\{^1\text{H}\}$ resonances were assigned with the aid of additional information from 1D & 2D NMR spectra: (H,H)-COSY, DEPT-135, HSQC and HMBC. All spectra were treated using Mestrenova software.

ESI-MS for the characterization of new compounds was performed on an ESI API 150EX and are reported as mass-per-charge ratio m/z (intensity in %, [assignment]). HR ESI-MS for the characterization of new compounds were performed on a QSTAR Pulsar or XL (AB/MDS Sciex) and are reported as mass-per-charge ratio m/z calculated and observed. MALDI-TOF MS were measured using a Bruker Daltonics Autoflex speed spectrometer.

5.1.4. Equipment used for Experiments

Air displacement micropipette calibrated for volumes 1 – 10 μL , 10 – 100 μL or 100 – 1000 μL from Vaudoux-Eppendorf (Switzerland) were used to manipulate aqueous or non-volatile solvents. Positive displacement micropipette calibrated for volumes 1 – 10 μL , 10 – 100 μL or 100 – 1000 μL were used to manipulate volatile solvents.

pH values of buffers were measured using a Consort C832 multi-parameter analyzer with a VWR glass membrane pH electrode. Before each use, the instrument was calibrated using Titrisol solutions from Merck at pH = 4.00 and 7.00. Deuterated sodium phosphate buffer was prepared by dissolving phosphoric acid (1 mmol, 119 mg, 85% D_3PO_4 in D_2O) in 10 mL D_2O ; pD adjustments were made with DCl (20 wt.% solution in D_2O) or NaOD (30 wt.% solution in D_2O) and the pH meter reading in D_2O was corrected ($\text{pD} = \text{pH meter reading} + 0.4$).^[212-213]

UV-Vis spectra were recorded on a JASCO V-650 spectrophotometer equipped with a temperature controller (25 °C) using a glass cell of 1 cm path length and are reported as maximal absorption wavelength λ in nm (extinction coefficient ϵ in $\text{M}^{-1}\text{cm}^{-1}$).

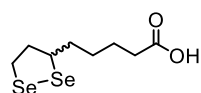
Fluorescence measurements were performed with a FluoroMax-4 spectrofluorometer (Horiba Scientific) equipped with a stirrer and a temperature controller (25 °C). Fluorescence spectra were corrected using instrument-supplied correction factors.

Fluorescence cellular imaging was performed using Leica SP5 or SP8 confocal, equipped with 63× oil immersion objective lens, or with an automated microscope ImageXpress from Molecular Devices equipped with a 40xpf lens. The images were treated using ImageJ 1.51s software.

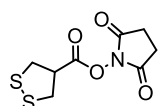
Flow cytometry measurements were performed using Beckman Coulter Gallios™ (6 colors 2 lasers) flow cytometer. The results were treated using Kaluza Analysis 1.1.11052.10190 software.

5.2. Synthesis

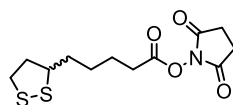
5.2.1. Thiol-Mediated Uptake of Vesicles



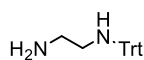
Compound 41 was synthesized following a published protocol.^[182]



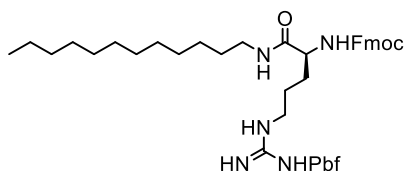
Compound 48 was synthesized following a published protocol.^[167–170]



Compound 50 was synthesized following a published protocol.^[58]

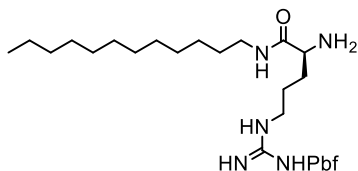


Compound 57 was synthesized following a published protocol.^[175–176]



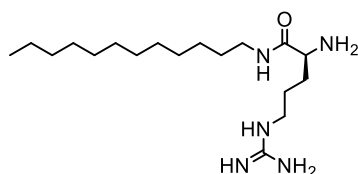
Compound 45. Compound **44** (1780 mg, 2.74 mmol) was dissolved in dry DMF (40 mL) at 0 °C. HATU (1050 mg, 2.77 mmol) and TEA (500 μ L, 3.58 mmol) were added followed by DA

(524 mg, 2.83 mmol) after 90 s. The solution was allowed to warm up from 0 °C to rt and stirred for 4 h under Ar atmosphere. EtOAc (100 mL) was then added and the organic layer was washed with H₂O, diluted KHSO₄ (pH 6.0), LiCl (5%) and brine (2 x 50 mL each). The organic layer was then dried with Na₂SO₄ and evaporated under reduced pressure. The mixture was purified by a flash column chromatography (SiO₂, CH₂Cl₂/MeOH 97:3 to 9:1, *R_f* 0.6 in CH₂Cl₂/MeOH 99:1) to give **45** as a sticky pale orange solid (1750 mg, 78%). Mp: 73 – 74 °C; [α]_D²⁰: +3.7 (c 0.10, CHCl₃); IR (neat): 3327 (w), 3136 (w), 2923 (m), 2853 (m), 1664 (w), 1620 (m), 1549 (s), 1448 (m), 1405 (w), 1370 (w), 1348 (w), 1291 (w), 1244 (m), 1192 (w), 1147 (m), 1100 (s), 1033 (w), 1011 (w), 993 (w), 967 (w), 900 (w), 845 (m), 816 (m), 785 (m), 725 (s), 658 (s), 642 (s), 618 (s), 564 (s), 529 (m), 517 (s); ¹H NMR (400 MHz, CD₃OD): 7.80 (d, ³*J* (H,H) = 7.6 Hz, 2H), 7.69 – 7.64 (m, 2H), 7.39 (t, ³*J* (H,H) = 7.4 Hz, 2H), 7.34 – 7.25 (m, 2H), 4.40 (d, ³*J* (H,H) = 6.7 Hz, 2H), 4.22 (t, ³*J* (H,H) = 6.7 Hz, 1H), 4.08 – 4.04 (m, 1H), 3.19 – 3.16 (m, 4H), 2.98 (s, 2H), 2.60 (s, 3H), 2.53 (s, 3H), 2.08 (s, 3H), 1.76 – 1.44 (m, 12H), 1.32 – 1.22 (m, 18H), 0.90 (t, ³*J* (H,H) = 6.8 Hz, 3H); ¹³C NMR (101 MHz, CD₃OD): 173.1 (C), 158.5 (C), 156.9 (C), 156.7 (C), 143.9 (C), 143.7 (C), 141.2 (C), 138.0 (C), 132.9 (C), 132.1 (C), 127.4 (2xCH), 126.8 (2xCH), 124.8 (2xCH), 124.6 (2xC), 119.5 (2xCH), 117.0 (C), 86.2 (C), 66.4 (CH₂), 54.8 (CH), 47.1 (CH), 42.5 (CH₂), 39.0 (CH₂), 31.7 (CH₂), 29.4 (2xCH₂), 29.3 (4xCH₂), 29.1 (2xCH₂), 29.0 (CH₂), 28.9 (CH₂), 27.3 (2xCH₃), 26.5 (CH₂), 22.3 (CH₂), 18.2 (CH₃), 17.0 (CH₃), 13.0 (CH₃), 11.1 (CH₃); MS (ESI, MeOH): 817 (100, [M+H]⁺).



Compound 46. To a solution of **45** (1750 mg, 2.14 mmol) dissolved in CH_2Cl_2 , DBU (1.6 mL, 11 mmol) was added and the solution was stirred for 3 h. The mixture was concentrated under reduced

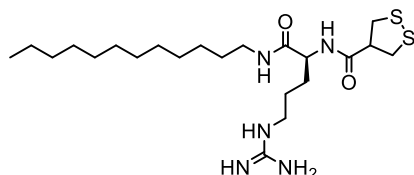
pressure and purified by a flash column chromatography (SiO_2 , $\text{CH}_2\text{Cl}_2/\text{MeOH}/\text{TEA}$ 97:3:0.1 to 9:1:0.1, R_f 0.5 in $\text{CH}_2\text{Cl}_2/\text{MeOH}$ 17:3) to give **46** as a sticky pale yellow solid (1420 mg, 94%). Mp: 97 – 98 °C; $[\alpha]_{\text{D}}^{20}$: +28 (c 0.10, CHCl_3); IR (neat): 3294 (w), 3130 (w), 2920 (m), 2852 (m), 1621 (m), 1545 (s), 1452 (m), 1421 (m), 1406 (m), 1374 (m), 1338 (w), 1296 (m), 1263 (m), 1206 (m), 1172 (m), 1152 (m), 1113 (s), 1087 (s), 1034 (m), 990 (m), 972 (m), 931 (w), 904 (w), 851 (m), 821 (m), 780 (m), 732 (m), 662 (s), 639 (s), 621 (s), 594 (m), 567 (s), 528 (m), 521 (m), 514 (m); ^1H NMR (400 MHz, CDCl_3): 7.56 (s, 1H), 6.59 (s, 1H), 6.44 (s, 2H), 3.54 – 3.51 (m, 1H), 3.27 – 3.17 (m, 4H), 2.97 (s, 2H), 2.59 (s, 3H), 2.52 (s, 3H), 2.11 (s, 3H), 1.83 – 1.79 (m, 1H), 1.66 – 1.60 (m, 3H), 1.32 – 1.26 (m, 18H), 0.90 (t, $^3J(\text{H,H}) = 6.8$ Hz, 3H); ^{13}C NMR (101 MHz, CDCl_3): 172.8 (C), 158.8 (C), 156.6 (C), 138.2 (C), 132.6 (C), 132.2 (C), 124.7 (C), 117.6 (C), 86.4 (C), 53.8 (CH), 43.2 (CH_2), 39.7 (CH_2), 31.9 (CH_2), 31.0 (CH_2), 29.7 (3x CH_2), 29.6 (CH_2), 29.5 (CH_2), 29.4 (2x CH_2), 29.2 (CH_2), 28.6 (2x CH_3), 27.1 (CH_2), 25.3 (CH_2), 22.7 (CH_2), 19.3 (CH_3), 18.0 (CH_3), 14.1 (CH_3), 12.5 (CH_3); MS (ESI, MeOH): 595 (100, $[\text{M}+\text{H}]^+$).



Compound 47. Compound **46** (262 mg, 370 μmol) was dissolved in a solution of TFA/ CHCl_3 1:1 (40 mL). The solution was stirred at rt for 2 h and concentrated under reduced pressure before purification by

trituration in Et_2O (50 mL). The solid was dried in vacuo overnight to give **47** as a colorless hygroscopic solid (183 mg, 87%). $[\alpha]_{\text{D}}^{20}$: +31 (c 0.10, CH_3OH);

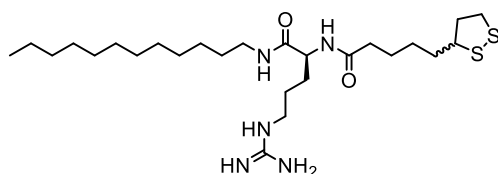
IR (neat): 3287 (w), 3189 (w), 3110 (w), 2925 (m), 2855 (m), 1660 (s), 1579 (m), 1467 (m), 1435 (m), 1370 (w), 1271 (w), 1183 (s), 1132 (s), 963 (w), 839 (m), 801 (m), 722 (s), 674 (m), 586 (m), 549 (m), 539 (m), 517 (s), 510 (s), 501 (m); ^1H NMR (400 MHz, CD_3OD): 3.78 (t, $^3J(\text{H,H}) = 6.2$ Hz, 1H), 3.15 – 3.12 (m, 4H), 1.89 – 1.78 (m, 2H), 1.63 – 1.54 (m, 2H), 1.48 – 1.41 (m, 2H), 1.27 – 1.19 (m, 18H), 0.80 (t, $^3J(\text{H,H}) = 6.8$ Hz, 3H); ^{13}C NMR (101 MHz, CD_3OD): 168.2 (C), 157.2 (C), 52.7 (CH), 40.4 (CH_2), 39.3 (CH_2), 31.7 (CH_2), 29.4 ($3\times\text{CH}_2$), 29.3 (CH_2), 29.1 (CH_2), 29.0 (CH_2), 28.9 (CH_2), 28.4 (CH_2), 26.6 (CH_2), 24.1 (CH_2), 22.3 (CH_2), 13.0 (CH_3); MS (ESI, MeOH): 343 (100, $[\text{M}+\text{H}]^+$).



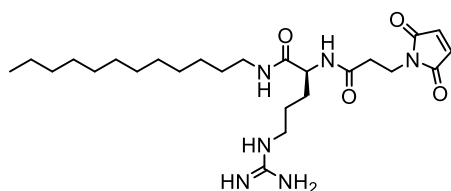
Compound 43. To a solution of **47** (43 mg, 75 μmol) dissolved in dry $\text{CH}_2\text{Cl}_2/\text{DMF}$ 4:1 (5 mL), compound **48** (35 mg, 140 μmol) was added before the addition of TEA (80 μL ,

540 μmol). The solution was stirred for 2 h before to be concentrated under reduced pressure at 30 $^\circ\text{C}$ and purified by trituration in Et_2O . The solid was purified by semi-preparative HPLC (R_t 16.3 min) to give compound **43** as a colorless solid (14 mg, 32%). Mp: 96 – 98 $^\circ\text{C}$; $[\alpha]_{\text{D}}^{20}$: –11 (c 0.10, CHCl_3); IR (neat): 3287 (m), 2921 (m), 2853 (w), 1635 (s), 1546 (m), 1468 (w), 1435 (w), 1374 (w), 1204 (m), 1182 (m), 1129 (m), 990 (w), 956 (w), 840 (m), 800 (m), 722 (m), 675 (m), 663 (m), 639 (m), 608 (m), 596 (m), 575 (m), 552 (m), 536 (m), 509 (s), 500 (s); ^1H NMR (400 MHz, CD_3OD): 4.23 (dd, $^3J(\text{H,H}) = 8.2$ Hz, 5.8 Hz, 1H), 3.32 – 3.05 (m, 9H), 1.79 – 1.70 (m, 1H), 1.63 – 1.38 (m, 5H), 1.23 – 1.19 (m, 18H), 0.80 (t, $^3J(\text{H,H}) = 6.8$ Hz, 3H); ^{13}C NMR (101 MHz, CD_3OD): 172.8 (C), 172.0 (C), 157.2 (C), 53.0 (CH), 51.4 (CH), 42.3 (CH_2), 41.9 (CH_2), 40.5 (CH_2), 39.1 (CH_2), 31.7 (CH_2), 29.4 (CH_2), 29.3 ($3\times\text{CH}_2$), 29.1 (CH_2), 29.0 ($3\times\text{CH}_2$), 26.6 (CH_2), 25.0 (CH_2), 22.3 (CH_2), 13.0 (CH_3); MS

(ESI, MeOH): 475 (100, [M+H]⁺); HRMS (ESI, +ve) calcd. for C₂₂H₄₄N₅O₂S₂⁺: 474.2931, found: 474.2933.

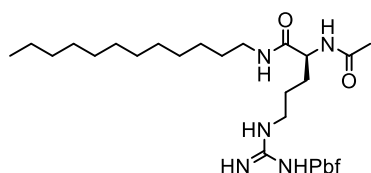


Compound 49. To a solution of **47** (20 mg, 35 μmol) dissolved in CH₂Cl₂/DMF 1:1 (2 mL), compound **50** (13 mg, 42 μmol) and TEA (50 μL, 370 μmol) were added and the solution was stirred under Ar atmosphere at rt for 2.5 h. The solution was then concentrated under reduced pressure at 30 °C and purified by trituration in Et₂O. The solid was dried in vacuo overnight and purified by semi-preparative HPLC (*R*_t 17.2 min) to give compound **49** as a colorless solid (11 mg, 48%). Mp: 116 – 118 °C; IR (neat): 3287 (m), 3192 (w), 2923 (m), 2853 (m), 1633 (s), 1539 (m), 1466 (m), 1435 (m), 1371 (w), 1312 (w), 1253 (w), 1200 (m), 1180 (s), 1130 (s), 968 (w), 926 (w), 893 (w), 837 (m), 800 (m), 721 (m), 648 (m), 590 (m), 529 (m), 509 (s); ¹H NMR (300 MHz, CD₃OD): 4.34 (dd, ³*J* (H,H) = 7.8 Hz, 5.5 Hz, 1H), 3.66 – 3.54 (m, 1H), 3.25 – 3.07 (m, 6H), 2.48 (sext, ³*J* (H,H) = 6.7 Hz, 1H), 2.29 (t, ³*J* (H,H) = 7.3 Hz, 2H), 1.96 – 1.42 (m, 13H), 1.33 – 1.31 (m, 18H), 0.92 (t, ³*J* (H,H) = 6.5 Hz, 3H); ¹³C NMR (101 MHz, CD₃OD): 174.6 (C), 172.3 (C), 157.2 (C), 56.2 (CH), 52.7 (CH), 40.6 (CH₂), 39.9 (CH₂), 39.1 (CH₂), 37.9 (CH₂), 35.2 (CH₂), 34.4 (CH₂), 31.7 (CH₂), 29.4 (2xCH₂), 29.3 (2xCH₂), 29.1 (CH₂), 29.0 (2xCH₂), 28.5 (2xCH₂), 26.6 (CH₂), 25.2 (CH₂), 25.0 (CH₂), 22.3 (CH₂), 13.0 (CH₃); MS (ESI, MeOH): 530 (100, [M+H]⁺); HRMS (ESI, +ve) calcd. for C₂₆H₅₁N₅O₂S₂⁺: 530.3557, found: 530.3559.



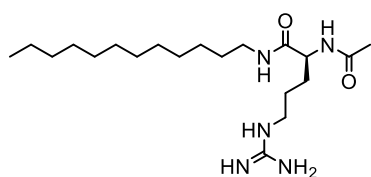
Compound 51. To a solution of **52** (47 mg, 280 μmol) in DMF (1.5 mL) were added sequentially a solution of HBTU (114 mg, 300 μmol) in DMF (2 mL), TEA (100 μL, 741 μmol) and a solution of compound **46** (92 mg, 160 μmol) in

DMF/CH₂Cl₂ (4:1, 5 mL) at 0 °C. The solution was allowed to warm up to rt and stirred for 2 h. After 2 h, TEA (100 µL, 741 µmol) was added and the solution was stirred for 3 h at rt. The solution was concentrated under reduced pressure and purified by trituration in Et₂O. The solid was dried in vacuo overnight and purified by semi-preparative HPLC (*R*_t 14.5 min) to give compound **51** as a colorless solid (35 mg, 36%). Mp: 118 – 119 °C; [α]_D²⁰: –13 (c 0.50, MeOH); IR (neat): 3350 (w), 3285 (w), 2923 (w), 2853 (w), 1695 (m), 1635 (m), 1542 (w), 1532 (w), 1464 (w), 1409 (w), 1377 (w), 1319 (w), 1201 (m), 1184 (m), 1129 (m), 957 (w), 831 (w), 800 (w), 721 (w), 695 (m), 590 (m), 569 (w), 555 (w), 544 (w), 530 (m), 511 (s); ¹H NMR (400 MHz, CD₃CN): 8.06 (s, 1H), 7.08 (d, ³*J* (H,H) = 7.7 Hz, 1H), 6.81 (s, 1H), 6.77 (s, 2H), 4.23 – 4.18 (m, 1H), 3.77 – 3.69 (m, 2H), 3.22 – 3.09 (m, 4H), 2.51 (t, ³*J* (H,H) = 7.0 Hz, 2H), 1.82 – 1.79 (m, 1H), 1.66 – 1.56 (m, 3H), 1.47 – 1.43 (m, 2H), 1.35 – 1.27 (m, 18H), 0.91 (t, ³*J* (H,H) = 6.6 Hz, 3H); ¹³C NMR (101 MHz, CD₃CN): 171.7 (C), 171.4 (C), 171.1 (C), 159.3 (C), 158.1 (C), 134.9 (2xCH), 53.1 (CH), 41.2 (CH₂), 39.4 (CH₂), 34.8 (CH₂), 34.6 (CH₂), 32.2 (CH₂), 30.0 (CH₂), 29.9 (3xCH₂), 29.7 (2xCH₂), 29.6 (2xCH₂), 27.1 (CH₂), 25.0 (CH₂), 23.0 (CH₂), 14.0 (CH₃); MS (ESI, CH₃CN): 494 (100, [M+H]⁺); HRMS (ESI, +ve) calcd. for C₂₅H₄₅N₆O₄⁺: 493.3497, found: 493.3485.



Compound 54. To a solution of **46** (114 mg, 161 µmol) dissolved in dry CH₂Cl₂ (5 mL), acetyl chloride was added (50 µL, 370 µmol) and the solution was stirred at rt. After 1.5 h, TEA (70 µL, 520 µmol) was added and the solution was stirred for 30 min at rt. The reaction mixture was concentrated under reduced pressure and purified by a flash column chromatography (CH₂Cl₂/MeOH 97:3 to 9:1, *R*_f 0.4 in CH₂Cl₂/MeOH 9:1) to give **54** as a pale yellow solid (96 mg, 94%). Mp: 91 – 92 °C; [α]_D²⁰: –17 (c 0.10, CHCl₃); IR (neat): 3266 (w), 3071 (w), 2975 (w), 2926 (m), 2855 (w), 2607 (w), 2532 (w), 2498 (w), 1633 (m), 1555 (m),

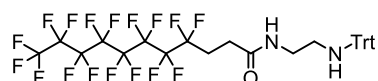
1445 (m), 1398 (m), 1371 (m), 1331 (w), 1289 (m), 1260 (w), 1241 (w), 1208 (w), 1166 (m), 1143 (m), 1091 (m), 1036 (w), 992 (w), 970 (w), 905 (w), 851 (w), 807 (m), 781 (w), 732 (m), 719 (w), 660 (m), 541 (s), 612 (m), 565 (s), 536 (s), 523 (s), 511 (m); ^1H NMR (400 MHz, CDCl_3): 7.26 (br s, 1H), 7.13 (d, $^3J(\text{H,H}) = 8.0$ Hz, 1H), 6.39 (s, 3H), 4.50 – 4.44 (m, 1H), 3.32 – 3.15 (m, 4H), 2.97 (s, 2H), 2.59 (s, 3H), 2.52 (s, 3H), 2.11 (s, 3H), 2.02 (s, 3H), 1.88 – 1.81 (m, 1H), 1.75 – 1.44 (m, 11H), 1.33 – 1.25 (m, 18H), 0.89 (t, $^3J(\text{H,H}) = 6.8$ Hz, 3H); ^{13}C NMR (101 MHz, CDCl_3): 171.9 (C), 171.0 (C), 158.8 (C), 156.5 (C), 138.2 (C), 132.6 (C), 132.2 (C), 124.7 (C), 117.6 (C), 86.5 (C), 53.4 (CH), 43.2 (CH₂), 39.7 (CH₂), 30.2 (CH₂), 29.7 (3xCH₂), 29.6 (2xCH₂), 29.4 (CH₂), 29.3 (2xCH₂), 28.6 (2xCH₃), 27.0 (CH₂), 25.6 (CH₂), 23.1 (CH₃), 22.7 (2xCH₂), 19.3 (CH₃), 18.0 (CH₃), 14.1 (CH₃), 12.5 (CH₃); MS (ESI, MeOH): 637 (100, $[\text{M}+\text{H}]^+$).



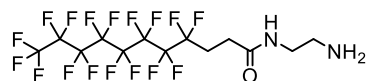
Compound 53. Compound **54** (91 mg, 140 μmol) was dissolved in TFA/ CHCl_3 1:1 (8 mL) mixture and stirred for 3.5 h at rt. The solution was concentrated under

reduced pressure and purified by trituration in Et_2O . The solid was purified by semi-preparative HPLC (R_t 14.2 min) to give **53** as a colorless solid (25 mg, 35%). Mp: 150 – 152 $^\circ\text{C}$; $[\alpha]_{\text{D}}^{20}$: -9.9 (c 0.10, MeOH); IR (neat): 3277 (w), 3261 (w), 2917 (m), 2850 (w), 1640 (s), 1560 (m), 1472 (w), 1440 (w), 1393 (w), 1373 (w), 1341 (w), 1300 (w), 1266 (w), 1233 (w), 1209 (m), 1187 (m), 1120 (m), 1067 (w), 1040 (w), 1014 (w), 969 (w), 950 (w), 932 (w), 843 (w), 799 (w), 784 (w), 722 (m), 603 (m), 576 (m), 541 (m), 517 (m), 510 (m); ^1H NMR (400 MHz, CD_3OD): 8.16 (d, $^3J(\text{H,H}) = 7.7$ Hz, 1H), 8.04 (br t, $^3J(\text{H,H}) = 5.3$ Hz, 1H), 4.36 – 4.30 (m, 1H), 3.25 – 3.17 (m, 4H), 3.23 – 3.07 (m, 6H), 2.02 (s, 3H), 1.89 – 1.81 (m, 1H), 1.72 – 1.58 (m, 3H), 1.56 – 1.48 (m, 2H), 1.36 – 1.31 (m, 18H), 0.92 (t, $^3J(\text{H,H}) = 6.8$ Hz, 3H); ^{13}C NMR (101 MHz, CD_3OD): 172.3 (C), 172.0 (C), 157.2 (C), 52.9 (CH), 40.6 (CH₂), 39.1 (CH₂),

31.7 (CH₂), 29.4 (CH₂), 29.3 (3xCH₂), 29.1 (CH₂), 29.0 (2xCH₂), 28.9 (CH₂), 26.6 (CH₂), 24.9 (CH₂), 22.3 (CH₂), 21.1 (CH₃), 13.0 (CH₃); MS (ESI, MeOH): 385 (100, [M+H]⁺); HRMS (ESI, +ve) calcd. for C₂₀H₄₁N₅O₂⁺: 384.3333, found: 384.3331.

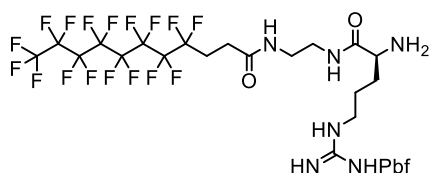


Compound 59. Compound **58** (146 mg, 296 μmol) was dissolved in dry DMF (3 mL) and cool down to 0 °C. HBTU (124 mg, 327 μmol), TEA (100 μL, 741 μmol) and **57** (92 mg, 300 μmol) were successively added and the reaction was stirred for 3 h at rt. EtOAc (100 mL) were added and the organic layer was washed with H₂O, LiCl (5%) and brine (2 x 30 mL each). The organic layer was dried with Na₂SO₄ and evaporated by reduced pressure. The mixture was purified by a flash column chromatography (SiO₂, CH₂Cl₂/MeOH 99:1, *R_f* 0.6 in CH₂Cl₂/MeOH 97:3) to give **59** as a colorless solid (179 mg, 78%). Mp: 58 – 59 °C; IR (neat): 3317 (w), 1669 (w), 1633 (m), 1599 (w), 1565 (w), 1534 (w), 1491 (w), 1448 (w), 1371 (w), 1334 (w), 1237 (m), 1197 (s), 1145 (s), 1117 (m), 1100 (m), 1034 (w), 982 (w), 960 (w), 903 (w), 849 (w), 778 (m), 749 (m), 700 (s), 656 (s), 621 (m), 607 (m), 585 (m), 558 (s), 530 (m), 518 (m), 504 (m); ¹H NMR (400 MHz, CDCl₃): 7.38 – 7.35 (m, 6H), 7.23 – 7.19 (m, 6H), 7.15 – 7.11 (m, 3H), 5.75 (t, ³*J* (H,H) = 5.6 Hz 1H), 3.30 (q, ³*J* (H,H) = 5.9 Hz, 2H), 2.51 – 2.38 (m, 4H), 2.26 (t, ³*J* (H,H) = 6.0 Hz, 2H); ¹³C NMR (101 MHz, CDCl₃): 169.8 (C), 145.6 (3xC), 128.5 (6xC), 127.9 (6xC), 126.5 (3xC), 70.7 (C), 43.3 (CH₂), 40.3 (CH₂), 27.2 – 26.8 (m, 2xCH₂); ¹⁹F NMR (282 MHz, CDCl₃): –80.7 (tt, ³*J* (F,F) = 9.9 Hz, ⁴*J* (F,F) = 2.2 Hz, 3F), –114.5 (t, ³*J* (F,F) = 15.3 Hz, 2F), –121.6 to –121.9 (m, 6F), –122.7 (br s, 2F), –123.4 (br s, 2F), –126.0 to –126.1 (m, 2F).



Compound 60. Compound **59** (175 mg, 225 μmol) was dissolved in TFA/CH₂Cl₂ (95:5) solution and stirred for 1 h at rt. The solution was concentrated by reduced pressure and purified by a flash column chromatography (SiO₂,

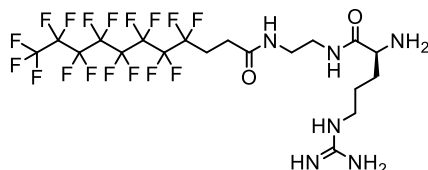
1H), 6.11 (s, 3H), 5.94 (d, 3J (H,H) = 8.2 Hz 1H), 4.33 – 4.23 (m, 3H), 4.09 (t, 3J (H,H) = 7.1 Hz, 1H), 3.34 – 3.20 (m, 6H), 2.86 (s, 2H), 2.53 – 2.27 (m, 10H), 1.63 – 1.49 (m, 4H), 1.35 (s, 6H); ^{13}C NMR (101 MHz, CDCl_3): 171.7 (C), 162.6 (C), 159.1 (C), 156.7 (C), 143.8 (C), 143.6 (C), 141.3 (2xC), 138.4 (C), 132.3 (C), 131.8 (C), 127.7 (2xCH), 127.0 (2xCH), 125.1 (C), 125.1 (2xCH), 124.9 (C), 120.0 (2xCH), 117.8 (C), 86.6 (C), 67.0 (CH_2), 53.9 (CH), 47.1 (CH), 43.1 (CH_2), 40.0 (CH_2), 39.5 (CH_2), 39.4 (CH_2), 36.6 (CH_2), 31.5 (CH_2), 28.5 (2x CH_3), 26.8 – 26.7 (m, 2x CH_2), 19.3 (CH_3), 18.0 (CH_3), 12.4 (CH_3); ^{19}F NMR (282 MHz, CDCl_3): –80.8 (tt, 3J (F,F) = 10.4 Hz, 4J (F,F) = 2.3 Hz, 3F), –114.6 (t, 3J (F,F) = 13.5 Hz, 2F), –121.7 to –121.9 (m, 6F), –122.7 (br s, 2F), –123.5 (br s, 2F), –126.0 to –126.2 (m, 2F); MS (ESI, MeOH): 1165 (100, $[\text{M}+\text{H}]^+$).



Compound 62. To a solution of **61** (160 mg, 137 μmol) dissolved in $\text{CH}_2\text{Cl}_2/\text{MeOH}$ (4:1), DBU (300 μL , 2.01 mmol) was added and the

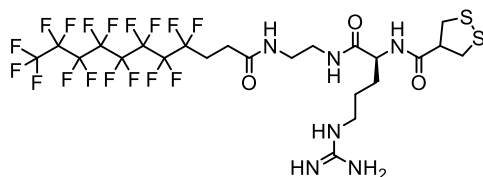
solution was stirred for 3 h at rt. The mixture was concentrated under reduced pressure and purified by a flash column chromatography (SiO_2 , $\text{CH}_2\text{Cl}_2/\text{MeOH}/\text{TEA}$ 9:1:0.1, R_f 0.4 in $\text{CH}_2\text{Cl}_2/\text{MeOH}$ 4:1) to give **62** as a colorless solid (118 mg, 81%). Mp: 88 – 90 $^\circ\text{C}$; $[\alpha]_{\text{D}}^{20}$: +17 (c 0.10, CHCl_3); IR (neat): 1653 (w), 1549 (w), 1449 (w), 1406 (w), 1372 (w), 1233 (w), 1203 (m), 1146 (m), 1095 (m), 1038 (w), 976 (w), 853 (w), 812 (w), 784 (w), 733 (w), 704 (w), 656 (w), 641 (w), 619 (w), 596 (w), 566 (w), 556 (w), 514 (s), 510 (s), 506 (m); ^1H NMR (400 MHz, CDCl_3): 3.40 – 3.30 (m, 3H), 3.02 – 3.01 (m, 2H), 2.59 – 2.50 (m, 10H), 2.10 (s, 3H), 1.75 – 1.69 (m, 1H), 1.61 – 1.55 (m, 3H), 1.47 (s, 6H); ^{13}C NMR (101 MHz, CD_3OD): 171.7 (C), 158.5 (C), 156.8 (C), 137.9 (C), 132.8 (C), 132.1 (C), 124.6 (C), 117.0 (C), 111.1 (C), 86.3 (C), 54.0 (CH), 42.5 (CH_2), 38.8 (CH_2), 38.6 (CH_2), 27.3 (2x CH_3), 26.3 – 26.2 (m, 2x CH_2), 18.1 (CH_3), 16.9 (CH_3), 11.0 (CH_3); ^{19}F NMR (282 MHz, CD_3OD): –

82.3 (tt, 3J (F,F) = 9.7 Hz, 4J (F,F) = 2.0 Hz, 3F), -115.6 to -115.7 (m, 2F), -122.6 to -122.9 (m, 6F), -123.7 (br s, 2F), -124.5 (br s, 2F), -127.2 to -127.3 (m, 2F); MS (ESI, MeOH): 944 (100, [M+H]⁺).



Compound 63. Compound **62** (115 mg, 109 μ mol) was dissolved in TFA/CH₂Cl₂ 1:1 (6 mL) and stirred at rt for 2 h. The mixture was

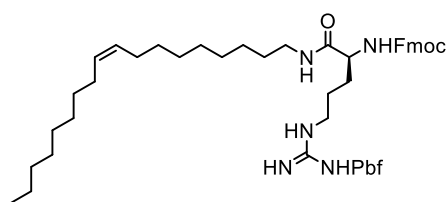
concentrated under reduced pressure and purified by trituration in Et₂O. The solid was dried in vacuo overnight to give **63** as a hygroscopic colorless solid (47 mg, 47%). $[\alpha]_D^{20}$: +1.3 (c 0.10, MeOH); IR (neat): 3268 (w), 3180 (w), 3089 (w), 2958 (w), 1660 (m), 1552 (w), 1447 (w), 1367 (w), 1349 (w), 1332 (w), 1200 (s), 1145 (s), 1073 (s), 975 (w), 871 (w), 801 (w), 777 (w), 703 (m), 654 (m), 605 (s), 576 (s), 556 (m), 516 (s), 506 (s); ¹H NMR (500 MHz, CD₃OD): 3.98 (t, ³*J* (H,H) = 6.5 Hz, 1H), 3.45 – 3.20 (m, 8H), 2.62 – 2.49 (m, 4H), 2.10 – 2.03 (m, 1H), 1.95 – 1.88 (m, 1H), 1.75 – 1.69 (m, 2H); ¹³C NMR (126 MHz, CD₃OD): 171.8 (C), 169.1 (C), 157.3 (C), 52.4 (CH), 39.8 (CH₂), 38.8 (CH₂), 38.5 (CH₂), 27.9 (CH₂), 26.4 – 26.1 (m, 2xCH₂), 23.2 (CH₂); ¹⁹F NMR (282 MHz, CD₃OD): –82.4 (tt, ³*J* (F,F) = 10.0 Hz, ⁴*J* (F,F) = 2.2 Hz, 3F), –115.6 to –115.7 (m, 2F), –122.6 to –122.9 (m, 6F), –123.7 (br s, 2F), –124.5 (br s, 2F), –127.2 to –127.3 (m, 2F); MS (ESI, MeOH): 691 (100, [M+H]⁺).



Compound 55. To a solution of **63** (47 mg, 51 μmol) dissolved in DMF/CH₂Cl₂ 3:1 (3 mL), compound **48** (19 mg, 75 μmol in 1.5 mL CH₂Cl₂) and

TEA (100 μ L, 741 μ mol) was added and the solution was stirred at rt for 4 h before the addition of 11 (31 mg, 124 μ mol) and TEA (100 μ L, 741 μ mol). The solution was stirred overnight before to remove the solvent by reduced pressure. The solid was dissolved in MeOH and purified by semi-preparative

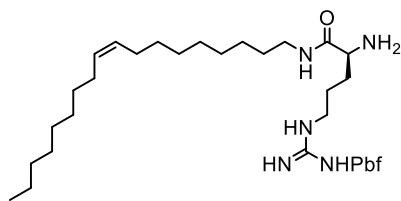
HPLC (R_t 12.5 min) to yield in compound **55** as a colorless solid (38 mg, 79%). Mp: 116 – 118 °C; $[\alpha]_D^{20}$: –14 (c 0.050, MeOH); IR (neat): 3101 (w), 2947 (w), 1653 (w), 1551 (w), 1467 (w), 1445 (w), 1351 (w), 1334 (w), 1198 (m), 1144 (m), 1110 (m), 1070 (m), 976 (w), 868 (w), 800 (w), 779 (w), 722 (w), 704 (w), 655 (w), 619 (w), 609 (m), 572 (m), 558 (m), 525 (m), 521 (m), 511 (s); ^1H NMR (500 MHz, CD_3OD): 4.31 (dd, $^3J(\text{H,H}) = 8.2$ Hz, 5.7 Hz, 1H), 3.44 – 3.20 (m, 11H), 2.58 – 2.52 (m, 4H), 1.90 – 1.84 (m, 1H), 1.73 – 1.62 (m, 3H); ^{13}C NMR (126 MHz, CD_3OD): 173.0 (C), 172.6 (C), 171.8 (C), 157.2 (C), 53.2 (CH), 51.4 (CH), 42.3 (CH_2), 41.9 (CH_2), 40.5 (CH_2), 38.9 (CH_2), 38.6 (CH_2), 28.7 (CH_2), 26.5 – 26.1 (m, 2x CH_2), 24.9 (CH_2); ^{19}F NMR (282 MHz, CD_3OD): –82.3 (tt, $^3J(\text{F,F}) = 10.1$ Hz, $^4J(\text{F,F}) = 2.3$ Hz, 3F), –115.6 to –115.7 (m, 2F), –122.6 to –122.8 (m, 6F), –123.7 (br s, 2F), –124.4 (br s, 2F), –127.2 to –127.3 (m, 2F); MS (ESI, MeOH): 823 (100, $[\text{M}+\text{H}]^+$); HRMS (ESI, +ve) calcd. for $\text{C}_{23}\text{H}_{28}\text{F}_{17}\text{N}_6\text{O}_3\text{S}_2^+$: 823.1387, found: 822.1356.



Compound 65. Compound **44** (380 mg, 586 μmol) was dissolved in dry DMF (6 mL) at 0 °C. HATU (237 mg, 624 μmol) and TEA (100 μL , 741 μmol) were added

followed by OA (164 mg, 613 μmol) after 90 s. The solution was allowed to warm up to rt and stirred for 2.5 h under Ar atmosphere. EtOAc (100 mL) was then added and the organic layer was washed with H_2O , LiCl (5%) and brine (3 x 20 mL each). The organic layer was then dried with Na_2SO_4 and concentrated under reduced pressure. The mixture was purified by a flash column chromatography (SiO_2 , $\text{CH}_2\text{Cl}_2/\text{MeOH}$ 97:3, R_f 0.4 in $\text{CH}_2\text{Cl}_2/\text{MeOH}$ 19:1) to give **65** as a pale yellow oil (419 mg, 79%). $[\alpha]_D^{20}$: –12 (c 0.10, CHCl_3); IR (neat): 3325 (w), 2925 (m), 2854 (w), 1710 (w), 1656 (w), 1618 (m), 1547 (m), 1450 (m), 1406 (w), 1371 (w), 1289 (w), 1243 (m), 1153 (m), 1094 (s), 1034 (m), 994 (w), 970 (w), 907 (w), 849 (w), 810 (w), 783 (w), 759 (m), 735 (s),

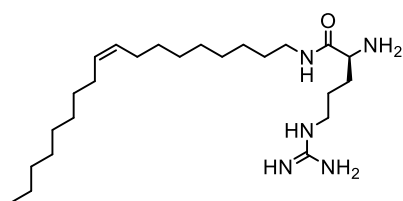
660 (s), 641 (m), 619 (m), 558 (s), 536 (m), 514 (s), 511 (s); ^1H NMR (400 MHz, CDCl_3): 7.66 (d, $^3J(\text{H,H}) = 7.6$ Hz, 2H), 7.48 (d, $^3J(\text{H,H}) = 7.4$ Hz, 2H), 7.29 (t, $^3J(\text{H,H}) = 7.4$ Hz, 2H), 7.21 – 7.15 (m, 2H), 6.93 (s, 1H), 6.14 (s, 2H), 5.93 (br d, $^3J(\text{H,H}) = 6.6$ Hz 1H), 5.30 – 5.24 (m, 2H), 4.26 – 4.04 (m, 4 H), 3.24 – 3.08 (m, 4H), 2.84 (s, 2H), 2.51 (s, 3H), 2.43 (s, 3H), 2.00 (s, 3H), 1.93 – 1.89 (m, 4H), 1.79 – 1.76 (m, 1H), 1.53 – 1.35 (m, 11H), 1.53 – 1.35 (m, 11H), 1.25 – 1.14 (m, 22H), 0.80 (t, $^3J(\text{H,H}) = 6.7$ Hz, 3H); ^{13}C NMR (101 MHz, CDCl_3): 171.8 (C), 158.9 (C), 156.6 (C), 156.4 (C), 143.7 (2xC), 141.2 (2xC), 138.4 (C), 132.6 (C), 132.3 (C), 129.9 (CH), 129.8 (CH), 127.7 (2xCH), 127.1 (2xCH), 125.1 (2xCH), 124.7 (C), 120.0 (2xCH), 117.6 (C), 86.4 (C), 67.1 (CH_2), 54.3 (CH), 47.1 (CH), 43.2 (CH_2), 39.8 (CH_2), 32.6 (CH_2), 31.9 (CH_2), 29.8 (CH_2), 29.7 (2x CH_2), 29.6 (CH_2), 29.5 (3x CH_2), 29.4 (CH_2), 29.3 (3x CH_2), 28.6 (2x CH_3), 27.2 (CH_2), 27.0 (CH_2), 25.4 (CH_2), 22.7 (CH_2), 19.3 (CH_3), 18.0 (CH_3), 14.1 (CH_3), 12.5 (CH_3); MS (ESI, MeOH): 899 (100, $[\text{M}+\text{H}]^+$).



Compound 66. To a solution of **65** (415 mg, 462 μmol) in CH_2Cl_2 , DBU (400 μL , 2.68 mmol) was added and the solution was stirred for 1 h at rt. The mixture was concentrated under

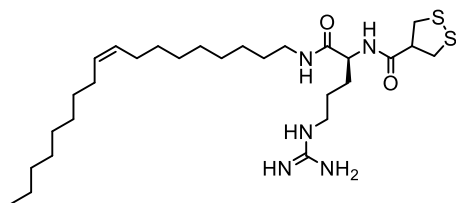
reduced pressure and purified by a flash column chromatography (SiO_2 , $\text{CH}_2\text{Cl}_2/\text{MeOH}/\text{TEA}$ 97:3:0.1 to 9:1:0.1, R_f 0.6 in $\text{CH}_2\text{Cl}_2/\text{MeOH}$ 17:3) to give **66** as a pale yellow oil (294 mg, 81%). $[\alpha]_{\text{D}}^{20}$: +12 (c 0.10, CHCl_3); IR (neat): 3322 (w), 2924 (m), 2854 (m), 1618 (m), 1549 (s), 1453 (m), 1402 (w), 1370 (w), 1294 (w), 1249 (m), 1152 (m), 1097 (s), 1035 (w), 994 (w), 969 (w), 905 (w), 848 (m), 809 (m), 784 (m), 730 (m), 720 (m), 661 (s), 640 (s), 618 (s), 599 (m), 560 (s), 539 (s); ^1H NMR (400 MHz, CD_3OD): 5.41 – 5.34 (m, 2H), 3.40 (t, $^3J(\text{H,H}) = 6.1$ Hz, 1H), 3.24 – 3.15 (m, 4H), 3.02 (s, 2H), 2.59 (s, 3H), 2.53 (s, 3H), 2.10 – 1.98 (m, 7H), 1.73 – 1.67 (m, 1H), 1.59 – 1.45 (m, 11H), 1.33 –

1.28 (m, 22H), 0.92 (t, 3J (H,H) = 6.7 Hz, 3H); ^{13}C NMR (101 MHz, CD_3OD): 158.5 (C), 156.7 (C), 138.0 (C), 132.9 (C), 132.1 (C), 130.1 (C), 129.5 (CH), 129.4 (CH), 124.6 (C), 117.0 (C), 86.3 (C), 54.0 (CH), 42.6 (CH_2), 39.0 (CH_2), 31.7 (CH_2), 29.5 (CH_2), 29.4 ($3\times\text{CH}_2$), 29.3 ($2\times\text{CH}_2$), 29.2 ($2\times\text{CH}_2$), 29.0 ($3\times\text{CH}_2$), 28.9 (CH_2), 27.3 ($2\times\text{CH}_3$), 26.7 ($2\times\text{CH}_2$), 26.6 (CH_2), 22.3 (CH_2), 18.2 (CH_3), 17.0 (CH_3), 13.0 (CH_3), 11.1 (CH_3); MS (ESI, MeOH): 677 (100, $[\text{M}+\text{H}]^+$).



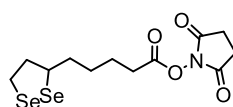
Compound 67. Compound **66** (293 mg, 371 μmol) was dissolved in TFA/ CHCl_3 1:1 (20 mL) and stirred at rt for 2.5 h. The mixture was concentrated under reduced pressure

and purified by trituration in Et_2O . The solid was dried in vacuo overnight to give **67** as a pale yellow hygroscopic solid (250 mg, quant.). $[\alpha]_{\text{D}}^{20}$: +7.1 (c 0.10, MeOH); IR (neat): 3301 (w), 3176 (w), 3116 (w), 2925 (m), 2855 (m), 1781 (w), 1665 (s), 1632 (m), 1570 (m), 1463 (w), 1373 (w), 1342 (w), 1292 (w), 1276 (w), 1200 (s), 1161 (s), 1135 (s), 1090 (s), 969 (w), 867 (m), 838 (m), 801 (m), 773 (m), 720 (s), 610 (s), 581 (s), 519 (m), 513 (s); ^1H NMR (400 MHz, CD_3OD): 5.42 – 5.35 (m, 2H), 3.74 (t, 3J (H,H) = 6.5 Hz, 1 H), 3.27 – 3.22 (m, 4H), 2.05 – 1.79 (m, 5H), 1.70 – 1.54 (m, 5H), 1.36 – 1.31 (m, 22H), 0.92 (t, 3J (H,H) = 6.7 Hz, 3H); ^{13}C NMR (101 MHz, CD_3OD): 168.4 (C), 157.3 (C), 129.3 (CH), 127.9 (CH), 52.6 (CH), 40.1 (CH_2), 39.3 (CH_2), 33.3 (CH_2), 32.2 (CH_2), 31.7 (CH_2), 29.4 ($2\times\text{CH}_2$), 29.2 (CH_2), 29.1 (CH_2), 28.9 ($3\times\text{CH}_2$), 28.2 (CH_2), 26.6 (CH_2), 24.7 ($2\times\text{CH}_2$), 23.6 (CH_2), 22.3 (CH_2), 13.0 (CH_3); MS (ESI, MeOH): 425 (100, $[\text{M}+\text{H}]^+$).



Compound 64. To a solution of **67** (42 mg, 64 μ mol) in $\text{CH}_2\text{Cl}_2/\text{DMF}$ 3:1 (3 mL), compound **48** (28 mg, 113 μ mol) in CH_2Cl_2 (1 mL) and TEA (80

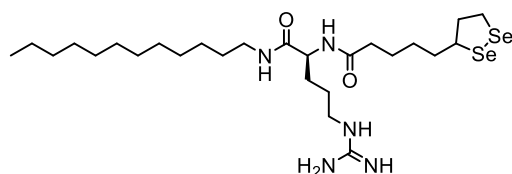
μ L, 538 μ mol) were added. The solution was stirred 2 h at rt under Ar atmosphere before to be concentrated under reduced pressure at 30 $^\circ\text{C}$ and purified by trituration in Et_2O . The solid was purified by semi-preparative HPLC (R_t 19.9 min) to give **64** as a colorless solid (6 mg, 14%). Mp: 106 – 108 $^\circ\text{C}$; $[\alpha]_D^{20}$: –17 (c 0.10, MeOH); IR (neat): 3286 (w), 2923 (m), 2853 (w), 1781 (w), 1708 (w), 1639 (s), 1547 (m), 1460 (w), 1372 (w), 1303 (w), 1216 (m), 1075 (s), 969 (m), 838 (w), 716 (m), 650 (s), 610 (s), 556 (s), 537 (s), 517 (s); ^1H NMR (500 MHz, CD_3OD): 5.41 – 5.53 (m, 2H), 4.35 (dd, $^3J(\text{H,H}) = 8.3$ Hz, 5.8 Hz, 1H), 3.34 – 3.16 (m, 9H), 2.07 – 1.98 (m, 3H), 1.90 – 1.83 (m, 1H), 1.74 – 1.51 (m, 6H), 1.38 – 1.31 (m, 22H), 0.92 (t, $^3J(\text{H,H}) = 6.7$ Hz, 3H); ^{13}C NMR (126 MHz, CD_3OD): 172.8 (C), 172.0 (C), 157.2 (C), 130.1 (CH), 129.5 (CH), 53.0 (CH), 51.4 (CH), 42.3 (CH_2), 41.9 (CH_2), 40.5 (CH_2), 39.1 (CH_2), 32.2 (CH_2), 31.7 (CH_2), 29.5 (CH_2), 29.4 (2x CH_2), 29.2 (CH_2), 29.0 (2x CH_2), 28.9 (CH_2), 28.8 (2x CH_2), 26.8 (CH_2), 26.7 (CH_2), 26.6 (CH_2), 25.0 (CH_2), 22.3 (CH_2), 13.1 (CH_3); MS (ESI, MeOH): 671 (40, $[\text{M}+\text{TFA}+\text{H}]^+$), 556 (100, $[\text{M}+\text{H}]^+$); HRMS (ESI, +ve) calcd. for $\text{C}_{28}\text{H}_{54}\text{N}_5\text{O}_2\text{S}_2^+$: 556.3713, found: 556.3722.



Compound 73. To a solution of **41** (44 mg, 150 μ mol) in THF (5 mL), DCC (35 mg, 170 μ mol) and NHS (23 mg, 200 μ mol) were successively added and the

solution was stirred at rt under Ar atmosphere. After 18 h and the formation of a precipitate, the mixture was filtered and dried under reduced pressure. The mixture was purified by two flash column chromatography (SiO_2 , $\text{CH}_2\text{Cl}_2/\text{acetone}$ 97:3, R_f 0.6 in $\text{CH}_2\text{Cl}_2/\text{acetone}$ 97:3 and PE/EtOAc 1:1, R_f 0.6

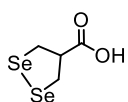
in PE/EtOAc 4:6) to give **73** as a dark brown oil (39 mg, 53%). IR (neat): 2933 (w), 1812 (w), 1781 (w), 1730 (s), 1456 (w), 1427 (w), 1364 (w), 1296 (w), 1248 (w), 1201 (s), 1152 (w), 1064 (s), 994 (w), 877 (w), 813 (w), 766 (w), 734 (w), 696 (w), 647 (m), 578 (w), 558 (w), 542 (w), 518 (w), 513 (w); ¹H NMR (400 MHz, CDCl₃): 3.91 – 3.78 (m, 1H), 3.31 – 3.20 (m, 2H), 2.95 – 2.84 (m, 1H), 2.77 (s, 4H), 2.61 – 2.42 (m, 3H), 1.82 – 1.65 (m, 4H), 1.57 – 1.43 (m, 2H); ¹³C NMR (101 MHz, CDCl₃): 169.1 (2xC), 168.4 (C), 52.2 (CH), 45.6 (CH₂), 35.1 (CH₂), 30.8 (CH₂), 29.3 (CH₂), 25.6 (2xCH₂), 24.3 (2xCH₂); UHPLC-MS: 399 (100, [M+H]⁺).



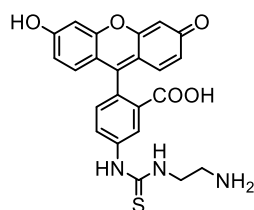
Compound 72. To solution of **47** (88 mg, 260 μmol) in DMF (1 mL), a solution of **73** (128 mg, 320 μmol) in

DMF (0.5 mL) and TEA (70 μL, 520 μmol) were successively added and the solution was stirred at rt under Ar for 5 h. The solution was then purified by trituration in Et₂O and semi-preparative HPLC to give **72** as a colorless solid (39 mg, 21%). IR (neat): 3448 (br, w), 2998 (w), 2914 (w), 1660 (w), 1436 (w), 1408 (w), 1312 (w), 1045 (s), 1025 (s), 952 (m), 934 (m), 899 (w), 823 (w), 760 (w), 698 (m), 668 (m), 613 (m), 593 (m), 580 (m), 565 (m), 547 (m), 525 (m), 513 (s); ¹H NMR (400 MHz, DMSO-*d*₆): 7.93 (d, ³*J* (H,H) = 8.1 Hz, 1H), 7.86 (t, ³*J* (H,H) = 6.1 Hz, 1H), 7.52 (t, ³*J* (H,H) = 5.7 Hz, 1H), 4.28 – 4.16 (m, 1H), 3.99 – 3.85 (m, 1H), 3.32 – 3.28 (m, 2H), 3.12 – 2.98 (m, 4H), 2.94 – 2.81 (m, 1H), 2.47 – 2.34 (m, 1H), 2.14 (t, ³*J* (H,H) = 7.3 Hz, 2H), 1.83 – 1.71 (m, 1H), 1.69 – 1.54 (m, 2H), 1.54 – 1.20 (m, 27H), 0.85 (t, ³*J* (H,H) = 7.1 Hz, 3H); ¹³C NMR (126 MHz, DMSO-*d*₆): 172.5 (C), 171.6 (C), 157.1 (C), 53.3 (CH), 52.5 (CH), 45.6 (CH₂), 40.9 (CH₂), 38.9 (CH₂), 35.4 (CH₂), 35.3 (2xCH₂), 31.8 (CH₂), 30.2 (CH₂), 29.8 (2xCH₂), 29.7 (CH₂), 29.5 (3xCH₂), 29.2 (2xCH₂), 26.8 (CH₂), 25.6 (CH₂), 25.5 (CH₂), 22.6 (CH₂), 14.4 (CH₃); UHPLC-MS: 626 (100, [M+H]⁺).

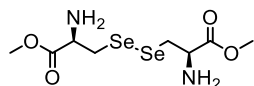
5.2.2. Delivery of Diselenide Probes



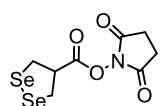
Compound 40 was synthesized following a published protocol.^[111]



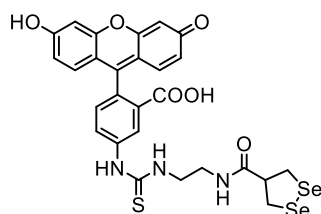
Compound 76 was synthesized following a published protocol.^[74]



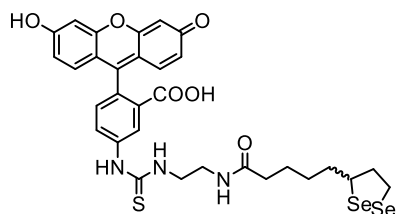
Compound 80 was synthesized following a published protocol.^[184]



Compound 75. To a solution of **40** (111 mg, 456 μ mol) in THF (5 mL), DCC (110 mg, 531 μ mol) and NHS (60.5 mg, 526 μ mol) were successively added and the solution was stirred at rt under Ar atmosphere. After 22 h and the formation of a precipitate, the mixture was filtered and dried under reduced pressure. The mixture was purified by flash column chromatography (SiO_2 , CH_2Cl_2 /acetone 49:1, R_f 0.6 in CH_2Cl_2 /acetone 24:1) to yield **75** as a dark brown oil (75.7 mg, 49%). IR (neat): 2931 (w), 2854 (w), 1808 (w), 1779 (m), 1727 (s), 1652 (w), 1423 (w), 1408 (w), 1359 (m), 1293 (w), 1247 (w), 1197 (s), 1063 (s), 992 (m), 934 (w), 909 (m), 809 (m), 725 (s), 643 (s), 577 (m), 554 (m), 513 (s), 509 (s), 501 (m); ^1H NMR (400 MHz, CDCl_3): 3.83 (quint, $^3J(\text{H,H}) = 6.9$ Hz, 1H), 3.63 – 3.57 (m, 4H), 2.78 (s, 4H); ^{13}C NMR (101 MHz, CDCl_3): 168.7 (2xC), 168.3 (C), 52.7 (CH), 31.6 (2xCH₂), 25.6 (2xCH₂); UHPLC-MS: 343 (100, $[\text{M}+\text{H}]^+$).

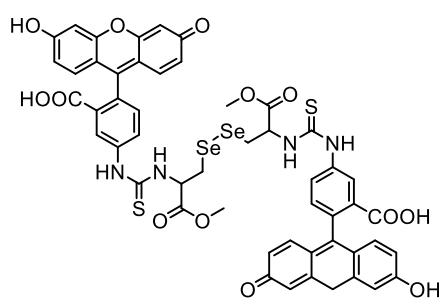


Compound 74. To a solution of **75** (61 mg, 180 μ mol) in DMF (0.5 mL), **76** (82 mg, 180 μ mol) in DMF (2.5 mL) was added and the solution was stirred for 4 h at rt. The mixture was purified by trituration in Et₂O (3 x 15 mL), reverse phase flash chromatography (90% H₂O / 10% CH₃CN + 0.1% TFA to 10% H₂O / 90% CH₃CN + 0.1% TFA) and semi-preparative HPLC (40% H₂O / 60% CH₃CN + 0.1% TFA to 30% H₂O / 70% CH₃CN + 0.1% TFA in 10 min, *R*_t = 4.8 min) to yield **74** as an orange solid (14 mg, 12%). Mp: 165 – 166 °C; IR (neat): 3244 (w), 3064 (w), 2929 (w), 2585 (w), 1635 (m), 1589 (m), 1534 (s), 1454 (m), 1383 (m), 1306 (m), 1268 (s), 1175 (s), 1117 (s), 992 (m), 966 (m), 915 (m), 843 (m), 795 (m), 764 (m), 718 (m), 694 (m), 668 (m), 639 (m), 596 (m), 574 (s), 546 (m), 522 (s), 514 (s), 509 (s); ¹H NMR (400 MHz, DMSO-*d*₆): 10.12 (br s, 1H), 10.01 (s, 1H), 8.29 (t, ³*J* (H,H) = 5.7 Hz, 1H), 8.17 (d, ⁴*J* (H,H) = 1.9 Hz, 1H), 8.05 (br s, 1H), 7.73 (br d, ³*J* (H,H) = 8.3 Hz, 1H), 7.19 (d, ³*J* (H,H) = 8.3 Hz, 1H), 6.68 (d, ⁴*J* (H,H) = 2.3 Hz, 2H), 6.62 (d, ³*J* (H,H) = 8.7 Hz, 2H), 6.57 (dd, ³*J* (H,H) = 8.7, ⁴*J* (H,H) = 2.3 Hz, 2H), 3.56 – 3.52 (m, 2H), 3.37 – 3.29 (m, 4H), 3.24 – 3.16 (m, 1H); ¹³C NMR (126 MHz, DMSO-*d*₆): 181.2 (C), 172.2 (C), 168.9 (C), 159.9 (2xC), 158.2 (C), 152.3 (2xC), 147.9 (C), 141.4 (C), 130.5 (CH), 129.5 (2xCH), 127.1 (C), 124.7 (CH), 117.6 (CH), 113.0 (2xCH), 110.1 (2xCH), 102.7 (2xCH), 57.3 (CH), 43.9 (CH₂), 38.6 (CH₂), 33.9 (¹*J* (Se,C) = 68 Hz, 2xCH₂); UHPLC-MS: 678 (100, [M+H]⁺).



Compound 77. To a solution of **76** (38 mg, 84 μ mol) in DMF (1 mL), **73** (31 mg, 78 μ mol) in DMF (1 mL) was added and the solution was stirred for 3 h at rt. The mixture was purified by trituration first in Et₂O (3 x 15 mL) and then in EtOAc (2 x 10 mL), and semi-

preparative HPLC (90% H₂O / 10% CH₃CN + 0.1% TFA to 10% H₂O / 90% CH₃CN + 0.1% TFA in 30 min, *R*_t = 22.6 min) to yield **77** as a pale brown solid (8 mg, 14%). Mp: 131 – 132 °C; IR (neat): 3266 (w), 3059 (w), 2927 (w), 2585 (w), 1671 (w), 1590 (s), 1538 (s), 1455 (m), 1424 (m), 1384 (m), 1308 (s), 1272 (s), 1192 (s), 1175 (s), 1119 (s), 994 (w), 972 (w), 916 (m), 848 (m), 795 (m), 765 (m), 719 (m), 692 (m), 669 (m), 638 (m), 598 (s), 581 (s), 564 (s), 546 (s), 529 (s), 502 (s); ¹H NMR (500 MHz, DMSO-*d*₆): 10.13 (br s, 1H), 10.04 (s, 1H), 8.18 (s, 1H), 8.05 (br s, 1H), 8.00 (br s, 1H), 7.73 (br s, 1H), 7.19 (d, ³*J* (H,H) = 8.2 Hz, 1H), 6.68 (d, ⁴*J* (H,H) = 2.4 Hz, 2H), 6.62 (d, ³*J* (H,H) = 8.7 Hz, 2H), 6.57 (dd, ³*J* (H,H) = 8.7 Hz, ⁴*J* (H,H) = 2.4 Hz, 2H), 3.94 – 3.88 (m, 1H), 3.63 – 3.53 (m, 2H), 3.32 – 3.25 (m, 4H), 2.87 – 2.80 (m, 1H), 2.44 – 2.36 (m, 1H), 2.09 (t, ³*J* (H,H) = 7.4 Hz, 2H), 1.79 – 1.71 (m, 1H), 1.63 – 1.47 (m, 3H), 1.32 (quint, ³*J* (H,H) = 7.7 Hz, 2H); ¹³C NMR (126 MHz, DMSO-*d*₆): 181.1 (C), 173.1 (C), 168.9 (C), 160.1 (C), 160.0 (2xC), 152.4 (2xC), 147.8 (C), 141.4 (C), 130.3 (CH), 129.5 (2xCH), 127.2 (C), 124.7 (CH), 117.5 (CH), 113.0 (2xCH), 110.2 (2xCH), 102.7 (2xCH), 53.3 (¹*J* (Se,C) = 62 Hz, CH), 45.6 (CH₂), 44.5 (CH₂), 38.1 (CH₂), 35.6 (CH₂), 35.3 (CH₂), 30.1 (¹*J* (Se,C) = 62 Hz, CH₂), 29.7 (CH₂), 25.4 (CH₂); UHPLC-MS: 734 (100, [M+H]⁺).



Compound 78. To a solution of **80** (108 mg, 153 μmol) in dry DMF (4.5 mL), TEA (50 μL, 360 μmol) and **81** (119 mg, 305 μmol) in DMF (1.5 mL) were successively added and the solution was stirred for 3 h at rt under Ar atmosphere. The

mixture was purified by trituration in Et₂O (3 x 15 mL) and reverse phase flash chromatography (90% H₂O / 10% CH₃CN + 0.1% TFA to 10% H₂O / 90% CH₃CN + 0.1% TFA) to afford **78** as an orange solid (77 mg, 44%). Mp: 143 – 144 °C; IR (neat): 3064 (br w), 2589 (w), 1719 (w), 1671 (w), 1637 (w), 1588

(m), 1537 (m), 1455 (m), 1385 (w), 1305 (m), 1269 (m), 1193 (m), 1174 (m), 1117 (m), 993 (w), 916 (w), 846 (m), 799 (w), 764 (w), 720 (m), 669 (m), 643 (w), 598 (m), 575 (m), 548 (m), 531 (m), 511 (s); ^1H NMR (500 MHz, DMSO- d_6): 10.36 (s, 2H), 10.14 (br s, 2H), 8.58 – 8.51 (m, 2H), 8.32 – 8.29 (m, 2H), 7.78 – 7.75 (m, 2H), 7.21 (d, 3J (H,H) = 8.3 Hz, 2H), 6.68 (d, 4J (H,H) = 1.8 Hz, 4H), 6.63 – 6.55 (m, 8H), 5.44 – 5.32 (m, 2H), 3.72 (s, 6H), 3.57 (dd, 2J (H,H) = 12.8 Hz, 3J (H,H) = 4.8 Hz, 2H), 3.46 (dd, 2J (H,H) = 12.8 Hz, 3J (H,H) = 8.2 Hz, 2H); ^{13}C NMR (126 MHz, DMSO- d_6): 181.2 (2xC), 171.3 (2xC), 168.9 (2xC), 160.0 (4xC), 152.3 (4xC), 148.0 (2xC), 141.4 (2xC), 130.0 (2xCH), 129.5 (4xCH), 127.0 (2xC), 124.7 (2xCH), 117.0 (2xCH), 113.1 (4xCH), 110.1 (4xC), 102.7 (4xCH), 57.6 (2xCH), 52.9 (2xCH₃), 31.3 (2xCH₂); UHPLC-MS: 1143 (10, [M+H]⁺), 571 (100, [M+2H]²⁺).

5.2.3. Activation of Polyarginine

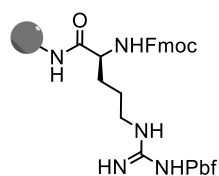
Compounds 96 – 113 were synthesized following a published protocol.^[166]

Preparation of Solutions for Solid Phase Peptide Synthesis.

Capping Mixture: 0.9 mL of acetic anhydride, 1.3 mL of 2,6-lutidine and 18 mL of DMF.

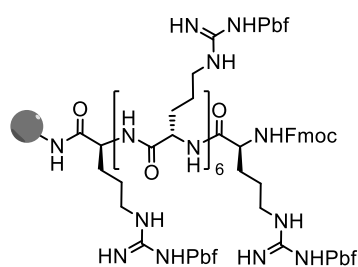
Fmoc Deprotection Solution: 20% vol. piperidine in DMF.

Base Solution: 1.96 mL DIPEA, 2.05 mL 2,6-lutidine were added to 5.54 mL NMP.



Compound 126. To a solution of **44** (97 mg, 0.15 mmol) in NMP (1 mL) were added HATU (56 mg, 0.26 mmol) followed by DIPEA (21 μL , 0.12 mmol) and 2,6-lutidine (7 μL , 0.06 mmol). The mixture was shaken for 5 min at rt, and then added to NovaPEG Rink amide resin (30 mg, initial loading 0.5 mmol/g). The reaction mixture was shaken for 13 h at rt and the resin was subsequently washed with DMF (3 x 5 mL) and CH₂Cl₂ (3 x 5 mL). The

remaining free amino groups were capped by adding Capping Mixture (1 mL), the reaction was shaken for 45 min at rt. Subsequently, the resin was washed with DMF (3 x 5 mL) and CH₂Cl₂ (3 x 5 mL). The loaded resin obtained was used in the next steps of synthesis with a loading of 0.2 mmol/g.



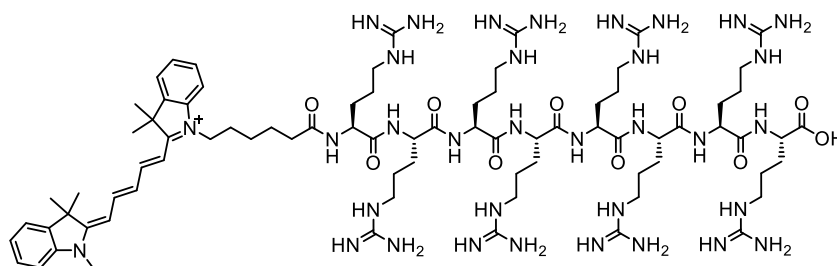
Compound 127.

Procedure 1. To **126** (5 mg) were added Fmoc Deprotection Solution (200 μ L). After 2 min, the resin was washed with DMF (1.8 mL) and the sequence was repeated a second time for 4 min. the resin was washed with DMF (2 x 1.8 mL) and CH₂Cl₂ (3 x 1.6 μ L) and DMF (3 x 1.8 mL).

Procedure 2. To a solution **44** (6 μ mol) in NMP (30 μ L) were added HATU (5 μ mol) in NMP (10 μ L), followed by Base Solution (5 μ L). The mixture was then added to the resin (5 mg). After 20 min the resin was filtered and washed with DMF (3 x 1.8 mL) and the sequence was repeated, then, the resin was washed with DMF (3 x 1.8 mL) and CH₂Cl₂ (3 x 1.8 mL).

Procedure 3. To the resin (5 mg) was added Capping Mixture (200 μ L). After 5 min, the resin was washed with DMF (3 x 1.8 mL).

Finally, procedure 1 – 3 were repeated 6 more times to give **127**.



Compound 119. To **127** (7.9 mg) was added a solution of 20% piperidine in DMF and the mixture was shaken for 4 h at 25 °C. The resin was washed with DMF (3 x 5 mL) and CH₂Cl₂ (3 x 5 mL). To the resin, Cy5-NHS (4 mg, 0.007 mmol) dissolved in NMP (300 µL) and TEA (10 µL) was added. The mixture was shaken for 4 h at 25 °C. The resin was washed with DMF (3 x 5 mL) and CH₂Cl₂ (3 x 5 mL). 150 µL of TFA was added to the resin and the mixture was shaken for 4 h at 25 °C. The resulting mixture was added to 1.5 mL of Et₂O and centrifuged. The supernatant was removed and the pellet was washed with 2 x 1.5 mL of Et₂O. The pellet was suspended in H₂O/ACN 1:1 mixture, the resin was filtered off and the filtrate was purified by reverse-phase chromatography to give product **119**. MALDI-MS (+ve, DHB matrix): 1732 ([M⁺]).

5.3. Methods

5.3.1. Vesicles Preparation

5.3.1.1. DSPC/DSPE-PEG₂₀₀₀ LUVs

A thin lipid film was obtained by evaporating a solution of 1,2-distearoyl-*sn*-glycero-3-phosphatidylcholine (7.5 mg, 9.5 µmol) and 1,2-distearoyl-*sn*-glycero-3-phosphoethanolamine-N-[amino(polyethylene glycol)-2000] (14 mg, 5 µmol) in MeOH/CHCl₃ 1:1 (1 mL) on a rotary evaporator and then drying it in vacuo overnight. The resulting film was hydrated with a buffer (1 mL, 30 mM SRB, 5 mM HEPES, 115 mM NaCl, pH 7.4) for 30 min, subjected to

freeze (liquid N₂)-thaw (65 °C water bath) cycles (10×) and extrusions (15×, 65 °C) through a polycarbonate membrane (pore size: 50, 100, 200 or 400 nm). Extravesicular components were removed by gel filtration (Sephadex G-50) with 5 mM HEPES, 172 mM NaCl, pH 7.4 buffer as eluent. Final conditions: ~2.5 mM lipids; inside: 30 mM SRB, 5 mM HEPES, 115 mM NaCl, pH 7.4; outside: 5 mM HEPES, 172 mM NaCl, pH 7.4. The vesicles were stored at 4 °C until used and kept for maximum one month.

5.3.1.2. *DSPC LUVs*

A thin film was obtained by evaporating 1,2-distearoyl-*sn*-glycero-3-phosphatidylcholine (7.9 mg, 10 µmol) in MeOH/CHCl₃ 1:1 (1 mL) on a rotary evaporator and then drying it in vacuo overnight. The resulting film was hydrated with a buffer (1 mL, 30 mM SRB, 5 mM HEPES, 115 mM NaCl, pH 7.4) for 30 min, subjected to freeze (liquid N₂)-thaw (65 °C water bath) cycles (10×) and extrusions (15×, 65 °C) through a polycarbonate membrane (pore size: 200 nm). Extravesicular components were removed by gel filtration (Sephadex G-50) with 5 mM HEPES, 172 mM NaCl, pH 7.4 buffer as eluent. Final conditions: ~2.5 mM lipids; inside: 30 mM SRB, 5 mM HEPES, 115 mM NaCl, pH 7.4; outside: 5 mM HEPES, 172 mM NaCl, pH 7.4. The vesicles were stored at 4 °C until used and kept for maximum one month.

5.3.1.3. *EYPC LUVs (SRB)*

A thin film was obtained by evaporating egg yolk phosphatidylcholine (25 mg, 32 µmol) in MeOH/CHCl₃ 1:1 (1 mL) on a rotary evaporator and then drying it in vacuo overnight. The resulting film was hydrated with a buffer (1 mL, 30 mM SRB, 5 mM HEPES, 115 mM NaCl, pH 7.4) for 30 min, subjected to freeze (liquid N₂)-thaw (40 °C water bath) cycles (10×) and extrusions (15×, 65 °C) through a polycarbonate membrane (pore size: 200 nm). Extravesicular components were removed by gel filtration (Sephadex G-50) with 5 mM HEPES, 172 mM NaCl, pH 7.4 buffer as eluent. Final conditions: ~5.4 mM

lipids; inside: 30 mM SRB, 5 mM HEPES, 115 mM NaCl, pH 7.4; outside: 5 mM HEPES, 172 mM NaCl, pH 7.4. The vesicles were stored at 4 °C.

5.3.1.4. *Brain PS/Rhod-PE LUVs*

A thin film was obtained by evaporating brain phosphatidylserine (8.1 mg, 9.8 μ mol) and 1,2-dipalmitoyl-*sn*-glycero-3-phosphoethanolamine-N-(lissamine rhodamine B sulfonyl) (0.25 mg, 0.2 μ mol) in MeOH/CHCl₃ 1:1 (1 mL) on a rotary evaporator and then drying it in vacuo overnight. The resulting film was hydrated with a buffer (1 mL, 5 mM TES, 100 mM NaCl, pH 7.4) for 30 min, subjected to freeze (liquid N₂)-thaw (40 °C water bath) cycles (5 \times) and extrusions (11 \times , 35 °C) through a polycarbonate membrane (pore size: 200 nm). The vesicles were stored at 4 °C until used and kept for maximum one month.

5.3.1.5. *Preparation of Vesicles for Thiol-Mediated Cellular Uptake*

Solutions of probes **43**, **49**, **51**, **53**, **55** and **64** in DMSO were added (1.0 – 7.5 μ L of 0.75 mM or 7.5 mM stock solution) to vesicle solution (30 μ L) at rt to reach the desired concentration (1 – 10 mol%) one day before cellular experiment. The solution was kept at 4 °C until dilution to 1 mL in Leibovitz's medium and incubation in cells.

5.3.1.6. *EYPC LUVs (CF)*

A thin lipid film was obtained by evaporating a solution of egg yolk phosphatidylcholine (25 mg, 32 μ mol) in MeOH/CHCl₃ 1:1 (1 mL) on a rotary evaporator and then drying it in vacuo overnight. The resulting film was hydrated with a buffer (1 mL, 50 mM CF, 10 mM sodium phosphate, 10 mM NaCl, pH 7.4) for 30 min, subjected to freeze (liquid N₂)-thaw (40 °C water bath) cycles (5 \times) and extrusions (15 \times , rt) through a polycarbonate membrane (pore size: 100 nm). Extravesicular components were removed by gel filtration (Sephadex G-50) with 10 mM sodium phosphate, 107 mM NaCl, pH 7.4 buffer

as eluent. Final conditions: ~5 mM EYPC; inside: 50 mM CF, 10 mM sodium phosphate, 10 mM NaCl, pH 7.4; outside: 10 mM sodium phosphate, 107 mM NaCl, pH 7.4. The vesicles were stored at 4 °C until used and kept for maximum 2 weeks.

5.3.1.7. Transport Activity in Fluorogenic LUVs

EYPC-LUV stock solutions (25 µL) were diluted with buffer solution (10 mM sodium phosphate, 107 mM NaCl, pH 7.4), placed in a thermostated fluorescence cuvette (25 °C) and gently stirred (total volume in the cuvette, 2000 µL; final lipid concentration, ~62.5 µM). CF efflux was monitored at λ_{em} 517 nm (λ_{ex} 492 nm) as a function of time after addition of activator (Na⁺ salt, 20 µL of concentrated solution in DMSO) at $t = 50$ s, polyarginine (HCl salt, 20 µL of 25 µM aqueous solution, 250 nM final concentration in the cuvette) at $t = 100$ s and 1.2% aqueous triton X-100 (40 µL of 1.2% aqueous solution, 0.024% final concentration) at $t = 500$ s. Fluorescence intensities were normalized to fractional emission intensity $I(t)$ using Equation 3:

$$I(t) = \frac{(I_t - I_0)}{(I_\infty - I_0)} \quad \text{Eq. 3.}$$

where $I_0 = I_t$ just before the addition of polyarginine, $I_\infty = I_t$ at saturation after lysis. Effective concentration EC_{50} and Hill coefficient n for activators were determined by plotting the fractional activity $Y (= I(t)$ at saturation just before lysis, $t = \sim 490$ s) as a function of activators concentration c and fitting them to the Hill Equation 4:

$$Y = Y_0 + \frac{Y_{max} - Y_0}{1 + (EC_{50}/c)^n} \quad \text{Eq. 4.}$$

where Y_0 is Y without activators, Y_{max} is Y with an excess of activators at saturation, EC_{50} is the concentration of activators required to reach 50% activity and n is the Hill coefficient.

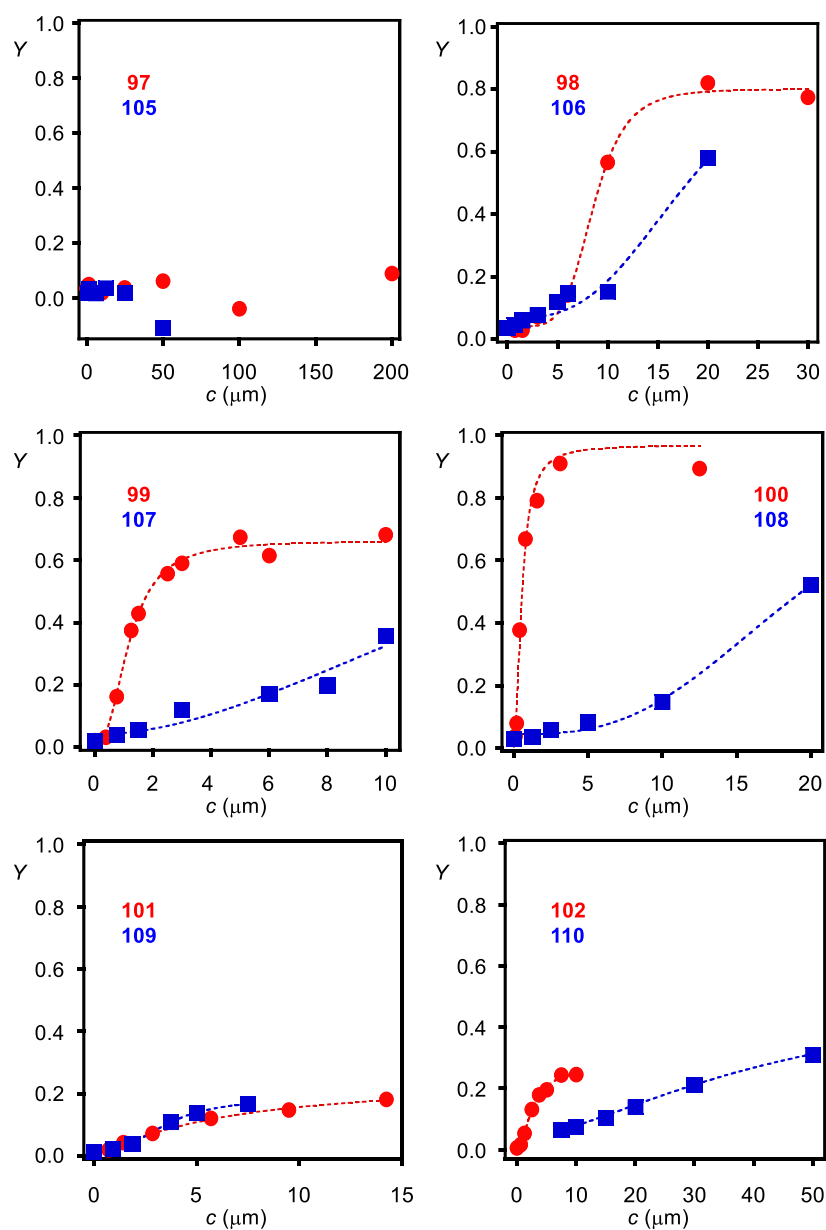


Figure 109. Transport activity in EYPC-LUVs in function of the concentration of the parallel (●) and antiparallel (■) ANI activators. The dashed lines correspond to the fit with Hill Equation 4.

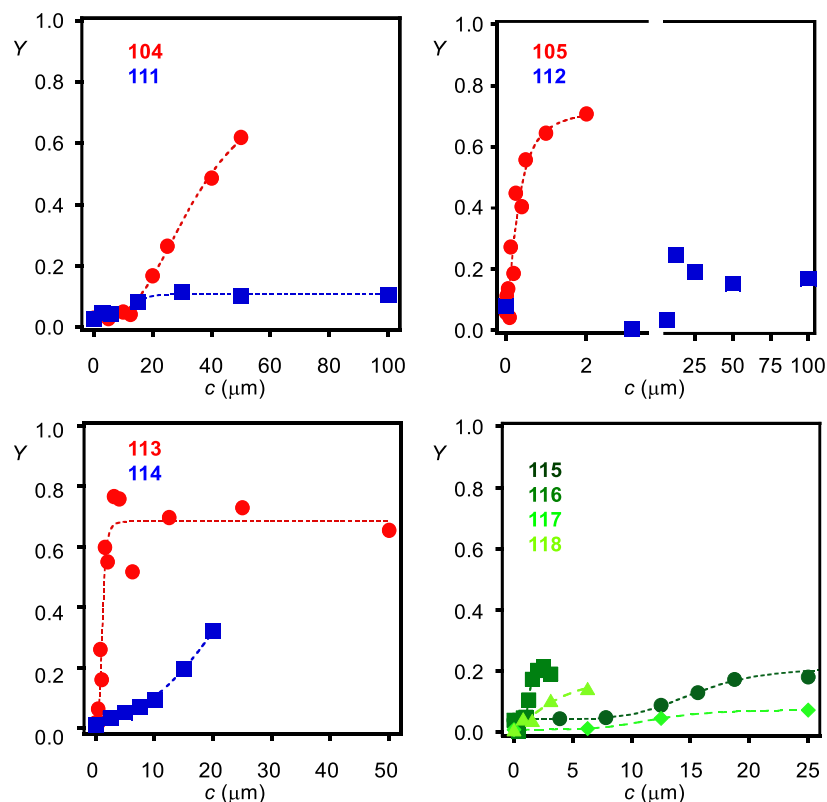


Figure 110. Transport activity in EYPC-LUVs in function of the concentration of the parallel (●) and antiparallel (■) ANI activators, and perfluorinated fatty acids (green). The dashed lines correspond to the fit with Hill Equation 4.

5.3.1.8. EYPC LUVs (empty)

A thin lipid film was obtained by evaporating a solution of egg yolk phosphatidylcholine (25 mg, 32 μmol) in MeOH/ CHCl_3 1:1 (1 mL) on a rotary evaporator and then drying it in vacuo overnight. The resulting film was hydrated with a buffer (1 mL, 10 mM sodium phosphate, 107 mM NaCl, pH 7.4) for 30 min, subjected to freeze (liquid N_2)-thaw (40 $^\circ\text{C}$ water bath) cycles (5 \times) and extrusions (15 \times , rt) through a polycarbonate membrane (pore size: 100 nm). The vesicles were stored at 4 $^\circ\text{C}$ until used and kept for maximum one month.

5.3.2. Cellular Experiments

5.3.2.1. Cell Culture

Human cervical cancer-derived HeLa Kyoto cells were cultured in minimum essential medium (MEM) containing 10% fetal bovine serum (FBS), 1% Penicillin / Streptomycin and 1% L-Glutamine. The cells were grown on a 25 cm³ tissue culture flask (TPD corporation) at 37 °C under 5% CO₂.

5.3.2.2. Confocal Microscopy

HeLa Kyoto cells were seeded at 5×10^4 cells/well on 35 mm glass-bottomed dishes (MatTek Corporation) and cultured overnight. After removing the medium, the cells were washed with PBS (2 x 1 mL) and with Leibovitz's medium (1 mL) before being treated as following:

Thiol-Mediated Uptake: cells were incubated with vesicle solution (1 mL in Leibovitz's medium). The cells were incubated for 1 – 8 h at 37 °C.

Delivery of Diselenolane: cells were incubated with fluorescent probes solution (1 mL, 1 – 100 μ M in Leibovitz's medium). The cells were incubated for 1 – 4 h at 37 °C. For experiment with the nucleus stained, Hoechst 33342 (1 μ L for a 10 μ g/mL in H₂O stock solution from Life Technologies) was added to the incubation mixture for the last 10 min.

Activation of Polyarginine: cells were incubated with activator solution (10 μ M final concentration in the dish in Leibovitz's medium) for 5 min before the addition of Cy5-CPP **119** (1 μ M final concentration in the dish in Leibovitz's medium). The cells were incubated for additional 15 min at 37 °C.

The media was removed by aspiration. Cells were washed with PBS containing 0.1 mg/mL heparin (3 x 1 mL) and with Leibovitz's medium (3 x 1 mL). The cells were kept in Leibovitz's medium during the microscope experiment. Distribution of fluorescence was analyzed without fixing using a

confocal laser scanning microscope (Leica SP5 or SP8) equipped with 63× oil immersion objective lens as following:

Thiol-Mediated Uptake: On Leica SP5, Ar laser was used as light source (4% laser power) with excitation wavelength 514 nm and emission 565 – 620 nm (Leica HyD™ detector).

Delivery of Diselenolane: On Leica SP5 microscope, Ar laser was used as light source (15% laser power) with excitation wavelength 488 nm and emission 498 – 535 nm (Leica HyD™ detector) for CF distribution. On Leica SP8 microscope, OPSL488 laser was used as light source (0.8% laser power) with excitation wavelength 488 nm and emission 501 – 550 nm (PMT detector) for CF distribution and Diode 405 laser was used as light source (6.5% laser power) with excitation wavelength 405 nm and emission 437 – 470 nm (PMT detector) for Hoechst 33342 distribution.

Activation of Polyarginine: On Leica SP5, HeNe 633 laser was used as light source (1 – 5% laser power) with excitation wavelength 633 nm and emission 650 – 700 nm (Leica HyD™ detector) for Cy5 distribution. Ar laser was used to detect the ANI core of activators (5% laser power) with excitation wavelength 458 nm and emission 500 – 541 nm (Leica HyD™ detector).

During CLSM analysis the sample was kept at 37 °C.

5.3.2.3. Colocalization Studies

HeLa Kyoto cells were seeded at 5×10^4 cells/well on 35 mm glass-bottomed dishes (MatTek Corporation) and cultured overnight. After removing the medium, the cells were washed with PBS (2 x 1 mL) and with Leibovitz's medium (1 mL) before being treated as following:

MitoTracker Green: cells were incubated with vesicle solution (1 mL in Leibovitz's medium) for 4 h at 37 °C. The last 15 min, MitoTracker Green FM (Life Technologies) was added to the dish (1 µL, final concentration: 100 nM).

MitoTracker Red: cells were incubated with 1 mL of compounds **74** or **77** (10 μ M in Leibovitz's medium) for 1 h at 37 °C. The last 20 min, MitoTracker Red CMXRos (Life Technologies) was added to the dish (final concentration: 500 nM).

LysoTracker Green: cells were incubated with vesicle solution (1 mL in Leibovitz's medium) for 4 h at 37 °C. The last 40 min, LysoTracker Green DND-26 (Life Technologies) was added to the dish (1 μ L, final concentration: 100 nM).

LysoTracker Red: cells were incubated with 1 mL of compounds **74** or **77** (10 μ M in Leibovitz's medium) for 1 h at 37 °C. The last 40 min, LysoTracker Red DND-99 (Life Technologies) was added to the dish (final concentration: 100 nM).

Dextran Green: cells were incubated with vesicle solution (950 μ L in Leibovitz's medium) for 4 h at 37 °C. The last 20 min, FITC-dextran (40 kDa, Sigma-Aldrich) was added to the dish (50 μ L, final concentration: 50 μ M).

Dextran Red: cells were incubated with 1 mL of compounds **74** or **77** (10 μ M in Leibovitz's medium) for 1 h at 37 °C. The last 20 min, Dextran Red (70 kDa, Life Technologies) was added to the dish (final concentration: 10 μ M).

After the incubation, the media was removed by aspiration. Cells were washed with PBS containing 0.1 mg/mL heparin (3 x 1 mL) and with Leibovitz's medium (3 x 1 mL). The cells were kept in Leibovitz's medium during the microscope experiment. Distribution of fluorescence was analyzed without fixing using a confocal laser scanning microscope (Leica SP5) equipped with 63 \times oil immersion objective lens. Ar laser was used as light source with excitation wavelength 488 nm and emission 492 – 534 nm (Leica HyDTM detector) for green fluorescent dyes; DPSS laser with excitation wavelength 561 nm and emission 571 – 650 nm for red fluorescent dyes. During CLSM analysis the sample was kept at 37 °C.

The colocalization quantification was performed using the ImageJ software (Ver. 1.51s), equipped with Coloc 2 plugin. The test was performed on at least 3 different pictures containing at least 5 cells each.

5.3.2.4. *Flow Cytometry*

HeLa Kyoto cells were seeded at 1×10^5 cells/well in a 6-well plate (BD Falcon) and cultured overnight. After removing the medium, the cells were washed with PBS (2 x 1 mL) and with Leibovitz's medium (1 mL) before being treated with appropriate solution (1 mL in Leibovitz's medium). The cells were incubated for 1 – 4 h at 37 °C then the media was removed by aspiration. Cells were washed with PBS containing 0.1 mg/mL heparin (1 mL) and with PBS (2 x 1 mL) before detachment by treatment with 0.05% trypsin-EDTA (1 mL) at 37 °C for 5 min. Cold MEM (1 mL) and cold PBS (2 mL) were added and the cells were collected and pelleted by centrifugation at $1400 \times g$ for 2 min. The supernatant was removed and the cells were washed with cold PBS (1 mL). The cells were re-suspended in PBS (600 μ L) containing Sytox Red (SR, 1 μ L/mL) and EDTA (0.02%). Fluorescent signals in cells were detected by laser excitation at 488 nm and emission at 525 nm or at 575 nm (at least 10000 events of live cells were collected) on a Beckman Coulter Gallios cytometer. Cells staining positive for SR were excluded from analysis. The experiments were done in triplicate.

For experiment in presence of serum, the procedure described before was applied, adding 10% FBS in the incubation medium. For 4 °C experiments, cells were preincubated in growing medium at 4 °C for 1 h. The same procedure described before was applied, using PBS solution at 4 °C for washing and performing the incubation in a 4 °C refrigerator. For inactivation of cell surface thiols, cells were preincubated with DTNB solution (1.2 mM in MEM) before incubation with appropriate solution. After incubation, the cells were treated in the same way as described before.

5.3.2.5. *Endocytosis Inhibition*

HeLa Kyoto cells were seeded at 1×10^5 cells/mL in a 6-well plate (BD Falcon) and cultured overnight. After removing the medium, the cells were incubated for 30 min at 37 °C under 5% CO₂ with 1 mL of one of the specific endocytosis inhibitors in MEM: chlorpromazine (CPZ, 30 µM), methyl- β -cyclodextrin (m β CD, 50 µM), wortmannin (wort, 50 nM) and cytochalasin B (cytoB, 10 µM). The solution was then removed by aspiration and the cells were washed twice with PBS. The cells were then treated with **77** (10 µM in MEM, 1 mL), containing the same amount of inhibitor. The cells were incubated for 1 h at 37 °C. The media was then removed by aspiration and the cells were washed three times with PBS before detachment with trypsin for 5 min at 37 °C. Cold MEM (1 mL) and cold PBS (2 mL) were added to each well and the cells were collected and pelleted by centrifugation at $1400 \times g$ for 2 min at 4 °C. The supernatant was removed and the cells were washed with cold PBS (1 mL). The supernatant was removed and the cells re-suspended in 600 µL PBS containing 1 µL/mL SR and 0.02% EDTA. Fluorescent signals in cells were detected by laser excitation at 488 nm and emission at 525 nm (at least 10000 events of live cells were collected) on a Beckman Coulter Gallios cytometer. Cells staining positive for SR were excluded from analysis. The experiments were done in triplicate.

5.3.2.6. *Automated Microscopy*

HeLa Kyoto cells were seeded at 1×10^4 cells/well in a 96-well plate (BD Falcon) and cultured overnight. The cells were then incubated for 4 h at 37 °C with vesicle solution (100 µL in Leibovitz's medium). Cells were washed using an automated plate washer (Plate washer EL406) with PBS (2 x 3 mL), PBS containing 0.1 mg/mL heparin (4 x 100 µL) and Leibovitz's medium (4 x 100 µL) before fixing with PFA (3%, 30 µL/well) for 15 min. The cells were washed with PBS (6 x 100 µL) and nuclei were stained with Hoechst H3570 (Life Technologies, 1:1000 in PBS, 30 µL/well) for 15 min before washing

with PBS (6 x 100 μ L). Cellular uptake was imaged on an automated microscope ImageXpress from Molecular Devices equipped with a 40xpf lens (λ_{ex} : 340 nm, λ_{em} : 488 nm for Hoechst, λ_{ex} : 554 nm, λ_{ex} : 568 nm for SRB). Every condition was performed in 4 wells and 25 pictures per well were taken.

5.3.2.7. *MTT Assay*

HeLa Kyoto cells were seeded with 100 μ L of cells suspension at 5×10^4 cells/mL in a 96-well plate (BD Falcon) and cultured 2 days. After removing the medium, the cells were incubated with 100 μ L of the desired CF-compound solution (10 or 100 μ M in MEM) for 24 h at 37 $^{\circ}$ C under 5% CO_2 . Then, MTT solution (10 μ L of 12 mM solution in sterile PBS) was added to each well. The cells were incubated for 4 h at 37 $^{\circ}$ C under 5% CO_2 . Finally, SDS solution (100 μ L of 100 g/L SDS in 0.01 M HCl) was added to each well and the cells were incubated for 2 h in the dark. The absorbance of the resulting solution was measured at 570 nm on a SpectraMax Plus 384 Microplate Reader from Molecular Devices and the results were treated with SOFTmax Pro 3.1.1 software.

5.3.3. Oxidation of DTT by Diselenolane

Solution of DTT (**33**, 250 μ L, 1 mM) in deuterated sodium phosphate buffer (100 mM, pD 8.0) was mixed with solution of **40** or **41** (250 μ L, 1 – 10 mM) in deuterated sodium phosphate buffer (100 mM, pD 8.0). The reaction mixture was transferred in a NMR tube and sealed with parafilm. Control experiment was performed by adding deuterated sodium phosphate buffer (250 μ L, 100 mM, pD 8.0) to **33** (250 μ L, 1 mM). ^1H NMR was measured on a Bruker 300 MHz spectrometer at different time until full conversion of **33** to **90**. The oxidation yield of DTT was calculated by comparing the integrals associated with protons of **33** (3.13 – 3.01 ppm, 2H) and of **90** (2.70 – 2.53 ppm, 4H).

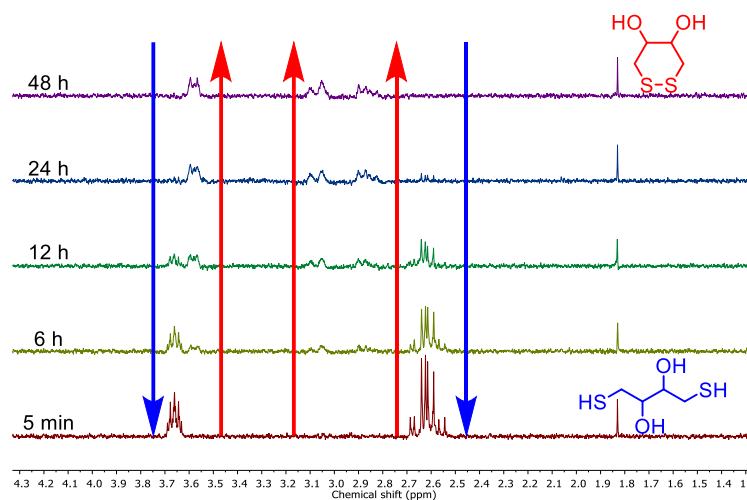


Figure 111. Representative ^1H NMR showing the reaction evolution of the oxidation of **33** to **90** at different time in deuterated phosphate buffer (100 mM, pD 8.0). Signals from **33** and **90** are shown with blue and red arrow respectively.

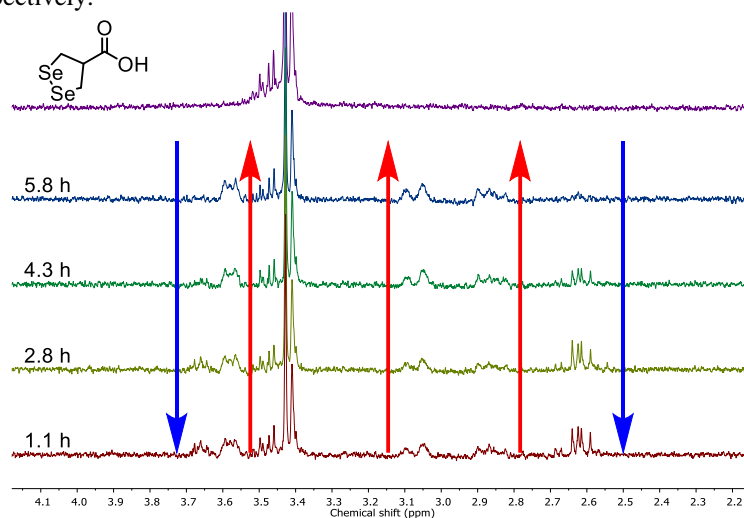


Figure 112. Representative ^1H NMR showing **40** and the reaction evolution of the oxidation of **33** to **90** in presence of **40** (1 mM) at different time in deuterated phosphate buffer (100 mM, pD 8.0). Signals from **33** and **90** are shown with blue and red arrow respectively.

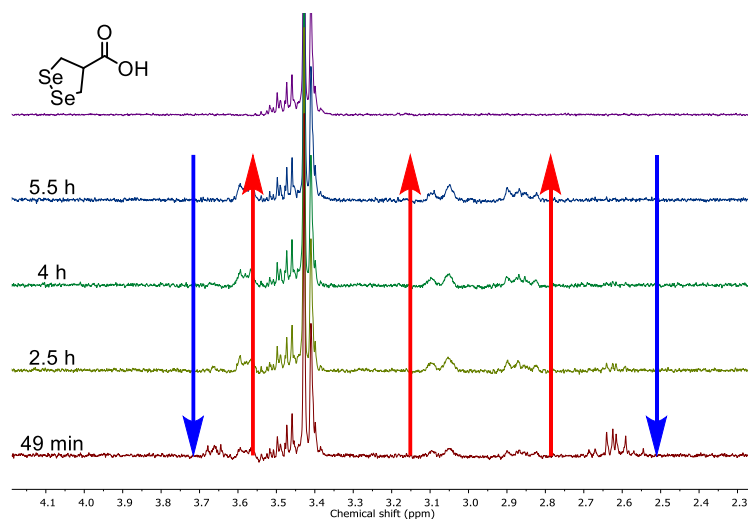


Figure 113. Representative ¹H NMR showing **40** and the reaction evolution of the oxidation of **33** to **90** in presence of **40** (2 mM) at different time in deuterated phosphate buffer (100 mM, pD 8.0). Signals from **33** and **90** are shown with blue and red arrow respectively.

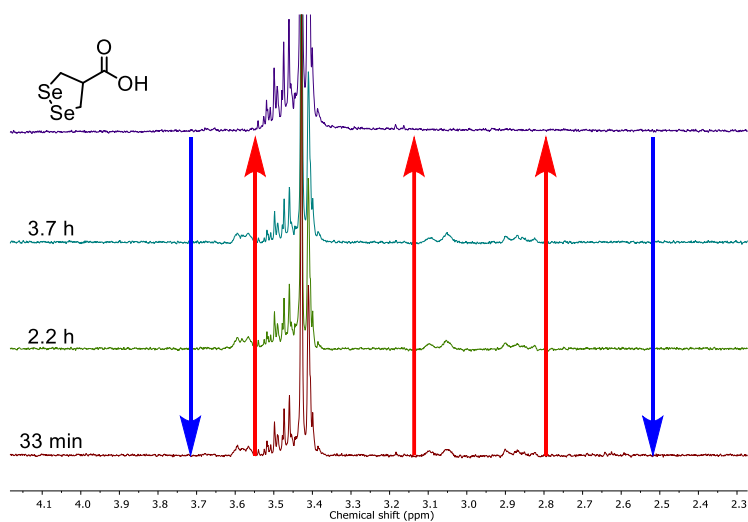


Figure 114. Representative ¹H NMR showing **40** and the reaction evolution of the oxidation of **33** to **90** in presence of **40** (5 mM) at different time in deuterated phosphate buffer (100 mM, pD 8.0). Signals from **33** and **90** are shown with blue and red arrow respectively.

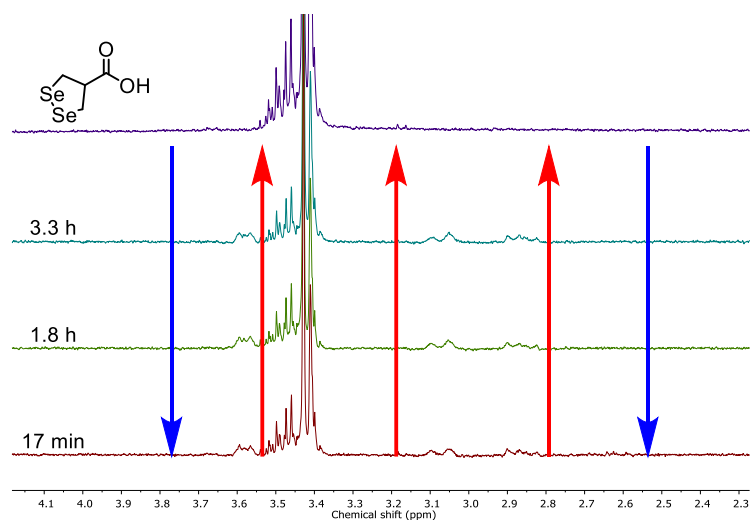


Figure 115. Representative ^1H NMR showing **40** and the reaction evolution of the oxidation of **33** to **90** in presence of **40** (10 mM) at different time in deuterated phosphate buffer (100 mM, pD 8.0). Signals from **33** and **90** are shown with blue and red arrow respectively.

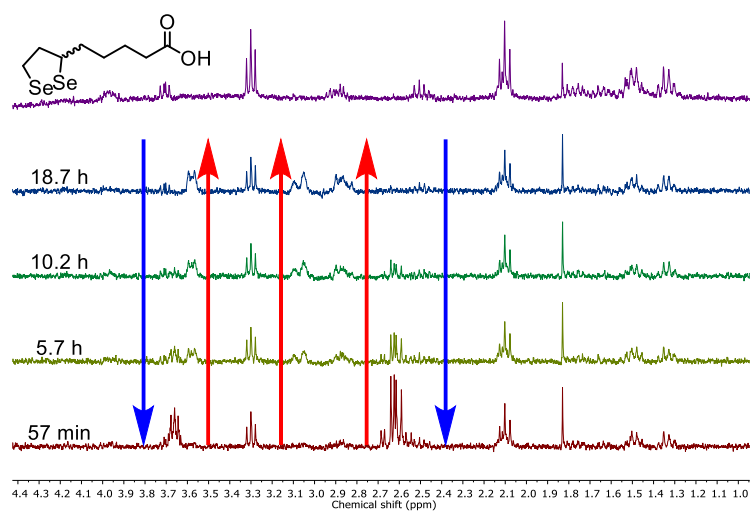


Figure 116. Representative ^1H NMR showing **41** and the reaction evolution of the oxidation of **33** to **90** in presence of **41** (1 mM) at different time in deuterated phosphate buffer (100 mM, pD 8.0). Signals from **33** and **90** are shown with blue and red arrow respectively.

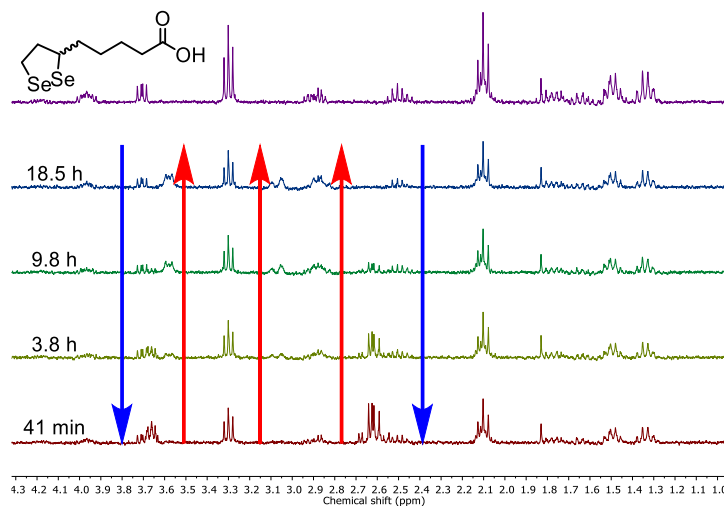


Figure 117. Representative ^1H NMR showing **41** and the reaction evolution of the oxidation of **33** to **90** in presence of **41** (2.5 mM) at different time in deuterated phosphate buffer (100 mM, pD 8.0). Signals from **33** and **90** are shown with blue and red arrow respectively.

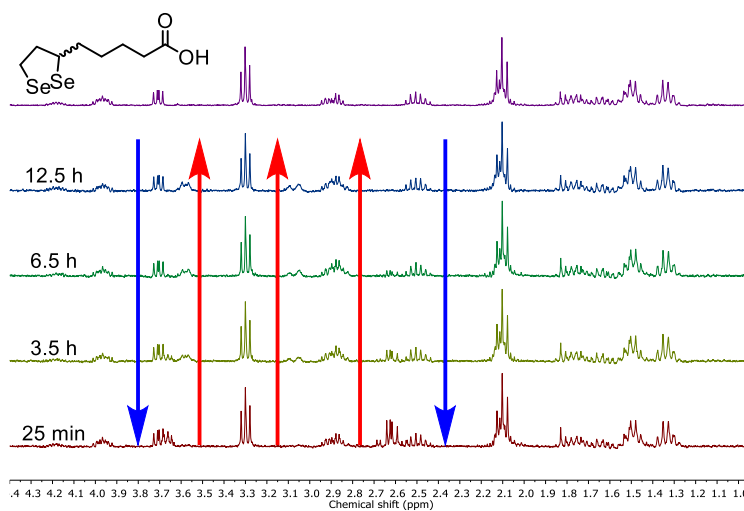


Figure 118. Representative ^1H NMR showing **41** and the reaction evolution of the oxidation of **33** to **90** in presence of **41** (5 mM) at different time in deuterated phosphate buffer (100 mM, pD 8.0). Signals from **33** and **90** are shown with blue and red arrow respectively.

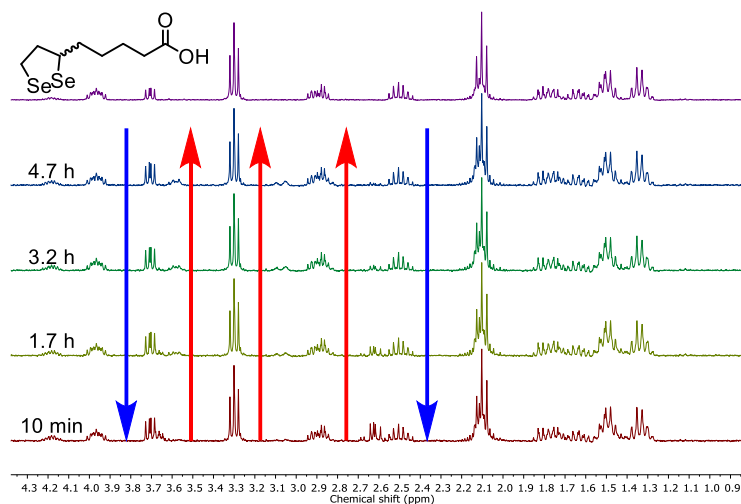


Figure 119. Representative ^1H NMR showing **41** and the reaction evolution of the oxidation of **33** to **90** in presence of **41** (10 mM) at different time in deuterated phosphate buffer (100 mM, pD 8.0). Signals from **33** and **90** are shown with blue and red arrow respectively.

5.3.4. Diselenolane Fluorescence Calibration

5.3.4.1. Closed Cycle Correction Factor

Stock solutions of **25**, **74** and **77** (10 mM in DMSO) were diluted to 1 μM solution of fluorescent compounds in PBS buffer (10 mM phosphate, 137 mM sodium chloride, 2.7 mM potassium chloride, pH 7.4). The fluorescence emission was then recorded from 500 nm to 700 nm upon excitation at 488 nm (slits 2 nm : 2 nm). Closed cycle correction factors were calculated by dividing the integrated emission intensity through the recorded spectral region of compound **25** by that of **74** or **77** (Table 4).

5.3.4.2. Open Cycle Correction Factor

Reduction of 40 and 41: TCEP (250 μL , 10 mM) in deoxygenated deuterated sodium phosphate buffer (100 mM, pD 8.0) was added to **40** or **41** (250 μL , 10 mM) in deoxygenated deuterated sodium phosphate buffer (100

mM, pD 8.0). The solution was transferred in a NMR tube and the spectrum was recorded on a Bruker 300 MHz spectrometer (Figure 74) to prove the reduction of diselenide using TCEP.

To obtain the open cycle correction factor, the fluorescent compounds (2 μ L, 100 μ M) were treated for 30 min with TCEP (2 μ L, 100 mM) before to be diluted to 1 μ M solution of fluorescent compounds in PBS buffer. The fluorescence emission was then recorded from 500 nm to 700 nm upon excitation at 488 nm (slits 1.2 nm : 1.2 nm). Open cycle correction factors were calculated by dividing the integrated emission intensity through the recorded spectral region of compound **25** by that of **74** or **77** (Table 4).

5.3.5. Absorbance and Fluorescence of CPP Activators

EYPC-LUVs (without encapsulated CF) stock solutions (25 μ L) were diluted with buffer solution (10 mM sodium phosphate, 107 mM NaCl, pH 7.4), placed in a thermostated fluorescence cuvette (25 °C) and gently stirred (total volume in the cuvette, 2000 μ L; final lipid concentration, ~62.5 μ M). The activators (3 μ M final concentration) were added to the solution and the absorption spectra were measured (Figure 120). The fluorescence spectra were recorded upon excitation at the absorption maxima for each activator (Figure 120).

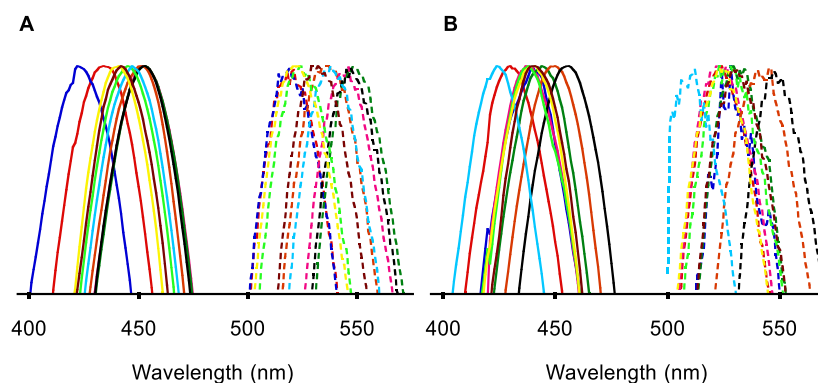


Figure 120. Absorbance and fluorescence (plain and dashed line respectively) spectra of all activators in LUVs. (A) **95**: blue; **96**: red; **97**: dark green; **98**: black; **99**: cyan; **100**: brown; **105**: purple; **106**: orange; **107**: light green; **108**: yellow. (B) **101**: blue; **102**: dark green; **103**: black; **104**: cyan; **109**: red; **110**: purple; **111**: orange; **112**: light green; **113**: brown; **114**: yellow.

5.4. Abbreviations

ANI	4-Amino-1,8-naphthalimide
Calcd	Calculated
CF	Carboxyfluorescein
CLSM	Confocal laser scanning microscopy
CPDs	Cell-penetrating poly(disulfide)s
CPPs	Cell-penetrating peptides
CuAAC	Copper-catalyzed alkyne-azide cycloaddition
Cy5	Cyanine 5
DA	Dodecylamine
DBU	1,8-Diazabicyclo[5.4.0]undec-7-ene
DCC	<i>N,N'</i> -Dicyclohexylcarbodiimide

DHB	2,5-Dihydrobenzoic acid
DMF	<i>N,N</i> -Dimethylformamide
DMSO	Dimethyl sulfoxide
DSPC	1,2-Distearoyl- <i>sn</i> -glycero-3-phosphatidylcholine
DSPE-PEG ₂₀₀₀	1,2-Distearoyl- <i>sn</i> -glycero-3-phosphoethanolamine- N-[amino(polyethylene glycol)-2000]
DTNB	5,5-Dithio-bis(2-nitrobenzoic acid)
DTT	Dithiothreitol
<i>EC</i> ₅₀	Effective concentration to reach 50% of activity
EDTA	Ethylenediaminetetraacetic acid
ETP	Epidithiodiketopiperazine
EYPC	Egg yolk phosphatidylcholine
FBS	Fetal bovine serum
FITC	Fluorescein isothiocyanate
Fmoc	Fluorenylmethyloxycarbonyl
FRET	Förster resonance energy transfer
GSH	Glutathione
HATU	<i>O</i> -(7-Azabenzotriazol-1-yl)- <i>N,N,N',N'</i> - tetramethyluronium hexafluorophosphate
HBTU	Tetramethyl-O-(1H-benzotriazol-1-yl)uronium hexafluorophosphate
HEPES	4-(2-Hydroxyethyl)-1-piperazineethanesulfonic acid
HPLC	High Pressure Liquid Chromatography
LUVs	Large unilamellar vesicles

MEM	Minimum essential medium
MTT	3-(4,5-Dimethylthiazol-2-yl)-2,5-diphenyltetrazolium bromide
NHS	<i>N</i> -Hydroxysuccinimide
NMP	<i>N</i> -Methyl-2-pyrrolidone
OA	Oleylamine
Pbf	2,2,4,6,7-Pentamethyl-dihydrobensofuran-5-sulfonyl
PBS	Phosphate buffered serum
PCC	Pearson's correlation coefficient
PDMS	Poly(dimethylsiloxan)
PE	Petroleum ether
PEG	Poly(ethylene glycol)
PFA	Paraformaldehyde
PMOXA	Poly(2-methyl-2-oxazoline)
pR	Poly-L-arginine
PS	Phosphatidylserine
PTSA	<i>p</i> -Toluenesulfonic acid
Quant	quantitative
R ₈	Octaarginine
rt	Room temperature
R _t	Retention time
R _f	Retention factor
Rhod-PE	1,2-dipalmitoyl- <i>sn</i> -glycero-3-phosphoethanolamine-N-(lissamine rhodamine B sulfonyl)

SDS	Sodium dodecyl sulfate
SR	Sytox red
SRB	Sulforhodamine B
t_{50}	Incubation time to reach 50% of the activity
TAMRA	Tetramethylrhodamine
TCEP	Tris(2-carboxyethyl)phosphine
TEA	Triethylamine
TES	N-[Tris(hydroxymethyl)methyl]-2-aminoethanesulfonic acid
TFA	Trifluoroacetic acid
THF	Tetrahydrofuran
Tris	Tris(hydroxymethyl)aminomethane
TRFC	Transferrin receptor protein 1
Trt	Trityl

Chapter 6

REFERENCES

- [1] Nisini, R.; Poerio, N.; Mariotti, S.; De Santis, F.; Fraziano, M. *Front. Immunol.* **2018**, *9*, 155.
- [2] Kaparissides, C.; Alexandridou, S.; Kotti, K.; Chaitidou, S. *Online J. Nanotechnol.* **2006**, *2*, 1–11.
- [3] Ray, M.; Lee, Y.-W.; Scaletti, F.; Yu, R.; Rotello, V. M. *Nanomedicine* **2017**, *12*, 941–952.
- [4] Isoglu, I. A.; Ozsoy, Y.; Isoglu, S. D. *Curr. Top. Med. Chem.* **2017**, *17*, 1469–1489.
- [5] Bazban-Shotorbani, S.; Hasani-Sadrabadi, M. M.; Karkhaneh, A.; Serpooshan, V.; Jacob, K. I.; Moshaverinia, A.; Mahmoudi, M. *J. Control. Release* **2017**, *253*, 46–63.
- [6] Aderem, A.; Underhill, D. M. *Annu. Rev. Immunol.* **1999**, *17*, 593–623.
- [7] Lim, J. P.; Gleeson, P. A. *Immunol. Cell Biol.* **2011**, *89*, 836–843.
- [8] Kaksonen, M.; Roux, A. *Nat. Rev. Mol. Cell Biol.* **2018**, *19*, 313–326.
- [9] Nabi, I. R.; Le, P. U. *J. Cell Biol.* **2003**, *161*, 673–677.
- [10] Zhu, M.; Nie, G.; Meng, H.; Xia, T.; Nel, A.; Zhao, Y. *Acc. Chem. Res.* **2013**, *46*, 622–631.
- [11] Damm, E.-M.; Pelkmans, L.; Kartenbeck, J.; Mezzacasa, A.; Kurzchalia, T.; Helenius, A. *J. Cell Biol.* **2005**, *168*, 477–488.
- [12] Ivanov, A. I. *Methods Mol. Biol.* **2008**, *440*, 15–33.
- [13] Geisow, M. J.; Evans, W. H. *Exp. Cell Res.* **1984**, *150*, 36–46.
- [14] Green, M.; Loewenstein, P. M. *Cell* **1988**, *55*, 1179–1188.
- [15] Frankel, A. D.; Pabo, C. O. *Cell* **1988**, *55*, 1189–1193.
- [16] Vivès, E.; Brodin, P.; Lebleu, B. *J. Biol. Chem.* **1997**, *272*, 16010–16017.
- [17] Derossi, D.; Joliot, A. H.; Chassaing, G.; Prochiantz, A. *J. Biol. Chem.* **1994**, *269*, 10444–10450.
- [18] Farkhani, S. M.; Valizadeh, A.; Karami, H.; Mohammadi, S.; Sohrabi, N.; Badrzadeh, F. *Peptides* **2014**, *57*, 78–94.

- [19] Rhee, M.; Davis, P. *J. Biol. Chem.* **2006**, *281*, 1233–1240.
- [20] Lin, Y.-Z.; Yao, S.; Veach, R. A.; Torgerson, T. R.; Hawiger, J. *J. Biol. Chem.* **1995**, *270*, 14255–14258.
- [21] Morris, M. C.; Depollier, J.; Mery, J.; Heitz, F.; Divita, G. *Nat. Biotechnol.* **2001**, *19*, 1173–1176.
- [22] Pooga, M.; Hällbrink, M.; Zorko, M.; Langel, U. *FASEB J.* **1998**, *12*, 67–77.
- [23] Wender, P. A.; Mitchell, D. J.; Pattabiraman, K.; Pelkey, E. T.; Steinman, L.; Rothbard, J. B. *Proc. Natl. Acad. Sci. U. S. A.* **2000**, *97*, 13003–13008.
- [24] Vocero-Akbani, A. M.; Heyden, N. Vander; Lissy, N. A.; Ratner, L.; Dowdy, S. F. *Nat. Med.* **1999**, *5*, 29–33.
- [25] Schwarze, S. R.; Ho, A.; Vocero-Akbani, A.; Dowdy, S. F. *Science* **1999**, *285*, 1569–1572.
- [26] Astriab-Fisher, A.; Sergueev, D. S.; Fisher, M.; Ramsay Shaw, B.; Juliano, R. L. *Biochem. Pharmacol.* **2000**, *60*, 83–90.
- [27] Sandgren, S.; Cheng, F.; Belting, M. *J. Biol. Chem.* **2002**, *277*, 38877–38883.
- [28] Sakai, N.; Matile, S. *J. Am. Chem. Soc.* **2003**, *125*, 14348–14356.
- [29] Rothbard, J. B.; Jessop, T. C.; Lewis, R. S.; Murray, B. A.; Wender, P. A. *J. Am. Chem. Soc.* **2004**, *126*, 9506–9507.
- [30] Herce, H. D.; Garcia, A. E.; Litt, J.; Kane, R. S.; Martin, P.; Enrique, N.; Rebollo, A.; Milesi, V. *Biophys. J.* **2009**, *97*, 1917–1925.
- [31] Hall, K.; Lee, T.-H.; Mechler, A. I.; Swann, M. J.; Aguilar, M.-I. *Sci. Rep.* **2014**, *4*, 5479.
- [32] Murayama, T.; Masuda, T.; Afonin, S.; Kawano, K.; Takatani-Nakase, T.; Ida, H.; Takahashi, Y.; Fukuma, T.; Ulrich, A. S.; Futaki, S. *Angew. Chem., Int. Ed.* **2017**, *56*, 7644–7647.
- [33] Di Pisa, M.; Chassaing, G.; Swiecicki, J.-M. *Biochemistry* **2015**, *54*, 194–207.
- [34] Perret, F.; Nishihara, M.; Takeuchi, T.; Futaki, S.; Lazar, A. N.; Coleman, A. W.; Sakai, N.; Matile, S. *J. Am. Chem. Soc.* **2005**, *127*, 1114–1115.
- [35] Kim, T.; Rothmund, T.; Kissel, T.; Kim, S. W. *J. Control. Release* **2011**, *152*, 110–119.
- [36] Takeuchi, T.; Kosuge, M.; Tadokoro, A.; Sugiura, Y.; Nishi, M.; Kawata, M.; Sakai, N.; Matile, S.; Futaki, S. *ACS Chem. Biol.* **2006**, *1*,

299–303.

- [37] Katayama, S.; Nakase, I.; Yano, Y.; Murayama, T.; Nakata, Y.; Matsuzaki, K.; Futaki, S. *Biochim. Biophys. Acta, Biomembr.* **2013**, *1828*, 2134–2142.
- [38] Candan, G.; Michiue, H.; Ishikawa, S.; Fujimura, A.; Hayashi, K.; Uneda, A.; Mori, A.; Ohmori, I.; Nishiki, T.; Matsui, H.; Tomizawa, K. *Biomaterials* **2012**, *33*, 6468–6475.
- [39] Gasparini, G.; Bang, E.-K.; Molinard, G.; Tulumello, D. V.; Ward, S.; Kelley, S. O.; Roux, A.; Sakai, N.; Matile, S. *J. Am. Chem. Soc.* **2014**, *136*, 6069–6074.
- [40] Kim, Y. H.; Park, J. H.; Lee, M.; Kim, Y.-H.; Park, T. G.; Kim, S. W. *J. Control. Release* **2005**, *103*, 209–219.
- [41] Luten, J.; van Nostrum, C. F.; De Smedt, S. C.; Hennink, W. E. *J. Control. Release* **2008**, *126*, 97–110.
- [42] Lee, Y. S.; Kim, S. W. *J. Control. Release* **2014**, *190*, 424–439.
- [43] Brülisauer, L.; Gauthier, M. A.; Leroux, J.-C. *J. Control. Release* **2014**, *195*, 147–154.
- [44] Kosower, N. S.; Kosower, E. M. *Int. Rev. Cytol.* **1978**, *54*, 109–160.
- [45] Soboll, S.; Gründel, S.; Harris, J.; Kolb-Bachofen, V.; Ketterer, B.; Sies, H. *Biochem. J.* **1995**, *311*, 889–894.
- [46] Lash, L. H.; Putt, D. A.; Matherly, L. H. *J. Pharmacol. Exp. Ther.* **2002**, *303*, 476–486.
- [47] Phillips, D. J.; Gibson, M. I. *Biomacromolecules* **2012**, *13*, 3200–3208.
- [48] Cho, H. Y.; Srinivasan, A.; Hong, J.; Hsu, E.; Liu, S.; Shrivats, A.; Kwak, D.; Bohaty, A. K.; Paik, H.; Hollinger, J. O.; Matyjaszewski, K. *Biomacromolecules* **2011**, *12*, 3478–3486.
- [49] Lee, Y.; Koo, H.; Jin, G.; Mo, H.; Cho, M. Y.; Park, J.-Y.; Choi, J. S.; Park, J. S. *Biomacromolecules* **2005**, *6*, 24–26.
- [50] Mullen, D. G.; Weigel, B.; Barany, G.; Distefano, M. D. *J. Pept. Sci.* **2010**, *16*, 219–222.
- [51] Oupický, D.; Li, J. *Macromol. Biosci.* **2014**, *14*, 908–922.
- [52] Sadownik, A.; Stefely, J.; Regen, S. L. *J. Am. Chem. Soc.* **1986**, *108*, 7789–7791.
- [53] Balakirev, M.; Schoehn, G.; Chroboczek, J. *Chem. Biol.* **2000**, *7*, 813–819.
- [54] Chung, Y. C.; Regen, S. L. *Macromolecules* **1991**, *24*, 5738–5739.

- [55] Sakai, N.; Lista, M.; Kel, O.; Sakurai, S.; Emery, D.; Mareda, J.; Vauthey, E.; Matile, S. *J. Am. Chem. Soc.* **2011**, *133*, 15224–15227.
- [56] Sakai, N.; Matile, S. *J. Am. Chem. Soc.* **2011**, *133*, 18542–18545.
- [57] Bang, E.-K.; Gasparini, G.; Molinard, G.; Roux, A.; Sakai, N.; Matile, S. *J. Am. Chem. Soc.* **2013**, *135*, 2088–2091.
- [58] Bang, E.-K.; Ward, S.; Gasparini, G.; Sakai, N.; Matile, S. *Polym. Chem.* **2014**, *5*, 2433–2441.
- [59] Chuard, N.; Gasparini, G.; Roux, A.; Sakai, N.; Matile, S. *Org. Biomol. Chem.* **2015**, *13*, 64–67.
- [60] Gasparini, G.; Matile, S. *Chem. Commun.* **2015**, *51*, 17160–17162.
- [61] Fu, J.; Yu, C.; Li, L.; Yao, S. Q. *J. Am. Chem. Soc.* **2015**, *137*, 12153–12160.
- [62] Yu, C.; Qian, L.; Ge, J.; Fu, J.; Yuan, P.; Yao, S. C. L.; Yao, S. Q. *Angew. Chem., Int. Ed.* **2016**, *55*, 9272–9276.
- [63] Yuan, P.; Zhang, H.; Qian, L.; Mao, X.; Du, S.; Yu, C.; Peng, B.; Yao, S. Q. *Angew. Chem., Int. Ed.* **2017**, *56*, 12481–12485.
- [64] Yuan, P.; Mao, X.; Chong, K. C.; Fu, J.; Pan, S.; Wu, S.; Yu, C.; Yao, S. Q. *Small* **2017**, *13*, 1700569.
- [65] Qian, L.; Fu, J.; Yuan, P.; Du, S.; Huang, W.; Li, L.; Yao, S. Q. *Angew. Chem., Int. Ed.* **2018**, *57*, 1532–1536.
- [66] Morelli, P.; Martin-Benlloch, X.; Tessier, R.; Waser, J.; Sakai, N.; Matile, S. *Polym. Chem.* **2016**, *7*, 3465–3470.
- [67] Morelli, P.; Matile, S. *Helv. Chim. Acta* **2017**, *100*, e1600370.
- [68] Morelli, P.; Bartolami, E.; Sakai, N.; Matile, S. *Helv. Chim. Acta* **2018**, *101*, e1700266.
- [69] Aubry, S.; Burlina, F.; Dupont, E.; Delaroche, D.; Joliot, A.; Lavielle, S.; Chassaing, G.; Sagan, S. *FASEB J.* **2009**, *23*, 2956–2967.
- [70] Yan, Y.; Wang, Y.; Joan, H. K.; Nice, E. C.; Caruso, F. *Adv. Mater.* **2011**, *23*, 3916–3921.
- [71] Torres, A. G.; Gait, M. J. *Trends Biotechnol.* **2012**, *30*, 185–190.
- [72] Torres, A. G.; Fabani, M. M.; Vigorito, E.; Williams, D.; Al-Obaidi, N.; Wojciechowski, F.; Hudson, R. H. E.; Seitz, O.; Gait, M. J. *Nucleic Acids Res.* **2012**, *40*, 2152–2167.
- [73] Rosenberg, L. E.; Crawhall, J. C.; Segal, S. *J. Clin. Invest.* **1967**, *46*, 30–34.
- [74] Gasparini, G.; Sargsyan, G.; Bang, E.-K.; Sakai, N.; Matile, S. *Angew.*

Chem., Int. Ed. **2015**, *54*, 7328–7331.

- [75] Foss, O.; Tjomsland, O. *Acta Chem. Scand.* **1958**, *12*, 1810–1818.
- [76] Stroud, R. M.; Carlisle, C. H. *Acta Cryst.* **1972**, *B28*, 304–307.
- [77] Rahman, R.; Safe, S.; Taylor, A. *Q. Rev., Chem Soc.* **1970**, *24*, 208–237.
- [78] Shefter, E.; Kalman, T. I. *J. Chem. Soc. D* **1969**, *0*, 1027b–1029.
- [79] Steinrauf, L. K.; Peterson, J.; Jensen, L. H. *J. Am. Chem. Soc.* **1958**, *80*, 3835–3838.
- [80] Clauss, A. D.; Nelsen, S. F.; Ayoub, M.; Moore, J. W.; Landis, C. R.; Weinhold, F. *Chem. Educ. Res. Pr.* **2014**, *15*, 417–434.
- [81] Abegg, D.; Gasparini, G.; Hoch, D. G.; Shuster, A.; Bartolami, E.; Matile, S.; Adibekian, A. *J. Am. Chem. Soc.* **2017**, *139*, 231–238.
- [82] Wiśniewski, J. R.; Ostasiewicz, P.; Duś, K.; Zielińska, D. F.; Gnad, F.; Mann, M. *Mol. Syst. Biol.* **2012**, *8*, 611.
- [83] Zong, L.; Bartolami, E.; Abegg, D.; Adibekian, A.; Sakai, N.; Matile, S. *ACS Cent. Sci.* **2017**, *3*, 449–453.
- [84] Gardiner, D. M.; Waring, P.; Howlett, B. H. *Microbiology* **2005**, *151*, 1021–1032.
- [85] Park, H. B.; Kwon, H. C.; Lee, C.-H.; Yang, H. O. *J. Nat. Prod.* **2009**, *72*, 248–252.
- [86] Overman, L. E.; Sato, T. *Org. Lett.* **2007**, *9*, 5267–5270.
- [87] Gao, W.; Li, T.; Wang, J.; Zhao, Y.; Wu, C. *Anal. Chem.* **2017**, *89*, 937–944.
- [88] Li, T.; Gao, W.; Liang, J.; Zha, M.; Chen, Y.; Zhao, Y.; Wu, C. *Anal. Chem.* **2017**, *89*, 8501–8508.
- [89] Kryukov, G. V.; Castellano, S.; Novoselov, S. V.; Lobanov, A. V.; Zehtab, O.; Guigó, R.; Gladyshev, V. N. *Science* **2003**, *300*, 1439–1443.
- [90] Takahashi, K.; Akasaka, M.; Yamamoto, Y.; Kobayashi, C.; Mizoguchi, J.; Koyaxna, J. *J. Biochem.* **1990**, *108*, 145–148.
- [91] Gasdaska, P. Y.; Gasdaska, J. R.; Cochran, S.; Powis, G. *FEBS Lett.* **2000**, *373*, 5–9.
- [92] Berry, M. J.; Banu, L.; Larsen, P. R. *Nature* **1991**, *349*, 438–440.
- [93] Liu, J.; Rozovsky, S. *Antioxid. Redox Signaling* **2015**, *23*, 795–813.
- [94] Bösl, M. R.; Takaku, K.; Oshima, M.; Nishimura, S.; Taketo, M. M. *Proc. Natl. Acad. Sci. U. S. A.* **1997**, *94*, 5531–5534.

- [95] Rosa, R. M.; Roesler, R.; Braga, A. L.; Saffi, J.; Henriques, J. A. P. *Braz. J. Med. Biol. Res.* **2007**, *40*, 1287–1304.
- [96] Marcondes Sari, M. H.; Zborowski, V. A.; Ferreira, L. M.; Jardim, N. S.; Barbieri, A. V.; Cruz, L.; Nogueira, C. W. *Eur. J. Pharm. Sci.* **2018**, *111*, 38–45.
- [97] Occai, B. K.; Hassan, W.; da Rocha, J. B. T. *Chem. Biol. Interact.* **2018**, *279*, 196–202.
- [98] Xu, H.; Cao, W.; Zhang, X. *Acc. Chem. Res.* **2013**, *46*, 1647–1658.
- [99] Ma, N.; Li, Y.; Xu, H.; Wang, Z.; Zhang, X. *J. Am. Chem. Soc.* **2010**, *132*, 442–443.
- [100] Ma, N.; Xu, H.; An, L.; Li, J.; Sun, Z.; Zhang, X. *Langmuir* **2011**, *27*, 5874–5878.
- [101] Han, P.; Li, S.; Cao, W.; Li, Y.; Sun, Z.; Wang, Z.; Xu, H. *J. Mater. Chem. B* **2013**, *1*, 740–743.
- [102] Zeng, X.; Zhou, X.; Li, M.; Wang, C.; Xu, J.; Ma, D.; Xue, W. *J. Mater. Sci., Mater. Med.* **2015**, *26*, 234.
- [103] Deepagan, V. G.; Kwon, S.; You, D. G.; Nguyen, V. Q.; Um, W.; Ko, H.; Lee, H.; Jo, D.-G.; Kang, Y. M.; Park, J. H. *Biomaterials* **2016**, *103*, 56–66.
- [104] Kunstelj, M.; Fidler, K.; Škrajnar, Š.; Kenig, M.; Smilović, V.; Kusterle, M.; Caserman, S.; Zore, I.; Porekar, V. G.; Jevševar, S. *Bioconjugate Chem.* **2013**, *24*, 889–896.
- [105] Yu, F.; Junyi, C.; Huaping, X.; Chantal, V. O.; Xi, Z.; Wim, D.; Mario, S. *Macromol. Rapid Commun.* **2012**, *33*, 798–804.
- [106] Zhang, X.; Xu, H.; Dong, Z.; Wang, Y.; Liu, J.; Shen, J. *J. Am. Chem. Soc.* **2004**, *126*, 10556–10557.
- [107] Liu, J.; Pang, Y.; Chen, J.; Huang, P.; Huang, W.; Zhu, X.; Yan, D. *Biomaterials* **2012**, *33*, 7765–7774.
- [108] Yiyan, H.; Yu, N.; Gang, C.; Li, X.; Youqing, S.; Zhongwei, G. *Adv. Mater.* **2014**, *26*, 1534–1540.
- [109] An, N.; Lin, H.; Yang, C.; Zhang, T.; Tong, R.; Chen, Y.; Qu, F. *Mater. Sci. Eng. C* **2016**, *69*, 292–300.
- [110] Zhai, S.; Hu, X.; Hu, Y.; Wu, B.; Xing, D. *Biomaterials* **2017**, *121*, 41–54.
- [111] Bergson, G. *Ark. Kemi* **1962**, *19*, 195–214.
- [112] Bergson, G. *Acta Chem. Scand.* **1957**, *11*, 1607–1608.
- [113] Bergson, G.; Biezais, A. *Ark. Kemi* **1961**, *18*, 143–149.

- [114] Bergson, G.; Claeson, G.; Schotte, L. *Acta Chem. Scand.* **1962**, *16*, 1159–1174.
- [115] Bergson, G. *Acta Chem. Scand.* **1961**, *15*, 1611–1613.
- [116] Matsugo, S.; Yan, L.-J.; Konishi, T.; Youn, H.-D.; Lodge, J. K.; Ulrich, H.; Packer, L. *Biochem. Biophys. Res. Commun.* **1997**, *240*, 819–824.
- [117] Hong, Y. S.; Jacobia, S. J.; Packer, L.; Patel, M. S. *Free Radical Biol. Med.* **1999**, *26*, 685–694.
- [118] Sergeeva, S. V.; Slepneva, I. A.; Khrantsov, V. V. *Free Radical Res.* **2001**, *35*, 491–497.
- [119] Hildebrandt, J.; Niksch, T.; Trautwein, R.; Häfner, N.; Görls, H.; Barth, M.-C.; Dürst, M.; Runnebaum, I. B.; Weigand, W. *Phosphorus, Sulfur Silicon Relat. Elem.* **2017**, *192*, 182–186.
- [120] Bachrach, S. M.; Walker, C. J.; Lee, F.; Royce, S. J. *Org. Chem.* **2007**, *72*, 5174–5182.
- [121] Bachrach, S. M.; Woody, J. T.; Mulhearn, D. C. *J. Org. Chem.* **2002**, *67*, 8983–8990.
- [122] Bangham, A. D. *Adv. Lipid Res.* **1963**, *1*, 65–104.
- [123] Etheridge, M. L.; Campbell, S. A.; Erdman, A. G.; Haynes, C. L.; Wolf, S. M.; McCullough, J. *Nanomedicine* **2013**, *9*, 1–14.
- [124] Sercombe, L.; Veerati, T.; Moheimani, F.; Wu, S. Y.; Sood, A. K.; Hua, S. *Front. Pharmacol.* **2015**, *6*, 286.
- [125] Akbarzadeh, A.; Rezaei-Sadabady, R.; Davaran, S.; Joo, S. W.; Zarghami, N.; Hanifehpour, Y.; Samiei, M.; Kouhi, M.; Nejati-Koshki, K. *Nanoscale Res. Lett.* **2013**, *8*, 102.
- [126] Huang, C.-H. *Biochemistry* **1969**, *8*, 344–352.
- [127] Deamer, D.; Bangham, A. D. *Biochim. Biophys. Acta, Biomembr.* **1976**, *443*, 629–634.
- [128] Dal Molin, M.; Verolet, Q.; Colom, A.; Letrun, R.; Derivery, E.; Gonzalez-Gaitan, M.; Vauthey, E.; Roux, A.; Sakai, N.; Matile, S. *J. Am. Chem. Soc.* **2015**, *137*, 568–571.
- [129] Angelova, M. I.; Dimitrov, D. S. *Faraday Discuss. Chem. Soc.* **1986**, *81*, 303–311.
- [130] Evans, E.; Kwok, R. *Biochemistry* **1982**, *21*, 4874–4879.
- [131] Munye, M. M.; Ravi, J.; Tagalakis, A. D.; McCarthy, D.; Ryadnov, M. G.; Hart, S. L. *Sci. Rep.* **2015**, *5*, 9292.
- [132] van Meer, G.; Voelker, D. R.; Feigenson, G. W. *Nat. Rev. Mol. Cell Biol.* **2008**, *9*, 112–124.

- [133] Sezgin, E.; Levental, I.; Mayor, S.; Eggeling, C. *Nat. Rev. Mol. Cell Biol.* **2017**, *18*, 361–374.
- [134] Hatakeyama, H.; Akita, H.; Harashima, H. *Biol. Pharm. Bull.* **2013**, *36*, 892–899.
- [135] Pangburn, T. O.; Petersen, M. A.; Waybrant, B.; Adil, M. M.; Kokkoli, E. *J. Biomech. Eng.* **2009**, *131*, 74005–74020.
- [136] Eloy, J. O.; Petrilli, R.; Trevizan, L. N. F.; Chorilli, M. *Colloids Surf., B* **2017**, *159*, 454–467.
- [137] Gaber, M.; Medhat, W.; Hany, M.; Saher, N.; Fang, J.-Y.; Elzoghby, A. *J. Control. Release* **2017**, *254*, 75–91.
- [138] Riaz, K. M.; Riaz, A. M.; Zhang, X.; Lin, C.; Wong, H. K.; Chen, X.; Zhang, G.; Lu, A.; Yang, Z. *Int. J. Mol. Sci.* **2018**, *19*, 195.
- [139] Kichler, A.; Remy, J. S.; Boussif, O.; Frisch, B.; Boeckler, C.; Behr, J. P.; Schuber, F. *Biochem. Biophys. Res. Commun.* **1995**, *209*, 444–450.
- [140] Olusanya, O. T.; Haj Ahmad, R. R.; Ibegbu, M. D.; Smith, R. J.; Elkordy, A. A. *Molecules* **2018**, *23*, 907.
- [141] Li, T.; Takeoka, S. *Int. J. Nanomedicine* **2013**, *8*, 3855–3866.
- [142] Li, T.; Takeoka, S. *Int. J. Nanomedicine* **2014**, *9*, 2849–2861.
- [143] Mandel, R.; Ryser, H. J.; Ghani, F.; Wu, M.; Peak, D. *Proc. Natl. Acad. Sci. U. S. A.* **1993**, *90*, 4112–4116.
- [144] Karala, A.; Ruddock, L. W. *FEBS J.* **2010**, *277*, 2454–2462.
- [145] Regen, S. L.; Czech, B.; Singh, A. *J. Am. Chem. Soc.* **1980**, *102*, 6638–6640.
- [146] Hub, H.; Hupfer, B.; Koch, H.; Ringsdorf, H. *Angew. Chem., Int. Ed.* **1980**, *19*, 938–940.
- [147] Johnston, D. S.; Sanghera, S.; Pons, M.; Chapman, D. *Biochim. Biophys. Acta, Biomembr.* **1980**, *602*, 57–69.
- [148] O'Brien, D. F.; Whitesides, T. H.; Klingbiel, R. T. *J. Polym. Sci., Polym. Lett. Ed.* **1981**, *19*, 95–101.
- [149] Palivan, C. G.; Goers, R.; Najer, A.; Zhang, X.; Car, A.; Meier, W. *Chem. Soc. Rev.* **2016**, *45*, 377–411.
- [150] Antonietti, M.; Förster, S. *Adv. Mater.* **2003**, *15*, 1323–1333.
- [151] Li, F.; Prevost, S.; Schweins, R.; Marcelis, A. T. M.; Leermakers, F. A. M.; Cohen Stuart, M. A.; Sudholter, E. J. R. *Soft Matter* **2009**, *5*, 4169–4172.
- [152] Chen, Q.; Schonherr, H.; Vancso, G. J. *Soft Matter* **2009**, *5*, 4944–

4950.

- [153] Kita-Tokarczyk, K.; Grumelard, J.; Haeefe, T.; Meier, W. *Polymer* **2005**, *46*, 3540–3563.
- [154] Dalhaimer, P.; Bates, F. S.; Aranda-Espinoza, H.; Discher, D. C. *R. Phys.* **2003**, *4*, 251–258.
- [155] Najer, A.; Wu, D.; Bieri, A.; Brand, F.; Palivan, C. G.; Beck, H.-P.; Meier, W. *ACS Nano* **2014**, *8*, 12560–12571.
- [156] Zhou, C.; Wang, M.; Zou, K.; Chen, J.; Zhu, Y.; Du, J. *ACS Macro Lett.* **2013**, *2* (11), 1021–1025.
- [157] Ken Wong, C.; Laos, A. J.; Soeriyadi, A. H.; Wiedenmann, J.; Curmi, P. M. G.; Gooding, J.; Marquis, C. J.; Stenzel, M. H.; Thordarson, P. *Angew. Chem., Int. Ed.* **2015**, *54*, 5317–5322.
- [158] Messenger, L.; Gaitzsch, J.; Chierico, L.; Battaglia, G. *Curr. Opin. Pharmacol.* **2014**, *18*, 104–111.
- [159] Discher, B. M.; Won, Y.-Y.; Ege, D. S.; Lee, J. C.-M.; Bates, F. S.; Discher, D. E.; Hammer, D. A. *Science* **1999**, *284*, 1143–1146.
- [160] Discher, D. E.; Eisenberg, A. *Science*. **2002**, *297*, 967–973.
- [161] Battaglia, G.; Ryan, A. J. *J. Am. Chem. Soc.* **2005**, *127*, 8757–8764.
- [162] Lomas, H.; Canton, I.; MacNeil, S.; Du, J.; Armes, S. P.; Ryan, A. J.; Lewis, A. L.; Battaglia, G. *Adv. Mater.* **2007**, *19*, 4238–4243.
- [163] Kumar, A.; Lale, S. V.; Mahajan, S.; Choudhary, V.; Koul, V. *ACS Appl. Mater. Interfaces* **2015**, *7*, 9211–9227.
- [164] Jia, L.; Cui, D.; Bignon, J.; Di Cicco, A.; Wdzieczak-Bakala, J.; Liu, J.; Li, M.-H. *Biomacromolecules* **2014**, *15*, 2206–2217.
- [165] Zhang, Y.; Wu, K.; Sun, H.; Zhang, J.; Yuan, J.; Zhong, Z. *ACS Appl. Mater. Interfaces* **2018**, *10*, 1597–1604.
- [166] Chuard, N.; Fujisawa, K.; Morelli, P.; Saarbach, J.; Winssinger, N.; Metrangolo, P.; Resnati, G.; Sakai, N.; Matile, S. *J. Am. Chem. Soc.* **2016**, *138*, 11264–11271.
- [167] Drake, C. R.; Aissaoui, A.; Argyros, O.; Thanou, M.; Steinke, J. H. G.; Miller, A. D. *J. Control. Release* **2013**, *171*, 81–90.
- [168] Glasoe, P. K.; Long, F. A. *J. Phys. Chem.* **1960**, *64*, 188–190.
- [169] Lees, W. J.; Whitesides, G. M. *J. Org. Chem.* **1993**, *58*, 642–647.
- [170] Schotte, L.; Ström, H. *Acta Chem. Scand.* **1956**, *10*, 687–688.
- [171] Viricel, W.; Mbarek, A.; Leblond, J. *Angew. Chem.* **2015**, *127*, 12934–12938.

- [172] Chuard, N.; Gasparini, G.; Moreau, D.; Lörcher, S.; Palivan, C.; Meier, W.; Sakai, N.; Matile, S. *Angew. Chem., Int. Ed.* **2017**, *56*, 2947–2950.
- [173] Schwendener, R. A.; Lagocki, P. A.; Rahman, Y. E. *Biochim. Biophys. Acta* **1984**, *772*, 93–101.
- [174] Lee Rodgers, J.; Nicewander, W. A. *Am. Stat.* **1988**, *42*, 59–66.
- [175] Wang, F.; Good, J. A. D.; Rath, O.; Kaan, H. Y. K.; Sutcliffe, O. B.; Mackay, S. P.; Kozielski, F. *J. Med. Chem.* **2012**, *55*, 1511–1525.
- [176] Magoulas, G. E.; Bariamis, S. E.; Athanassopoulos, C. M.; Papaioannou, D. *Tetrahedron Lett.* **2010**, *51*, 1989–1993.
- [177] Marsh, E. N. G. *Acc. Chem. Res.* **2014**, *47*, 2878–2886.
- [178] Zhang, W.; Curran, D. P. *Tetrahedron* **2006**, *62*, 11837–11865.
- [179] Lörcher, S.; Meier, W. *Eur. Polym. J.* **2017**, *88*, 575–585.
- [180] Ite, F.; Chami, M.; Najer, A.; Lörcher, S.; Wu, D.; Dinu, I. A.; Meier, W. *Macromolecules* **2014**, *47*, 7588–7596.
- [181] Chuard, N.; Poblador-Bahamonde, A. I.; Zong, L.; Bartolami, E.; Hildebrandt, J.; Weigand, W.; Sakai, N.; Matile, S. *Chem. Sci.* **2018**, *9*, 1860–1866.
- [182] Xu, F.; Yang, Z.-Z.; Zhang, S.-J. *Phosphorus, Sulfur Silicon Relat. Elem.* **2013**, *188*, 1312–1319.
- [183] Ferris, A. F. *J. Org. Chem.* **1955**, *20*, 780–787.
- [184] Haratake, M.; Matsumoto, S.; Ono, M.; Nakayama, M. *Bioconjug. Chem.* **2008**, *19*, 1831–1839.
- [185] Rasmussen, B.; Sorensen, A.; Gottfredsen, H.; Pittelkow, M. *Chem. Commun.* **2014**, *50*, 3716–3718.
- [186] Günther, W. H. H. *J. Org. Chem.* **1967**, *32*, 3931–3933.
- [187] Steinmann, D.; Nauser, T.; Koppenol, W. H. *J. Org. Chem.* **2010**, *75*, 6696–6699.
- [188] Thapa, B.; Schlegel, H. B. *J. Phys. Chem. A* **2016**, *120*, 8916–8922.
- [189] Corbett, J. F. *J. Chem. Educ.* **1972**, *49*, 663.
- [190] Günther, W. H. H.; Mautner, H. G. *J. Med. Chem.* **1964**, *7*, 229–232.
- [191] Günther, W. H. H. *J. Org. Chem.* **1966**, *31*, 1202–1205.
- [192] Santi, C.; Santoro, S.; Testaferri, L.; Tiecco, M. *Synlett* **2008**, *10*, 1471–1474.
- [193] Silverstein, S. C.; Steinman, R. M.; Cohn, Z. A. *Annu. Rev. Biochem.* **1977**, *46*, 669–722.

- [194] Los, D. A.; Murata, N. *Biochim. Biophys. Acta, Biomembr.* **2004**, *1666*, 142–157.
- [195] Wang, L. H.; Rothberg, K. G.; Anderson, R. G. *J. Cell Biol.* **1993**, *123*, 1107–1117.
- [196] Rodal, S. K.; Skretting, G.; Garred, Ø.; Vilhardt, F.; van Deurs, B.; Sandvig, K. *Mol. Biol. Cell* **1999**, *10*, 961–974.
- [197] Spiro, D. J.; Boll, W.; Kirchhausen, T.; Wessling-Resnick, M. *Mol. Biol. Cell* **1996**, *7*, 355–367.
- [198] Kjekken, R.; Mousavi, S. A.; Brech, A.; Griffiths, G.; Berg, T. *Biochem. J.* **2001**, *357*, 497–503.
- [199] Davies, P.; Allison, A. C. *Front Biol.* **1978**, *46*, 143–160.
- [200] Dougherty, D. A. *Acc. Chem. Res.* **2013**, *46*, 885–893.
- [201] Schottel, B. L.; Chifotides, H. T.; Dunbar, K. R. *Chem. Soc. Rev.* **2008**, *37*, 68–83.
- [202] Gorteau, V.; Bollot, G.; Mareda, J.; Perez-Velasco, A.; Matile, S. *J. Am. Chem. Soc.* **2006**, *128*, 14788–14789.
- [203] Zhao, Y.; Cotellet, Y.; Avestro, A.-J.; Sakai, N.; Matile, S. *J. Am. Chem. Soc.* **2015**, *137*, 11582–11585.
- [204] Cotellet, Y.; Benz, S.; Avestro, A.-J.; Ward, T. R.; Sakai, N.; Matile, S. *Angew. Chem., Int. Ed.* **2016**, *55*, 4275–4279.
- [205] Liu, L.; Cotellet, Y.; Avestro, A.-J.; Sakai, N.; Matile, S. *J. Am. Chem. Soc.* **2016**, *138*, 7876–7879.
- [206] Fujisawa, K.; Beuchat, C.; Humbert-Droz, M.; Wilson, A.; Wesolowski, T. A.; Mareda, J.; Sakai, N.; Matile, S. *Angew. Chem., Int. Ed.* **2014**, *53*, 11266–11269.
- [207] Fujisawa, K.; Humbert-Droz, M.; Letrun, R.; Vauthey, E.; Wesolowski, T. A.; Sakai, N.; Matile, S. *J. Am. Chem. Soc.* **2015**, *137*, 11047–11056.
- [208] Zhao, Y.; Beuchat, C.; Domoto, Y.; Gajewy, J.; Wilson, A.; Mareda, J.; Sakai, N.; Matile, S. *J. Am. Chem. Soc.* **2014**, *136*, 2101–2111.
- [209] Herce, H. D.; Garcia, A. E.; Cardoso, M. C. *J. Am. Chem. Soc.* **2014**, *136*, 17459–17467.
- [210] Nishihara, M.; Perret, F.; Takeuchi, T.; Futaki, S.; Lazar, A. N.; Coleman, A. W.; Sakai, N.; Matile, S. *Org. Biomol. Chem.* **2005**, *3*, 1659–1669.
- [211] DeRouchey, J.; Hoover, B.; Rau, D. C. *Biochemistry* **2013**, *52*, 3000–3009.
- [212] Bayer, T. S.; Booth, L. N.; Knudsen, S. M.; Ellington, A. D. *RNA* **2005**,

11, 1848–1857.

- [213] Gasparini, G.; Bang, E.-K.; Montenegro, J.; Matile, S. *Chem. Commun.* **2015**, 51, 10389–10402.
- [214] Baumann, P.; Balasubramanian, V.; Onaca-Fischer, O.; Sienkiewicz, A.; Palivan, C. G. *Nanoscale* **2013**, 5, 217–224.
- [215] Heinisch, T.; Langowska, K.; Tanner, P.; Reymond, J.; Meier, W.; Palivan, C.; Ward, T. R. *ChemCatChem* **2013**, 5, 720–723.
- [216] Qian, Z. M.; Li, H.; Sun, H.; Ho, K. *Pharmacol. Rev.* **2002**, 54, 561–587.
- [217] McMahon, T. C.; Stanley, S.; Kazyanskaya, E.; Hung, D.; Wood, J. L. *Org. Lett.* **2012**, 14, 4534–4536.
- [218] Self, W. T.; Tsai, L.; Stadtman, T. C. *Proc. Natl. Acad. Sci. U. S. A.* **2000**, 97, 12481–12486.
- [219] Novakov, I. A.; Shulevich, Y. V.; Zakharova, Y. A.; Chang, L. T. D.; Dukhanina, E. G.; Navrotskii, A. V. *Russ. Chem. Bull.* **2015**, 64, 597–604.
- [220] Wang, Y.; Zhu, L.; Wang, Y.; Li, L.; Lu, Y.; Shen, L.; Zhang, L. W. *ACS Appl. Mater. Interfaces* **2016**, 8, 35106–35113.
- [221] Singh, R.; Whitesides, G. M. *J. Am. Chem. Soc.* **1990**, 112, 1190–1197.
- [222] Danehy, J. P.; Elia, V. J. *J. Org. Chem.* **1972**, 37, 369–373.
- [223] Unger, F.; Liehl, E. GB 2 148 296 A, **1985**.